NASA

DEVELOPMENT OF ADVANCED HIGH-TEMPERATURE HEAT FLUX SENSORS

By:
W. H. Atkinson and R. R. Strange

UNITED TECHNOLOGIES CORPORATION
POWER SECTOR
PRATT & WHITNEY AIRCRAFT GROUP
COMMERCIAL PRODUCTS DIVISION

Prepared for:
NATIONAL AERONAUTICS AND SPACE ADMINISTRATION

NASA Lewis Research Center
Contract NAS 3-22133

1. Report No. NASA CR-165618	2. Government Accession No.	3. Recipient's Catalog No.
4. Title and Subtitle DEVELOPMENT OF ADVANCED HIGH-TEMPERATURE HEAT FLUX SENSORS		5. Report Date September 1982
		6. Performing Organization Code
7. Author(s) W. H. Atkinson and R. R. Strange		8. Performing Organization Report No. PWA-5723-27
		10. Work Unit No.
9. Performing Organization Name and Address United Technologies Corporation Pratt & Whitney Aircraft Group Commercial Products Division - East Hartford, CT		11. Contract or Grant No. NAS 3-22133
		13. Type of Report and Period Covered Contractor Report
12. Sponsoring Agency Name and Address National Aeronautics and Space Administration Washington, D. C. 20546		14. Sponsoring Agency Code

15. Supplementary Notes

Project Manager, Howard Hobart
NASA Lewis Research Center, Cleveland OH 44135

16. Abstract

Various configurations of high-temperature heat flux sensors were studied to determine their suitability for use in experimental combustor liners of advanced aircraft gas turbine engines. It was determined that embedded thermocouple sensors, laminated sensors, and Gardon gauge sensors, were the most viable candidates. Sensors of all three types were fabricated, calibrated, and endurance tested. All three types of sensors met the fabricability, survivability, and accuracy requirements established for their application.

17. Key Words (Suggested by Author(s)) Gas Turbine Engine Combustors Embedded Thermocouple Sensors Laminated Sensors Gardon Gauges	18. Distribution Statement		
19. Security Classif. (of this report) Unclassified	20. Security Classif. (of this page) Unclassified	21. No. of Pages	22. Price*

N83-10044 #

FOREWORD

TABLE OF CONTENTS

TABLE OF CONTENTS (Continued)

LIST OF ILLUSTRATIONS

LIST OF ILLUSTRATIONS (Continued)

LIST OF ILLUSTRATIONS (Continued)

LIST OF ILLUSTRATIONS (Continued)

LIST OF ILLUSTRATIONS (Continued)

SUMMARY

The overall objectives of the program were to analyze various types of heat flux sensors and, using the results of that analysis, fabricate and test miniature high temperature heat flux sensors suitable for installation in experimental combustor liners of advanced aircraft gas turbine engines.

A literature survey was conducted to review the state of the art of heat flux sensor technology. Preliminary analyses were then performed to investigate possible sensor configurations for the application. One-dimensional heat flux sensors and Gardon gauges were identified as the most promising candidates. A series of component and construction technique evaluation tests were performed to determine the feasibility of various sensor configurations. On the basis of the results of those tests, final designs of three sensor configurations were generated and thermally analyzed. Two of these configurations, the embedded thermocouple sensors and the laminated sensors, were selected by NASA for continued development. Work on the third type, the Gardon gauge, was continued at no cost to NASA as an alternate sensor configuration. Sensors of all three types were fabricated, calibrated, and endurance tested. The conclusions that were drawn from this program are identified below.

o   Sensors of three types were fabricated that met the geometrical requirements and could withstand the environmental conditions.

o   Calibration data from both primary and transfer calibration techniques confirm that the accuracy goal of ±5 percent of the nominal full scale heat flux of 1×10^6 watts per square meter was met.

o   Thermal cycle tests and thermal soak tests indicated that the sensors are capable of surviving extended periods of exposure to burner environmental conditions.

o   A large number of sensor failures were observed. The primary cause of the failures was identified as leadwire failure external to the sensors. Corrective actions in the handling and protection of the leadwires have been identified that should minimize the failure rate.

INTRODUCTION

2.1 BACKGROUND

Designing combustor liners and turbine airfoils which are durable and use a minimum amount of cooling air requires a complete knowledge of heat flux characteristics throughout the hot section of modern gas turbine engines. Although analytical models have been developed to predict heat fluxes, the technology is not currently available to measure heat flux directly on hot section components. Such measurements are required to enable modification and/or verification of analytical procedures used to design combustor liners and turbine airfoils for longer hot section life while minimizing the amount of cooling required, thus maintaining efficiency and economy. Therefore, it is necessary to design miniature heat flux sensors for these high temperature, high pressure applications. These sensors are designed to measure heat flux per unit area (kw/m^2). This quantity will be referred to as heat flux throughout the report.

The measurement of heat loads in the hot section is complicated by several factors. The temperature levels are sufficiently high so that high temperature resistant materials must be used to fabricate the sensors and leads. Extreme temperature gradients exist along the surface of the hot section components which increase the need for small sensors. Finally, thermal and electrical insulation is required in many sensor designs to enhance one-directional heat flow. The presence of the heat flux sensor may disturb the thermal profile where it is installed and alter the heat flux relative to the unperturbed liner. Therefore, care must be exercised in selecting the material properties and geometry of the insulation to minimize the surface temperature perturbation. The presence of the sensor and its installation into the test hardware produces a pronounced effect on the sensor calibration accuracy which must be accounted for.

2.2 SENSOR ANALYSIS CRITERIA

The above considerations dictate that the criteria used to evaluate sensor viability should include survivability, accuracy, and fabricability.

2.2.1 Survivability

The sensor must be capable of surviving in the hot section environment where metal temperatures to 1250K, pressure to 40 atmospheres, pressure drops of up to 1.5 atmospheres across the combustor liner, and heat flux to two million watts per square meter must be tolerated. The sensor must also be compatible with the products of combustion, thermal shock, and thermal cycling conditions that exist in the hot section.

2.2.2 Accuracy

The heat flux accuracy goal of +5-10 percent of the nominal full scale heat flux of 1×10^6 w/m^2 requires that any viable sensor must only disturb the

heat flux pattern a minimum amount, particularly where sensor accuracy is a strong function of operating condition. Therefore, the sensor must not cause large thermal or aerodynamic variations in the sensing area.

2.2.3 Fabricability

Viable sensors, and their components, must be fabricated using cost effective, repeatable techniques that either currently exist or could be developed at acceptable risk under contract.

2.3 SCREENING OF CANDIDATE SENSORS

A study was undertaken to identify sensor candidates that most adequately satisfied the above criteria. The stepwise approach used in the study includes:

o   literature survey to define state-of-the-art heat flux sensors,

o   selection of sensor type suitable for high temperature/high flux operation in aircraft gas turbine engine combustor liners,

o   preliminary design of suitable sensors,

o   thermal analysis of preliminary designs,

o   fabrication and testing of sensor components,

o   selection of designs for fabrication and testing,

o   thermal analysis of final designs,

o   fabrication of sensors,

o   calibration testing,

o   endurance testing.

Section 3.0 of this report describes the screening process that led to the selection of the final candidate sensors; Section 4.0 presents a description of the design, fabrication and testing of the final sensors; Section 5.0 presents the sensor test results; and Section 6.0 presents the conclusions and recommendations of the program. The more detailed data from the program are presented in Appendices A through E.

4

SENSOR SELECTION BY PRELIMINARY ANALYSIS, DESIGN AND TESTING

3.1 LITERATURE SURVEY

A computer assisted literature survey was performed to identify the state-of-the-art in heat flux sensor development. This survey was conducted through the United Technologies Research Center library using interlibrary loans on requested materials. Initially, materials were requested with publication dates from 1965 to the present. Subsequent findings indicated the existence of important articles and papers with earlier publication dates and these were also obtained. The references resulting from this survey are listed in Appendix A. The information was separated into four categories:

1. steady state sensors (including Gardon gauges) that appeared applicable to the present contract,

2. transient sensors,

3. miscellaneous sensors that were not applicable to the present contract,

4. calibration methods.

The following is a discussion of the significant items identified under each of the above categories.

3.1.1 Steady State Sensors

The steady state sensors are classified as sensors whose operation is based on heat conduction through a thermal barrier. One-dimensional steady state sensors determine the heat flux by measuring the temperature differential across a material of known thermal conductivity. There have been a wide variety of configurations that have been used in the construction of these sensors, providing flexibility in design with regard to size, geometry and materials. The thermal barrier may be installed in the test section, placed on one surface of the test section, or the wall of the test section may be used as the thermal barrier. Several configurations of existing one-dimensional sensors are illustrated in Figure 3.1-1 and are discussed below.

The simplest form of a one-dimensional steady state heat flux sensor is formed by placing a surface thermocouple on both the hot and cold side of the test section. The test section itself then forms the thermal barrier for the one-dimensional sensor. Since simply placing wires on the surface would cause a large boundary layer disturbance, various techniques may be used to maintain the aerodynamic integrity of the test section. Such techniques include embedding the thermocouple in the wall of the test section, use of sputtered thin film thermocouples, or installing foil thermocouples cemented in ceramic coatings on the surface of the test section. Depending on the particular installation, data may be obtained either by measuring both hot and cold side temperature or a differential output signal may be measured directly.

HEAT SOURCE

AIRFOIL

SURFACE THERMOCOUPLES

HEAT SOURCE

AIRFOIL

INSULATION

THERMOELECTRIC MATERIAL B

THERMOELECTRIC MATERIAL A (SENSOR OUTPUT)

LAMINATED SENSOR

HEAT SOURCE

THERMOPILE OUTPUT

AIRFOIL

THIN THERMOPILE ON SURFACE

HEAT SOURCE

AIRFOIL

THERMOCOUPLES

GARDON GAUGE
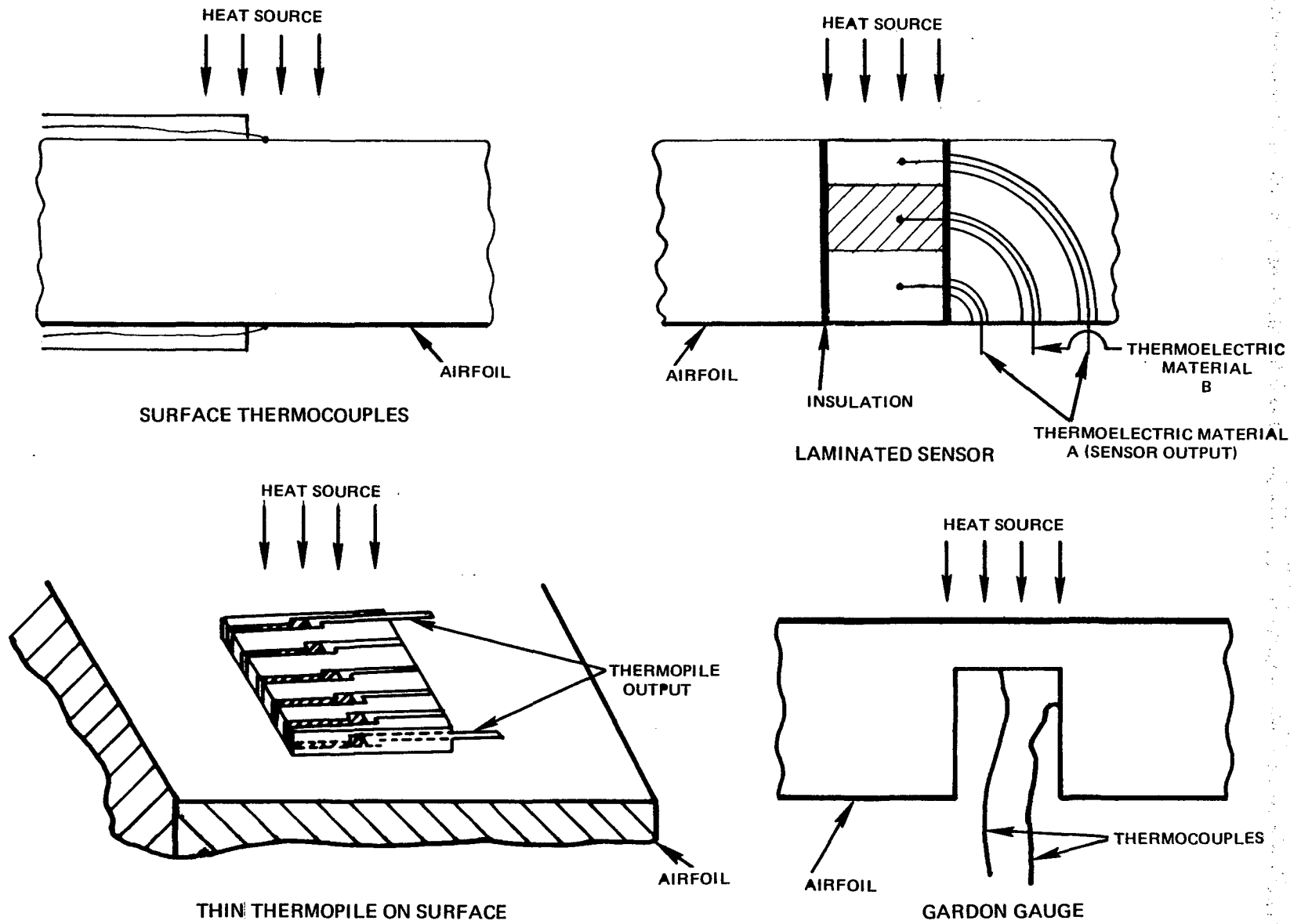
Figure 3.1-1   General Configurations of Steady State Heat Flux Sensors

Another type of one-dimensional sensor is the laminated steady state sensor. In this sensor, the thermoelectric junctions are formed by a direct metal-to-metal bond between layers of the thermoelectric materials. This is designed to remove the location of thermoelectric junctions from any thermal perturbations introduced by the leadwires. Overall thermal perturbations introduced by the laminated sensor may be minimized by matching the thermal conductivity of the sensor materials to that of the surrounding combustor liner.

A third type of one-dimensional sensor may be formed by placing a thin thermopile on either the hot or cold combustor liner surface. The thermal barrier in these sensors is very thin and a multijunction pair thermopile is used to increase the output voltage of the sensor. This type of sensor is widely used for low temperature applications but it is not readily available for high temperature applications. The advantage of these sensors is that they are installed on the surface and do not require modification of the combustor liner. The disadvantage is that the multijunction pair thermopile required to increase the output also increases the size of the active area of the sensor.

Due to the overall advantages in design flexibility and materials selection for the one-dimensional sensor type, several forms of one-dimensional steady state heat flux sensors were chosen for further investigation.

The Gardon gauge is a form of the steady state sensor that operates on the principle of radial heat conduction in a thin metallic foil rather than linear heat conduction through a thermal barrier. The gauge is constructed by forming a thin foil over a hole in the combustor liner. A differential thermocouple is formed by attaching one wire to the center of the rear face of the foil and the second wire to the surrounding combustor liner. The heat flux entering the foil of the Gardon gauge flows from the foil center to the periphery of the gauge on the combustor liner. This sets up a temperature difference between the foil and liner. The heat flux seen by the sensor is proportional to the difference between the temperatures of the liner and the foil and can be found using the conduction equation in radial form.

The disadvantage of the Gardon gauge is that these sensors can cause large thermal perturbations in the area of the sensor. However, Gardon gauges have some advantages over other sensors. According to Gardon (11), these gauges are adaptive to high fluxes and the sensors are rugged. These sensors also have rapid response time (59), and are relatively insensitive to liner temperature. W. A. Clayton (15) has studied several different methods for improving the performance of this type of sensor. By using materials different from conventional foil calorimeters, he has been able to improve the high temperature performance without loss of sensitivity.

It was determined that Gardon gauges showed sufficient potential to allow the design to be further evaluated.

3.1.2 Transient Sensors

Transient sensor operation is based on either the heat capacity equation, or the transient form of the heat conduction equation, and requires a net change

in heat flux to the sensor to yield data. The sensor area is part of a heat sink of known physical and thermal properties.

Slug calorimeters, which are a typical type of transient sensor, are constructed with a slug that is mounted in a thermally insulated housing. Thermocouples are attached to the body of the slug and track the time-temperature history of the sensor as in Kraabel's sensor (16).

The thin foil transient heat flux sensor uses a thin layer of foil as a very small slug. The foil is placed over a hole in the test specimen with a thermocouple attached to the center of the rear face of the sensor. These sensors are used in a variety of environments including spacecraft, boiler furnaces, and aircraft.

Another type of transient sensor is the one-dimensional transient heat flux sensor. It is constructed from the same materials as the skin in which it is embedded. It is also the same thickness as the skin material. The sensor is thermally isolated from the skin by a thin layer of insulation. A thermocouple is applied to the front face of the sensor surface and tracks the time-temperature history. Considering this sensor as an insulated rod, the heat flux can then be calculated using the conduction equation.

The advantages of transient sensors are that they are reasonably simple to fabricate, rugged, easy to use, and can be developed to give fast response to thermal perturbations.

One of the disadvantages of these sensors is that they are transient and require a step change in net heat flux to the sensor to yield data. Under steady state conditions, or under transients that are slow compared to sensor response time, these sensors yield no data. Since the goal of this program is to measure steady state heat flux through the combustor, and since cycling a gas turbine engine quickly enough to simulate a step change to the combustor is difficult, obtaining sufficiently accurate information from any transient sensor to predict steady state heat flux would not be feasible. Therefore, transient heat flux sensors are not considered viable candidates for the combustor liner application.

3.1.3 Miscellaneous Sensor Types

Other types of sensors include radiometers and I^2R heat flux sensors. The latter consist of a number of resistively heated strips, each of which is monitored by two thermocouples at known distances. The strips are heated until a uniform temperature is reached. Cooling air is then applied to the surface and the power to the strips is adjusted until the same uniform temperature is regained. The power needed to regain uniformity represents the heat transfer and is calculated from the voltage drop across the thermocouple leads and current through the strips. Radiometers are most often thermopiles with a window and respond only to radiant heat loads. These were not considered to be of interest for the specified total steady state heat flux application and were not researched further.

8

3.1.4 Calibration Methods

Because of slight fabrication differences from sensor-to-sensor and the fact that the sensor will produce small perturbations in local heat flux, they must be individually calibrated to achieve the accuracy goals specified for this program. This can be done by subjecting the sensor to an accurately known heat flux and measuring its output which will be a microvolt signal related to the heat flux through the sensor. A known heat flux can be applied by conductive, convective or radiative means.

Conductive calibrations are performed by placing a heater on one side of the sensor and a heat sink on the other side. The edges of the sensor are either well insulated or surrounded by guard heaters to prevent heat loss. A conductive calibration may be absolute if the input power is measured and all the heat losses from the back side of the heater and sensor edges are known. More frequently, the conductive calibrations are comparative where the sensor being calibrated is placed in series with a sensor of known characteristics.

A second method of calibration makes use of a convective heat source. This method is not used frequently because it is difficult to obtain reproducibility in the air flow and temperature characteristics of the source.

Radiative calibrations are the most widely used because they are relatively easy to conduct, are straightforward to analyze, and are capable of producing high heat loads. In radiative calibrations, the sensor is exposed to a heat load from a high temperature source. The sensor is coated to provide a surface with known absorptance and emittance. A radiant calibration can be an absolute calibration if the total heat balance of the system can be defined from thermal and dimensional measurements, or it can be comparative where the output of the sensor is compared with the output of a standard sensor with known characteristics. For absolute calibrations, it is desirable to operate in a vacuum environment to eliminate convective heat transfer effects. The geometry of the radiative calibration devices must be designed to produce a known view factor from the source to the sensor if absolute calibrations are desired. This is most easily accomplished by positioning the sensor close to the surface of a heat source that is considerably larger than the sensor.

Because of the high temperatures and high heat loads involved in this program, conductive and convective methods would be difficult to implement. It was decided that the most effective and easily controllable approach would be to use a well defined radiative heat flux.

3.2 ANALYTICAL SCREENING OF CANDIDATE SENSORS

Several sensor types which were identified during the literature search were subjected to preliminary thermal analysis. The purpose of that analysis was to evaluate the amount of perturbation to the thermal and heat flux distribution caused by the sensors.

An analysis was conducted for a flat Hastelloy plate, with and without thermal gradients imposed on the plate surfaces. These served as baselines for sensor analyses. Temperature and heat flux distributions within five percent of these baselines were chosen as design goals.

The sensor analyses were performed using Pratt & Whitney Aircraft's Thermal Calculation (TCAL) program. This program performs three-dimensional finite difference heat transfer analyses. The program allows materials properties (thermal conductivity and specific heat) to vary with temperature and allows both transient and steady state analyses to be performed.

For the purposes of this analysis, the heat load on the sensors was assumed to be strictly convective. The hot and cold side boundary conditions were chosen to give representative heat fluxes and combustor liner temperatures. The uniform hot and cold side conditions chosen were:

A. hot side gas temperature of 2030K with a heat transfer coefficient of 1470 watts/meter^{2}K,

B. cold side gas temperature of 810K with a heat transfer coefficient   of 2550 watts/meter^{2}K.

To evaluate the effect of thermal gradients, the analysis was then repeated with a hot side gas temperature gradient of approximately 44K/centimeter imposed on the sensors.

The results of the early computer runs were used to modify the geometry of the various sensor designs to better achieve the design goals. The end results of these analyses showed that it would be possible to build several types of one-dimensional heat flux sensors that introduced acceptably small thermal perturbations to meet the initial design goals. In addition, it was determined that it would be possible to construct Gardon Gauges which introduced hot side thermal perturbations within the design goals.

Once the preliminary thermal analyses were completed, more detailed analyses were performed to determine the validity of the assumption of constant heat flux across the sensor. These analyses were performed using STAN5, a computer program developed for NASA by Stanford University. The program performs a step-wise, finite element solution of the boundary layer dynamics for a flat plate given the free stream conditions, the plate thermal distributions, and the initial shape of the thermal boundary layer; the solution chosen provided Stanton number as a function of the distance from the start of the boundary layer. The Stanton number can be directly related to the convective heat transfer coefficient.

A ceramic strip, the width of a nominal sensor, was used to introduce the thermal perturbation in the boundary layer. The strip was placed at five locations downstream from the start of the boundary layer, giving variations in turbulence from laminar to turbulent flow.

The hydrodynamic flow field that was simulated in this analysis was one-dimensional as would be expected in a typical combustor section. In addition, the diameter of the sensor was small relative to the curvature of the combustor liner, making the flat plate analysis a reasonable approximation.

An iterative solution was planned to determine the affect of variable heat transfer coefficients across the sensors. The STAN 5 analysis would be used to define the variation in h across the sensor. The h distribution from STAN 5 would be used in TCAL to determine a new surface temperature distribution for STAN 5. The above procedure was to be repeated until the h distribution and the surface temperature distribution converged. In addition, a continuous curve was fit through the sensor area using the unperturbed data before and after the sensor. The mean values of these functions represent the heat transfer coefficients that would have existed over the sensor area without the sensor installed which allowed calculation of the error due to the assumption of constant surface temperature and h distributions. After the first iteration, the error was less than 2 percent for all cases except where the flow was transitional. In that case, the error was 3 percent. These errors represent negligible error in the sensor heat flux and verify our assumptions of constant hot side surface conditions.

The preliminary analysis provided the results identified below.

1. Three basic types of heat flux sensors were identified for consideration:

    o   one-dimensional sensors,

    o   Gardon gauges,

    o   transient sensors.

2. The one-dimensional sensors and Gardon gauges were found to be the most suitable sensor types for miniature, high temperature, high heat flux applications in aircraft gas turbine engine combustors.

3. The transient sensors were not considered feasible because of the problems associated with introducing a step change in heat input to the combustor liners.

The results of the preliminary analysis were used to complete preliminary designs and thermal analyses on a large number of sensor designs. Five designs which appeared to offer the highest probability of meeting the contract objectives were chosen for further evaluation in the sensor component test program:

o   embedded thermocouple sensors,

o   thermocouples cemented in a ceramic coating,

o   laminated sensors,

o   Gardon gauges,

o   thin thermopile on hot side surface.

3.3 LABORATORY TESTING OF COMPONENTS

The purpose of the laboratory tests was to identify materials and fabrication techniques for production of sensors that were fabricable, survivable, and had desirable output characteristics. The results of those tests were to be used to choose, with approval from NASA, two sensor types for further development. The tests conducted were:

o   thermoelectric characterization tests,

o   diffusion bonding tests,

o   electrical insulation tests,

o   thermal ageing tests,

o   thermal cycling tests.

3.3.1 Thermoelectric Characterization Tests

The combustor liners for which the high temperature miniature heat flux sensors are being developed are manufactured from Hastelloy-X. It was considered desirable to use Hastelloy-X for the heat flux sensor bodies to minimize any thermal disturbance introduced by the heat flux sensors. Several of the sensor types could also make use of Hastelloy-X as part of the thermoelectric circuit. Tests were, therefore, conducted to determine the thermoelectric characteristics of various thermoelectric materials vs. Hastelloy-X. The results of those tests are summarized in Figure 3.3-1 which shows the output of various materials vs. Hastelloy-X as a function of temperature. These data were then combined with the known temperature dependent thermal conductivity of Hastelloy-X to calculate the sensitivity that each of the thermoelements would yield in a one-dimensional steady state heat flux sensor with a Hastelloy-X body. As shown in Figure 3.3-2, the results indicate that the most desirable materials to pair with Hastelloy-X from a thermoelectric standpoint were Constantan, due to its high output level, and Alumel which has an acceptably high output level and small sensitivity variation with temperature over the range of interest.

3.3.2 Diffusion Bonding Tests

For the laminated sensor to be successful, good electrical and mechanical bonds between the layers of laminate are required. It is also important to prevent voids in the bond line which could cause unacceptable thermal perturbations. Diffusion bonding was felt to have the highest probability of yielding the required high quality bonds. To minimize costs, a diffusion bonding method that utilized differential thermal expansion was chosen. Shown in Figure 3.3-3, this method eliminates the need for large presses. The sensors to be bonded are stacked inside a TZM yoke. TZM is an alloy of Molybdenum (containing small amounts of Titanium and Zirconium) with a coefficient of thermal expansion of approximately 7×10^{-6}/K compared to approximately 14×10^{-6}/K for typical nickel alloys. When this yoke is heated in a vacuum furnace, the stack containing the sensors attempts to expand more than the external yoke. This generates the force needed for diffusion bonding.

12
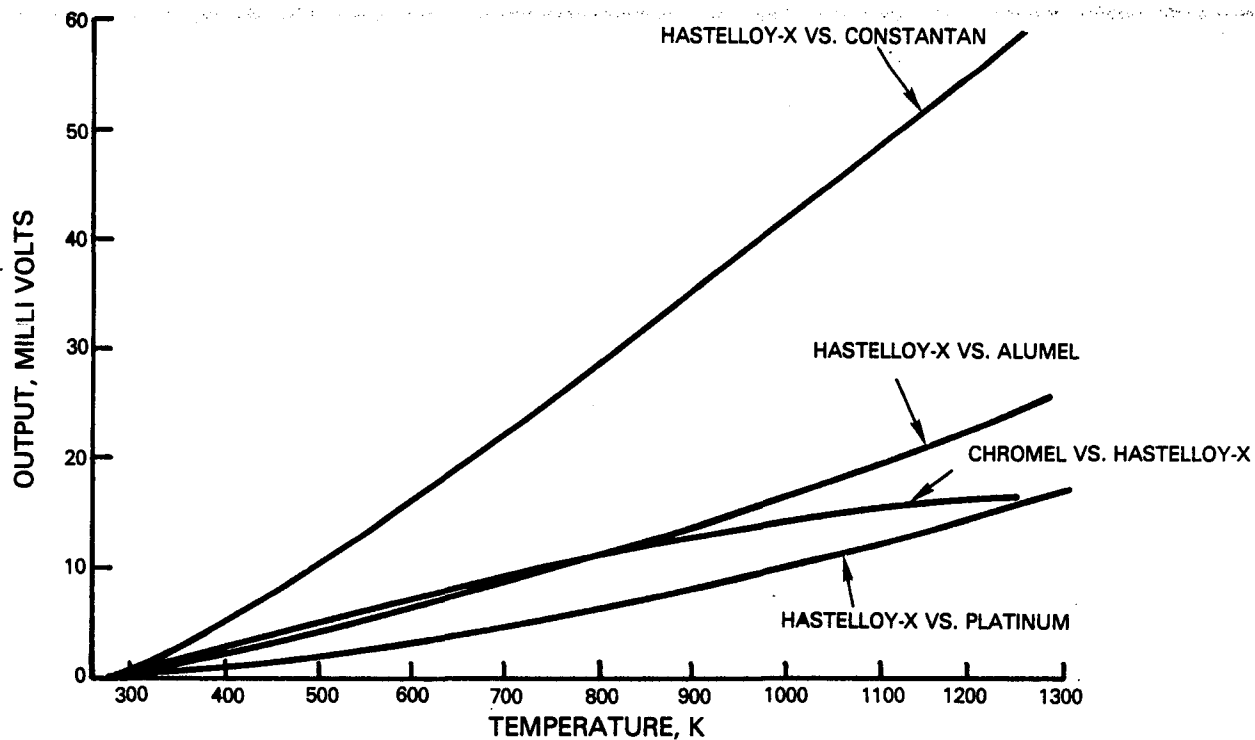
Figure 3.3-1   Output from Various Thermoelements Paired with Hastelloy-X
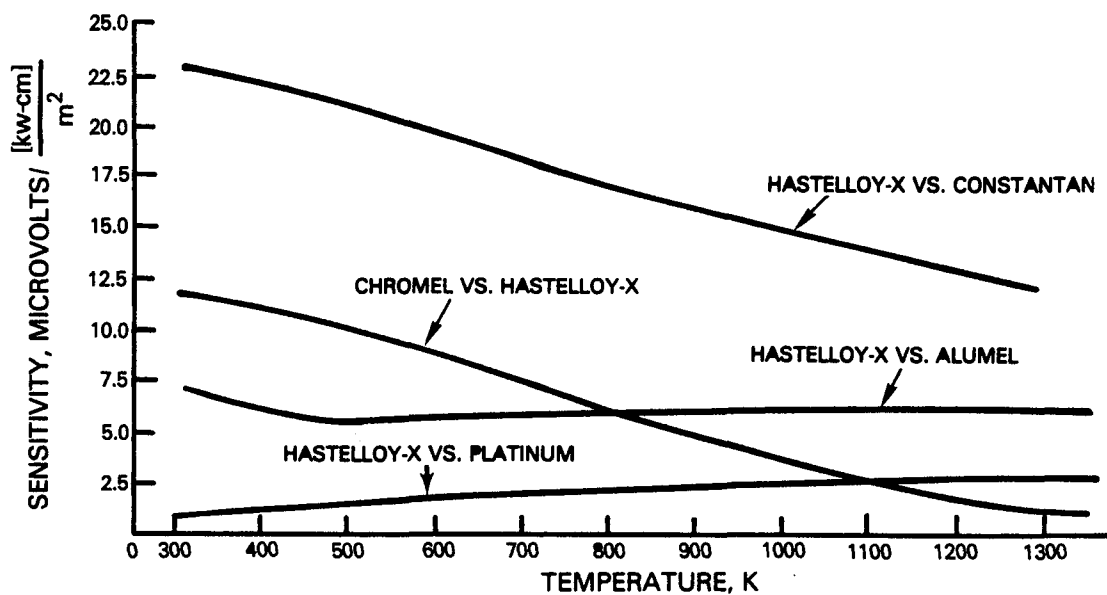
Figure 3.3-2   Sensitivity of Various Thermoelements Paired with Hastelloy-X

13
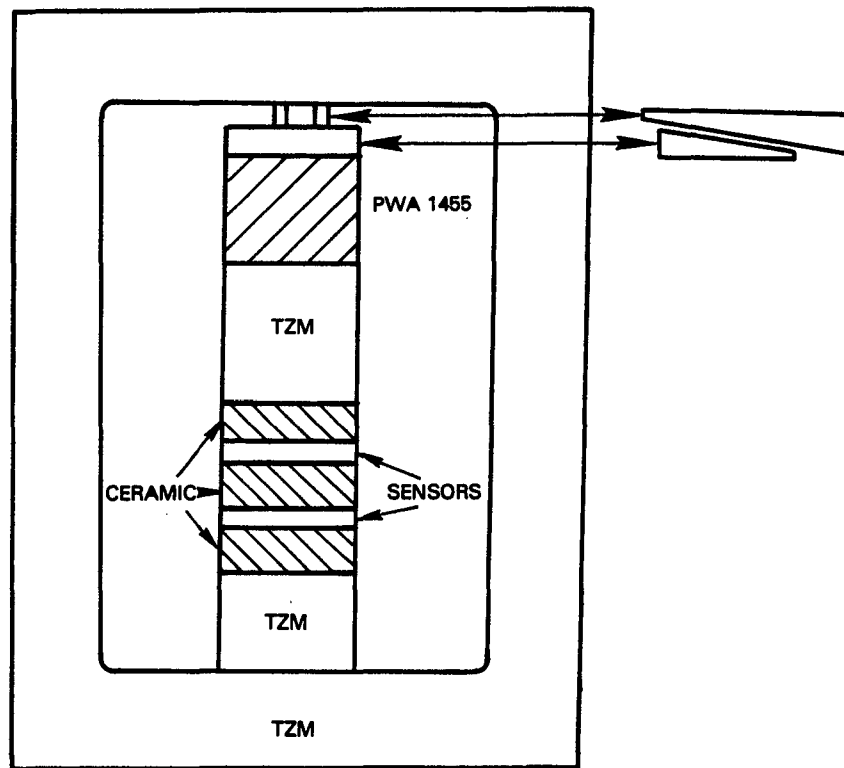
BONDING TEMPERATURE =1400K
BONDING TIME = 4 HRS
BACKGROUND PRESSURE = 0.07 PASCAL .

Figure 3.3-3   General Arrangement for Diffusion Bonding Laminated Materials by
               Differential Thermal Bonding

The bonding force obtained can be controlled by varying the relative amount of
nickel alloy (PWA 1455) and TZM in the sensor stack. Tests were run where
Chromel, Alumel, and Constantan were diffusion bonded to Hastelloy-X. In
addition, since it was considered possible that formation of aluminum oxide on
the surface of the Alumel could cause bonding problems, some Alumel samples
were flashed with a thin (0.0005 cm) nickel plate prior to bonding.

Following bonding, some of the samples were peel tested. These tests showed
that the strength of the bond lines was comparable to that of the bulk
materials. Some of the samples were sectioned and etched. Figures 3.3-4
through 3.3-7 show representative micrographs for each material diffusion
bonded to Hastelloy-X. All bond lines were uniform and free of voids. These
tests showed that any of the materials of interest could be diffusion bonded
to Hastelloy-X in a cost effective manner and that the resulting bonds were of
high quality. To eliminate any possibility of future oxide problems with
Alumel bonds, nickel flashing was used as a standard procedure for all further
Alumel bonding.

14
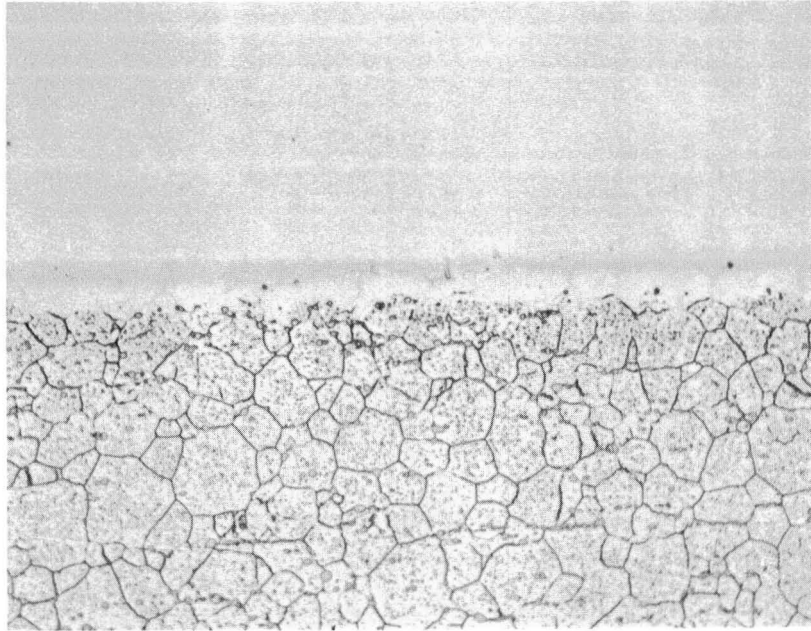
Figure 3.3-4 Photomicrograph of Alumel (Top) to Hastelloy-X (Bottom)
Diffusion Bond (Mag: 200X)
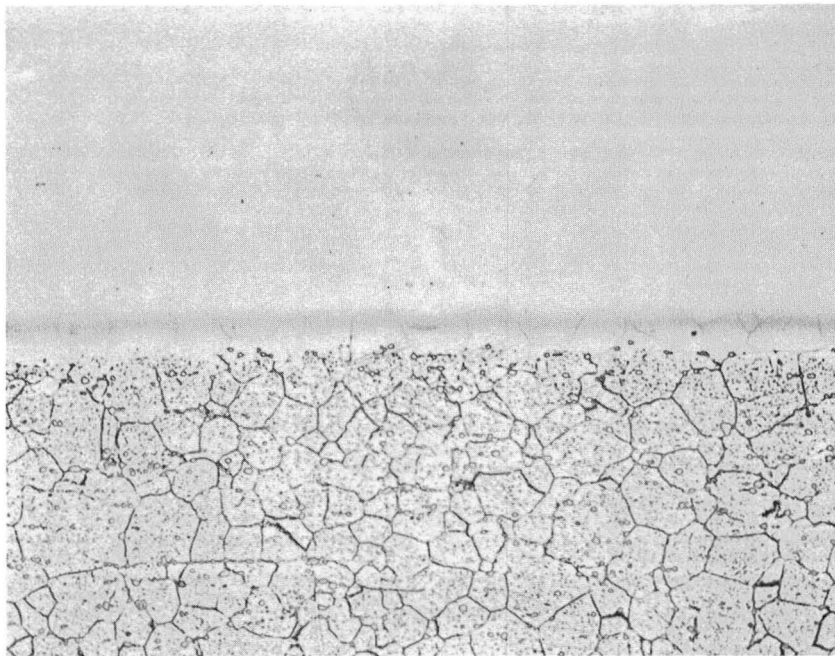
Figure 3.3-5 Photomicrograph of Alumel (Top) to Hastelloy-X (Bottom)
Diffusion Bond with a 0.0005 centimeter Nickel Plate on the
Alumel before Bonding (Mag: 200X)
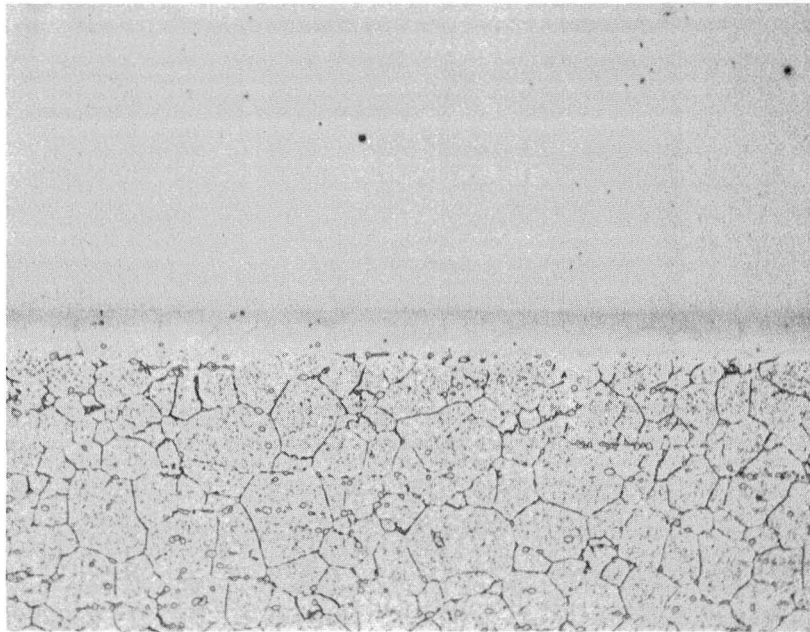
Figure 3.3-6   Photomicrograph of Chromel (Top) to Hastelloy-X (Bottom)
                Diffusion Bond (Mag: 200X)
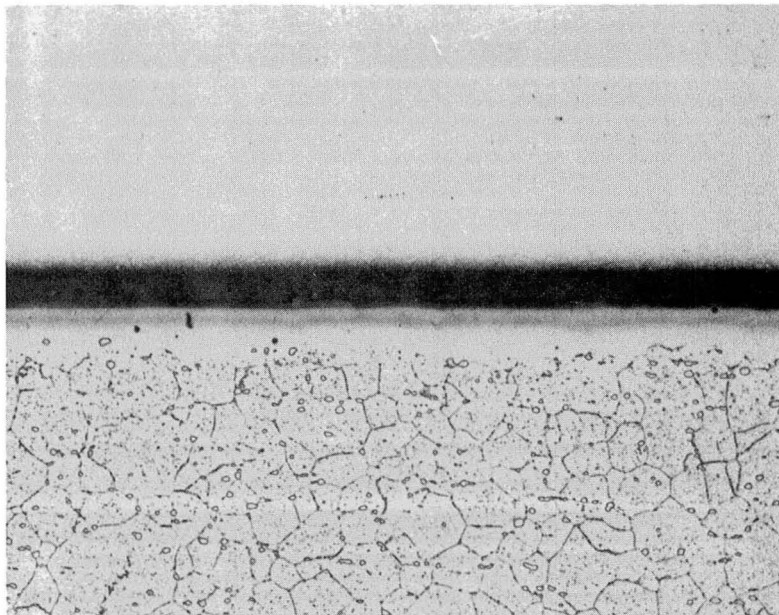
Figure 3.3-7   Photomicrograph of Constantan (Top) to Hastelloy-X (Bottom)
                Diffusion Bond (Mag: 200X)

16

3.3.3 Electrical Insulation Tests

Since several of the proposed sensor types could make use of ceramic cement as a high temperature electrical insulator, tests were conducted to investigate the resistivity characteristics of various ceramic cements. Figure 3.3-8 shows the results of a typical test where three commercially available ceramic cements were cycled from room temperature to 1260K, held for approximately 50 hours, and returned to room temperature. For this particular test, one ceramic (Sermabond P-1) showed a variation in resistance with time at temperature while the two other ceramics tested did not. The results of this test program showed that there were several commercially available ceramic cements with sufficient resistivity at the temperatures of interest to act as an insulator in these sensors.
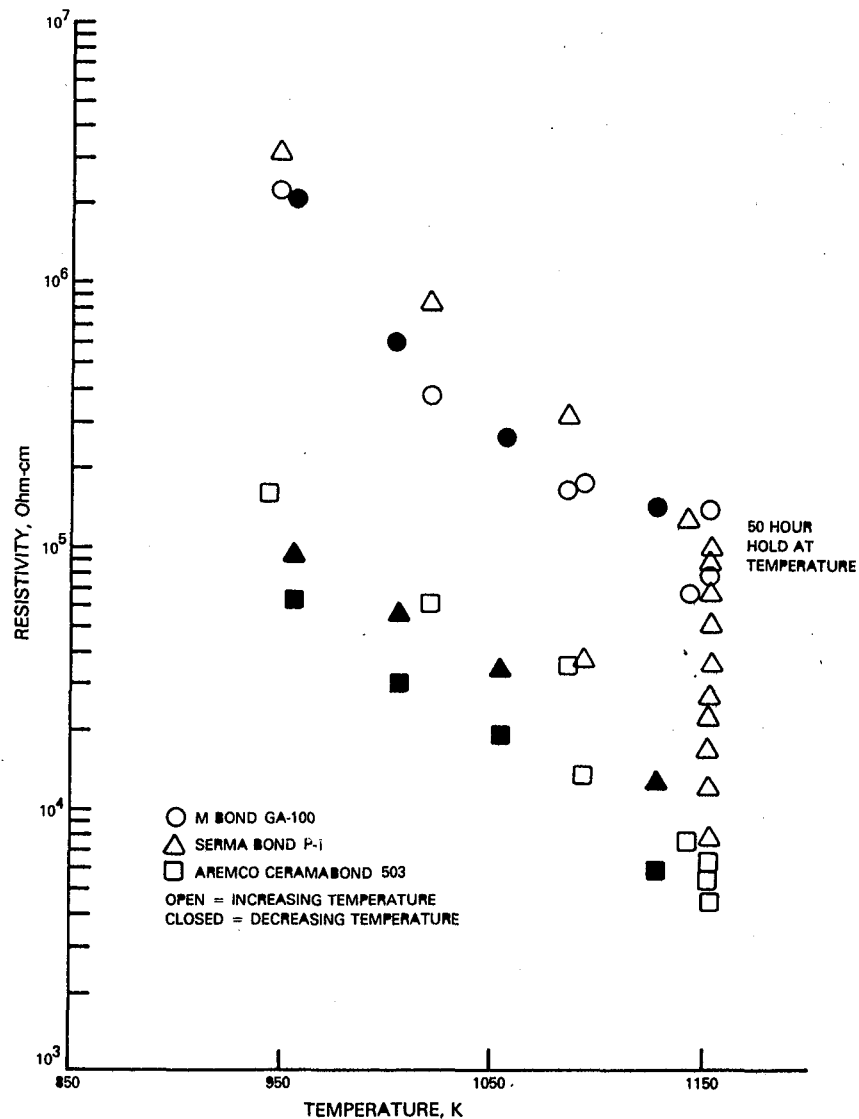
Figure 3.3-8   Plot of the Electrical Resistance versus Temperature for Various Ceramic Cements

3.3.4 Thermal Ageing Tests

Thermal ageing tests were run to investigate the stability with time as well as the survivability of the fine gauge sheathed lead wires that would be used in the sensors. These tests were run in a laboratory oven with capability of testing to temperatures in excess of 1550K. Figure 3.3-9 shows a typical test sample being installed in the oven while Figure 3.3-10 shows the test setup at the start of a test. To obtain data over extended periods in a cost effective manner, data were recorded automatically on a microcomputer-based data acquisition system shown in Figure 3.3-11. Figure 3.3-12 shows channel assignments for a typical test while Figure 3.3-13 shows representative data taken during the warmup period of one of the tests.
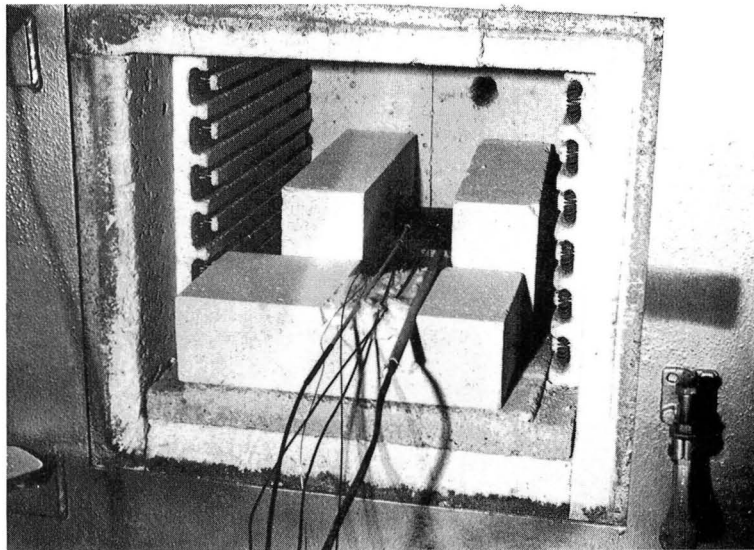
Figure 3.3-9   Internal View of Oven Used for Thermal Ageing Tests Showing Placement of Samples

Commercially available wire of various gauges containing various thermoelements were tested as well as sheathed Hastelloy-X wire that was produced at Pratt & Whitney Aircraft. Tests were conducted both with exposed thermocouple junctions (Figure 3.3-14) and with junctions protected by various ceramic cements (Figure 3.3-15).
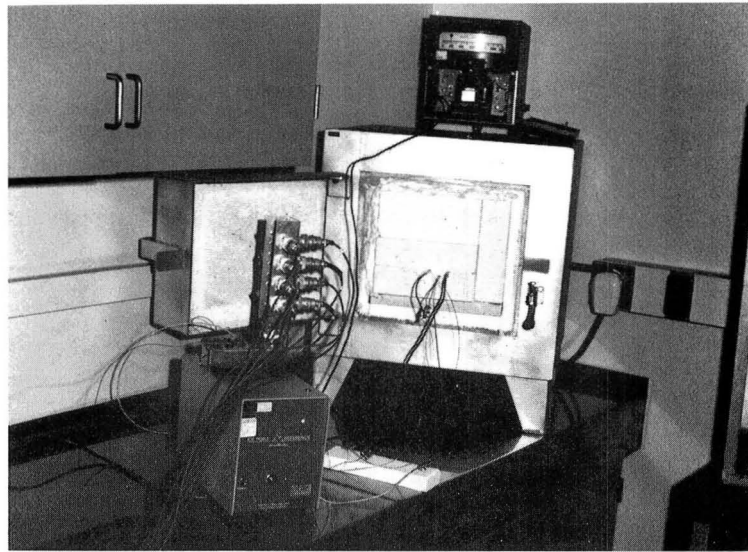
Figure 3.3-10 External View of Oven Used for Thermal Ageing Tests Showing Firebrick Closure

Figure 3.3-11 Data Acquistion System Used for All Test Programs

TYPE K THERMOCOUPLE AGING TEST 4

CHANNEL ASSIGNMENTS

```
CHANNEL   0 PT 10% RH   + PLATINUM  - .062 IN SHEATH
CHANNEL   1 CHROMEL     + ALUMEL    - .010 IN SHEATH SINGLE CONDUCTOR
CHANNEL   2 CHROMEL     + PLATINUM -
CHANNEL   3 ALUMEL      + PLATINUM -
CHANNEL   4 CHROMEL     + ALUMEL    - .010 IN SHEATH
CHANNEL   5 CHROMEL     + PLATINUM -
CHANNEL   6 ALUMEL      + PLATINUM -
CHANNEL   7 CHROMEL     + ALUMEL    - .006 IN SHEATH SINGLE CONDUCTOR
CHANNEL   8 CHROMEL     + PLATINUM -
CHANNEL   9 ALUMEL      + PLATINUM -
CHANNEL  10 PT 10% RH   + PLATINUM - .062 IN SHEATH
```

DATA TEST STARTED 12/12/80

Figure 3.3-12 Data System Channel Assignments for Thermocouple Ageing Tests

AGING TESTS ELAPSED TIME 90 MIN

DATE TEST STARTED 12/12/80

TIME OF DATA POINT 164304

CHANNEL	MILLIVOLTS	DEGREES F	LOOP RESIST	DEVIATION MICROV.
00	4.734	1023.19	3.1	5.-
01	22.672	1017.81	126.1	150.-
02	17.898	1020.88	92.4	62.-
03	4.778-	1006.67	50.1	83.
04	22.879	1026.54	189.1	56.
05	18.093	1031.21	129.9	133.
06	4.791-	1009.30	76.0	71.
07	22.813	1023.76	413.5	9.-
08	18.004	1026.46	309.9	43.
09	4.814-	1014.14	120.4	47.
10	4.745	1025.13	3.1	5.

TIME OF DATA POINT 165804

CHANNEL	MILLIVOLTS	DEGREES F	LOOP RESIST	DEVIATION MICROV.
00	6.051	1253.78	2.0	4.-
01	28.211	1252.73	123.1	44.-
02	22.279	1255.49	89.3	16.
03	5.935-	1243.35	52.8	56.
04	28.366	1259.36	189.0	110.
05	22.451	1264.86	127.7	188.
06	5.919-	1240.04	80.6	72.
07	28.254	1254.55	418.5	1.-
08	22.355	1259.60	309.7	91.
09	5.903-	1236.74	128.1	89.
10	6.060	1255.46	2.0	4.

Figure 3.3-13 Representative Data from Thermocouple Ageing Tests Taken during Heat-up Period

20
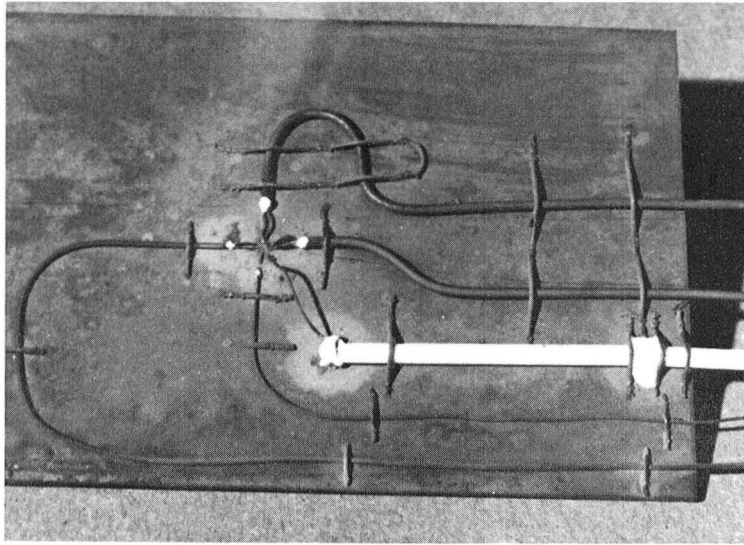
Figure 3.3-14 Thermocouple Ageing Test Sample Plate with Exposed Thermocouple Junctions after 50 hour Test
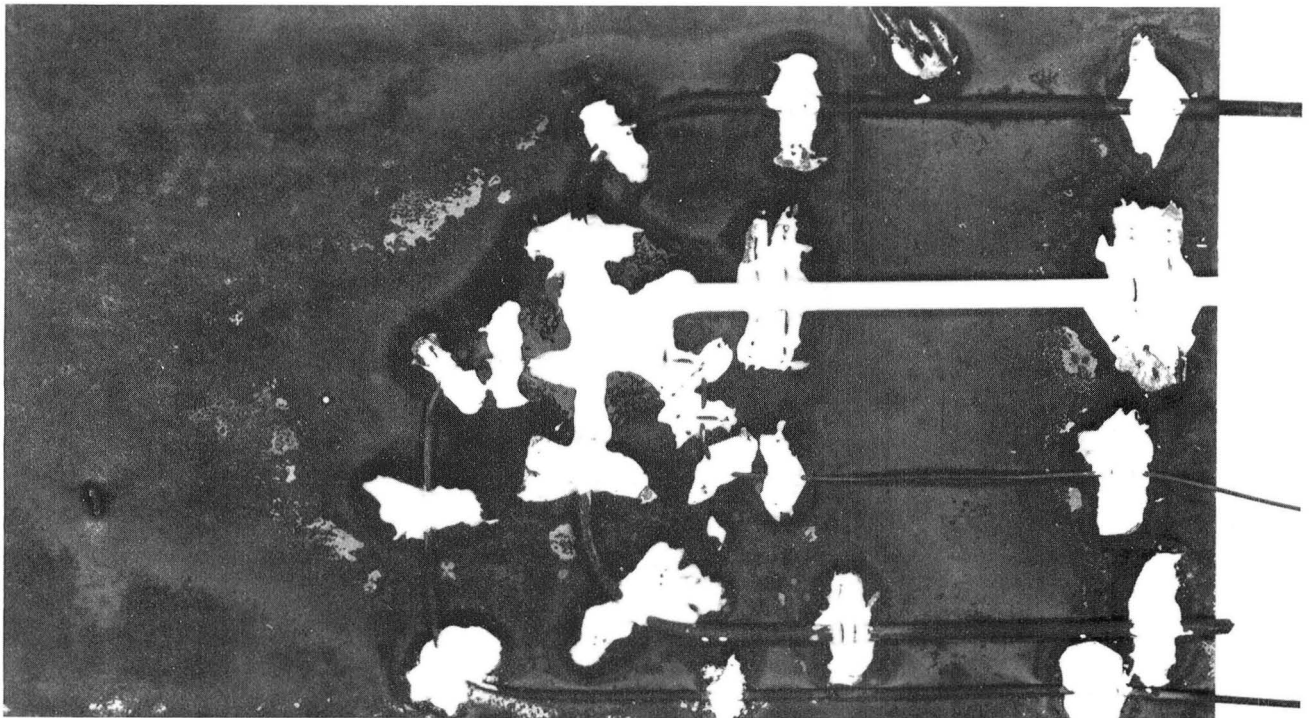
Figure 3.3-15 Thermocouple Ageing Test Sample Plate with Ceramic Covered Thermocouple Junctions after 50 hour Test

As expected, the tests with exposed junctions showed severe oxidation for all thermoelements except platinum in 50 hours at 1250K. Junction failures were often experienced before the end of the test period. It was found that protecting the wires with ceramic cement provided substantial protection to the junctions and yielded acceptable junction life. Also, as expected, heavier gauge wires were found to have better survivability than fine gauge wires. The finest wires tested (0.015 cm sheath outer diameter) were found to be unacceptable both in terms of stability and survivability. This confirmed results obtained previously by NASA (reference 53 of Appendix A). Both single and dual conductor Chromel and Alumel wires of 0.025 cm sheath outer diameter were found to have acceptable stability and lifetimes. Commercial sheathed Hastelloy-X wire was not available within the time restraints of this contract. We were able to swage Hastelloy-X wire with a sheath outer diameter of approximately 0.060 cm that had acceptable lifetimes for use under this contract.

3.3.5 Thermal Cycling Tests

Thermal cycling tests were conducted to investigate the effect of thermal cycling on component durability. The tests were conducted in front of the high intensity quartz lamp bank shown in Figure 3.3-16. Test samples were mounted in front of the lamp and impingement cooling was supplied to the back of the samples. Figure 3.3-17 shows a test sample mounted in the thermal cycling facility. Both rig operation and data reduction were controlled by the same microcomputer-based data system used for the thermal ageing tests.
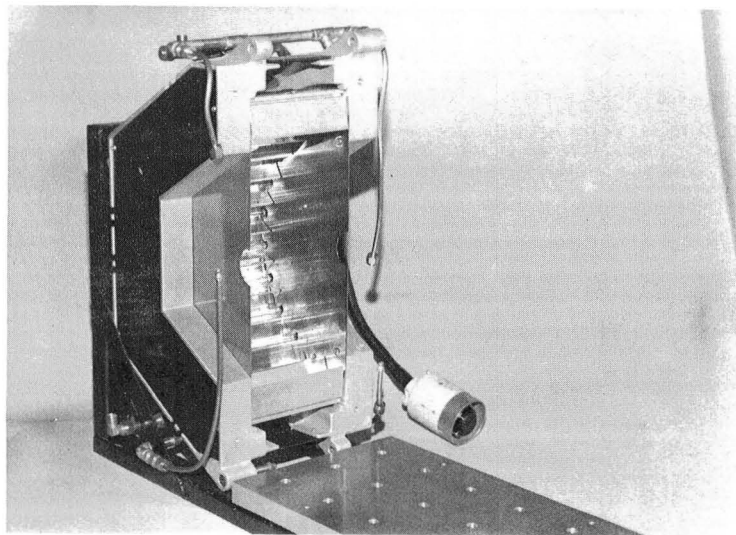
Figure 3.3-16 Quartz Lamp Bank Heat Source
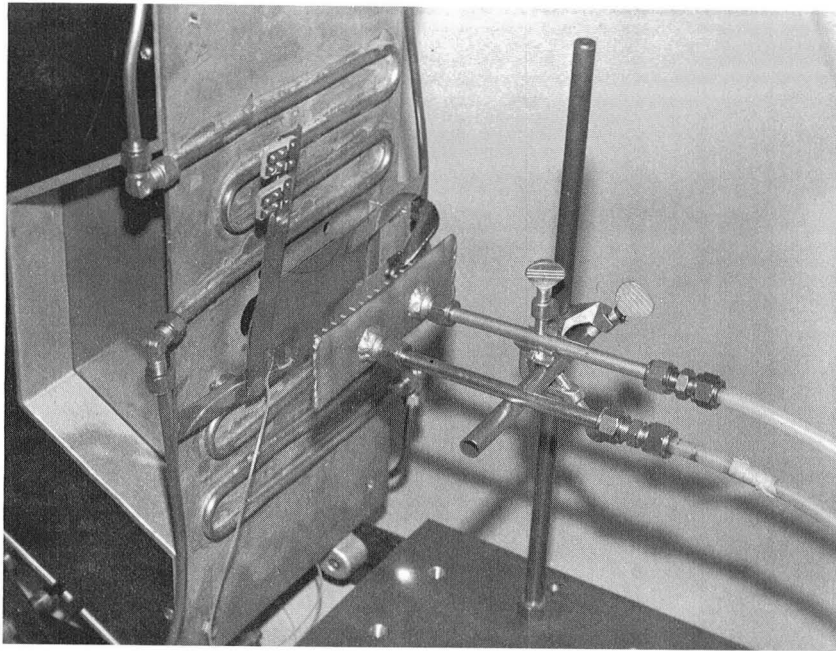
Figure 3.3-17 Sample Mounting Arrangement for Component Tests with Quartz Lamp Bank Showing the Plenum to Supply Cooling Air

Thermal cycle testing of the diffusion bonded materials showed no indications of delamination as the result of thermal cycling. Both single and dual conductor Chromel and Alumel sheathed wires with 0.025 cm sheath diameters were embedded in Hastelloy-X plates and cycled repeatedly. These wires generally survived beyond the 50 cycle goal. Most ceramics, when applied to flat Hastelloy-X plates, were found to peel after a few cycles due to the stresses caused by the widely different coefficients of expansion of the Hastelloy-X and the ceramics. When the plates were grooved and the ceramics installed in the grooves, excellent results were obtained. Figure 3.3-18, for example, shows a test sample with three ceramics installed in grooves with 0.025 cm diameter Type K sheathed thermocouples in a Hastelloy-X plate. This sample was cycled 48 times to temperatures of approximately 1250K and twice to temperatures of approximately 1450K. The ceramics maintained good adhesion throughout the test sequence and the thermocouples survived intact.
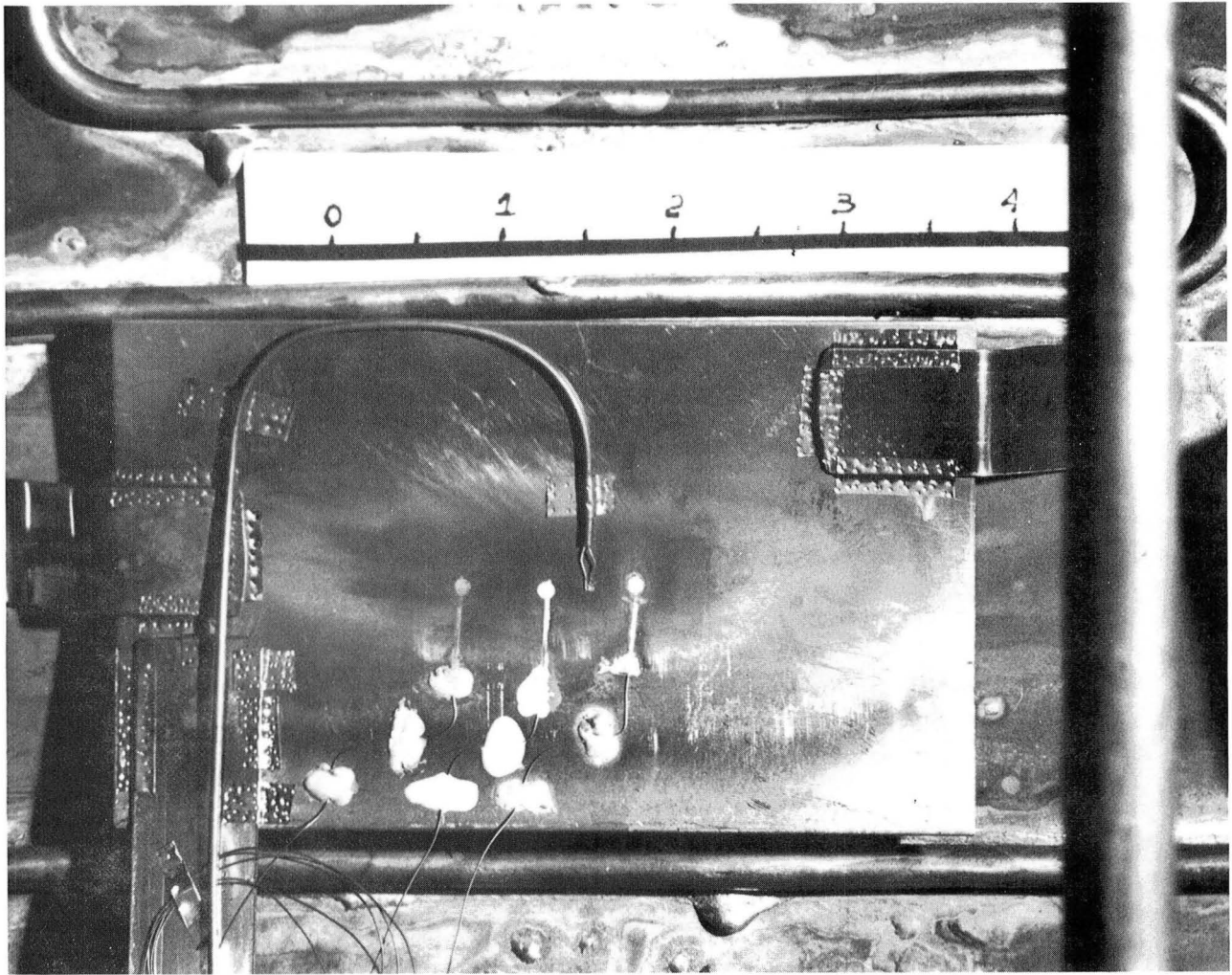
Figure 3.3-18 Ceramic Cement Sample Plate after 50 cycles in front of Quartz Lamp Bank

Peeling of the ceramic from the flat plates indicated that the fabrication of thin thermopiles and foil thermocouples on the surface would involve high risk. The proposed installation method for thermopiles and foil thermocouples was to cement them to the surface with a ceramic cement. The thin thermopile sensors also pose problems as a result of the changes in thermal conductivity of the thermal barrier materials with temperature. The literature values of thermal conductivity for three common high temperature materials were used to calculate the change in the calibration constant with temperature for a thermopile sensor fabricated with these materials as thermal barriers. The

data plotted in Figure 3.3-19 are the the factors by which the room temperature calibration constant must be multiplied to account for thermal barrier temperature. The dotted line represents a material with a constant thermal conductivity with temperature and, hence, a steady calibration constant over the temperature range. The test results and analyses of the thermal barrier conductivities indicated that both thin thermopiles and thermocouples cemented in a ceramic coating on the surface would require considerable materials development and thus, were eliminated from further consideration.
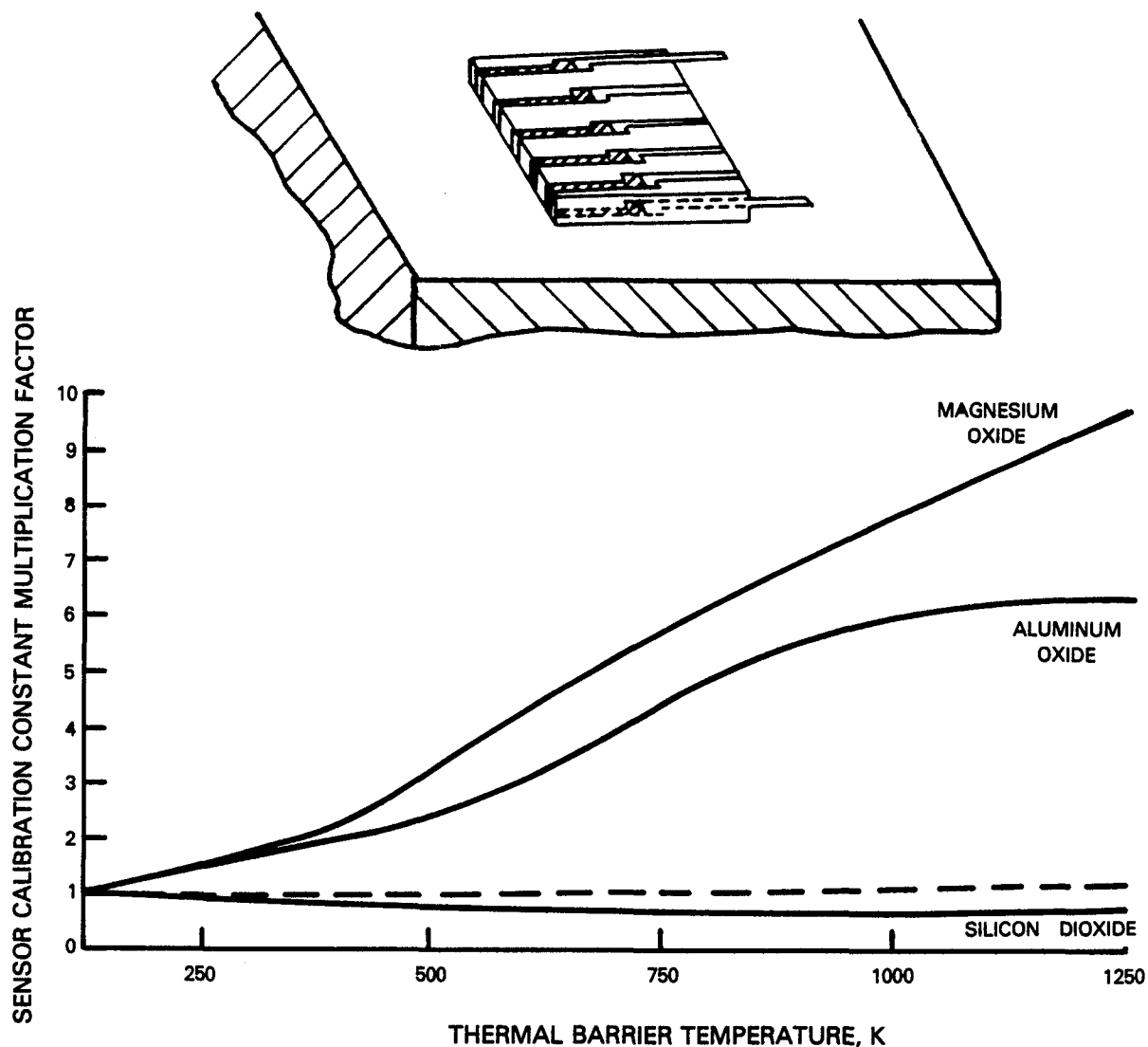
Figure 3.3-19 Plot of Calibration Shift with Temperature in a Thin Thermopile Sensor with Various Thermal Barrier Materials

3.4 SUMMARY AND CONCLUSIONS

Several conclusions can be drawn from the results of this sequence of laboratory tests.

o   Hastelloy-X would be a suitable thermoelectric material for sensor fabrication.

o   A durable laminated sensor could be formed by diffusion bonding.

o   Fine sheathed thermocouple wires (0.025 cm diameter) were stable and durable enough for sensor construction.

o   Ceramics peeled when applied to flat Hastelloy-X plates but survived well when applied to grooves.

Based on these results, it was recommended that three sensor types be considered for further development:

o   embedded thermocouples,

o   laminated sensors,

o   Gardon gauges.

SECTION 4.0

DESIGN, FABRICATION AND TESTING OF SENSORS

4.1 DESIGN OF SENSORS

The embedded thermocouple sensor and the laminated sensor were chosen by NASA
for development. It was also agreed that Pratt & Whitney Aircraft would
continue development of the Gardon gauges at no additional cost to the
contract. Based on the results from the laboratory testing of components, as
well as its stability at elevated temperatures, Alumel was chosen as the most
desirable thermoelectric material to be paired with Hastelloy-X in
construction of these sensors.

TCAL analyses of the type discussed in Section 3.2 were performed on the final
sensor designs using the materials and geometries of the actual physical
construction of the sensors. The embedded thermocouple sensors and the
laminated sensors were found to meet all sensor design goals discussed in
Section 3.2. The hot side thermal perturbation introduced by the Gardon gauge
sensor was also found to be within the design goals.

4.1.1 Design of Embedded Thermocouple Sensors

The design of embedded thermocouple sensors utilized both dual and single
conductor sheathed wire. Figure 4.1-1 shows a schematic of the design
utilizing dual conductor sheathed wire. In this design, a grounded Type K
thermocouple is embedded in both the hot side and the cold side of the sensor.
The sensor output is obtained from the differential output of the Alumel wires
from the two thermocouples. The type K thermocouples give reference
temperatures near both the hot and cold sensor surfaces.
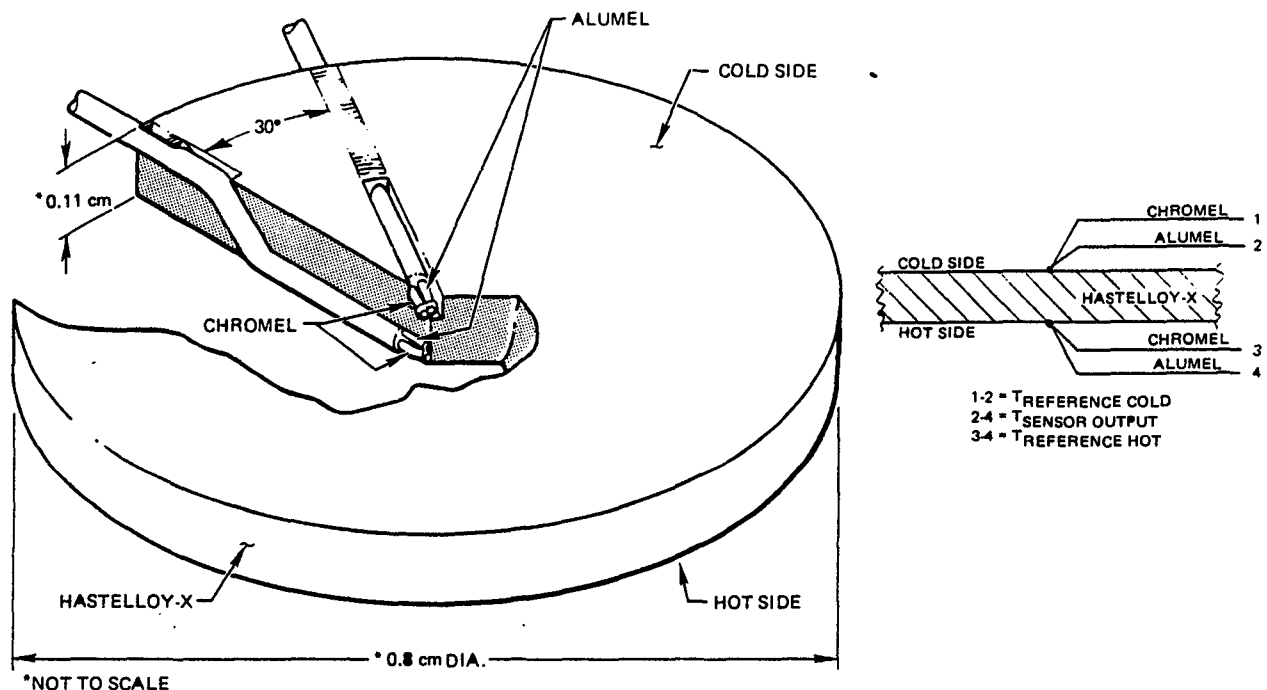
Figure 4.1-1   Construction Details and Electrical Schematic of the Embedded
               Thermocouple Sensor Fabricated with Dual Conductor Swaged Wire

27

Figure 4.1-2 shows a schematic of the embedded thermocouple design utilizing single conductor sheathed wire. The single conductor allowed use of a heavier gauge conductor while maintaining an external sheath diameter of 0.025 cm. In this design, sheathed Alumel wires with grounded junctions were embedded in both the hot and cold side of the sensor. In addition a sheathed Chromel wire with a grounded junction was embedded in the cold side of the sensor. The sensor output is obtained from the two Alumel wires and the reference temperature is obtained from the Chromel and Alumel wire on the cold side of the sensor.
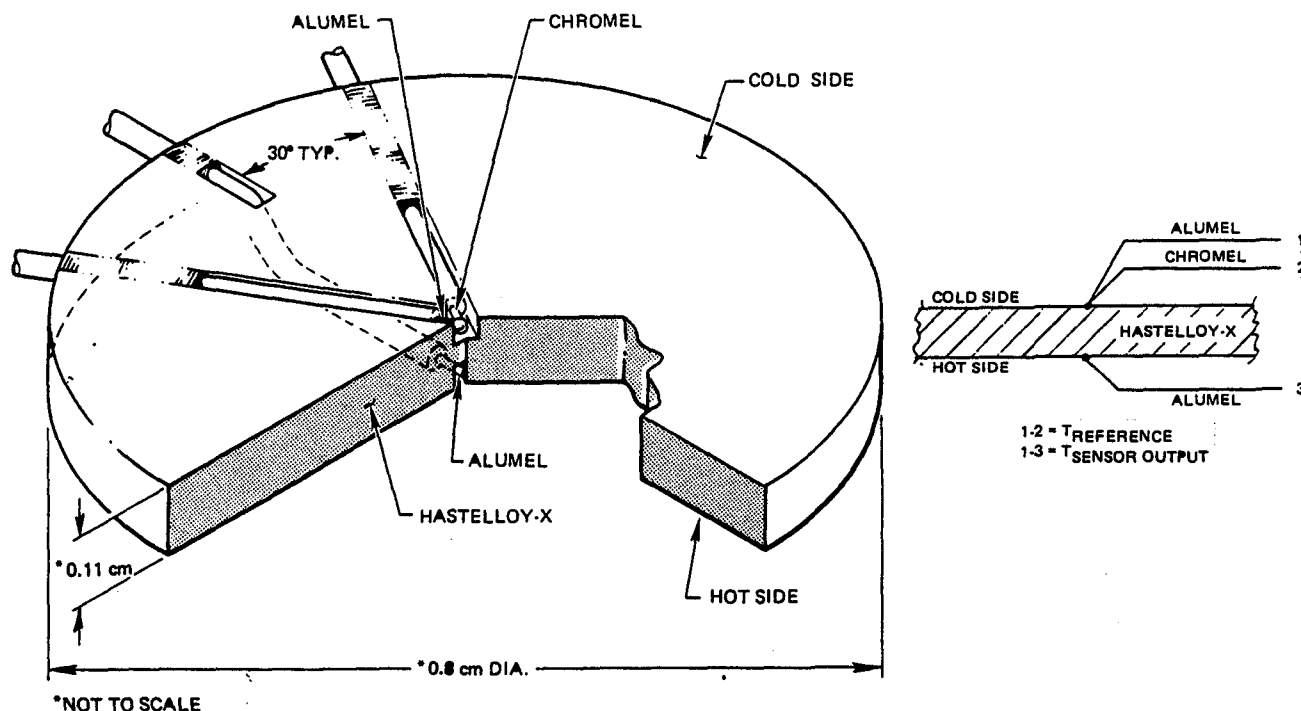
Figure 4.1-2   Construction Details and Electrical Schematic of the Embedded Thermocouple Sensor Fabricated with Single Conductor Swaged Wire

4.1.2   Design of Laminated Sensor

Figure 4.1-3 shows a schematic of the design of a laminated heat flux sensor. This sensor is composed of a 0.046 cm thick layer of Alumel diffusion bonded between two 0.034 cm thick layers of Hastelloy-X. The ceramic filled groove electrically insulates the Alumel and cold side Hastelloy-X layers in the sensor from the surrounding liner. M Bond GA100 cement was chosen to fill the groove based on component test results and the desirable working characteristics of that cement. The sensor output is obtained from a sheathed Hastelloy-X wire attached to the hot side Hastelloy-X layer and a sheathed Hastelloy-X wire attached to the insulated cold side Hastelloy-X layer. Sensor reference temperature may be obtained from a sheathed Alumel wire attached to the cold side Hastelloy-X layer and the Hastelloy-X wire from the cold side layer. In the construction of these sensors, care must be taken that the sheaths of neither the Alumel wire nor cold side Hastelloy-X wire contact the sensor itself, otherwise they will supply a current path across the ceramic insulation.
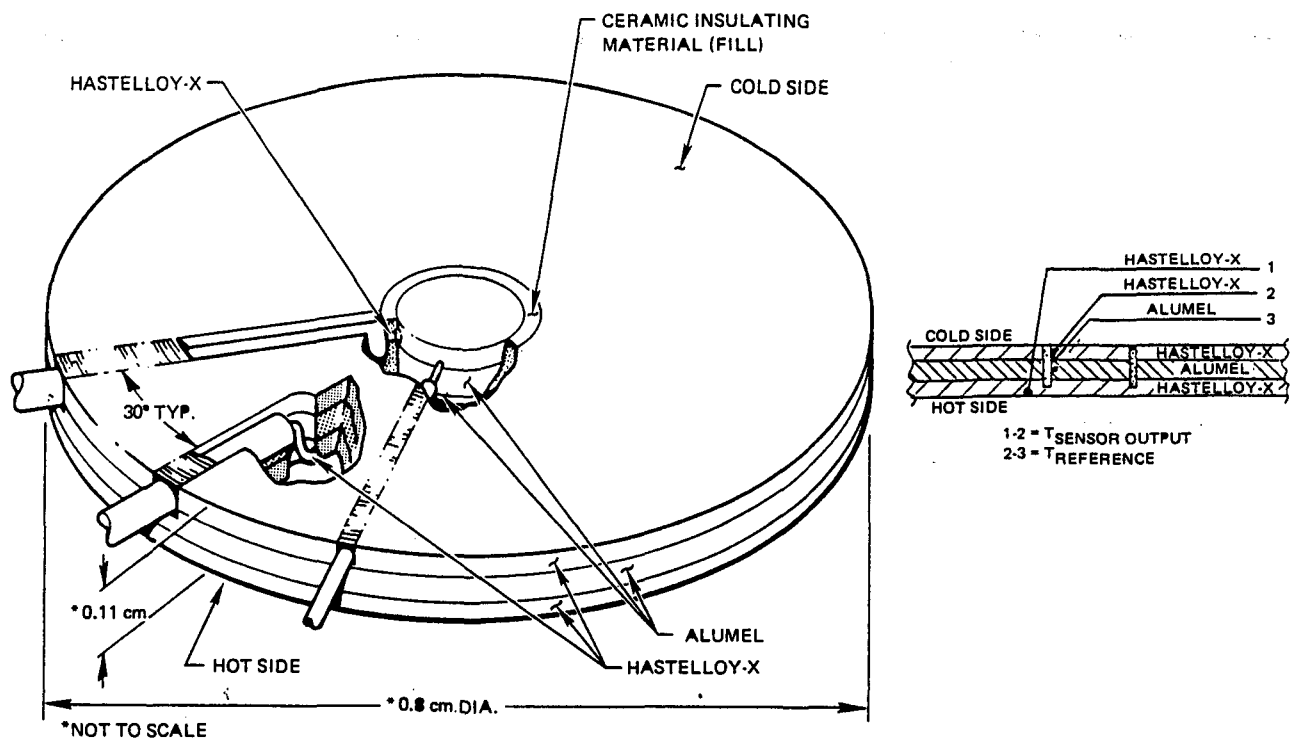
Figure 4.1-3   Construction Details and Electrical Schematic of the Laminated Sensor

4.1.3   Design of Gardon Gauge

In view of the availability of the laminated material, the Gardon gauge was designed to be fabricated from the same material used for the laminated sensor. Figure 4.1-4 shows a schematic of the final Gardon gauge design. In this design, sheathed Alumel wires were attached to both the center of the Gardon gauge "foil" and the Alumel layer of the sensor. A Chromel wire was also attached to the Alumel layer of the sensor. Sensor output is obtained from the two Alumel wires while the reference temperature is obtained from the Chromel and Alumel wires attached to the mid-layer of the sensor. The Gardon gauge "foil" thickness was chosen as a nominal 0.020 centimeter based on trade studies conducted to evaluate sensor sensitivity vs. induced thermal perturbation. The Gardon gauge was designed to have the rear cavity either covered with a thin foil to provide aerodynamic integrity or filled with ceramic. Tests were conducted on Gardon gauge G-1 both with the rear cavity covered with a thin foil and filled with M-Bond GA100 ceramic cement (see Appendix E for data). Both configurations yielded acceptable results. The ceramic filled design was chosen as the preferred configuration for all further testing because it was more easily fabricated and the ceramic cement supplied mechanical support and oxidation protection for the fine wires within the rear cavity of the Gardon gauge.
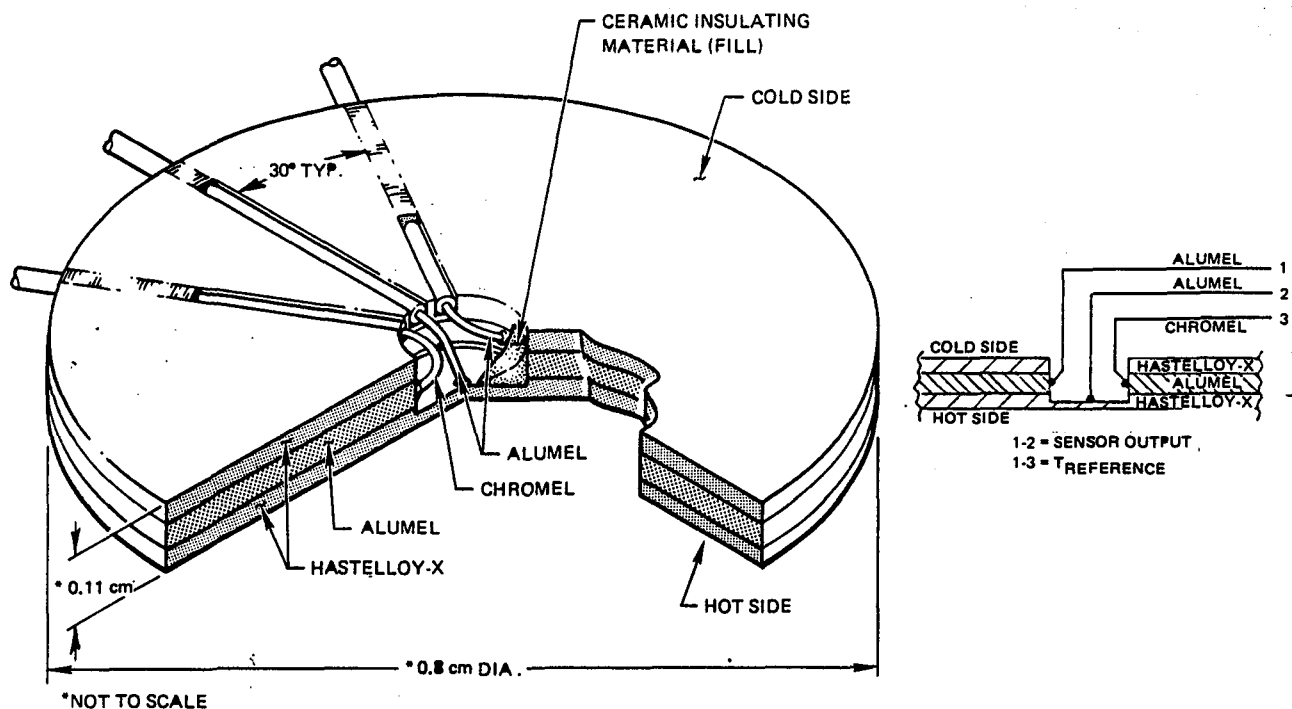
Figure 4.1-4 Construction Details and Electrical Schematic of the Gardon Gauge Sensor

4.2 FABRICATION OF SENSORS

During design of the heat flux sensors, consideration was given to the fabrication and installation procedures required. The sensors were intended for use in a wide variety of combustor liners having various diameters and louver designs. To achieve the required universality, the fabrication process included the ability to produce any desired amount of curvature. During installation, a lip or a taper on the sensor would prevent the sensor from falling into the flowpath of the engine. However, this configuration would require precision machining of both the combustor liner and the sensor to produce a fit flush with the combustor wall. Precision machining of a sensor mounting hole in a fully assembled annular combustor liner is a difficult and expensive operation. It was determined that a circular hole could easily be installed in a combustor liner, and the hole can be reamed with a precision reamer to a close tolerance. This would then only require that the sensor body be machined to a close tolerance. The sensor would be welded into the liner. The pressure differential across a combustor liner does not exert a large force on the sensor and, hence the weld does not have to exhibit great strength. In the unlikely event of a complete failure, all sensor designs provide a minimum of two leadwires on the cold surface side to restrain the sensor from entering the engine flowpath. A detailed description of the sensor fabrication and installation procedure is given below.

PAGE
31
MISSING

4.2.6 Installation of Swaged Wires

The swaged thermocouple wires are installed in the grooves and held in place by fillet wires of Hastelloy-X or Chromel which are resistance welded in place. After the thermoelectric junctions are made by resistance welding, the entire groove is filled with the fillet wire, and the surface of the groove is ground smooth.

4.2.7 Installation of the Ceramic Insulation

The groove in the laminated sensor and the rear cavity in the Gardon gauge are filled with GA100 ceramic material to provide aerodynamic integrity on the cold side surface. The ceramic is cured at 340K for one hour then the temperature is slowly raised to 590K and held for one hour. After curing, any excess ceramic material is removed from the surface by sanding.

4.2.8 Installation of the Sensor in the Combustor Liner

After fabrication and calibration, the sensor is installed in the combustor liner and welded around the circumference. For actual practice, it is recommended that advanced techniques such as laser welding be evaluated for the process. Figure 4.2-1 shows a sample sensor laser welded into a test plate. This welding was performed by JEC Lasers, Inc. of Paterson, N.J. as a demonstration of feasibility. Figure 4.2-2 shows a cross section of the weld and indicates that the penetration is sufficiently shallow to protect the lead wires coming off the rear face of the sensor. For the laboratory testing of the sensors, resistance welding is used to install the sensors in 7.0 centimeter diameter test plates so that the sensor can be removed from the plate after testing. Figure 4.2-3 shows one of the sensors installed in a test plate by the resistance welding technique. This sensor had been heavily resistance welded to obtain a pressure tight seal for an experimental program. Sensors intended for actual use in combustor liners would only be tack welded lightly in a few places. This would allow removal of the sensor from the calibration plate without distortion or damage to the sensor. After the sensors are installed, the lead wires are strapped down to the cold side surface to provide mechanical support.

4.3 TESTING OF SENSORS

The test program conducted on the heat flux sensors had two primary goals. The first goal was to establish the sensor calibration characteristics. This was accomplished by comparative calibrations using a commercially available heat flux sensor as a reference and by absolute calibrations to confirm the validity of the comparative calibrations. The second goal was to demonstrate the durability and reliability of the sensors. Thermal cycle and thermal soak tests were used to provide this demonstration. A summary of the test program is provided in Table 4.3-I.
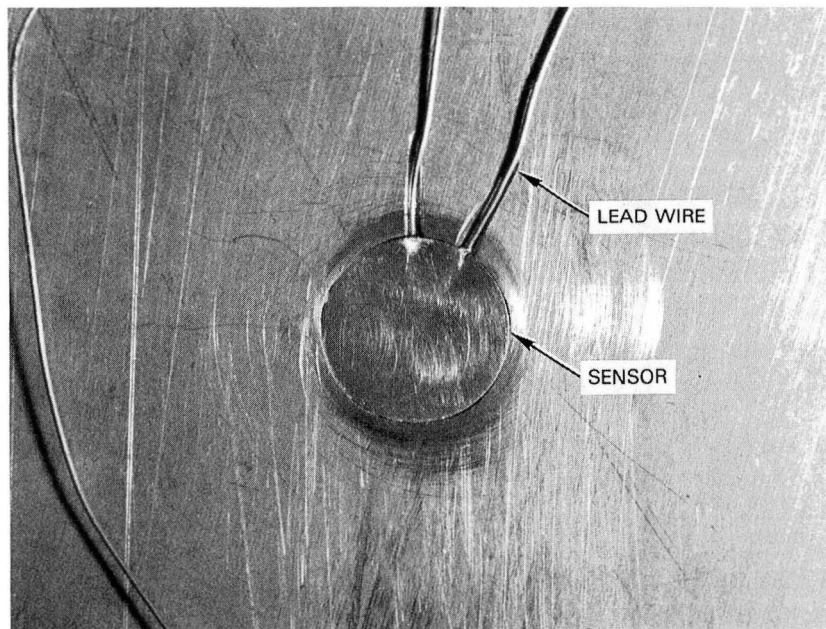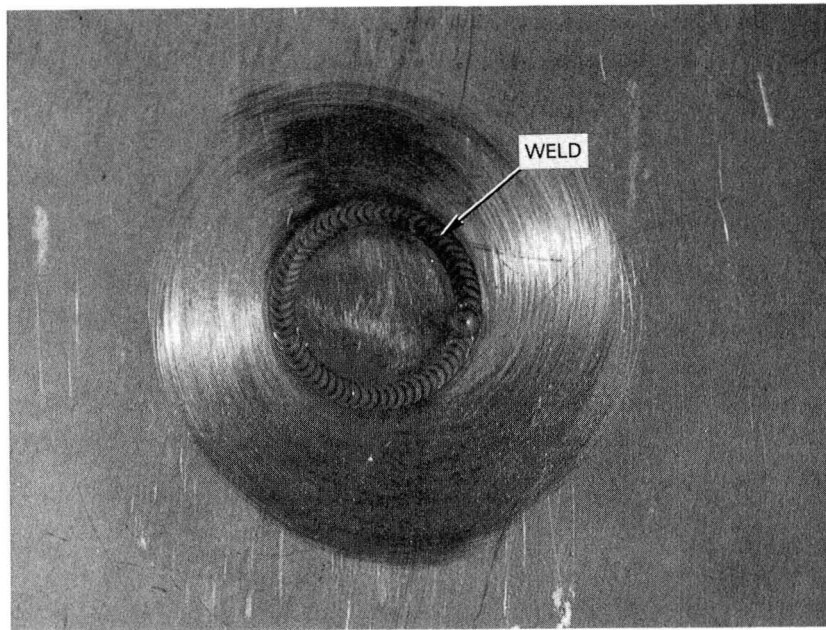
Figure 4.2-1 Hot (Top) and Cold (Bottom) Surface Views of a Sensor Installed in a Test Plate by Laser Welding
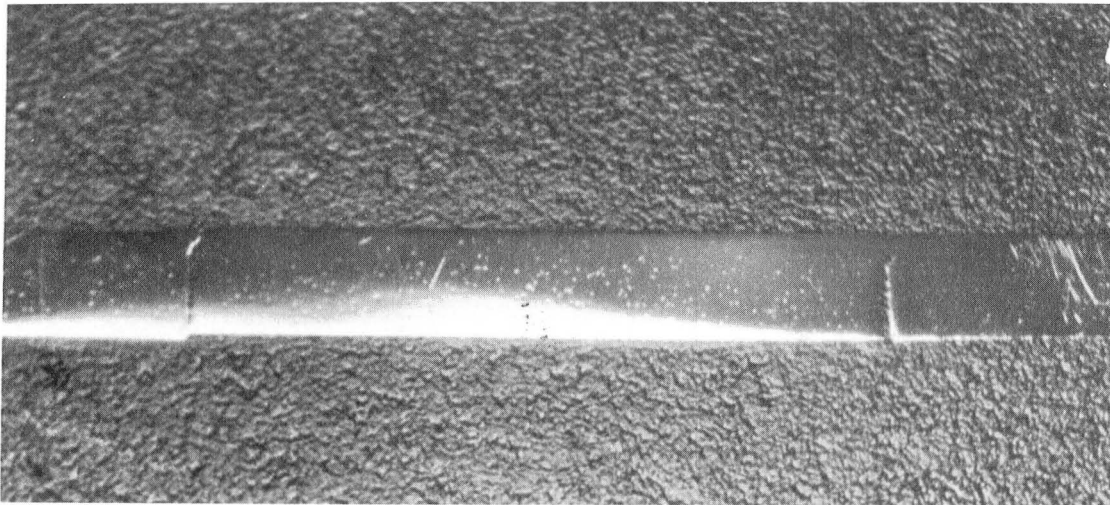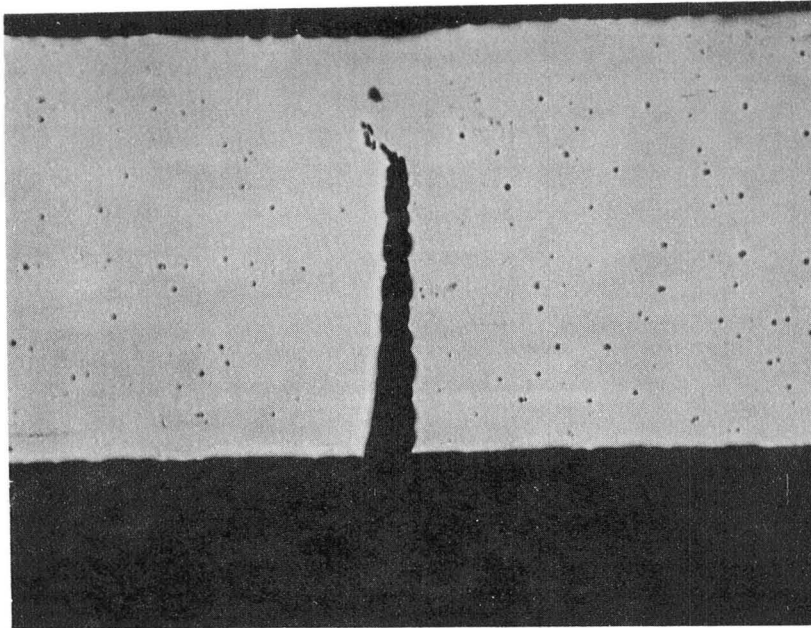
Figure 4.2-2   Photomicrograph of a Cross Section of a Sensor Installed in a
Test Plate by Laser Welding with an Enlargement of the Weld Area
to Show Depth of Weld Penetration
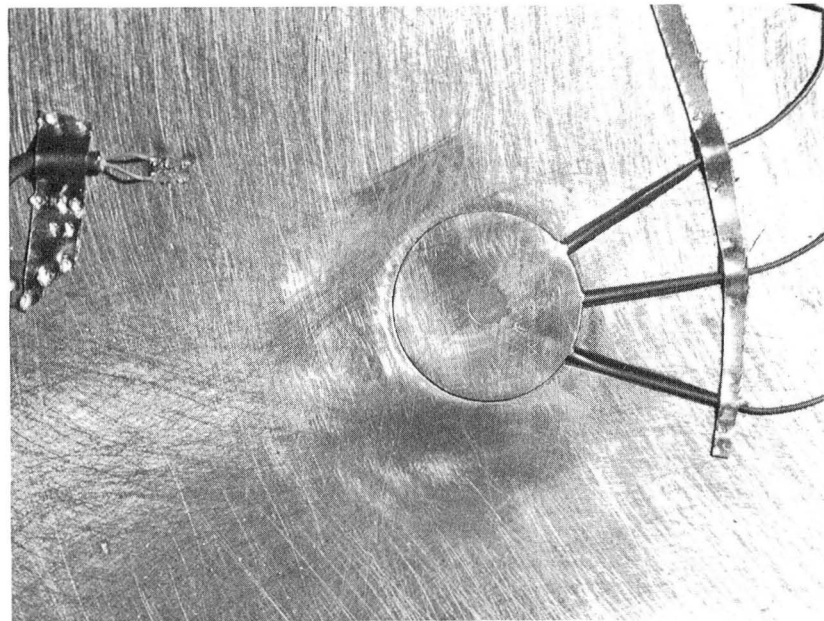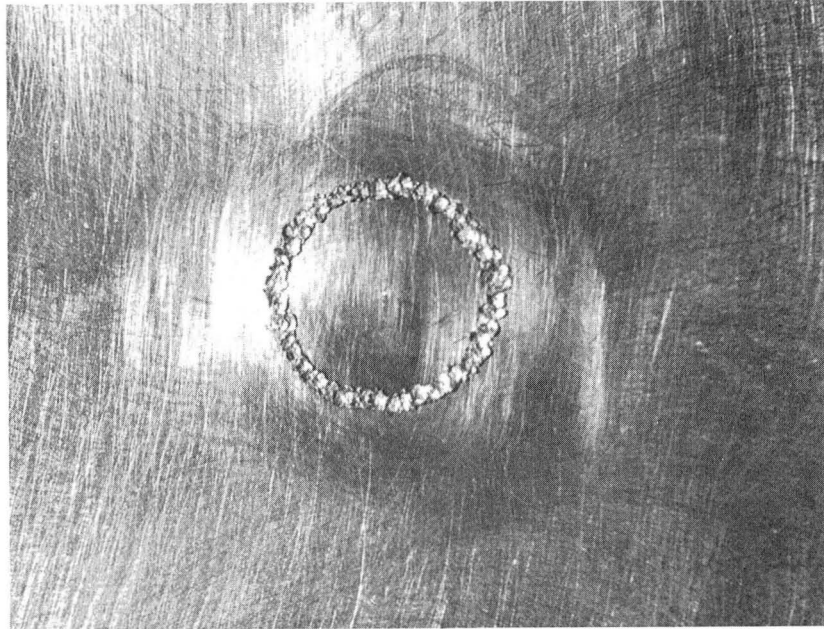
Figure 4.2-3 Hot and Cold Surface Views of a Sensor Installed in a Test Plate
by Resistance Welding

TABLE 4.3-I

SUMMARY OF TEST PROGRAM

	Sensor Type			
	Embedded Thermocouple Sensors			
	Single	Dual		
	Conductor	Conductor	Gardon	Laminated
Test Type	Swaged Wire	Swaged Wire	Gauges	Sensors ·
Comparative Calibration Tests	4	7	9	11
Absolute Calibration Tests	0	1	3	0
Thermal Cycle Tests	0	0	2	2
Thermal Soak Tests	1	1	1	1

4.3.1 Test Fixtures

A pair of calibration fixtures were designed and fabricated to permit the testing and calibration of sensors both in the three filament vacuum apparatus and in the quartz lamp bank. An exploded view of the fixture for the quartz lamp bank is shown in Figure 4.3-1. The sensor to be tested was mounted in a circular calibration plate 7.0 centimeters in diameter. The sensor was resistance welded into the plate around the circumference of the hot side surface of the sensor. It was found that the resistance welding would produce a vacuum tight seal for the sensor when cold but was prone to leakage when heated and the calibration plate bowed. In cases where severe leakage occurred, the problem was corrected by rewelding the sensor into the plate. The plate was held onto the body of the fixture by a water cooled flange, and a metal O-ring was used as a seal. The sensor was cooled during calibration and test by cooling air impinging on the cold side surface of the sensor. In quartz lamp bank testing, the fixture was open on the back and in the three filament vacuum apparatus, the fixture was sealed and provided with inlet and outlet ducts for the cooling air. The sensor leadwires were routed out through the outlet air duct.
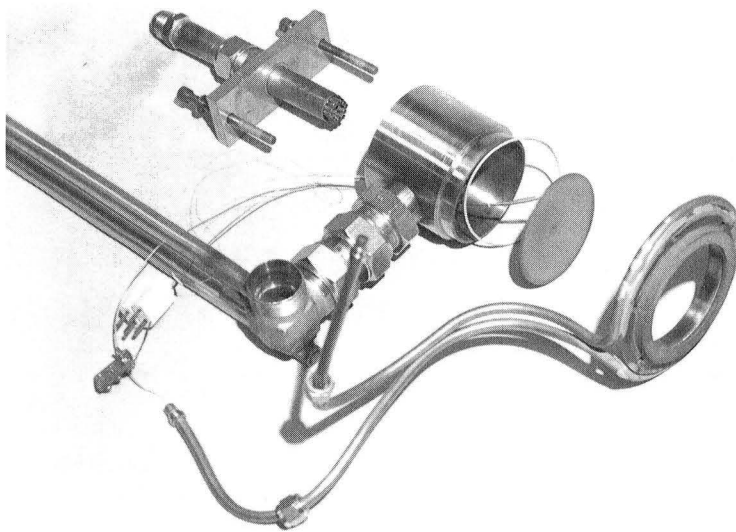
Figure 4.3-1   Exploded View of Calibration Fixture to Position the Test
                 Sensor in Front of the Quartz Lamp Bank

4.3.2 Data Recording Equipment

Throughout the calibration and test programs, data were recorded and reduced
using the same microcomputer system used earlier for testing of components.
Data from the tests were stored in tabular form on floppy diskettes. Use of
this system allowed real time corrections to be applied to the calibration
data. In addition, the data files allowed later statistical analysis of the
data, presentation of summary results in English or SI units, and automated
graphical representation of test results through use of a digital plotter
interfaced to the system.

4.3.3 Quartz Lamp Bank Calibration Facility

The comparative calibration tests were run using the same quartz lamp bank
shown in Figure 3.3-16 that had been used to thermally cycle sensor
components. A Hy-Cal asymptotic calorimeter was used as a reference sensor to
monitor the incident heat flux. The sensor to be calibrated was mounted in a
plate 7.0 centimeters in diameter and coated with a material of known
emittance and absorptance. The plate was then mounted in a fixture in front of
the lamp. The Hy-Cal sensor was mounted on one side of the fixture at the same
distance from the lamp. Impingement air was used to cool the back side of the
sensor. Figures 4.3-2 and 4.3-3 show the sensor installed for calibration.
During the calibration sequence, data were taken at different incident heat
flux levels with both a constant sensor temperature and a constant impingement
air flow. The incident heat flux, sensor temperature and sensor microvolt
output were measured during the calibration. The heat flow through the sensor
was determined by calculating the heat absorbed into the sensor and
subtracting the heat losses from reradiation and convection. A discussion of
the calculation procedure is given in Appendix B. The sensor sensitivity
(microvolt output per unit heat flux transmitted) was also calculated to
detect changes in output due to varying sensor temperature or heat flux levels.
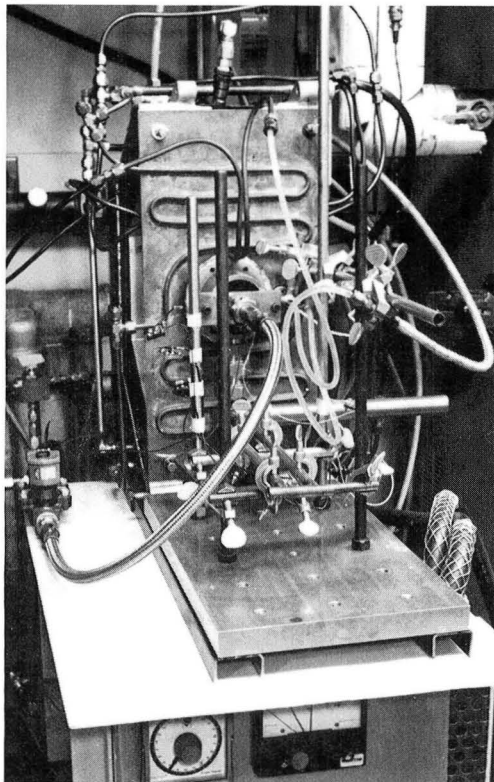
Figure 4.3-2   Quartz Lamp Bank with
                Sensor Calibration Fix-
                ture and Reference Hy-
                Cal Sensor Installed
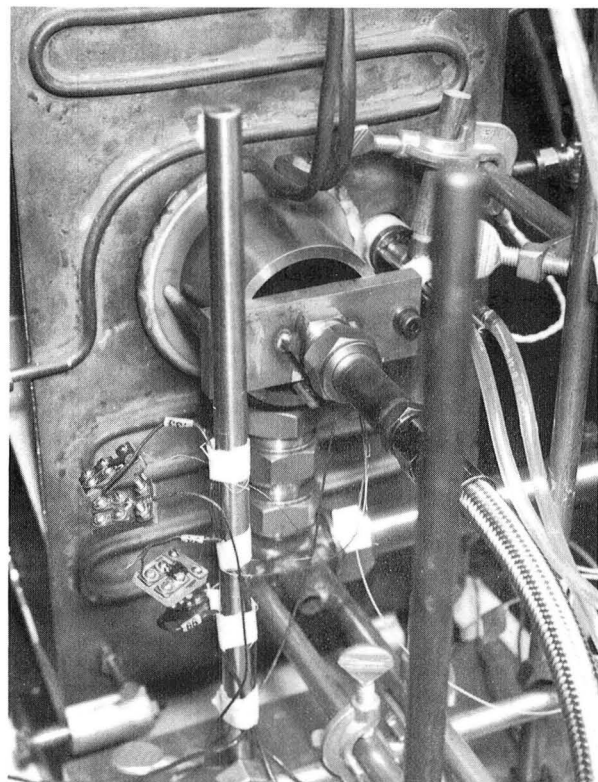
Figure 4.3-3   Closeup View of Cali-
                bration Fixture and
                Reference Hy-Cal Sen-
                sor Installed on the
                Quartz Lamp Bank

4.3.4   Three Filament Calibration Source

Absolute calibrations were performed using the three filament vacuum
calibration facility shown in Figures 4.3-4, 4.3-5, and 4.3-6. The sensor
mounting configuration was identical to that in the quartz lamp bank facility
to provide interchangability of samples. The three filament vacuum facility
applied the additional constraint that the mounting of the sensor in the
calibration plate must be a leak-free weld. The heat source was provided by
three electrically heated graphite filaments. The sensor under test was
mounted on one side of the center filament and a Hy-Cal reference sensor was
mounted on the opposite side. The top and bottom filaments acted as guard
filaments to reduce heat losses from the edge of the center filament which
ensured a constant filament temperature. The filament temperature, Hy-Cal
sensor output, test sensor temperature and test sensor microvolt output were
measured during the test. The heat flux incident on the test sensor was
calculated from the filament temperature and the geometrical constants of the
test setup. An independent determination of the heat flux was provided by the
Hy-Cal sensor. The heat flux transmitted through the sensor was then
calculated as described in Appendix B. Figure 4.3-7 presents comparisons of:

1. the absolute calibration data against the filament temperature,

2. data from a Hy-Cal asymptotic calorimeter in the vacuum calibration facility,

3. data from another Hy-Cal asymptotic calorimeter in the quartz lamp bank facility.
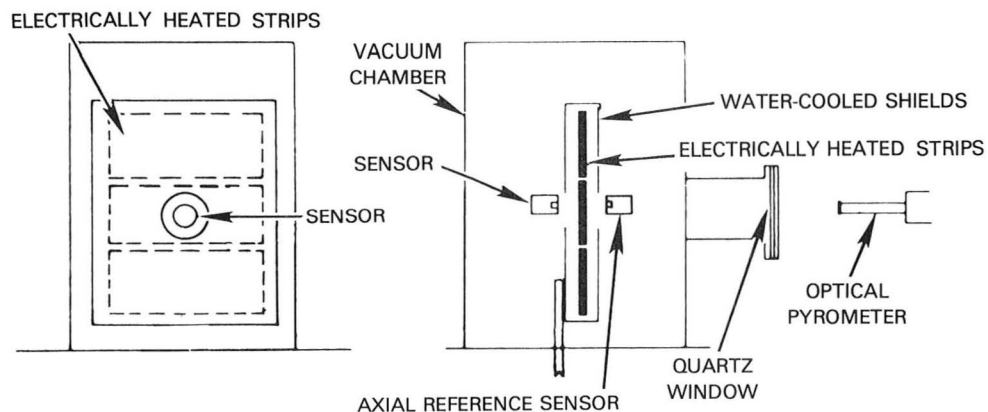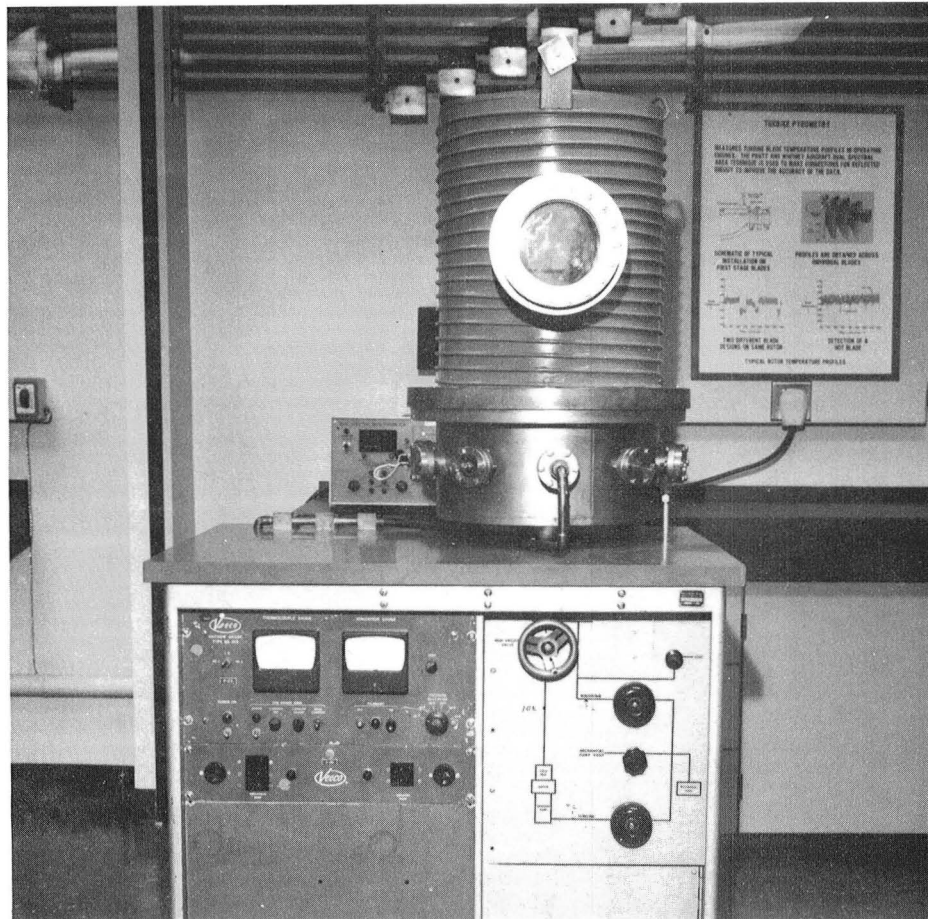
Figure 4.3-4 External View and Schematic of Three Filament Vacuum Calibration Facility
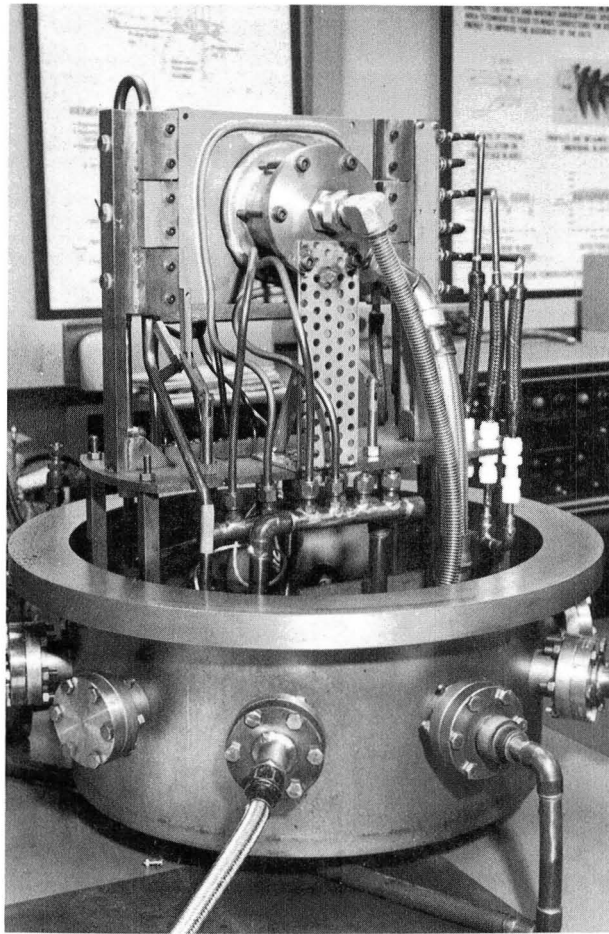
Figure 4.3-5   Internal View of Three Filament Vacuum Calibration Facility
Showing the Calibration Fixture and Heat Shield

The agreement shown confirms that the calibration data obtained in the quartz
lamp bank facility is valid and can be verified by another independent
measurement technique.

At high heat flux levels in the vacuum calibration facility, the measured heat
flux was reduced by inadvertantly copper plating the surface of the sensor
causing a decrease in the absorptance of the surface. The source of the copper
plating was traced to overtemperatured heat shields. The cooling on the heat
shields has been improved, and the shields are being chrome plated to
eliminate this problem on future runs.

40
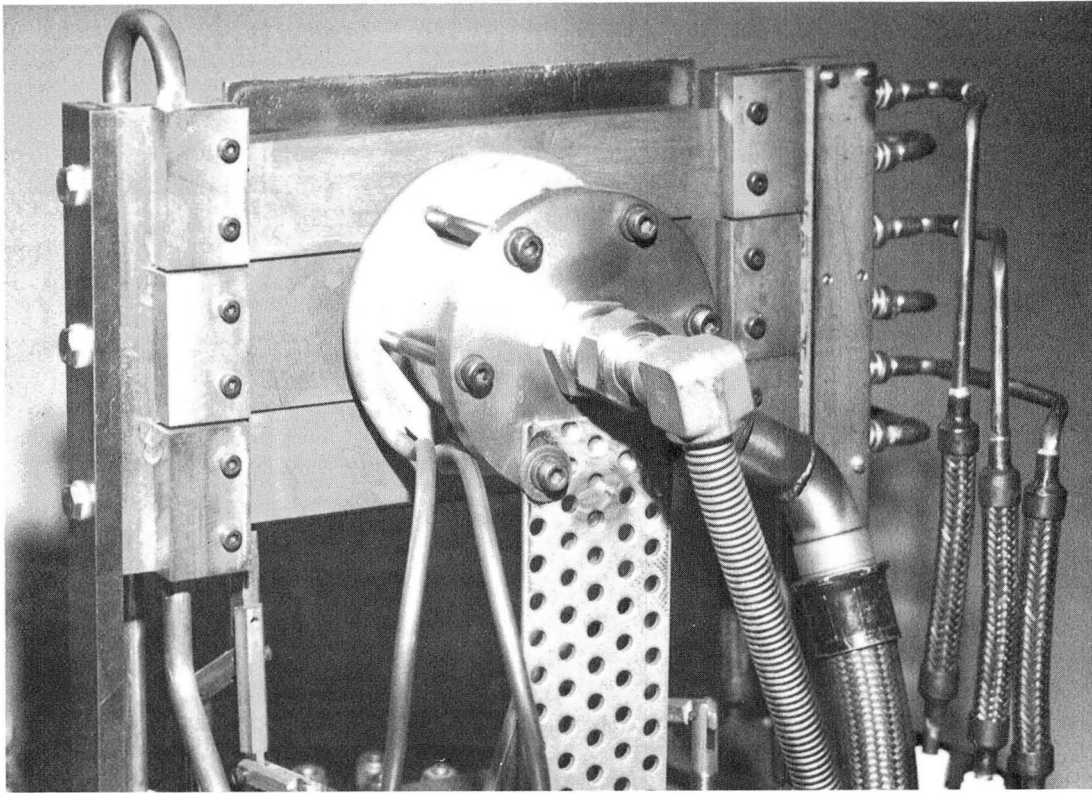
Figure 4.3-6   Internal View of Three Filament Vacuum Calibration Facility with the Heat Shield Removed to Expose the Filaments
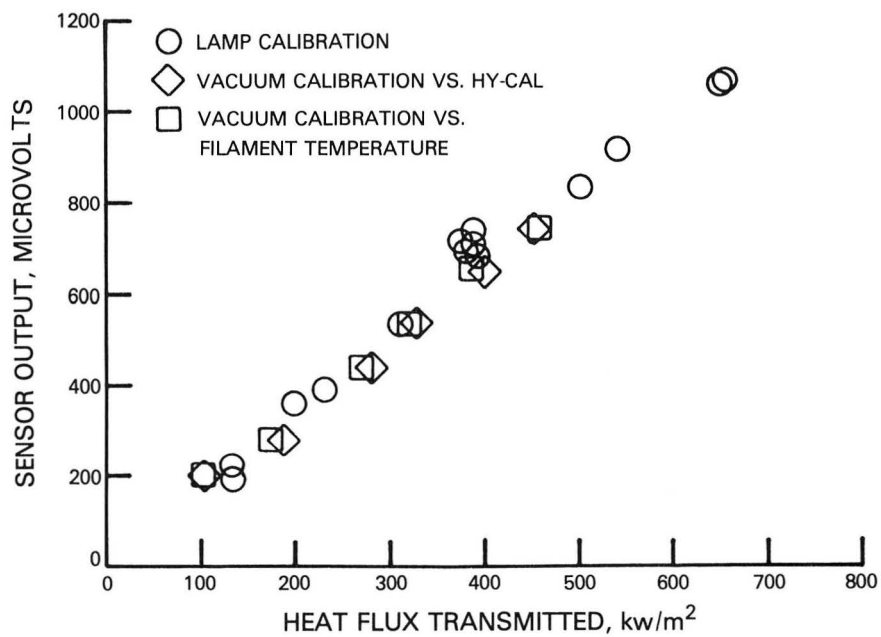
Figure 4.3-7   Plot Showing Comparison of Absolute and Comparative Calibrations for Gardon Gauge Sensor G-4

4.3.5 Thermal Cycling Tests

The thermal cycling tests were conducted with the quartz lamp bank facility. A cycle consisted of rapid heating to 1200K, with a transmitted heat flux of approximately 560 kw/m^2, and holding this condition for 1.8 minutes. The heat source was then shut down and the sample allowed to cool for 5.2 minutes. Data were acquired twice during each cycle, once 1.5 minutes after the lamps were turned on and again 3.5 minutes after the lamps were turned off. Figure 4.3-8 shows the channel assignments and Figures 4.3-9 and 4.3-10 show data from a hot and cold cycle on sensor G-9. Of the five sensors that were thermal cycled, two survived through the full 50 cycles. The comparison of calibration data before and after the cyclic endurance tests are shown in Figures 4.3-11 and 4.3-12. The failures of the three sensors were all traced to broken leadwires external to the sensors. This breakage was a result of leadwire vibration caused by the cooling air impinging on the back of the sensor. This problem has been minimized by providing better support for the leadwires during both calibration and thermal cycling tests.

4.3.6 Thermal Soak Tests

The thermal soak test was conducted by ageing one sensor of each type in an oven for 50 hours at approximately 1175K. The test setup is shown in Figure 4.3-13. Sensors T-2, D-3, L-1, and G-3 were used in this test. The sensor resistance, i.e., the resistance of the differential thermocouple, was monitored during the test. A plot of the data from this test is given in Figure 4.3-14. There is considerable variation among the sensors as was expected. Sensor T-2 had the highest resistance because of the extremely fine gauge Alumel conductors in the dual conductor swaged wire. Sensors D-3 and G-3 had significantly lower resistance due to the larger gauge Alumel conductors in the single conductor swaged wire used in these sensors. The laminated sensor (L-1) had an intermediate level resistance. The sensor had heavier gauge wire; however, the wire was Hastelloy-X with a higher resistivity than Alumel. As the sensors were heated, the resistance increased due to the lower electrical conductivity of both Hastelloy-X and Alumel at elevated temperatures. The resistance of the sensors remained constant during the thermal soak and returned to the initial value upon cool down. These results showed that the leadwires physically survived the test without burnout or severe loss of cross sectional area due to oxidation. Attempts to recalibrate the sensors after the thermal soak produced erratic results with low microvolt output from all four sensors. Heat was applied locally along the length of the leadwires, and it was found that secondary junctions had formed in numerous areas, with the most significant junctions located in the gradient area where the leadwires exited the oven. This test showed that the sensors and leadwires could physically survive the 50 hour endurance test. The leads, however, developed thermoelectric problems external to the sensors. In addition to addressing leadwire problems, Pratt & Whitney Aircraft is currently procuring a quartz lamp bank that will allow ageing tests to be conducted under conditions more representative of what would actually be experienced by the sensors under active rig or engine test conditions.

N A S A

GARDON GAUGE THERMAL CYCLING TESTS
SENSOR G-9

CHANNEL ASSIGNMENTS
CHANNEL   10 VOLTAGE TO LAMP CONTROL
CHANNEL   11 HYCAL S/N 86212 ON EDGE
CHANNEL   13 C/A THERMOCOUPLE ON EDGE OF SENSOR
CHANNEL   14 ALUMEL VS. ALUMEL

ENGINEERING UNITS ARE:
DEGREES FAHRENHEIT FOR TEMPERATURES
BTU/SEC FT**2 (INCIDENT) FOR HEAT FLUX

DATA TEST STARTED 11-05-81

Figure 4.3-8   Data System Channel Assignments for Thermal Cycling Tests

CYCLE   49

TIME OF DATA POINT 142514

CHANNEL	MILLIVOLTS	ENGINEERING UNITS
10	6804.170	65.689
11	4.422	63.119
13	36.115	1599.532
14	.506	.000

Q HYCAL-Q PREDICTED FROM LAMP VOLTAGE -.31
Q HYCAL CORRECTED TO CENTER OF LAMP 65.36

LOSS MODEL RESULTS
Q ABSORBED (E=.9) 58.841
FRONT FACE RERADIATION (E=.9) 7.922
CONVECTION (H=3 BTU/FT**2 SEC) TG=250   1.124
Q TRANSMITTED 49.793

SENSOR SENSITIVITY -MICROVOLTS/(BTU/SEC FT**2)   10.116

CHANNEL   13   RESISTANCE   52
CHANNEL   14   RESISTANCE   51

Figure 4.3-9   Representative Data from Hot Portion of a Thermal Cycling Test

TIME OF DATA POINT 143044

CHANNEL	MILLIVOLTS	ENGINEERING UNITS
10	6955.060	69.203
11	.030	.428
13	2.503	142.905
14	.000-	.000

Q HYCAL-Q PREDICTED FROM LAMP VOLTAGE -68.766
Q HYCAL CORRECTED TO CENTER OF LAMP .438

LOSS MODEL RESULTS
Q ABSORBED (E=.9) .394
FRONT FACE RERADIATION (E=.9) 0
CONVECTION (H=3 BTU/FT**2 SEC) TG=250   0
Q TRANSMITTED .393

SENSOR SENSITIVITY -MICROVOLTS/(BTU/SEC FT**2) -1.016

CHANNEL 13 RESISTANCE 82
CHANNEL 14 RESISTANCE 45

Figure 4.3-10 Representative Data from Cold Portion of a Thermal Cycling Test
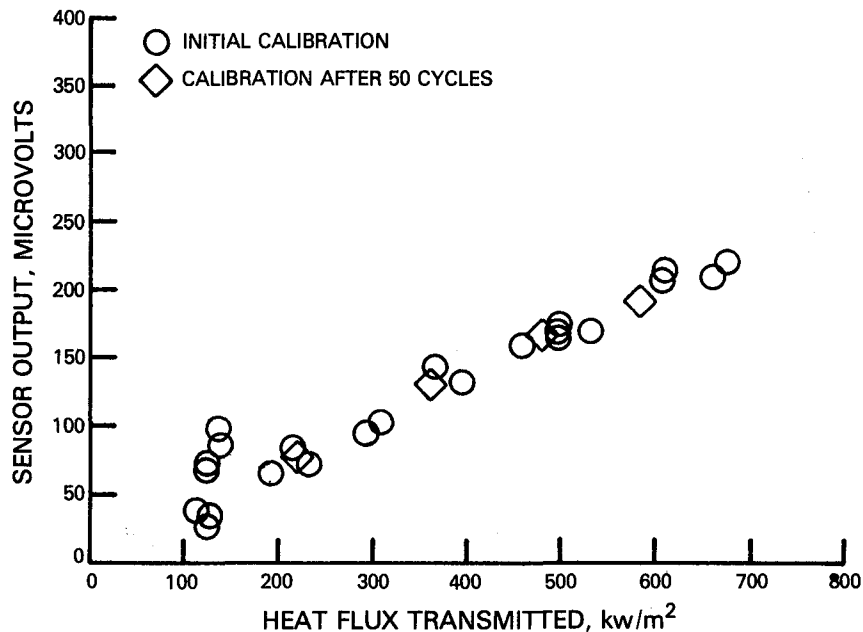
Figure 4.3-11 Plot Showing the Comparison of Calibration Data before and after
the Thermal Cycling Test on Laminated Sensor L-3
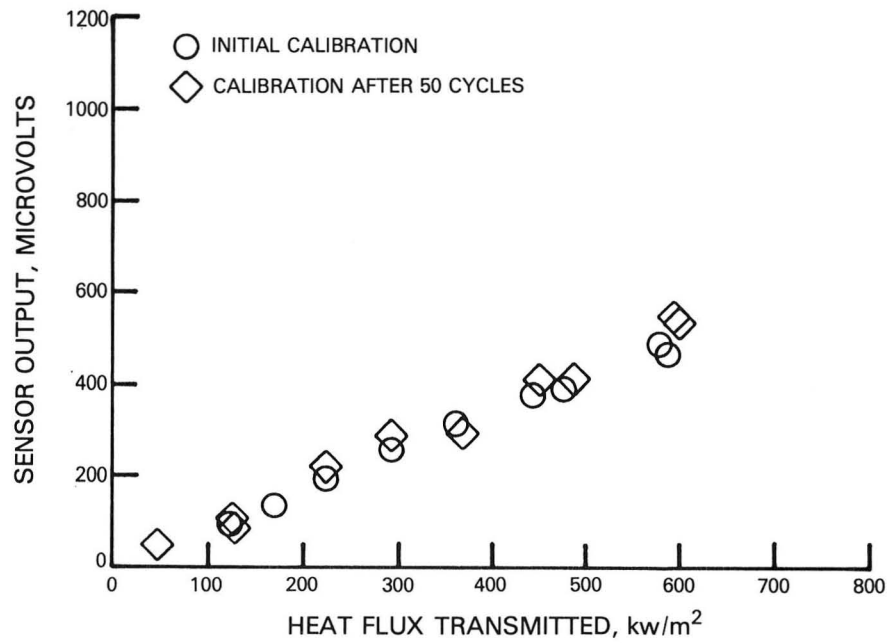
Figure 4.3-12 Plot Showing the Comparison of Calibration Data before and after the Thermal Cycling Test on Gardon Gauge Sensor G-9
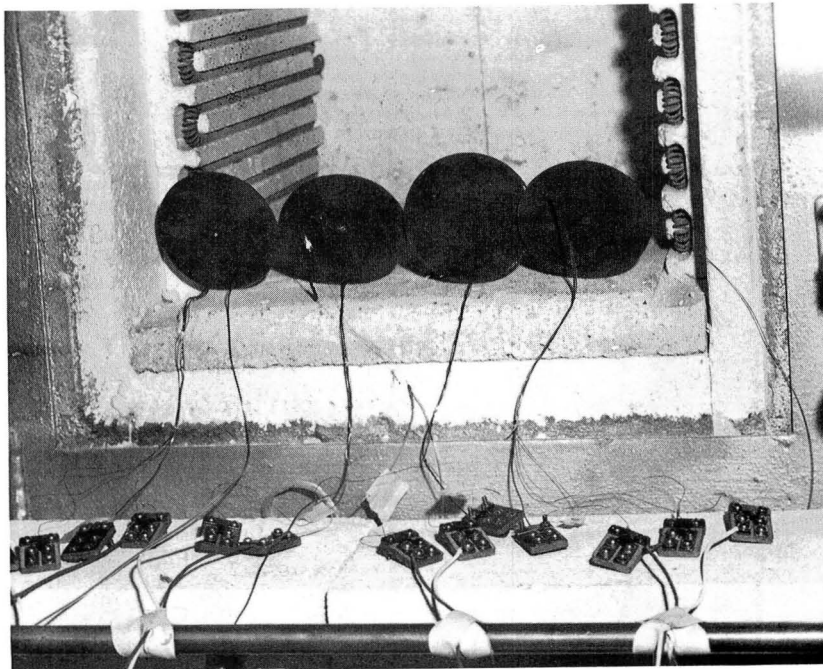
Figure 4.3-13 Sensors in Oven after 50 hour Thermal Ageing Test
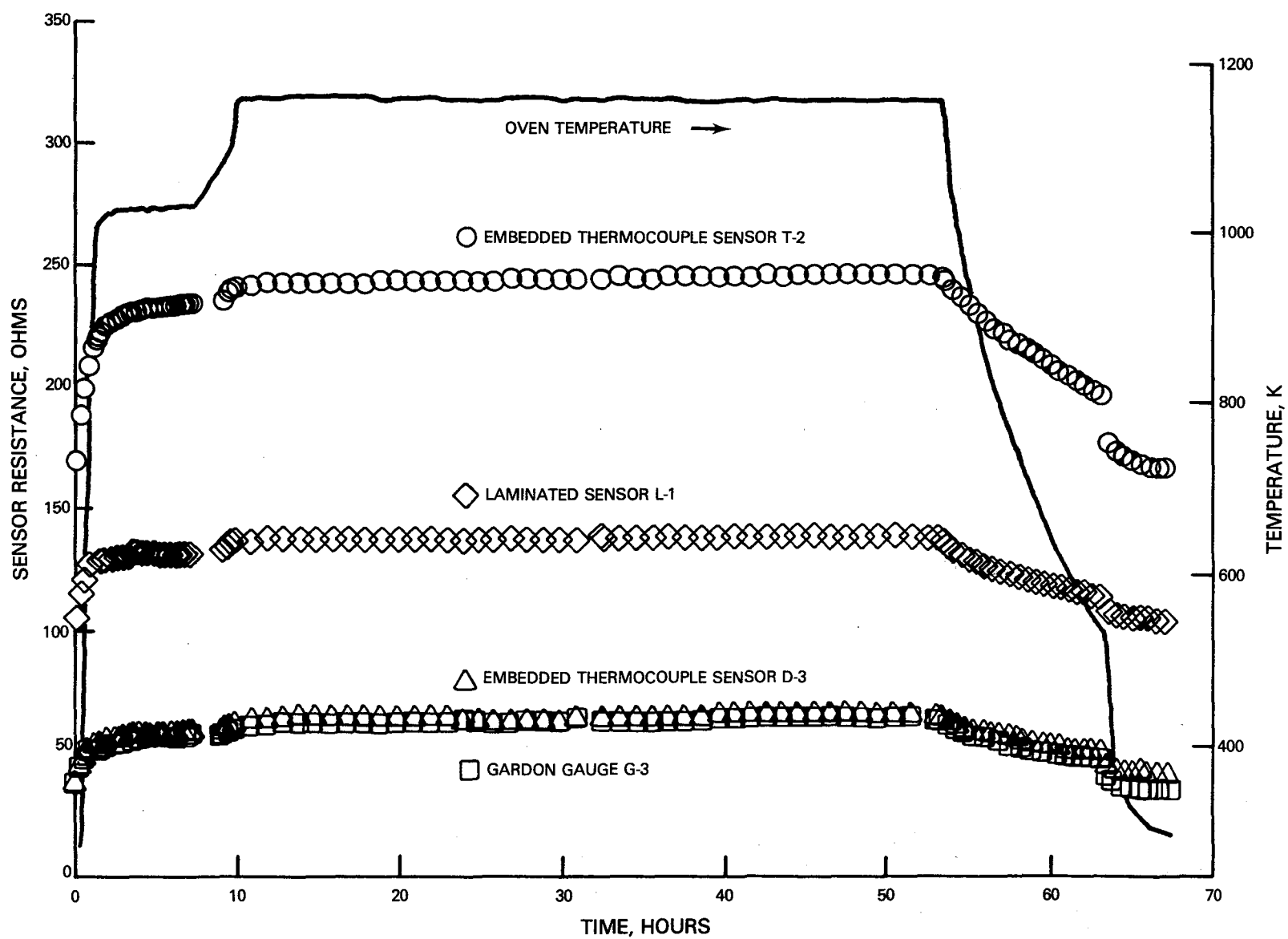
Figure 4.3-14 Plot of Oven Temperature and Sensor Electrical Resistance During
Thermal Ageing Test

SECTION 5.0

SENSOR TEST RESULTS

5.1 ACCURACY SUMMARY

The sensor accuracy goal was to achieve ±5 percent of 1×10^6 Watt/m^2 even though ±10 percent accuracy would be acceptable. The calibration curves for all the sensors are presented in Appendices C, D and E along with the ±5 percent and ±10 percent error bands. The individual data points are represented by the symbols. The least squares fit of the data forced through the origin is shown by the solid line. The two short dashed lines represent the ±5 percent error bands and the two long dashed lines represent the ±10 percent error bands. For the majority of the sensors of each type, all the data falls within the ±5 percent error band. For each of the sensor types however, there are a few sensors which exhibit increased scatter in the data, but still fall generally within the ±10 percent error band. Any sources of nonrepeatability related either to the sensors themselves or the sensor calibration system will be reflected as scatter in the data. An error discussion is presented in Appendix B. System bias is believed to be small. Section 4.3.3 and Figure 4.3-7 compare data taken by three different calibration techniques in two different calibration devices. There is no detectable rig-to-rig or technique-to-technique bias in this data.

5.2 SURVIVABILITY SUMMARY

Twenty-two of the thirty-nine sensors fabricated failed during the program. The dominant failure mode for all the sensor types was failure of the leadwires external to the sensors. Twenty of the sensors experienced leadwire failures. The two other sensors that failed developed opens in the thermocouple circuits, and the location of these opens was determined to be internal to the sensors.

The leadwire failures can be attributed to two general causes. The first cause of leadwire failure was breakage resulting from handling during fabrication and mounting of the sensors. There were several factors contributing to these failures:

1. while sensor components had been tested earlier, several sensors of the first type constructed (embedded thermocouples - single conductor swaged wire) failed during construction or installation. This reflects the "learning curve" process where techniques for sensor construction were being developed.

2. The swaged wire was stripped back in the miniature thermocouple lab by the use of mechanical strippers. This technique, which is routinely used successfully for heavier gauge thermocouple wire, tended to twist the sheath on the fine gauge wire for approximately 2.5 centimeters back from the junction area. Consequently, the leadwire exiting the side of the sensor was embrittled, and prone to failure. This problem was identified during post test inspection, and the technique for stripping the wire is being modified to eliminate the problem in the future.

3. Several of the sensors were used in multiple tests. This required
   extensive handling that eventually contributed to lead wire failure.

The second general cause of leadwire failure was vibration of the leadwires
behind the sensor by the air used to cool the back of the sensors. The wires
in this case had been somewhat embrittled by exposure to high temperature,
increasing the risk of breakage from the vibration. The technique for
installing the sensors in the calibration plate was modified to support
leadwires firmly at close intervals during calibration and cyclic testing.
This greatly reduced the number of this type of failure during later testing.

5.3 TEST RESULTS FOR EMBEDDED THERMOCOUPLE SENSORS - SINGLE CONDUCTOR SWAGED
    WIRE

A total of 10 embedded thermocouple sensors, designated D-1 through D-10, were
constructed using single conductor swaged wire and tested. A summary of the
test program is given in Table 5.3-I. The individual sensor calibrations are
presented in Appendix C.

TABLE 5.3-I

TEST RESULTS OF EMBEDDED THERMOCOUPLE SENSORS - SINGLE CONDUCTOR SWAGED WIRE

Serial Number	Status	Lamp Calibration	Vacuum Calibration	Thermal Cycle	Thermal Soak	Comments
D-1	Good	X				
D-2	Failed	X				Leadwire Failure During Calibration
D-3	Failed	X			X	Leadwire Failure After Thermal Soak
D-4	Good	X				Delivered to NASA at 11/13/81 Oral Briefing
D-5	Failed					Leadwire Failure During Installation in Rig
D-6	Failed					Leadwire Failure During Installation
D-7	Failed					Leadwire Failure During Installation

48

TABLE 5.3-I (Continued)

Serial Number	Status	Lamp Calibration	Vacuum Calibration	Thermal Cycle	Thermal Soak	Comments
D-8	Failed					Leadwire Failure During Construction
D-9	Failed					Leadwire Failure During Construction
D-10	Failed					Leadwire Failure During Construction

These sensors were the first type to be fabricated and tested, and six out of ten were failed by mechanical means during fabrication and installation. The failure rate on subsequent sensors was dramatically reduced by improvements in the fabrication techniques.

The failure of sensor D-2 during the lamp calibration was traced to vibration of the leadwire by the cooling air impinging on the back of the sensor. Sensor D-3 failed when subjected to a 50 hour thermal soak test at near maximum hot side temperature. This problem was traced to secondary junctions in the leadwires.

Figure 5.3-1 is a plot of the least squares fit of the sensor microvolt output versus heat flux transmitted for sensor D-1. As anticipated, this line passes close to the origin (zero output at zero heat flux transmitted). Figures 5.3-2 and 5.3-3 show the least squares fit of the sensor sensitivity versus heat flux transmitted and sensor reference temperatures. Both these curves are relatively flat, indicating that no correction to the sensor output is required to account for sensor temperature or heat flux level.

5.4 TEST RESULTS FOR EMBEDDED THERMOCOUPLE SENSOR - DUAL CONDUCTOR SWAGED WIRE

A total of nine embedded thermocouple sensors using dual conductor swaged wire, designated as T-1 through T-9, were fabricated and tested. A summary of the test program is given in Table 5.4-I. The individual sensor calibrations are presented in Appendix C.

One of the dual conductor swaged wire sensors was damaged during fabrication and one was damaged during installation in the calibration rig. Sensor T-3 failed during vacuum calibration and sensor T-4 failed during thermal cycling, both due to leadwire failures external to the sensor. These failures were a result of leadwire vibration caused by the cooling air impinging on the back of the sensor. Sensor T-6 failed during the quartz lamp calibration. One of the thermocouples opened during test, and the location was determined to be internal to the sensor.

Figure 5.3-1   Least Squares Plot of Calibration Data for Embedded
Thermocouple Sensor D-1
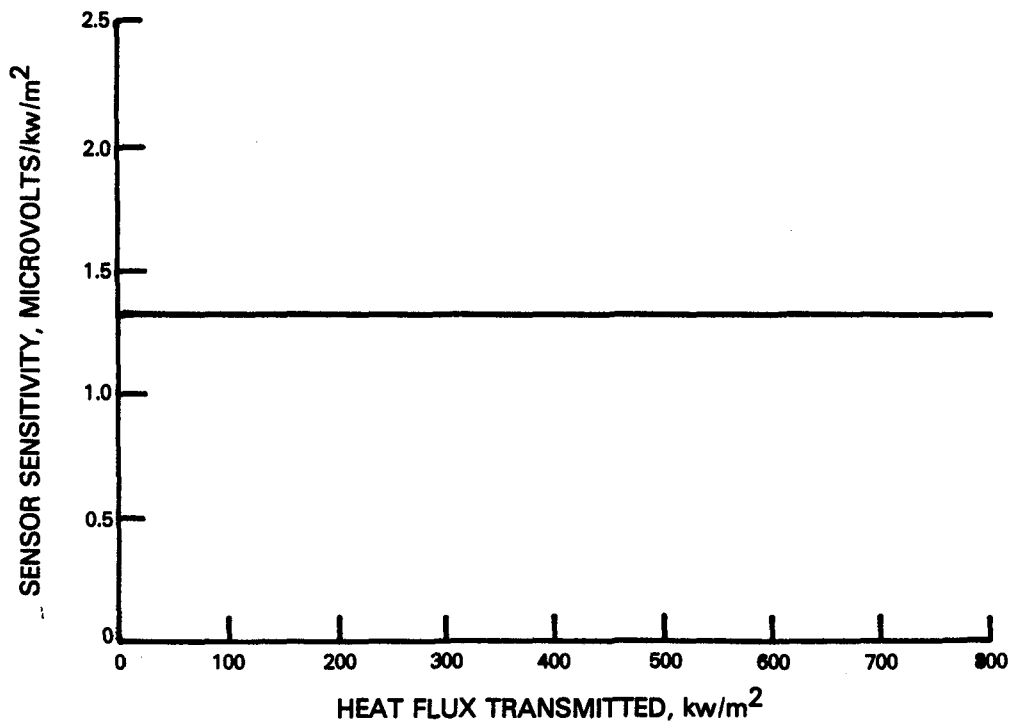
Figure 5.3-2   Least Squares Plot of Sensor Sensitivity versus Transmitted
Heat Flux for Embedded Thermocouple Sensor D-1
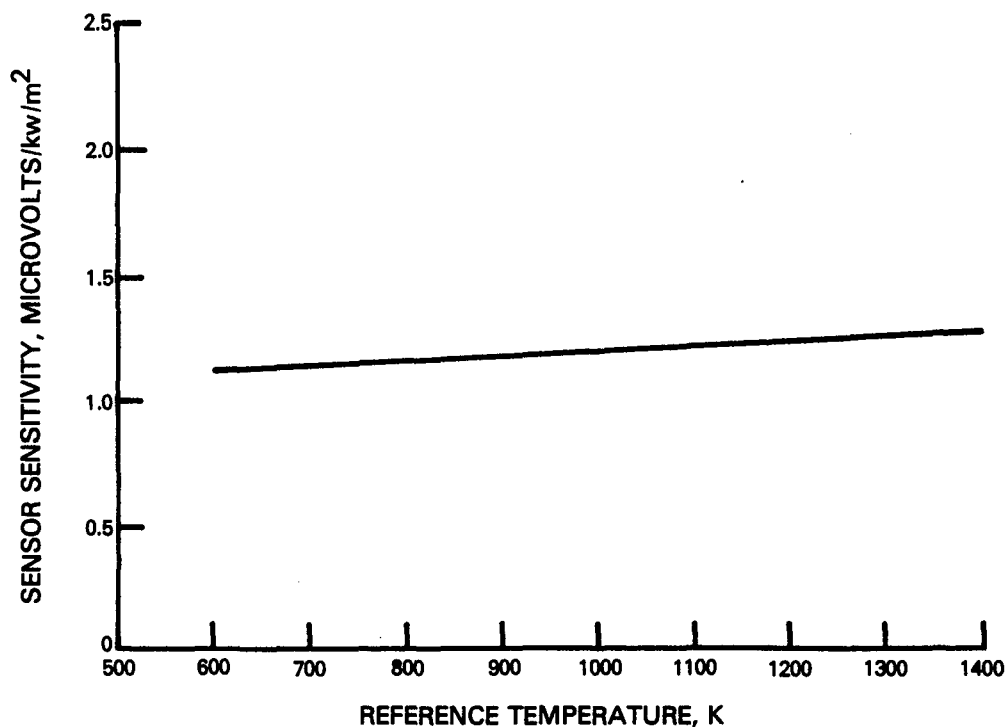
Figure 5.3-3   Least Squares Plot of Sensor Sensitivity versus Sensor
                   Reference Temperature for Embedded Thermocouple Sensor D-1

TABLE 5.4-I

TEST RESULTS OF EMBEDDED THERMOCOUPLE SENSORS - DUAL CONDUCTOR SWAGED WIRE

Serial Number	Status	Lamp Calibration	Vacuum Calibration	Thermal Cycle	Thermal Soak	Comments
T-1	Good	X				
T-2	Failed	X			X	Leadwire Failure After Thermal Soak
T-3	Failed	X	X			Leadwire Failure During Vacuum Calibration

TABLE 5.4-I (Continued)

Serial Number	Status	Lamp Calibration	Vacuum Calibration	Thermal Cycle	Thermal Soak	Comments
T-4	Failed	X				Leadwire Failure During Initial Calibration
T-5	Good	X				
T-6	Failed	X				Open Thermocouple Internal to the Sensor During Lamp Calibration
T-7	Good	X				Delivered to NASA at 11/13/81 Oral Briefing
T-8	Failed					Leadwires Cut During Installation in Rig
T-9	Failed					Bad Weld on Leadwire Damaged During Construction

Figure 5.4-1 is a plot of the least squares fit of the sensor microvolt output versus heat flux transmitted for sensor T-1. As anticipated, the line passes close to the origin (zero output at zero heat flux transmitted). Figures 5.4-2 and 5.4-3 show the least squares fit of the sensor sensitivity versus heat flux through the sensor and sensor reference temperature. The sensor sensitivity versus both heat flux transmitted and sensor reference temperature are relatively flat, indicating that no correction to the sensor output is required to account for sensor temperature or heat flux level.
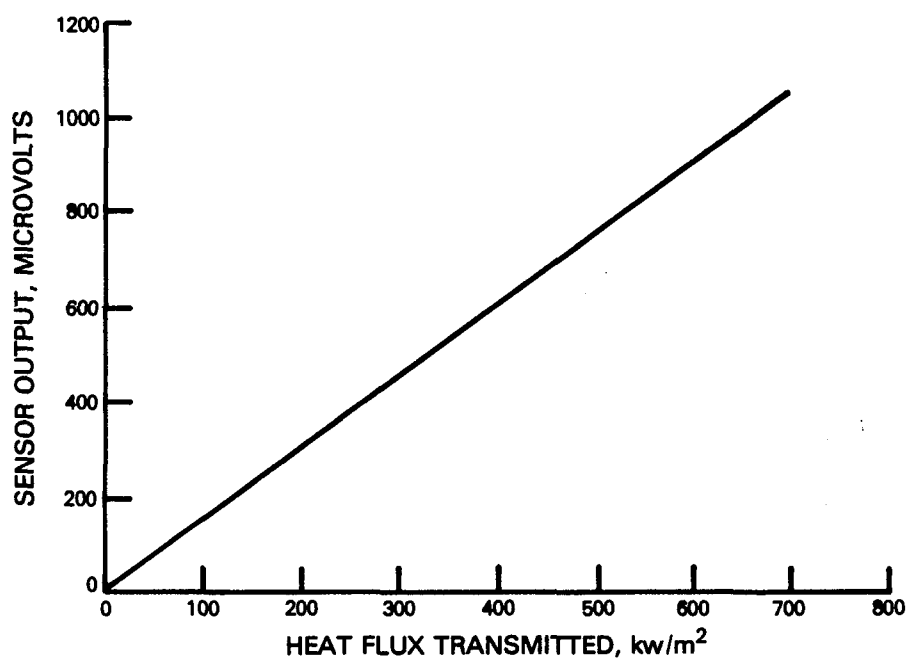
Figure 5.4-1   Least Squares Plot of Calibration Data for Embedded
                 Thermocouple Sensor T-1
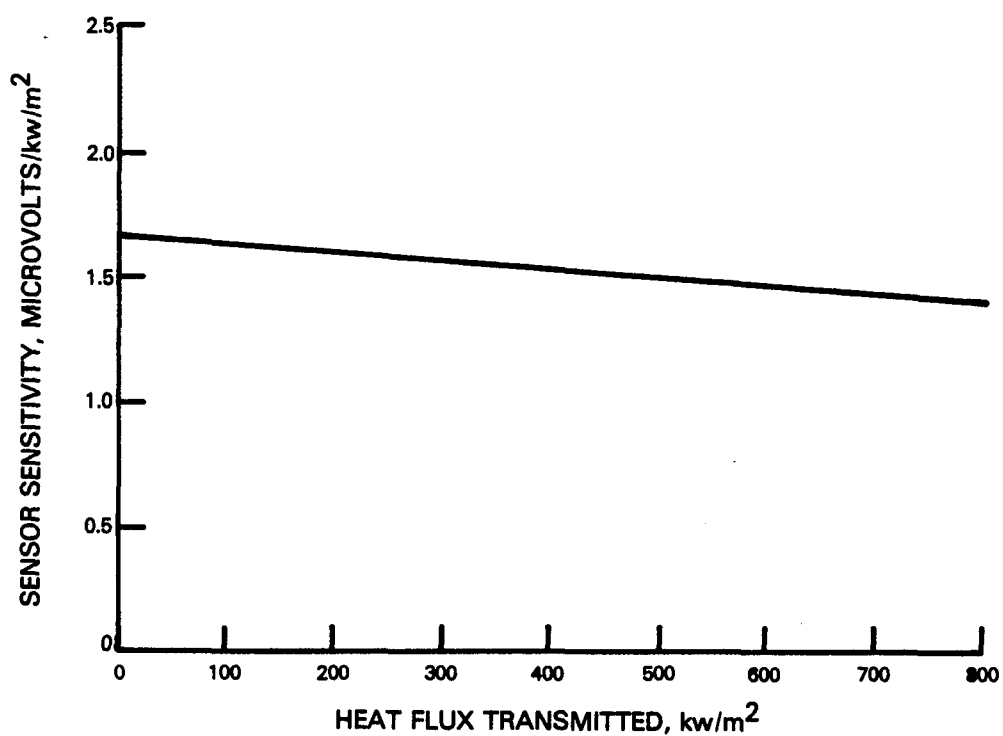
Figure 5.4-2   Least Squares Plot of Sensor Sensitivity versus Transmitted
                 Heat Flux for Embedded Thermocouple Sensor T-1
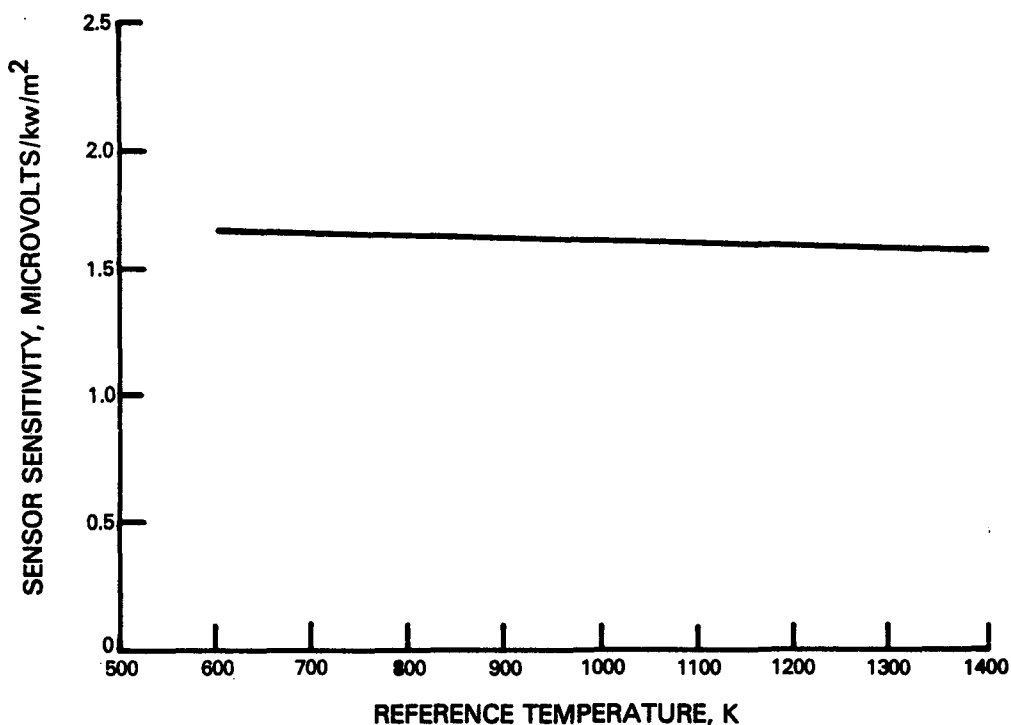
Figure 5.4-3   Least Squares Plot of Sensor Sensitivity versus Sensor
Reference Temperature for Embedded Thermocouple Sensor T-1

5.5 TEST RESULTS FOR LAMINATED SENSORS

A total of eleven laminated sensors, designated L-1 through L-11, were
fabricated and tested. A summary of the test program is given in Table 5.5-I
and the individual sensor calibrations are presented in Appendix D.

TABLE 5.5-I

TEST RESULTS OF LAMINATED SENSORS

Serial Number	Status	Lamp Calibration	Vacuum Calibration	Thermal Cycle	Thermal Soak	Comments
L-1	Failed	X			X	Open Thermocouple Internal to the Sensor During Calibration After Thermal Soak
L-2	Failed	X		X		Leadwire Failure During Thermal Cycle
L-3	Good	X		X		Delivered to NASA at 11/13/81 Oral Briefing

54

TABLE 5.5-I (Continued)

TEST RESULTS OF LAMINATED SENSORS

Serial Number	Status	Lamp Calibration	Vacuum Calibration	Thermal Cycle	Thermal Soak	Comments
L-4	Good	X				
L-5	Good	X				
L-6	Good	X				
L-7	Good	X				
L-8	Good	X				
L-9	Good	X				
L-10	Good	X				
L-11	Good	X				

Of the eleven laminated sensors fabricated and tested, only two sensors failed, one during thermal cycle testing and one after the thermal soak test. Sensor L-1 developed an open thermocouple during recalibration after the thermal soak and the location of the open was determined to be internal to the sensor. Sensor L-2 experienced a leadwire failure during the thermal cycle test. Sensor L-3 successfully completed the thermal cycle test. In large part, the reduced failure rate of these sensors can be attributed to the fact that these sensors were fabricated and tested last, and the experience in fabrication techniques and leadwire support procedures was evident.

The dashed line in Figure 5.5-1 is a plot of the least squares fit of the sensor microvolt output versus heat flux transmitted for sensor L-11. This curve does not pass near the origin (zero output at zero transmitted heat flux). The cause of the discrepancy was found to be varying sensor sensitivity with sensor temperature. Figures 5.5-2 and 5.5-3 are the least squares fit of the sensor sensitivity versus heat flow through the sensor and sensor temperature. The plot of sensitivity versus heat flow through the sensor is nearly flat, indicating that no correction is required to account for heat flux level. The plot of sensor sensitivity versus sensor temperature has a significant slope, indicating that accuracy might be gained by correcting the output to account for changes in sensor temperature.
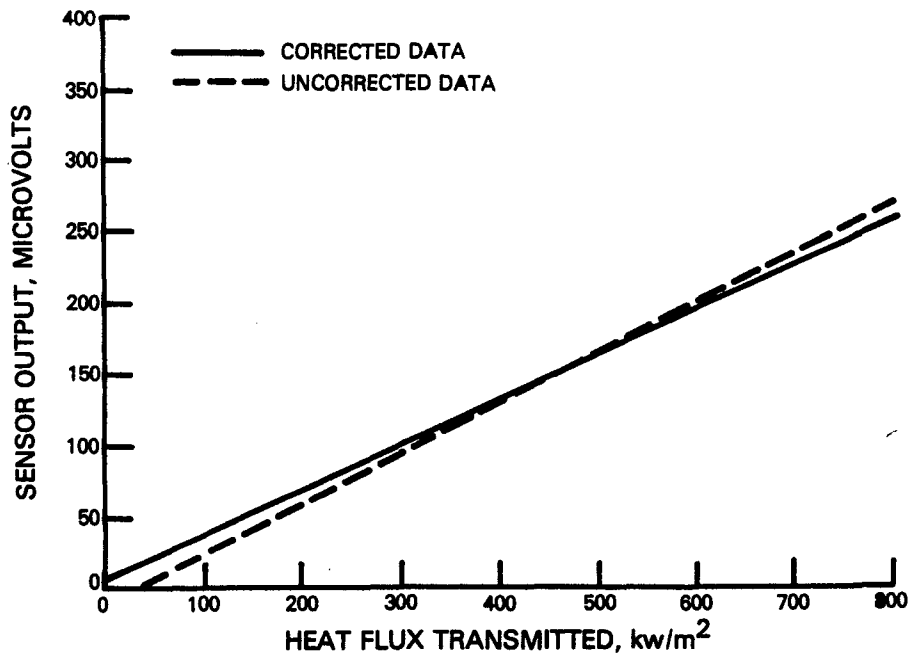
Figure 5.5-1 Least Squares Plot of Calibration Data for Laminated Sensor L-11
Showing Comparison of Raw and Corrected Data
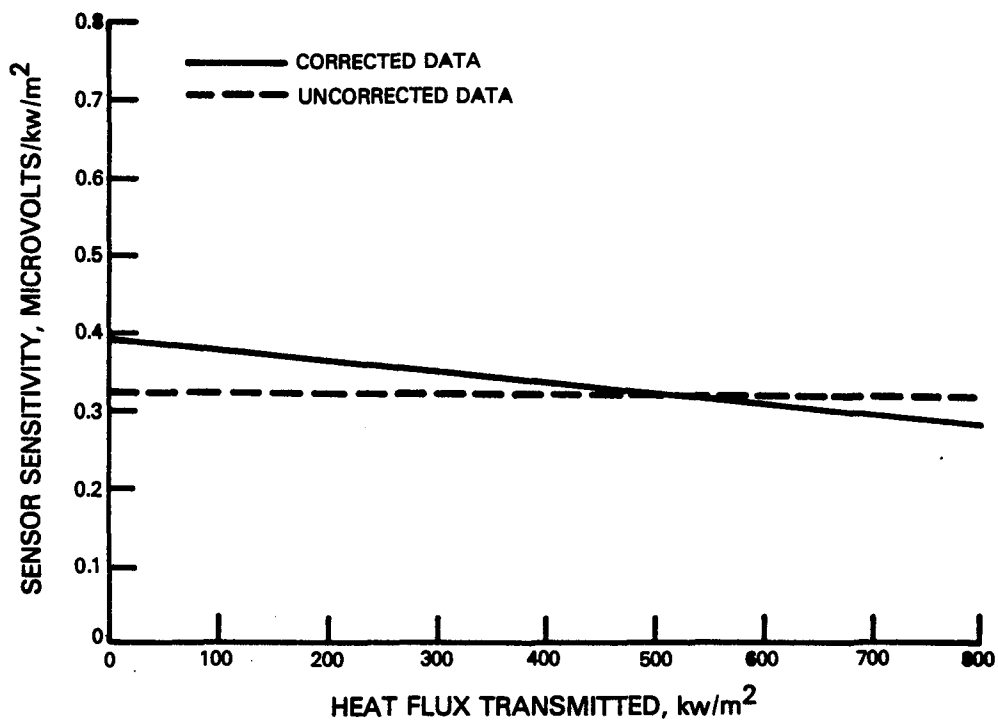
Figure 5.5-2 Least Squares Plot of Sensor Sensitivity versus Transmitted Heat
Flux for Laminated Sensor L-11 Showing Comparison of Raw and
Corrected Data
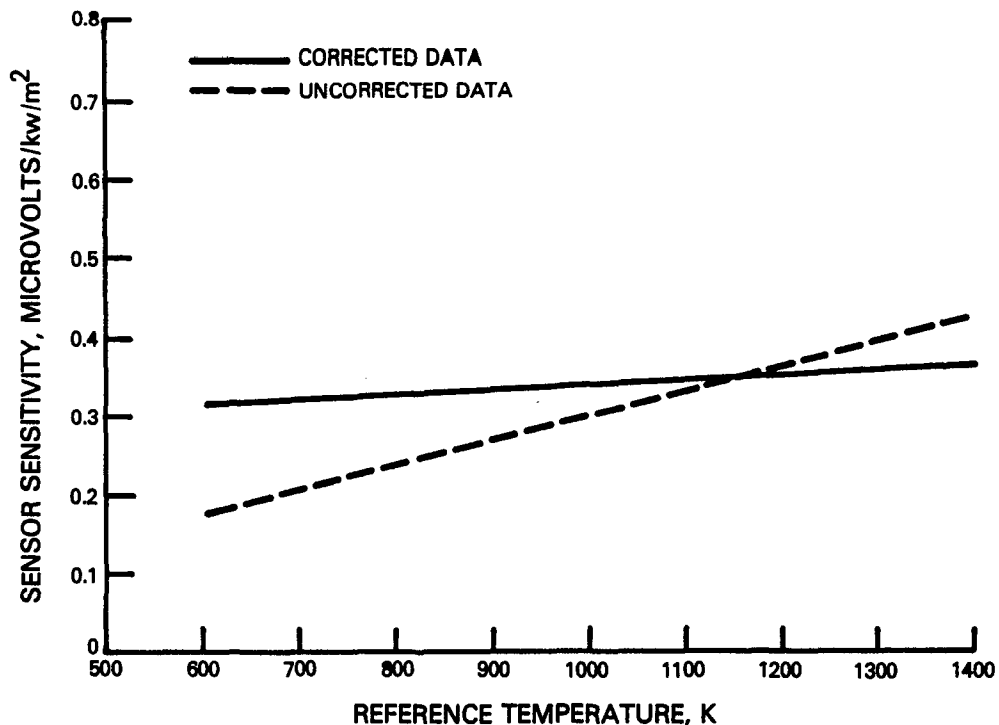
Figure 5.5-3   Least Squares Plot of Sensor Sensitivity versus Sensor Reference
Temperature for Laminated Sensor L-11 Showing Comparison of Raw
and Corrected Data

The slope of sensor sensitivity versus sensor reference temperature plot,
shown by the dashed line in Figure 5.5-3, is positive. This is typical for all
the laminated sensors. Statistical techniques discussed in Appendix B were
used to obtain the best overall slope of these curves which was 2.54×10^{-4}
microvolts/kw/m²/K. That correction was then applied to correct all the data
to a constant temperature of 1150K. The least squares fits to the corrected
data are shown as the solid lines in Figures 5.5-1 through 5.5-3. The
correction causes the output curve to go closer to the origin and results in
nearly flat slopes for the sensor sensitivity vs. heat flux and temperature
curves.

5.6   TEST RESULTS FOR GARDON GAUGE SENSORS

A total of nine Gardon Gauge sensors, designated G-1 through G-9, were
fabricated and tested. A summary of the test program is given in Table 5.6-I
and the individual sensor calibrations are presented in Appendix E.

TABLE 5.6-I

TEST RESULTS OF GARDON GAUGE SENSORS

Serial Number	Status	Lamp Calibration	Vacuum Calibration	Thermal Cycle	Thermal Soak	Comments
G-1	Failed	X	X			Leadwire Failure During Handling
G-2	Failed	X				Leadwire Failure During Calibration
G-3	Failed	X			X	Bad Temperature Profile-Suspect Poor Lamination Leadwire Failure After Thermal Soak
G-4	Good	X	X			Delivered to NASA at 11/13/81 Oral Briefing
G-5	Failed	X				Leadwire Failure During Calibration
G-6	Failed	X		X		Leadwire Failure During Thermal Cycle
G-7	Failed	X				Leadwire Failure During Calibration
G-8	Good	X	X			
G-9	Good	X		X		

Sensor G-1 was calibrated initially with an air cavity covered with Hastelloy-X foil, and then rebuilt with the rear cavity filled with ceramic. When tested, it was determined that the gauge performs satisfactorily with both construction techniques, with a reduced but still acceptable output and sensitivity with the ceramic filled cavity. Figure 5.6-1 shows the comparison of calibration data for sensor G-1 with the air filled and ceramic filled

cavities. Fabricability and survivability considerations favored the ceramic filled Gardon gauge, and this construction was adopted for all further testing. Sensors G-1, G-4, and G-8 were used for absolute calibrations in the three filament vacuum rig. Sensor G-3 exhibited an uneven temperature profile during the initial calibration which was traced to a lamination defect. This sensor was then used for the thermal aging tests. Sensors G-6 and G-9 were used for thermal cycling tests. Of the nine Gardon gauge sensors fabricated and tested, six sensors failed during calibration testing. All of these were traced to leadwire failures.
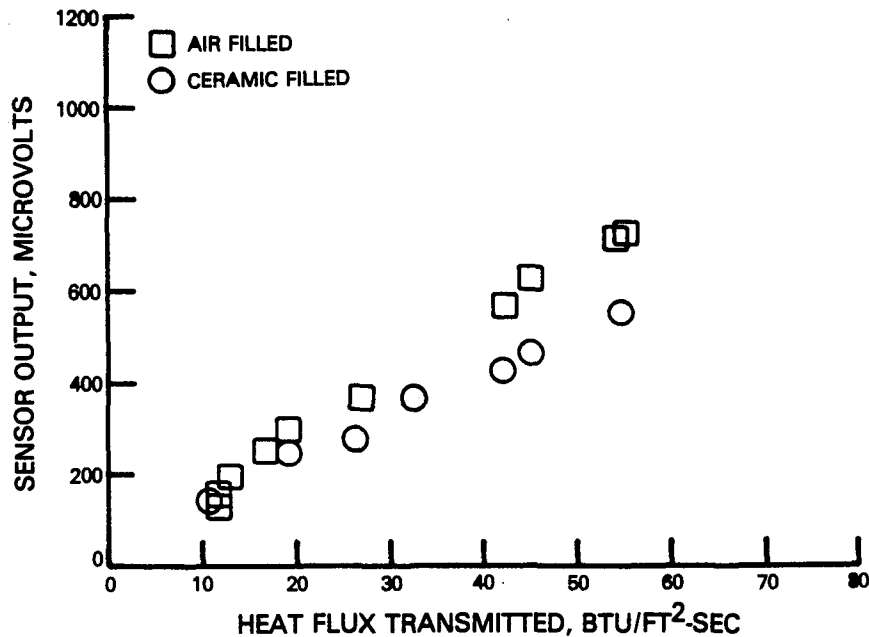
Figure 5.6-1   Plot Showing Comparison of Calibration Data for an Air Filled and a Ceramic Cement Filled Gardon Gauge Sensor

Figure 5.6-2 is a plot of the least squares fit of the sensor microvolt output versus heat flux transmitted for sensor G-9. As anticipated, this line passes close to the origin (zero output at zero heat flux transmitted). Figures 5.6-3 and 5.6-4 are plots of the least squares fit of sensor sensitivity versus heat flux through the sensor and sensor temperature. These plot are both very close to flat, indicating that there is no correction of the sensor output required to account for sensor temperature or heat flux level.
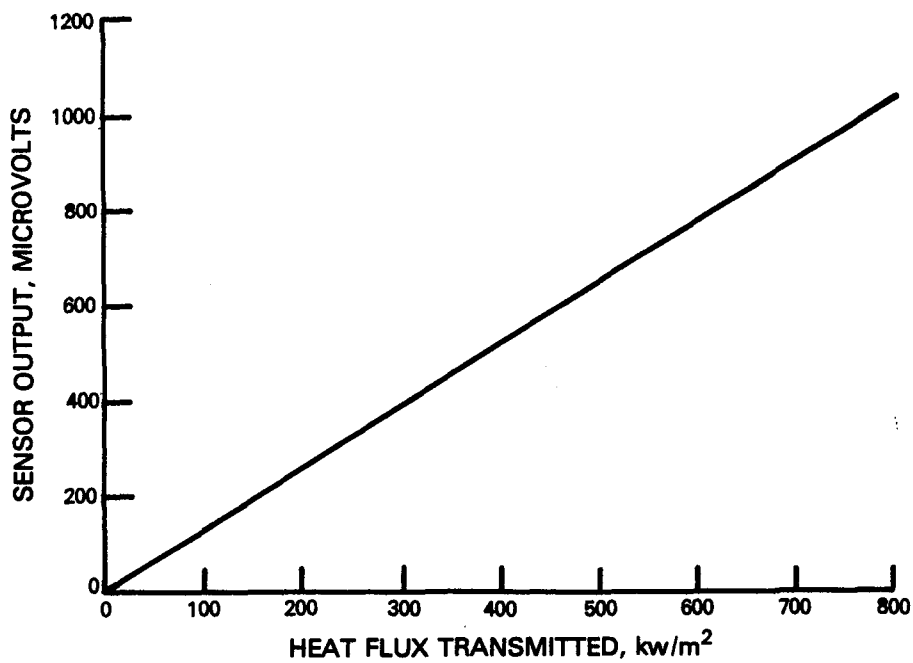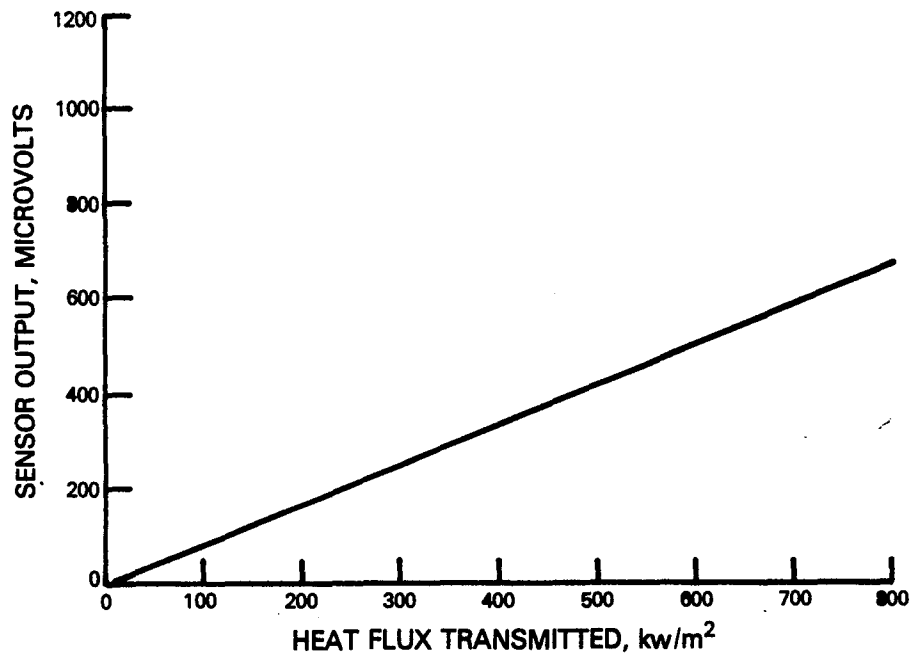
Figure 5.6-2   Least Squares Plot of Calibration Data for Gardon Gauge
                Sensor G-9
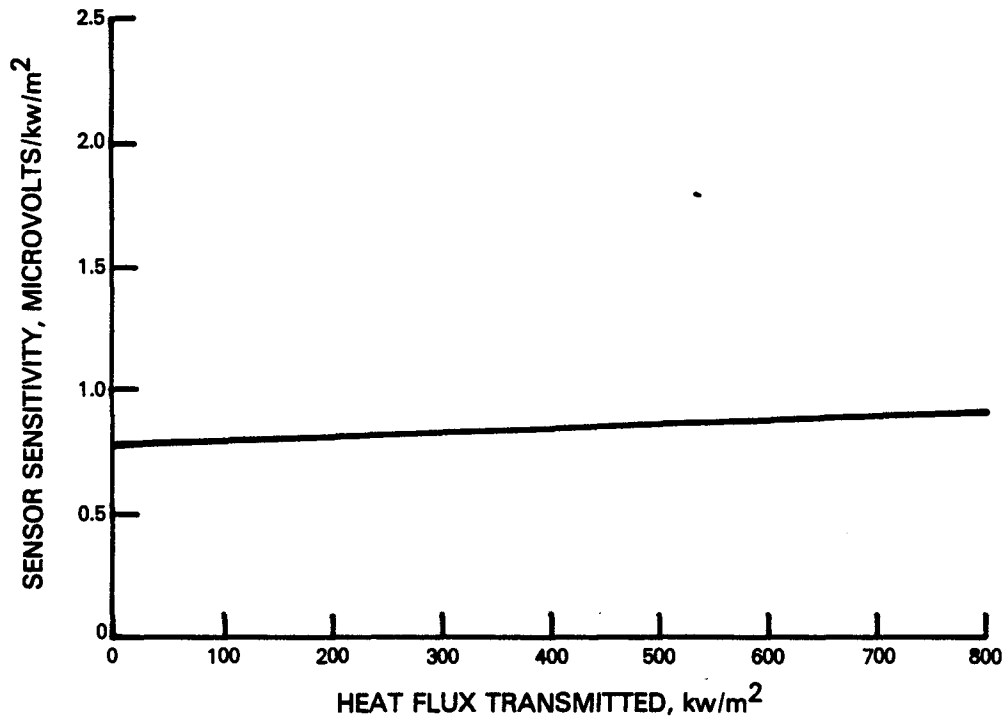
Figure 5.6-3   Least Squares Plot of Sensor Sensitivity versus Transmitted
                Heat Flux for Gardon Gauge Sensor G-9
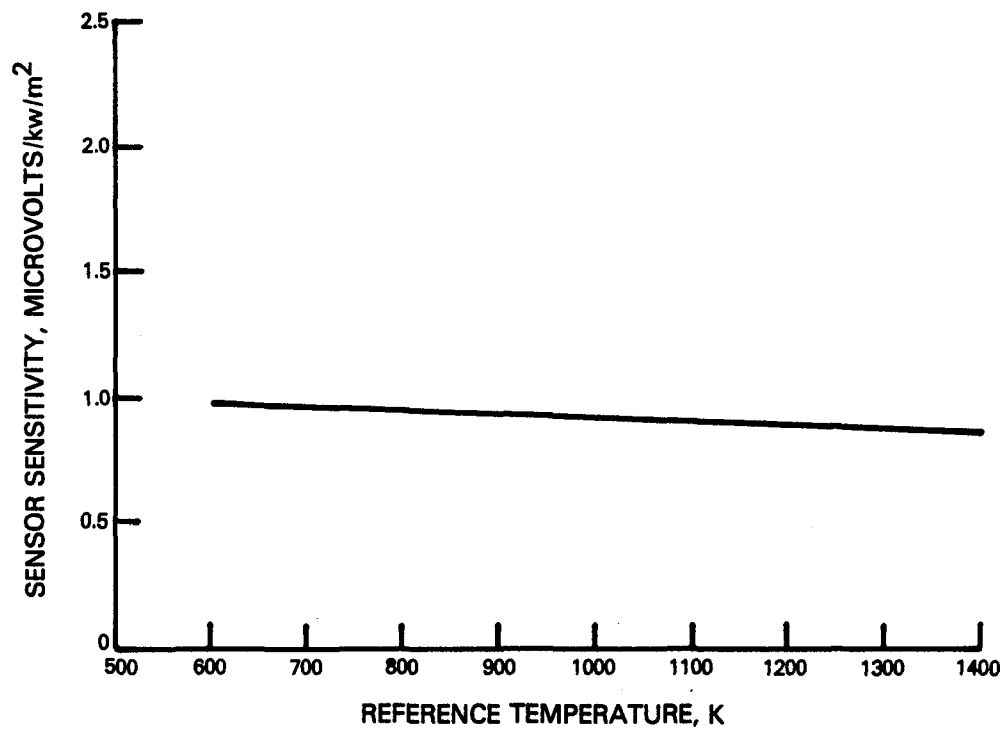
Figure 5.6-4   Least Squares Plot of Sensor Sensitivity versus Sensor
                 Reference Temperature for Gardon Gauge Sensor G-9

SECTION 6.0

CONCLUSIONS AND RECOMMENDATIONS

Sensors were fabricated according to three different designs that met the goals set forth in the requirements of physical size, durability under the anticipated environmental conditions, and accuracy.

The embedded thermocouple sensors, laminated sensors and Gardon gauge sensors all were fabricated with external dimensions not exceeding 0.8 centimeter in diameter and 0.115 centimeter in thickness. The actual sensor area in the laminated sensors and the Gardon gauge sensors is 0.152 centimeter in diameter. In the case of the embedded thermocouple sensors, the actual sensor active area is undefined, but is estimated to be less than 0.2 centimeter in diameter.

The sensors were shown to be capable of withstanding fifty thermal cycles from near room temperature and negligible heat flow to 1175K and 50 kw/m^2, and of repeating the initial calibration values after the cyclic testing. The sensors were also shown to maintain a constant resistance throughout a fifty hour thermal soak at approximately 1175K, indicating that oxidation of the thermoelectric elements was not a significant factor.

The accuracy of each type of sensor was found to be within +5 percent of 1x10^6 Watts/m^2 for the majority of the individual sensors. A few sensors of each type were found to exhibit more scatter in the data and to produce accuracies in the +10 percent range. The cause for this variation between sensors is not known, but it is suspected to result from problems with intermittant secondary junctions in the leadwires.

The embedded thermocouple sensors were found to produce stable accurate results and are the preferred sensors. These sensors experienced a very high mortality rate due to leadwire failures, but this is attributed more to problems in fabrication and handling procedures than to a problem in the sensor design.

The laminated sensors were found to exhibit a change in sensitivity with changing sensor temperature. This required that an empirical correction be made to the data. After correction, the data from the sensors exhibited the accuracy required. These sensors are considered the third preference because of the correction required to the data.

The Gardon gauge sensors were found to produce stable and accurate results and are considered as second preference only from the standpoint that they tend to cause a larger thermal perturbation than the embedded thermocouples. This thermal perturbation is only a problem in convective heating situations where the gas temperature is close to the combustor liner temperature.

The fabrication of all three types of sensors is a labor intensive effort and there is no significant difference in cost or complexity of fabrication between the sensor types.

The dominant failure mode for all the sensor types was failure of the lead-wires external to the sensors. Twenty of the thirty-nine sensors experienced leadwire failures. Two of the remaining sensors developed opens in the thermocouple circuits, and the location of these opens was determined to be internal to the sensors. The leadwire failures can be attributed to two general causes; 1) breakage resulting from handling during fabrication and mounting of the sensors; and 2) vibration of the leadwires behind the sensor caused by the cooling air used to cool the back of the sensors.

No bias errors were detected between the two calibration devices used or between the three calibration techniques employed. Repeatability errors in the testing would appear as scatter in the calibration data.

Some scatter in the data and some of the inconsistancies in output between sensors of the same type could be explained by secondary junctions in the swaged wire. The single conductor Chromel and Alumel swaged wire used for sensor construction was approximately twelve years old, and had an unspecified INCONEL sheath. The Hastelloy-X swaged wire was fabricated in-house, and the consistency of this wire could account for some of the observed data scatter.

Specific recommendations for improving the fabricability, durability and repeatability of the sensors are listed below.

o   Use new swaged wire for the fabrication of the sensors and improve inspection requirements for the wire.

o   Modify fabrication techniques to strip the swaged wire with a resistance welder rather than a mechanical stripper, and minimize the flexing of the wire during installation.

o   Install the sensor into the calibration plate with a few tack welds rather than a continuous weld to minimize handling and make removal of the sensor easier.

o   Support leadwires firmly at close intervals during calibration and cyclic testing.

o   Use lightweight connectors on the swaged wire to minimize stresses on the wire caused by the weight of the connectors.

APPENDIX A

LITERATURE SURVEY BIBLIOGRAPHY

Steady State Heat Flux Sensor References

References for steady state heat flux sensors are listed below. Important information was found in Hager (1)(2); Spitzer (8); and the Gardon gauge references (11 through 15).

1) N. E. Hager, Jr., "Making and Applying a Thin-Foil Heat Flux Sensor," INSTRUMENTATION TECHNOLOGY, October, 1967.

2) N. E. Hager, Jr., "Thin Foil Heat Meter Applications," ISA Preprint #P11-2-PHYMMID-67.

3) E. H. Schulte and R. F. Kohl, "Low-Temperature High-Sensitivity Sensor," Solid State Sensors Symposium, Minneapolis, Minn., Sept. 1968.

4) "Present Status of Convective Calibration Tests of One-Dimensional Heat Flux Sensors in the UAC Research Hypersonic Wind Tunnel," HTM-362, August 23, 1965.

5) "Thin Film Heat Transfer Gage," NASA Tech Brief 68-10051.

6) W. E. Haupin, "Heat Flow Meters for Industrial Furnaces," ISA Preprint #16.7-4-64.

7) S. E. Nydick, "Thermal Analysis of a Thin Wafer Heat Flux Transducer Backed by a Finite Heat Sink," ISA Preprint #16.5-4-66.

8) C. R. Spitzer, "Fabrication and Application of Thin Film Heat-Transfer Gages," NASA Report LWP-91.

9) E. A. Brown, R. J. Charlson, and D. L. Johnson, "Steady-State Heat Flux Gauge," May 21, 1961.

10) E. W. Northover and J. A. Hitchcock, "A Heat Flux Meter for Use in Boiler Furnaces," JOURNAL OF SCIENTIFIC INSTRUMENTATION, Vol. 44, 1967.

11) R. Gardon, "An Instrument for the Direct Measurement of Intense Thermal Radiation,". Review of Scientific Instruments, Vol. 24, N.5, May 1953.

12) R. Gardon, "A Transducer for the Measurement of Heat-Flow Rate," ASME Transaction, November, 1960.

13) R. H. Kirchhoff, "Response of Finite-Thickness Gardon Heat-Flux Sensors," ASME TRANSACTIONS, Ser. C (USA), Vol. 94, No. 2, May, 1972, Coden: JHIRAD, pp. 244-5.

14) E. W. Malone, "Design and Calibration of Thin-Foil Heat Flux Sensors," ISA TRANSACTIONS, Vol. 7, NO3, 1968.

15) W. A. Clayton, "High Temperature Circular Foil Heat Flux Gage," Proceedings of 26th International Instrumentation Symposium, Seattle Wash., 1980.

Transient Sensor References

Of the references listed below for transient heat flux sensors, the most important were Kraabel, et. al. (16); and Pfeifer, et. al. (19).

16) J. S. Kraabel, J. W. Baughn, and A. A. McKillop, "Isothermal Heat Flux Sensor," University of California at Davis, ASME Paper No. 78-WA/HT-14, Presented at ASME Meeting December 10-15, 1978, Coden: ASMSA4, 6 pp.

17) L. D. Russell, "Calorimeter Probes for Measuring High Thermal Flux," Ames Research Center, NASA, Moffett Field, California, April, 1979, 13 pp.

18) R. D. Ulrich and G. D. Coffin, "An Analysis and Discussion of Heat Flux Meters."

19) HTM-362 G. D. Pfeifer and B. U. Lewandowski to J. J. Wesbecher Present Status of: (1) Accuracy Determination of a Hy-Cal Asymptotic Calorimeter* Heat Flux Sensor and (2) One Dimensional Heat Flux Sensor Radiation Calibration, May 24, 1965.

20) H. Higuchi and D. J. Peake, "Bi-Directional, Buried-Wire Skin-Friction Gage," Report No. N79-14330/1ST, Ames Research Center, NASA, Moffett Field, California, November, 1978, 27 pp.

21) YU. F. Gortyshov, I. M. Varfolomeev, and R. A. Yaushev, "On the Study of Heat Transfer with the Aid of a Local Heat Flux Sensor," SOVIET AERONAUT, Vol. 21, No. 3, 1978, Coden: SOAEA4, pp. 25-27.

22) Down, M. G., and Hause, A., "Measurement of Heat Flux and Pressure in a Turbine Stage", ASME Paper 81-GT-88.

23) "Fast-Acting Calorimeter," NASA Tech Brief 67-10192.

24) E. E. Covert and A. F. Gollnick, Jr., "Design and Calibration of a Small Heat Transfer Gage and its Application," AIAA Paper 68-535.

25) K. E. Starner, "Use of Thin-Skinned Calorimeters for High Heat Flux Arc-Jet Measurements," ISA TRANSACTIONS, Vol. 7, No. 3, 1968.

26) R. C. Bachmann, J. T. Chamber, and W. H. Giedt, "Investigation of Surface Heat-Flux Measurements with Calorimeters," ISA Trans. 65.

27) D. Dutoya, "Flux de Chaleur Transfere par un Ecoulement en Combustion Turbulente (Heat Flux Transferred by a Flow in Turbulent Combustion)," Off Natl d'Etud et de Rech Aerosp, Chatillon (France), at Sixth International Heat Transfer Conf., Toronto (Canada), August 7-11, 1978. Published by National Research Council of Canada, Toronto, 1978. Available from Hemisphere Publ Corp., Washington, D. C., Vol. 2, pp. 19-24.

28) E. W. Northover, "The Cerl Dometer: A Radiant Heat Flux and Tube Metal Temperature Measurement System for Highly Rated Boilers," Central Electricity Generating Board, London (England), 1978, 12pp.

29) H. Yanowitz and P. Beckman, "A New Heat Flux Gage for Use on Recessive Surfaces," ISA Preprint #16.12-5-66.

30) J. W. Baughn, "Measurements of Heat Flux to Models in a Hyperthermal Wind Tunnel," ISA Preprint #16.7-3-64.

31) S. A. Gordon, "On the Limits on Wall-Thickness in the Thin-Wall Calorimeter Heat Flux Gauge," ASME TRANSACTIONS, May, 1964.

32) Bachmann, Giedt, Chambers and Foley, "Investigation of Surface Heat-Flux Measurements with Calorimeters," ISA Preprint #16.19-3-64.

33) E. W. Malone, "Fast Response High Output Heat Flux Sensor," ISA Preprint #16.15-3-66.

Miscellaneous Sensor References

Articles containing information on different types of sensors, sensor systems, discussions of heat flux, and research in heat transfer were used to gain a better background and understanding of heat flux transducers. Of the references listed, the most interesting were Gerashchenko (38); Hobbs, et. al. (40); "Instrumentation in the Aerospace Industry' (39); and "Research in the Area of Thermal Measurement" (47).

34) D. A. Gerashchenko, "Fundamentals of Heat Measurement," NASA, Washington, D. C., August, 1979, 234 pp.

35) Hobbs, Kinzie and Witherspoon, "Research Trends in Heat Flux Transducers," AIAA Paper 69-661.

36) "Instrumentation in the Aerospace Industry," Vol. 24, No. 913944, in "Test Measurement," Vol. 15, PROCEEDINGS OF THE INTERNATIONAL INSTRUMENTATION SYMPOSIUM, 24TH, 1978,

37) R. D. Stottle, "Direct Heat Transfer Measurements .... Watch Your Step!," ISA Preprint #16.7-2-64.

38) H. F. Poppendiek, "Why Not Measure Heat Flux Directly?," ENVIRONMENTAL QUARTERLY, March, 1969.

39) G. N. Dul'nev, V. A. Kuz'min, N. V. Pilipenko, and S. V. Tikhonov, "Special Features of Measurement of Nonstationary Heat Fluxes by Heat Meters Implementing the Auxiliary Wall Method," Leningrad Institute of Precision Mechanics & Optics (USSR), in JOURNAL OF ENGINEERING PHYSICS, Vol. 32, No. 5, May, 1977, Coden: JEPHAL, pp. 492-497.

40) YU. I. Yunkerov, "Analysis of Measurement Errors of Convective Heat-Transfer Coefficient Using a Thin-Walled Heat-Flux Sensor," INZH.-FIZ. ZH. (USSR), Vol. 35, No. 2, August 1978, Coden: INFZA9, pp. 243-9. Translated In: JOURNAL OF ENGINEERING PHYSICS (USA), Vol. 35, No. 2, August, 1978, Coden: JEPHAL, pp. 917-21.

41) G. A. Surkov, F. B. Yurevich, and S. D. Skakun, "Some Research in the Area of the Determination of Non-Steady Heat Fluxes," A. V. Lykon Institute of Heat & Mass Exchange, Academy of Science of the B SSR, JOURNAL OF ENGINEERING PHYSICS, Vol. 33, No. 6, December, 1977, Coden: JEPHAL, pp. 1475-1480.

42) "Research in the Area of Thermal Measurements (Selected Articles)," Foreign Technology Division, Wright-Patterson Air Force Base, Ohio, Rpt. No. FTD-ID (ES) T-0215-77, March 7, 1977, 52 pp.

43) London, G. YE., "Gas Temperature and Heat Flux in Short-Lived Gasdynamic Processes," HEAT TRANSFER (Sov. Res.)(USA), Vol. 7, No. 3, May-June, 1975, Coden: HTSRAD, pp. 152-7,

44) "Heat-Flux Gage Measurements on a Flat Plate at a Mach Number of 4.6 in the Vsd High Speed Wind Tunnel, a Feasibility Test (LA28)," Space Division, Chrysler Corporation, New Orleans, La., December, 1975, 109 pp.

45) E. W. Northover, "The Cerl Fluxprobe - A Portable, Direct Reading, Radiant Heat Flux Measuring Device." Central Electricity Generating Board, Rpt. No. TD8-286, London (England), August, 1977, 6 pp.

46) L. Bogdan, "Transient Heat Transfer Measurement with Thin-Film Resistance Thermometers--Data Reduction Techniques," Final Report (Apr-Sep 67), Cornell Aeronautical Lab, Inc., Buffalo, N. Y., No. UR68-00-556, October 1967, 111 p.

47) S. A. Guerrieri and R. J. Hanna, "Local Heat Flux in a Vertical Duct with Free Convection in Opposition to Forced Flow," Final Report, Delaware Univ, Newark, 31 December 1952, 100p.

48) D. L. Baker, M. R. Wool, and J. W. Schaefer, "Development of Total and Radiative Heat Flux Measurement Systems for Rocket Nozzle Applications," Final Report, Aerotherm Corporation, Mountain View, California, August, 1970, 196 p.

49) J. R. Ellison and H. I. Binder, "Evaluation of a Heat-Flux Measurement System," Technical Report No. C7635F1 AD-865 583/9ST, Air Force Rocket Propulsion Lab, Edwards Air Force Base, California, November, 1969, 46 p.

50) J. R. Ellison, "Evaluation of a Heat Flux Measurement System (Test No. 2)," Technical Report, Air Force Rocket Propulsion Lab, Edwards Air Force Base, California, December, 1970, 41 pp.

51) Richard D. Baxter, "Heat Flux Measuring System," Patent, National Aeronautics & Space Administration, Filed June 2, 1965, Patent Granted February 6, 1968.

52) D. W. Hill, Jr and D. K. Smith, "Flat Plate Heat Flux and Pressure Measurement in a MOL Scaled Thruster Plume at 400,000-Ft Altitude," Final Report, Arnold Engineering Development Center, Arnold Air Force Station, Tenn., May 1969, 51 p.

53) R. Holanda, "Evaluation of Miniature Single-Wire Sheathed Thermocouples for Turbine Blade Temperature Measurement", NASA Technical Memorandum 79173, June 1979.

54) M. C. Ziemke, "Heat Flux Transducers," Instruments and Control Systems, Vol. 40, December 1967.

55) M G. Dunn and A. Hause, "Measurement of Heat Flux and Pressure in a Turbine Stage", ASME Paper 81-GT-88, March 1981.

56) "Annual Book of ASTM Standards", Part 41, 1981.

57) Russell W. Claus, "Spectral Frame Radiance from a Tubular Can Combustor", NASA Technical Paper 1722, February 1981.

Calibration Method References

58) Ash, Weller, and Wright, "Sources of Error in Vacuum Calibration of Heat Flux Sensors," Review of Scientific Instruments, Vol. 41, No. 7, July 1970.

59) F. V. Bernstein and B. Kinchen, "The Development and Evaluation of a Radiative Heat Source for the Calibration of Transient and Steady-State Heat Flux Sensors," ISA TRANSACTIONS, Vol. 8, No. 2, 1969.

60) G. D. Pfeifer and G. Mikk, "A Comparison and Evaluation of Several Radiant Energy Methods for Calibrating Heat Flux Sensors," ISA Preprint #16.15-2-66.

61) L. K. Holtermann, "Radiant Heat Source Facility for Calibration and Simulation Testing," ISA TRANSACTIONS, Vol. 6, No. 2.

62) D. L. Rall and F. C. Stempel, "A Discussion of the Standardized Procedure for Calibrating Heat Flux Transducers," ISA Preprint #16 7-1-64.

APPENDIX B

CALCULATION PROCEDURES, ERROR DISCUSSION AND ERROR ANALYSIS

B-1.0 APPROACH TO CALCULATION

In all testing conducted on the heat flux sensors, the measured parameters were incident heat flux, sensor voltage output, and sensor reference temperature. The calibration desired for the sensor is the sensor output as a function of the heat flow through the sensor. The sensor is subjected to changing conditions on both the hot and cold surfaces when it is installed in a combustor liner, hence the heat flow through the sensor is the only meaningful result that can be obtained from the sensor. The heat flow through the sensor is calculated by determining the heat flux absorbed by the sensor and subtracting the heat loss from radiation and convection off the front face. Described below are the quantities that are calculated.

B-1.1 Heat Flux Absorbed

The sensors were all coated with Zynolite High Temperature Black Paint prior to calibration. This paint has been found to have a stable emittance and absorptance in air of 0.89 over the wavelength range of interest at temperatures up to 1350K. The heat flux absorbed is determined by multiplying the incident heat flux by the 0.89 absorptance value.

B-1.2 Transmitted Heat Flux

The transmitted heat flux was calculated by subtracting the radiation heat loss and convection heat loss off the front face of the sensor from the heat flux absorbed. The radiation loss off the front face of the sensor is calculated using an emittance value of 0.89 and the calculated front face temperature. For tests conducted in the quartz lamp bank facility, the convection loss was calculated using an experimentally determined value of 394K for the temperature within the quartz lamp bank and a heat transfer coefficient of 0.017 kw/m^{2}K. For tests in the three filament vacuum rig, no convection loss was used. The calculation is run iteratively with the front face temperature calculation to converge on a solution.

B-1.3 Sensor Front Face Temperature

The sensor front face temperature is determined by estimating the depth of the reference temperature measurement, and back calculating the surface temperature using the transmitted heat flux and the thermal conductivities of the materials. In the embedded thermocouple sensors, the reference temperature junction was estimated to be one half the wire diameter below the surface. In the laminated sensor, the reference junction depth was taken as 0.09 centimeter below the sensor hot side surface. For the Gardon gauge sensors, the depth was estimated as the midpoint of the Alumel layer in the sensor. The front face temperature calculation is made iteratively with the transmitted heat flux to converge on a solution. The front face temperature of the Gardon gauge sensors was also calculated by adding the differential temperature between the center of the foil and the Alumel layer to the reference temperature, and this produced virtually the same result as with the estimated depth of the reference junction.

B-1.4 Sensor Sensitivity

The sensor sensitivity is calculated by dividing the sensor microvolt output by the heat flux transmitted. This quantity provides a means to determine if the unit output of the sensor is a function of sensor temperature or heat flux levels. The sensitivities of the embedded thermocouple sensors and the Gardon gauge sensors are essentially constant with both sensor temperature and heat flux levels. For the laminated sensors, the sensitivity is constant with heat flux level, but increases with increasing sensor temperature. This indicates that to achieve maximum accuracy from the laminated sensors, a temperature dependent sensor sensitivity must be used.

B-1.5 Laminated Sensor Output Correction

As mentioned above and in the text of the report, the laminated sensors showed a variation in sensitivity with sensor temperature. The sensitivity was consistently found to be higher at higher temperatures for these sensors. While these sensors were the only type to use Hastelloy-X leadwires with an Alumel thermal barrier, no basis could be found in the the material or thermoelectric properties of Alumel or Hastelloy-X to account for the variation. Statistical techniques were, therefore, used to derive a common correction factor for the sensor type.

A least squares line was fit to the sensitivity vs. temperature curve for each of the laminated sensors. Since small errors in heat flux can cause large errors in sensitivity at low heat flux levels, the data was weighted by the heat flux transmitted through the sensor. The resulting slopes of the least squares lines were found to be distributed roughly lognormally. The fifty percentile point from that distribution (a slope of 2.54×10^{-4} microvolts/kw/m^2/K) was then used to correct all data from all laminated sensors to a constant temperature of 1150K. This correction significantly reduced the scatter in the data. In addition, the corrected curves yield a sensor output near zero for zero transmitted heat flux as should be expected from the sensor. No such corrections were required for either the embedded thermocouple sensors or the Gardon gauge sensors.

B-2.0 SAMPLE CALCULATION

To illustrate the above procedure, a sample calculation is presented below. This example corresponds to the third data point in the calibration of sensor L-11.

B-2.1 Incident Heat Flux

The incident heat flux was measured using a Hy-Cal asymptotic calorimeter mounted on one side of the test fixture in front of the quartz lamp bank. The Hy-Cal reading was corrected for the small, experimentally determined, heat flux difference between the location of the Hy-Cal and the sensor. The resulting basic calibration results for this point were:

Incident Heat Flux	608 kw/m^2
Reference Temperature	1074K
Sensor Output	138 microvolts

72

B-2.2 Heat Flux Absorbed

Since the sensor was coated with a material of known absorptance, 0.89, the absorbed heat flux is given by:

$$Q_{Absorbed} = (0.89) \ (Q_{incident}) = (0.89) \ (608)$$
$$Q_{Absorbed} = 541 \ kw/m^2$$

B-2.3 Heat Flux Transmitted

Front Face Radiation Loss - For a first pass, the sensor hot side temperature was assumed to be equal to the sensor reference temperature. The average temperature within the quartz lamp bank to which the sensor reradiates was determined experimentally to be approximately 394K.

$Q_{Reradiation} = \epsilon \ \sigma \ (T_S^4 - T_{wall}^4)$ using the 0.89 sensor emittance and $\sigma =$ $5.67 \times 10^{-11} \ kw/m^2/K^4$:

$$Q_{Reradiated} = 0.89 \times 5.67 \times 10^{-11} \ (1074^4 - 394^4)$$
$$Q_{Reradiated} = 66 \ kw/m^2$$

Front Face Convection Loss - The front face convection loss was calculated using an air temperature within the quartz lamp bank of 394K and a convective heat transfer coefficient of 0.017 kw/m^2K. This heat transfer coefficient, which was based on a test conducted to investigate the effect of lamp cooling air, is roughly twice that which would be expected from free convection.

$$Q_{Convection} = 0.017 \ (1074 - 394) = 12 \ kw/m^2$$

Transmitted Heat Flux - The heat flux transmitted is given by:

$$Q_{Transmitted} = Q_{Absorbed} - Q_{Reradiated} - Q_{Convected}$$
$$= 541 - 66 - 12$$
$$Q_{Transmitted} = 463 \ kw/m^2$$

Sensor Front Face Temperature

At this point, the sensor front face temperature will be calculated based on sensor reference temperature, the transmitted heat flux, the known reference junction location, and the known temperature dependent thermal conductivities of the sensor materials.

The temperature increase across any layer of the sensor is given by:

$$\Delta T = Q_T \ \Delta X/k$$

where;

Q_T = Q transmitted
ΔX = thickness of the layer
k = thermal conductivity of the layer.

Therefore, to calculate the temperature rise between the reference thermocouple and the hot side surface, we need only to sum the temperature rise across each layer of the sensor above the reference thermocouple junction. Since the Q transmitted is the same for all layers:

$$\Delta T = Q_T \sum_{i=1}^{n} \Delta X_i / k_i$$

Figure B-1 presents a schematic of the conduction layers for the laminated sensor. The conduction path between the reference junction location and the hot side surface consists of approximately 0.009 centimeter of Hastelloy-X, 0.046 centimeter of Alumel, 0.034 more centimeter of Hastelloy-X, and 0.001 centimeter of the high emittance coating. At a temperature of 1074K, the thermal conductivities are:

Hastelloy-X = 0.025 kw/m K
Alumel = 0.050 kw/m K
Coating (assumed) = 0.00175 kw/m K

The temperature rise between the reference thermocouple junction location and the hot side surface is, therefore:

$$\Delta T = 463 \left[\frac{0.00009}{0.025} + \frac{0.00046}{0.050} + \frac{0.00034}{0.025} + \frac{0.00001}{0.00175} \right]$$

$$\Delta T = 15K \text{ and}$$

$$T_{hot\ side} = 1089K$$

Recursive Calculation

This new hot side temperature is now substituted into the calculation for the heat flux transmitted. The resulting transmitted heat flux is used to calculate a new hot side temperature, etc. The result quickly converges on:

$$Q_{Transmitted} = 460 \text{ kw/m}^2$$

$$T_{hot\ side} = 1088K$$
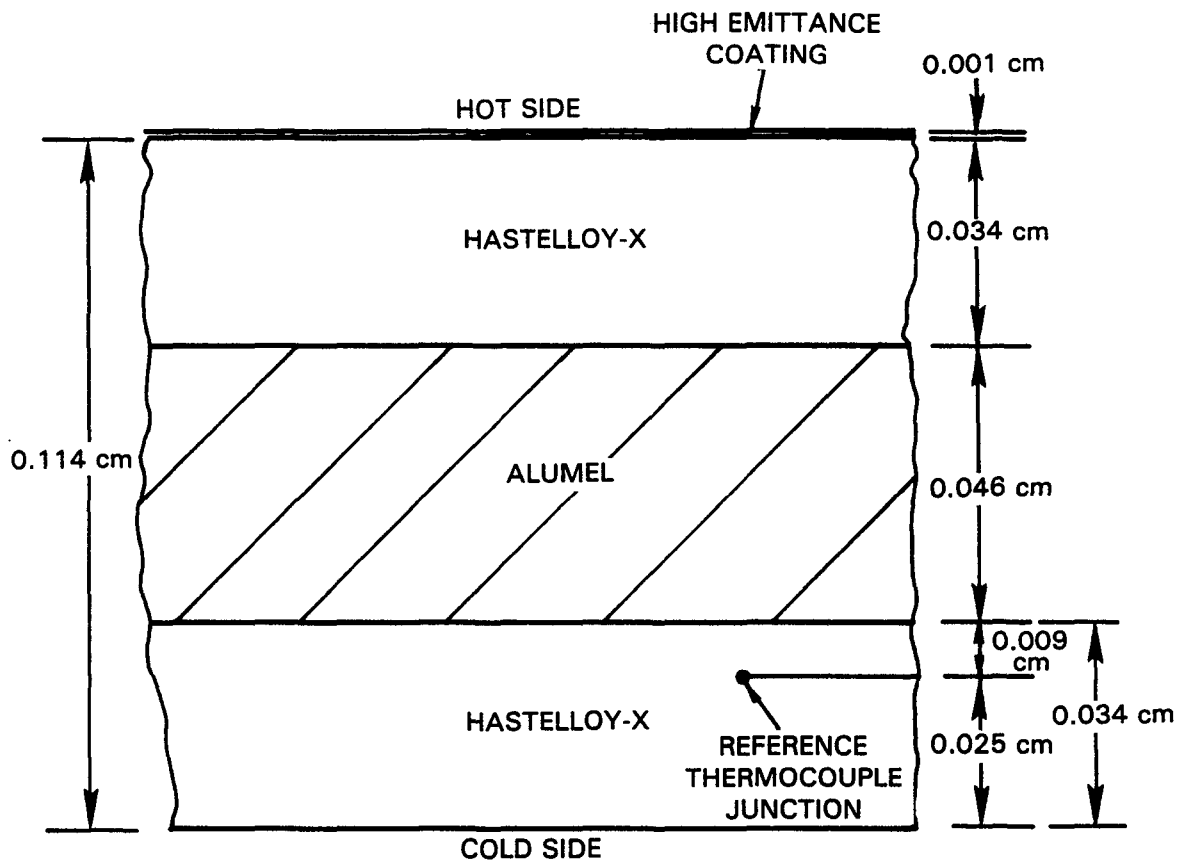
Figure B-1 Conduction Layers for Laminated Sensor

B-2.4 Sensor Sensitivity

The sensor sensitivity may now be calculated for the data point as:

Sensitivity = microvolt output/unit heat flux transmitted

= 139/460

Sensitivity = 0.300 microvolts/kw/m^2

Laminated Sensor Output Correction

The previous step would complete the calculations for all sensor types except the laminated sensors. As discussed in the Basic Approach to Calculations Section, the laminated sensors showed a variation in sensitivity with sensor temperature. All data from these sensors were, therefore, corrected to a constant sensor temperature of 1150K. As discussed earlier, the "best" common correction factor for the laminated sensors was found to be 2.54x10^{-4} microvolts/kw/m^2/K. Since this calibration point was at 1074K, sensor reference temperature:

$$\text{(Sensitivity at 1150K)} = \text{(Sensitivity at 1074K)} + 2.54\times10^{-4} \text{ (1150 -1074)}$$

$$= 0.300 + 0.019$$

$$= 0.319 \text{ microvolts/kw/m}^2$$

In actual use, this is the only correction required as explained in Appendix D. To permit corrected data plots, however, the sensor output was corrected to a nominal temperature of 1150K.

The output corrected to 1150K may be found as:

$$\text{(Output at 1150K)} = \text{(Sensitivity at 1150K) } (Q_{Transmitted})$$

$$= (0.319) \ (459.80)$$

$$= 147 \text{ microvolts.}$$

B-3.0 ERROR DISCUSSION

The magnitude and importance of the various possible error sources will be a function of the sensor operating condition ($Q_{Absorbed}$, $T_{Surface}$, etc.). That subject is discussed more fully in the error analysis presented in Section B-4.0. A good qualitative feel for the relative importance of the various parameters can, however, be obtained by investigating a typical data point. The point that will be discussed here is the same data point from sensor L-11 that was used for the previous sample calculation. This is an intermediate level heat flux point at relatively high temperature.

Table B-I lists those parameters that are used in the calculation of sensor sensitivity. Those parameters preceded by an asterisk are felt to be accurately known and, as such, are sources of negligible error. Those parameters will not be discussed further. The remaining parameters are discussed further. The approach that will be taken is to analytically investigate the affect that a variation in each parameter would have on the calculated sensor sensitivity (calibration constant).

B-3.1 Incident Heat Flux

Figure B-2 shows the calculated effect of variations in the value of the incident heat flux on the calculated sensor sensitivity. A +1.0 percent variation in the incident heat flux results in a +1.1 percent variation in the calculated sensor sensitivity. This indicates, as expected, that care must be taken in measuring the incident heat flux.

76

PARAMETERS ENTERING CALCULATION OF SENSOR SENSITIVITY

o   Incident Heat Flux
o   Sensor Microvolt Output
o   Absorptance of Hot Side Coating Layer
o   Reference Temperature
o   Reference Thermocouple Junction Location
o   *Stephan-Boltzman Constant
o   Temperature Within the Quartz Lamp Bank
o   Sensor Hot Side Convective Heat Transfer Coefficient
o   *Thickness of Sensor Alumel Layer
o   *Thickness of Sensor Hastelloy-X Layers
o   Thickness of Hot Side Coating Layer
o   *Thermal Conductivity of Alumel
o   *Thermal Conductivity of Hastelloy-X
o   Thermal Conductivity of Hot Side Coating Layer

Those parameters preceded by an * are assumed to be sources of
negligible error.
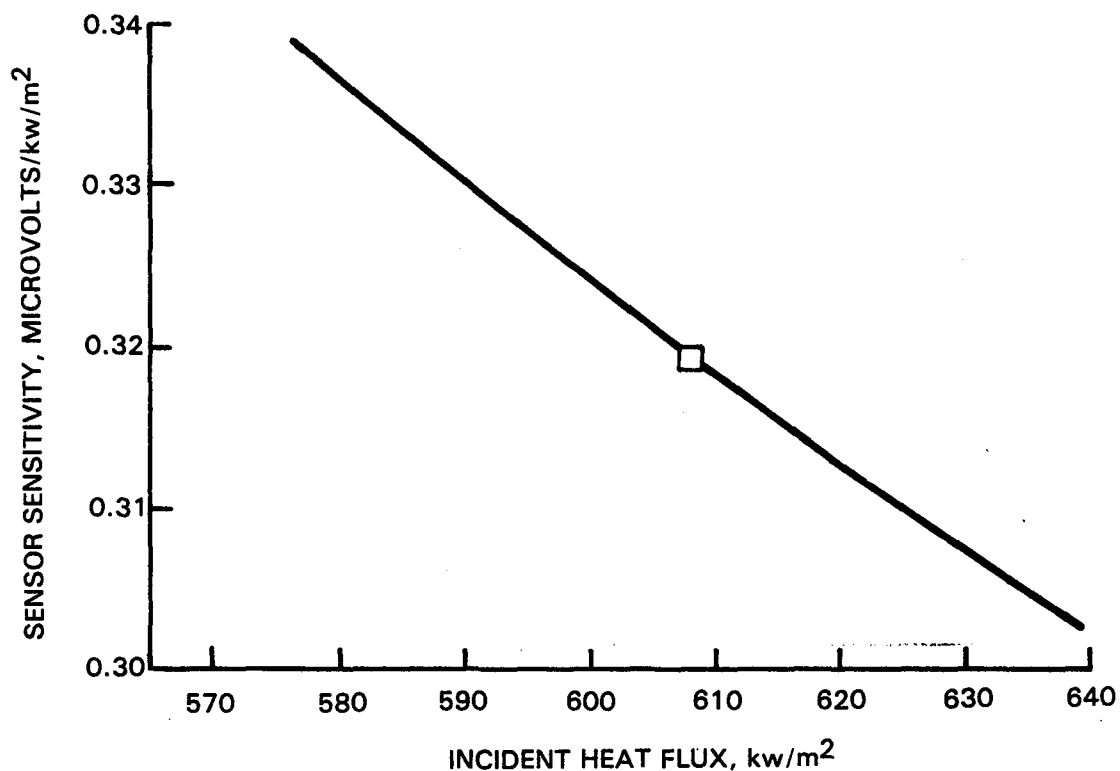
Figure B-2   Calculated Effect of Variation in Incident Heat Flux on
             Calculated Sensor Sensitivity

B-3.2 Sensor Output

Figure B-3 shows the calculated effect of variations in the sensor output on the calculated sensor sensitivity. A +1.0 percent variation in the sensor output results in a +0.94 percent variation in the sensor sensitivity. This differs slightly from the +1.0 percent to be expected because of the output correction for the laminated sensor discussed earlier. An accurate microvolt meter must, therefore, be used to measure the sensor output voltage.
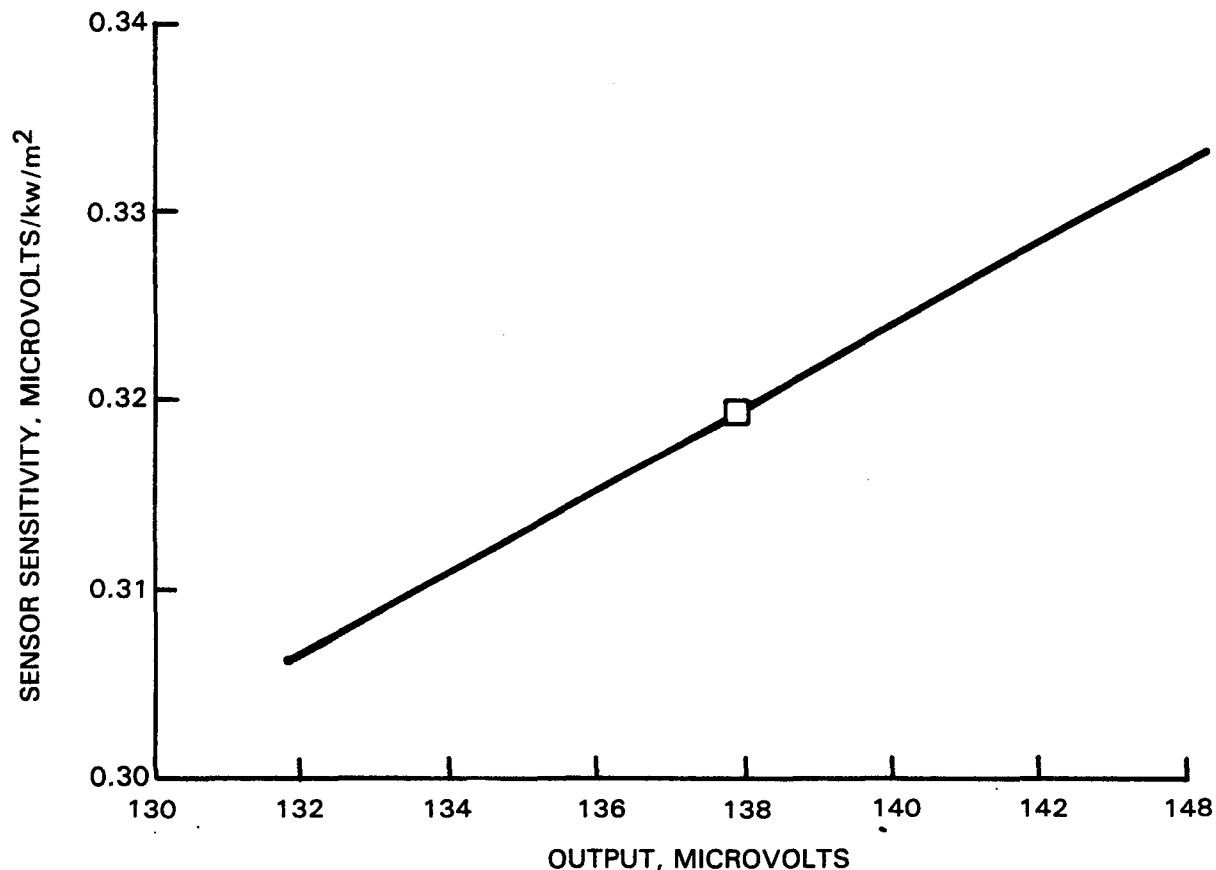
Figure B-3   Calculated Effect of Variation in Sensor Output on Calculated Sensor Sensitivity

B-3.3 Absorptance of Hot Side Coating Layer

Figure B-4 shows the calculated effect of variations in the absorptance of the hot side coating layer has on the calculated sensor sensitivity. A +1.0 percent variation in the coating emittance value results in a +0.96 percent variation in the sensor sensitivity. This confirms the sensitivity of the calibration to the absorptance of the hot side surface, and verifies the need for a coating with known absorptance.
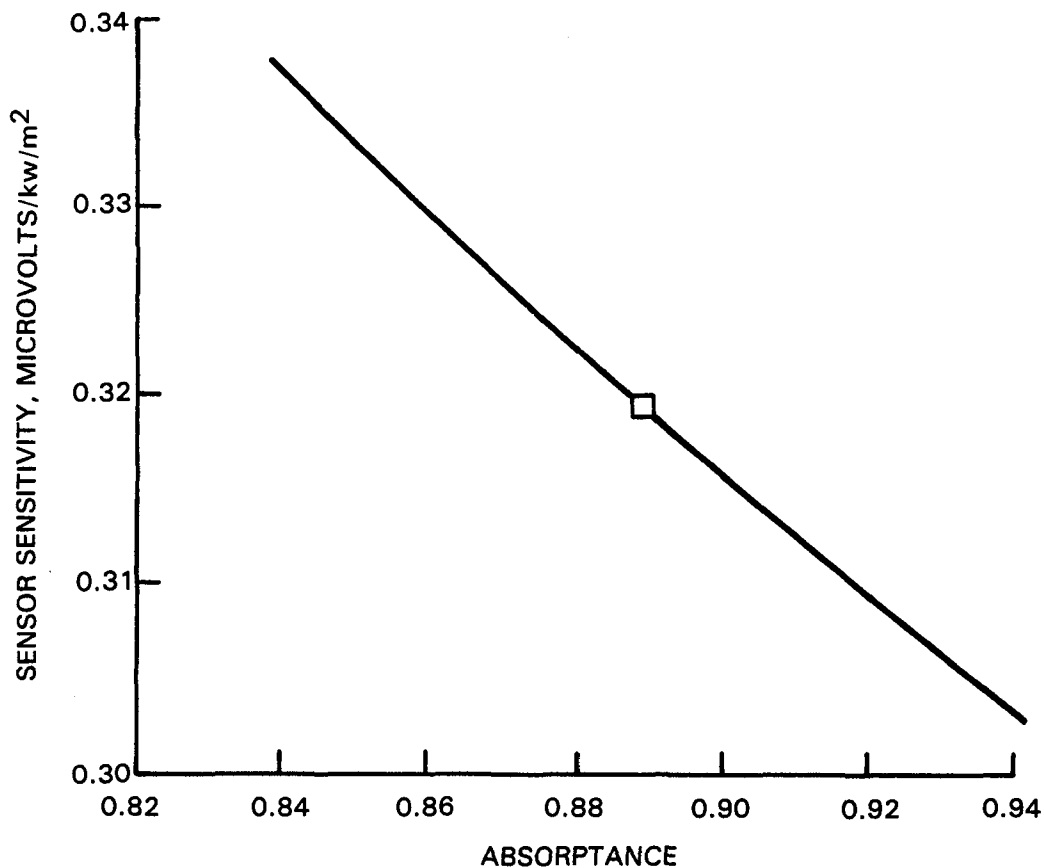
Figure B-4   Calculated Effect of Variation in Absorptance of Hot Side
             Coating on Calculated Sensor Sensitivity

B-3.4 Reference Temperature

Figure B-5 shows the calculated effect of a variation in sensor reference
temperature on the calculated sensor sensitivity. A +10K variation in the
reference temperature only results in a +0.22 percent variation in sensor
sensitivity. The calibration results are therefore, quite insensitive to
moderate errors in determination of the reference temperature.

B-3.5 Reference Thermocouple Junction Location

Figure B-6 shows the effect of a variation in sensor reference location on the
calculated sensor sensitivity. Only a +0.08 percent variation in sensor
sensitivity results from a +0.0075 centimeter variation in the reference
junction location. This +0.0075 centimeter variation in junction location
equates to a +22 percent variation in the placement of the thermocouple
junction within the 0.034 centimeter Alumel layer or a +6.6 percent variation
of the junction location within the total thickness of the sensor. Because of
the slight variation in sensor sensitivity, the calculation results are very
insensitive to errors in determination of reference junction location.
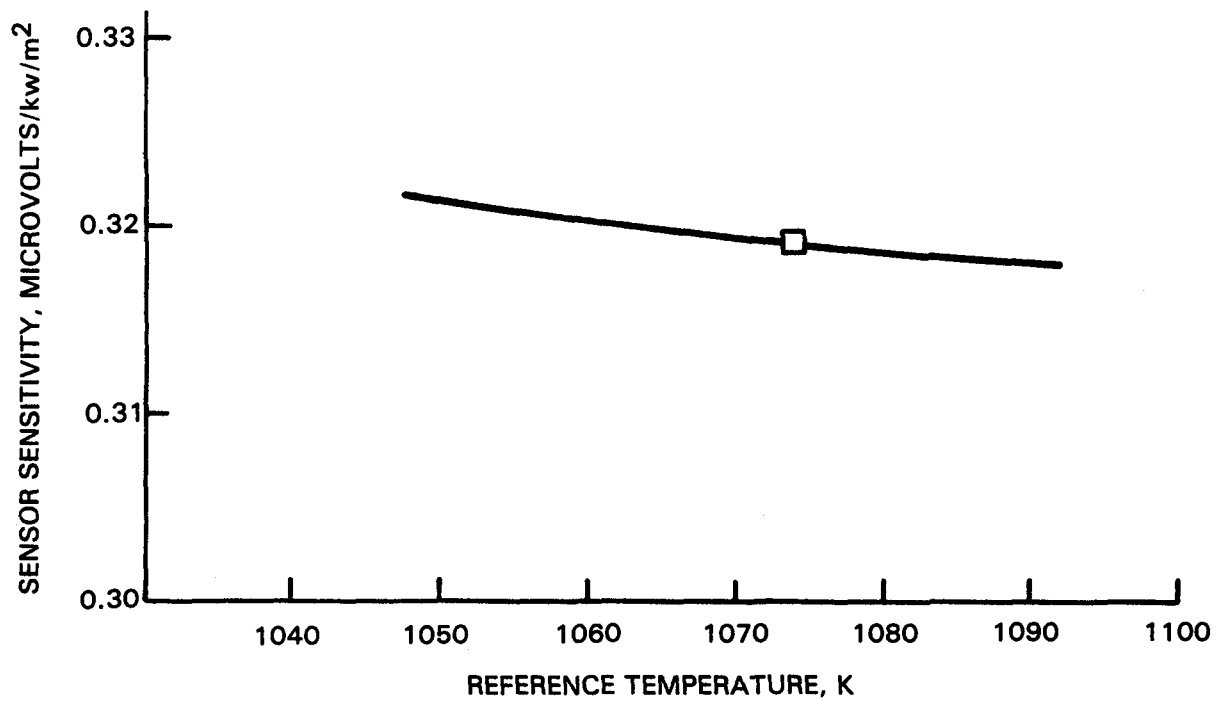
Figure B-5   Calculated Effect of Variation in Reference Temperature on Calculated Sensor Sensitivity
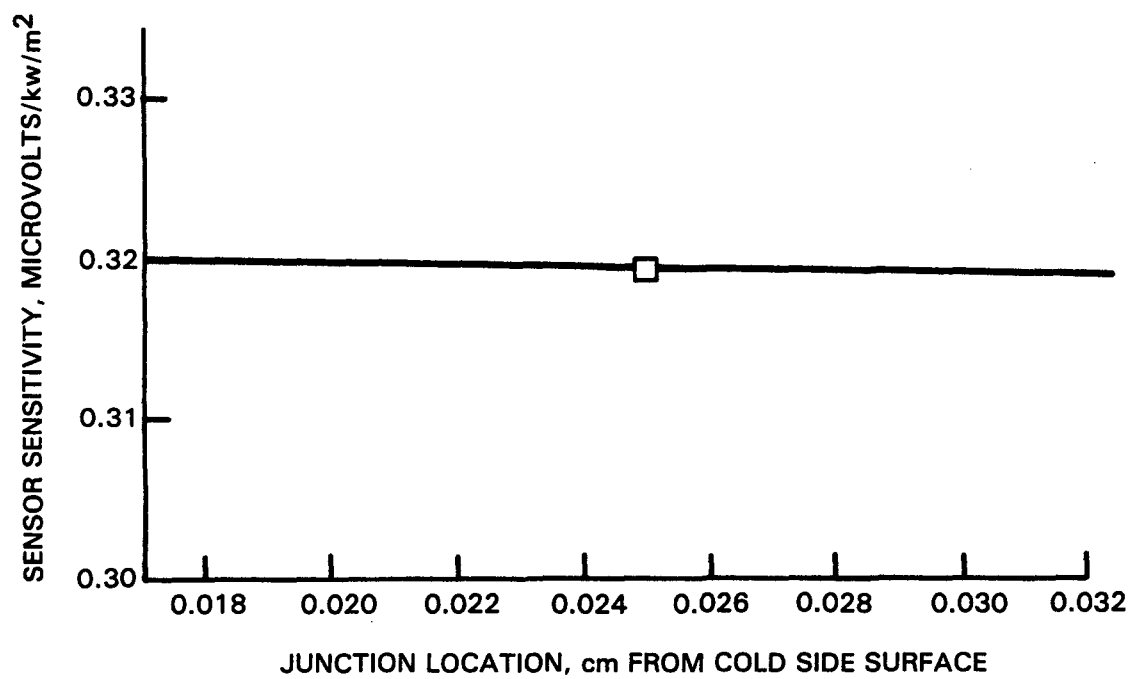
Figure B-6   Calculated Effect of Variation in Reference Junction Location on Calculated Sensor Sensitivity

B-3.6 Temperature within the Quartz Lamp Bank

Figure B-7 shows the calculated effect of a variation in the temperature within the quartz lamp bank on the calculated sensor sensitivity. The temperature primarily effects the convective loss from the sensor although it also enters the radiation loss calculation. A +50K variation in the assumed temperature within the quartz lamp bank results in a +0.13 percent variation in the sensor sensitivity. The calculation results are, therefore, quite insensitive to the temperature within the quartz lamp bank.
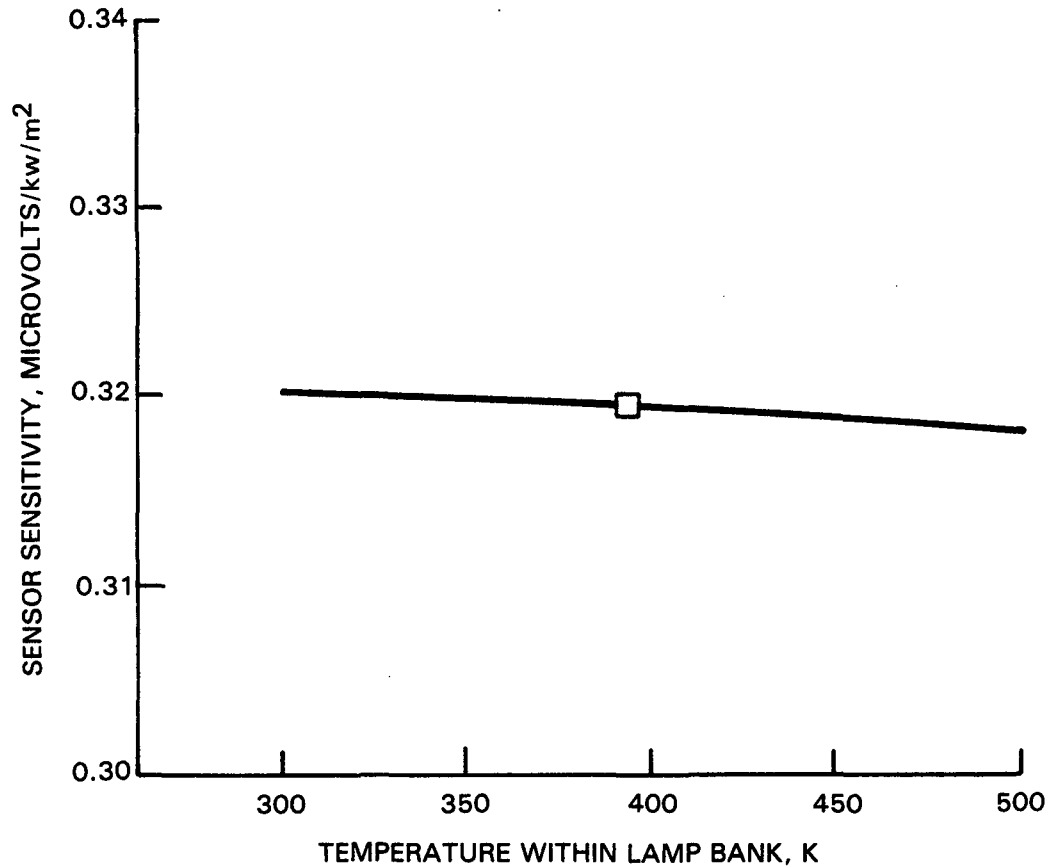
Figure B-7   Calculated Effect of Variation in Temperature within Quartz Lamp Bank on Calculated Sensor Sensitivity

B-3.7 Hot Side Heat Transfer Coefficient

Figure B-8 shows the calculated effect of a variation in the hot side heat transfer coefficient on the calculated sensor sensitivity. A +50 percent variation in the assumed heat transfer coefficient results in a +1.19 percent variation in sensor sensitivity. The calculation results are, therefore, relatively insensitive to moderate errors in the hot side heat transfer coefficient.
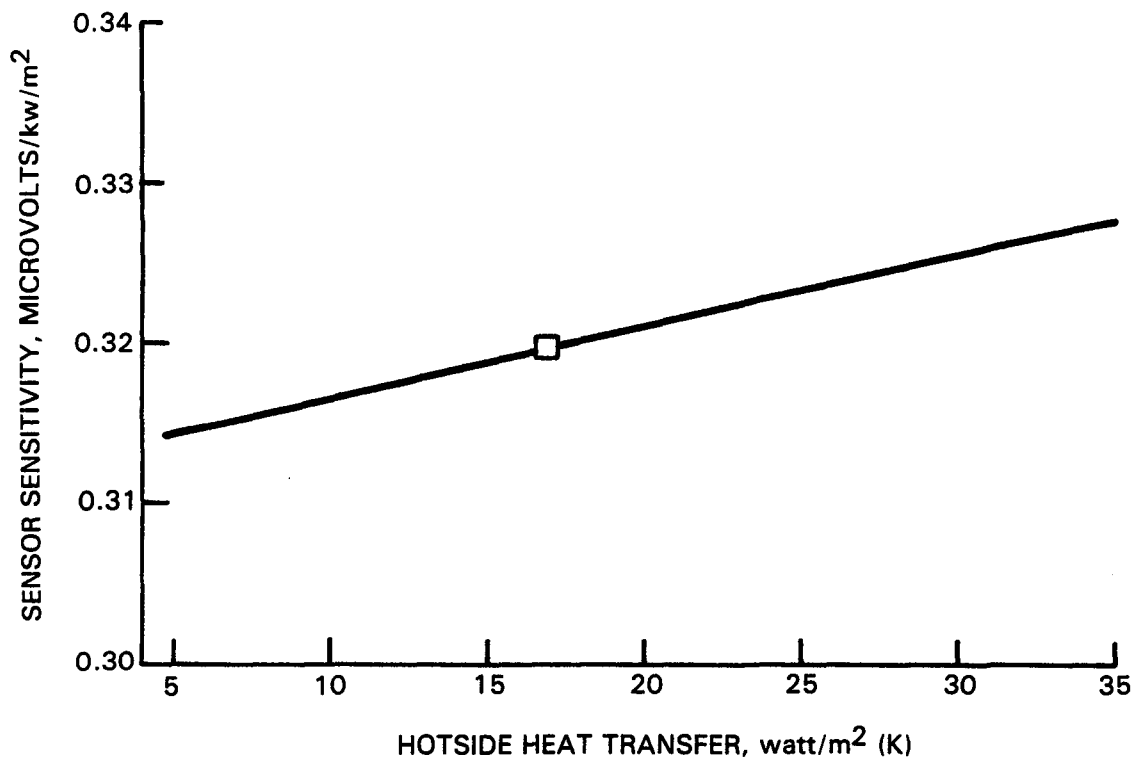
Figure B-8   Calculated Effect of Variation in Hot Side Heat Transfer
              Coefficient on Calculated Sensor Sensitivity

B-3.8 Thickness of the Hot Side Coating Layer

Figure B-9 shows the calculated effect of a variation in the thickness of the
hot side coating layer on the calculated sensor sensitivity. A +100 percent
variation in the coating layer thickness results in a +0.15 percent variation
in the calculated sensor sensitivity. The calculation results are very
insensitive to even large errors in this parameter.

B-3.9 Thermal Conductivity of Hot Side Coating Layer

Figure B-10 shows the calculated effect of a variation in the thermal
conductivity of the hot side coating layer on the calculated sensor
sensitivity. Varying this value from half the assumed value to infinity
results in a +0.15 percent variation in the calculated sensor sensitivity. The
calculation results are, therefore, very insensitive to even large errors in
this parameter.
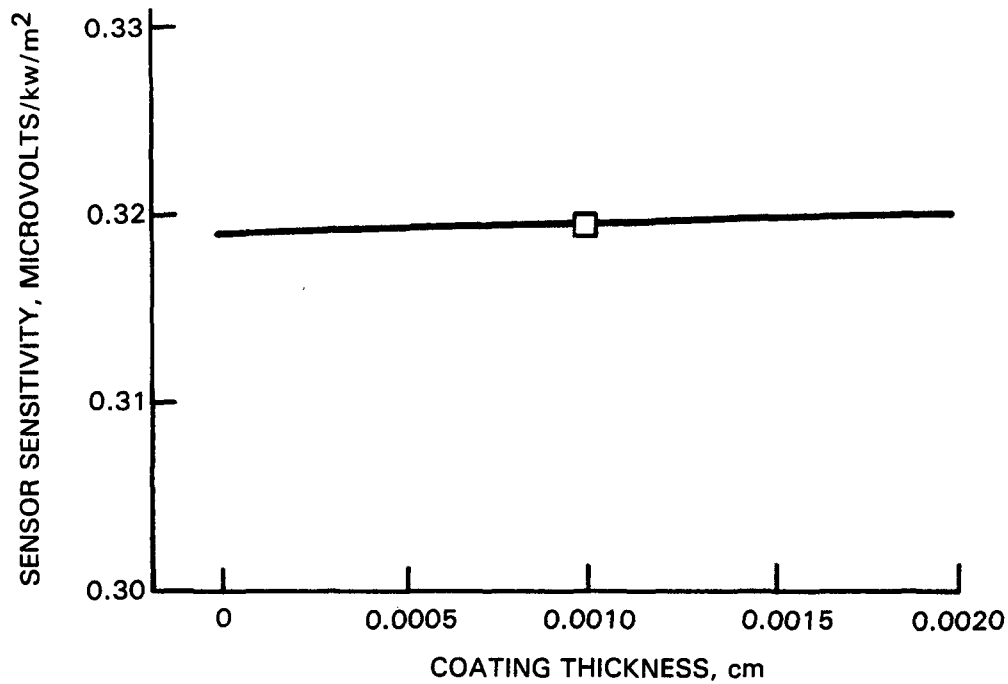
Figure B-9   Calculated Effect of Variation in Thickness of Hot Side Coating
Layer on Calculated Sensor Sensitivity
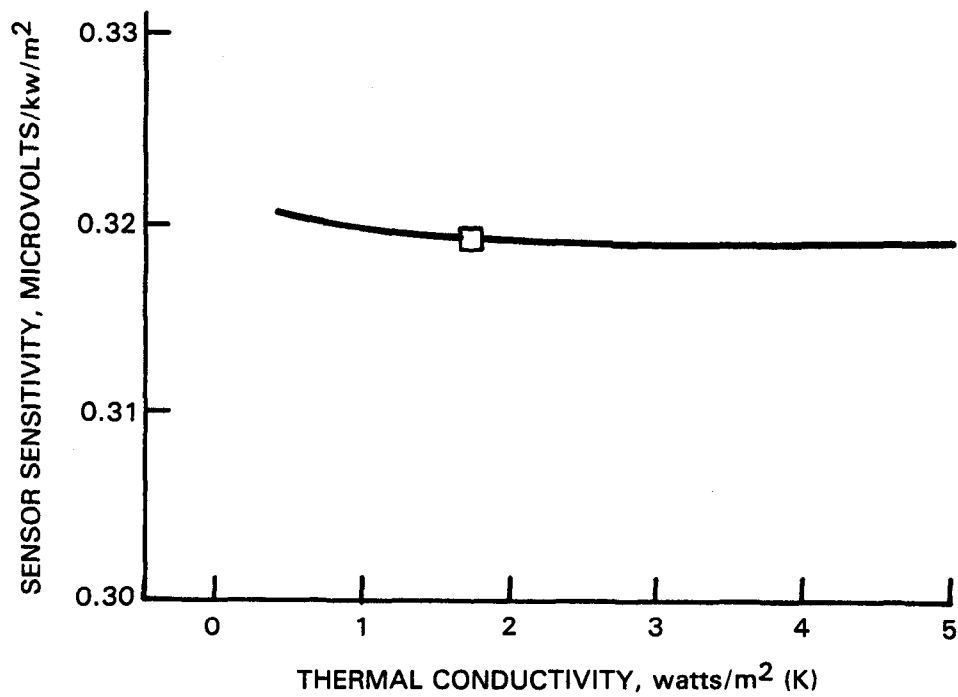
Figure B-10   Calculated Effect of Variation in Thermal Conductivity of Hot
Side Coating Layer on Calculated Sensor Sensitivity

B-3.10 Summary

For most cases of interest, uncertainty in the sensor calibration results will be dominated by any errors in the incident heat flux, sensor output, and absorptance of the sensor hot side coating. Care should be used to determine those parameters accurately. Large variations in the hot side heat transfer coefficient and the sensor reference temperature could yield moderate errors and should be avoided. All other error sources should introduce negligible calibration uncertainty.

B.4.0 ERROR ANALYSIS

Identified below are the symbols to be used in the following discussion.

Q_i = Incident heat flux on the sensor

T_R = Sensor reference temperature

V_T = Sensor output

Q_A = Heat flux absorbed by the sensor

Q_T = Heat flux transmitted through the sensor

Q_R = Heat flux loss from the sensor front face by radiation

Q_C = Heat flux loss from the sensor front face by convection

α = Absorptance of the coating on the sensor

ϵ = Emittance of the coating on the sensor

h = Heat transfer coefficient

S = Sensor sensitivity

T_S = Sensor surface temperature

T_E = Temperature within the quartz lamp bank

k = Thermal conductivity

L = Length of conduction path

σ = Stefan-Boltzmann constant

δx = Uncertainty in x

B-4.1 Formulation of the Problem

The parameters actually measured during sensor calibration are:

Q_i = Incident heat flux on the sensor

T_R = Sensor reference temperature

V_T = Sensor output.

84

We then must calculate

$$Q_A = \alpha Q_i$$

$$Q_T = Q_A - Q_R - Q_C$$

where:

$$Q_R = \varepsilon \sigma \ (T_S^4 - T_E^4)$$

$$Q_C = h \ (T_S - T_E)$$

so:

$$Q_T = \alpha \ Q_i - \varepsilon \sigma \ (T_S^4 - T_E^4) - h \ (T_S - T_E) \qquad \qquad 1$$

and sensitivity = V_T/Q_T but T_S is unknown.

From the conduction equation we find that

$$Q_T = \frac{k}{L} \ (T_S - T_R)$$

and

$$T_S = T_R + \frac{L}{k} \ Q_T.$$

B-4.2 Approximations

It is shown above that

$$T_S = T_R + \frac{L}{k} \ Q_T = T_R + \frac{L}{k} \ (\alpha \ Q_i - Q_R - Q_C).$$

L/k is 0.035 and $Q_R + Q_C <150$. So, to within an accuracy of 5K, we may write:

$$T_S \approx T_R + \frac{L\alpha}{k} \ Q_i$$

and we may substitute that expression into equation 1 to yield

$$Q_T = \alpha \ Q_i - \varepsilon \ \sigma \ [(T_R + \frac{L\alpha}{k} \ Q_i)^4 - T_E^4] - h(T_R + \frac{L\alpha}{k} Q_i - T_E) \ . \qquad \qquad 2$$

T_R, which is 600, is $(L\alpha/k)$ Q_i, which is 31. So we may expand the fourth power expression and save only the two high order terms in T_R to obtain

$$Q_T \approx \alpha Q_i - \epsilon \sigma(T_R^4 - T_E^4) - 3 \epsilon \sigma T_R^3 \frac{L\alpha}{k} Q_i - h (T_R - T_E) - \frac{hL\alpha}{k} Q_i \; .$$

As mentioned earlier, over the ranges of wavelengths and temperatures of interest, the coating used has been shown to have an $\epsilon = \alpha = 0.89$. So we set $\epsilon = \alpha$ to obtain

$$Q_T = \alpha Q_i - \alpha\sigma (T_R^4 - T_E^4) - 3 \alpha\sigma T_R^3 \frac{L\alpha Q_i}{k} - h(T_R - T_E) - \frac{\alpha h L Q_i}{k} \qquad\qquad 3$$

B-4.3 Differentiation

Equation 3 may be differentiated to yield the results shown in Table B-II.

TABLE B-II

RESULTS OF DIFFERENTIATION

$$\partial Q_T / \partial Q_i = \alpha - 3\alpha^2\sigma T_R^3 \frac{L}{k} - \frac{hL\alpha}{k}$$

$$\partial Q_T / \partial \alpha = Q_i - \sigma (T_R^4 - T_E^4) - 6\alpha\sigma T_R^3 \frac{L}{k} Q_i - \frac{hL}{k} Q_i$$

$$\partial Q_T / \partial T_R = -4\alpha\sigma T_R^3 - 9 \alpha^2\sigma T_R^2 \frac{L}{k} Q_i - h$$

$$\partial Q_T / \partial T_E = 4\alpha\sigma T_E^3 + h$$

$$\partial Q_T / \partial h = - T_R + T_E - \frac{L\alpha}{k} Q_i$$

$$\partial Q_T / \partial L = - \frac{3\alpha^2\sigma T_R^3}{k} Q_i - \frac{h\alpha}{k} Q_i$$

$$\partial Q_T / \partial k = \frac{3\alpha^2\sigma T_R^3 L Q_i}{k^2} + \frac{hL\alpha}{k^2} Q_i$$

86

We can now use nominal values to get a feel for the relative size of the various terms in each partial derivative:

$$\alpha = \epsilon = 0.89$$

$$\sigma = 5.67 \times 10^{-11} \text{ kw/m}^2/\text{K}^4$$

$$h = 0.017 \text{ kw/m}^2/\text{K}$$

$$T_E = 394\text{K}$$

T_R in range $600 < T_R < 1200\text{K}$

Q_i in range $200 < Q_i < 800 \text{ kw/m}^2$

$$L/k = \sum_{i \text{ layers}} L_i/k_i \text{ in range } 0.010 < L/k < 0.032$$

0.02 will be used for a nominal value, with $L \approx 0.00058$ m and $k \approx 0.029$ kw/m K.

Using this range of values in each partial,

a) $\quad \partial Q_T/\partial Q_i = \underbrace{\alpha}_{} - 3 \underbrace{\alpha^2 \sigma T_R^3 \frac{L}{k}}_{} - \underbrace{\frac{hL\alpha}{k}}_{}$

magnitudes $\quad$ 0.89 $\quad$ < 0.006 $\quad$ < 0.0004

so $\quad \partial Q_T/\partial Q_i \approx \alpha$.

That indicates that any error in the incident heat flux is directly related to an error in the transmitted heat flux through the absorptance term, α.

b) $\quad \partial Q_T/\partial \alpha = \underbrace{Q_i}_{} - \underbrace{\sigma T_R^4}_{} + \underbrace{\sigma T_E^4}_{} - \underbrace{6\sigma T_R^3 \alpha \frac{L}{k} Q_i}_{} + \underbrace{\frac{hL}{k} Q_i}_{}$

magnitudes $\quad$ 0-1000 $\quad$ 7.5 to 120 $\quad$ < 2 $\quad$ < 11 $\quad$ < 1

so $\quad \partial Q_T/\partial \alpha \approx Q_i - \sigma T_R^4$

Uncertainty in the absorptance is reflected both as uncertainty in the absorbed heat flux and in hot side reradiation correction. The error in the absorbed heat flux depends on the incident heat flux while the uncertainty in the reradiated heat flux depends on the fourth power of the sensor temperature.

c) $\quad \partial Q_T/\partial T_R = \underbrace{-4 \alpha \sigma T_R^3}_{} - \underbrace{9\alpha^2 \sigma T_R^2 \frac{L}{k} Q_i}_{} - \underbrace{h}_{}$

magnitudes $\quad$ 0.044 to 0.35 $\quad$ < 0.01 $\quad$ 0.017

so $\quad \partial Q_T/\partial T_R \approx 4\alpha \sigma T_R^3$

This is independent of Q_i. The size of this term is, however, strongly dependent on the sensor temperature T_R^3. This is because uncertainty in T_R effects accuracy primarily through uncertainty in the hot side reradiation term.

d) $\partial Q_T / \partial T_E = \underbrace{4a\sigma T_E^3}_{} + \underbrace{h}_{}$

  magnitudes   0.013   0.017

so, since these terms are comparable in magnitude,

$$\partial Q_T / \partial T_E = 4a\sigma T_E^3 + h.$$

Uncertainties in the temperature within the quartz lamp bank are reflected as uncertainties in the hot side convection and reradiation losses. Again this is independent of Q_i.

e) $\partial Q_T / \partial h = \underbrace{-T_R}_{} + \underbrace{T_E}_{} - \underbrace{\frac{L\alpha}{k} Q_i}_{}$

  magnitudes   600 to 1200   394   17

so $\partial Q_T / \partial h \approx - (T_R - T_E)$

As would be expected, uncertainly in the hot side heat transfer coefficient is reflected in uncertainty in the transmitted heat flux dependent on the size of the temperature difference between the sensor and the temperature within the quartz lamp bank. Again this is independent of Q_i.

f) $\partial Q_T / \partial L = \underbrace{(-3a\sigma T_R^3}_{} - \underbrace{h)}_{} \frac{Q_i \alpha}{k}$

  magnitudes   0.033 to 0.27   0.017

so $\partial Q_T / \partial L \approx -3 \, a^2 \sigma T_R^3 \, \frac{Q_i}{k}$

An error in the conduction thickness L is propagated to an error in transmitted heat flux through a term containing heat flux multiplied by the third power of the sensor temperature. This is because uncertainty in the conduction length results in an uncertainty in the surface temperature (proportional to Q_i). This results in an uncertainty in the reradiation loss (proportional to T^3).

g) $\partial Q_T / \partial k$ $(3 \, a\sigma T_R^3 + \underbrace{h)}_{} \frac{L\alpha}{k^2} Q_i$

  magnitudes 0.033 to 0.27   0.017

and $\partial Q_T / \partial k \approx 3 \, a^2 \sigma T_R^3 \frac{LQ_i}{k^2}$

88

This is the same general form as the previous terms. Any uncertainty in k is reflected as an uncertainty in the reradiation loss.

B-4.4 Numerical Evaluation

Section B-4.3 indicated that most of the partial derivatives were functions of either heat flux level, sensor temperature level or both. This indicates that there are four cases that should be considered.

Low Temperature - Low Heat Flux
Low Temperature - High Heat Flux
High Temperature - Low Heat Flux
High Temperature - High Heat Flux

The expressions in Table B-II were used to calculate numerical values for these four cases. The results are shown in Table B-III. Our estimate for the uncertainty values of the various parameters are given in Table B-IV. Under the assumption that the errors are random, that is the errors in the various parameters are not correlated, the uncertainty in Q_T may be calculated as:

$$\delta^2 Q_T = \left(\frac{\partial Q_T}{\partial Q_i}\right)^2 \delta^2 Q_i + \left(\frac{\partial Q_T}{\partial \alpha}\right)^2 \delta^2 \alpha + \left(\frac{\partial Q_T}{\delta T_R}\right)^2 \delta^2 T_R + \left(\frac{\partial Q_T}{\partial T_E}\right)^2 \delta^2 T_E + \left(\frac{\partial Q_T}{\partial h}\right)^2 \delta^2 h^2$$

$$+ \left(\frac{\partial Q_T}{\partial L}\right)^2 \delta^2 L + \left(\frac{\partial Q_T}{\partial k}\right)^2 \delta^2 k$$

TABLE B-III

NUMERICAL VALUES OF PARTIAL DERIVATIVES
OF Q TRANSMITTED

| Partial | Units | T_R = 600K | | T_R = 1200K | |
		Q_i = 200 kw/m^2	Q_i = 800 kw/m^2	Q_i = 200 kw/m^2	Q_i = 800 kw/m^2
$\partial Q_T/\partial Q_i$		0.889	0.889	0.885	0.885
$\partial Q_T/\partial \alpha$	(kw/m^2)	194	793	80	673
$\partial Q_T/\partial T_R$	(kw/m^{2}K)	-0.0620	-0.0642	-0.374	-0.381
$\partial Q_T/\partial T_E$	(kw/m^{2}K)	0.0295	0.0295	0.0295	0.0295
$\partial Q_T/\partial h$	(K)	-210	-220	-810	-820
$\partial Q_T/\partial L$	(kw/m^3)	-308	-1250	-1736	-6942
$\partial Q_T/\partial k$	(K/m)	6.16	25.0	34.7	139

TABLE B-IV

UNCERTAINTY VALUES

	$T_R = 600K$		$T_R = 1200K$	
Parameter	$Q_i =$ 200 kw/m^2	$Q_i =$ 800 kw/m^2	$Q_i =$ 200 kw/m^2	$Q_i =$ 800 kw/m^2
δQ_i (kw/m^2) $\pm$(1 percent FS + 1 percent Reading)	12	18	12	18
$\delta \alpha$ $\pm$1 percent low temperature 2 percent high temperature	0.0089	0.0089	0.0178	0.0178
δT_R(K) $\pm$ (5K + 1 percent of value)	11	11	17	17
δT_E(K) ($\pm$50K)	50	50	50	50
δh (kw/m^{2}K) ($\pm$25 percent)	0.00425	0.00425	0.00425	0.00425
δL(m) ($\pm$ 0.012 centimeter)	0.00012	0.00012	0.00012	0.00012
δk (kw/mK) ($\pm$25 percent)	0.00715	0.00715	0.00715	0.00715

The values of each of the uncertainty terms as well as the resulting uncertainty in Q_T is presented in Table B-V.

It can be seen that virtually all error in Q_T is due to three sources. The uncertainty in Q_i is important in all cases. Errors in α become important in high heat flux cases, and errors in T_R become important in high temperature cases. If these sources of scatter were reduced significantly, uncertainty in h could become important in high temperature cases. Uncertainty in T_E, L, and K should introduce insignificant scatter. While the uncertainty in the transmitted heat flux is typically only 1 to 2 percent of the nominal full scale heat flux of 10^6 w/m^2, the uncertainty as a percent of the transmitted heat flux can be quite large especially for the low heat flux-high temperature case where the reradiated heat flux correction is large.

B-4.5 Uncertainty in Output Voltage and Sensor Sensitivity

The transmitted heat flux is then combined with the measured output voltage, V_T, to obtain the sensor sensitivity:

$$S = \frac{V_T}{Q_T} .$$

UNCERTAINTY IN Q_T

Parameter	$T_R = 600K$		$T_R = 1200K$	
	$Q_i =$ 200 kw/m^2	$Q_i =$ 800 kw/m^2	$Q_i =$ 200 kw/m^2	$Q_i =$ 800 kw/m^2
$\left(\dfrac{\partial Q_T}{\partial Q_i}\right)^2 (\delta Q_i)^2 =$	114	256	113	254
$\left(\dfrac{\partial Q_T}{\partial \alpha}\right)^2 (\delta\alpha)^2 =$	3.0	50	2.0	144
$\left(\dfrac{\partial Q_T}{\partial T_R}\right)^2 (\delta T_R)^2 =$	0.46	0.50	40	42
$\left(\dfrac{\partial Q_T}{\partial T_E}\right)^2 (\delta T_E)^2 =$	2.2	2.2	2.2	2.2
$\left(\dfrac{\partial Q_T}{\partial h}\right)^2 (\delta h)^2 =$	0.80	0.87	12	12
$\left(\dfrac{\partial Q_T}{\partial L}\right)^2 (\delta L)^2 =$	-	0.02	0.04	0.69
$\left(\dfrac{\partial Q_T}{\partial k}\right)^2 (\delta k)^2 =$	-	0.03	0.06	0.99
$(\delta Q_T)^2$ (kw/m^2)^2 =	120	309	169	456
δQ_T (kw/m^2) =	11.0	17.6	13.0	21.3
Q_T (kw/m^2) =	169	702	59.2	589
δQ_T (percent of 10^3 kw/m^2) =	1.1	1.8	1.3	2.1
δQ_T (percent of Q_T) =	6.5	2.5	22.0	3.6

This may be differentiated straight forwardly to yield:

$$\delta S = \frac{\partial S}{\partial V_T} \, \delta V_T + \frac{\partial S}{\partial Q_T} \, \delta Q_T$$

$$\delta S = \left(\frac{1}{Q_T}\right) \delta V_T - \left(\frac{V_T}{Q_T^2}\right) \delta Q_T$$

or, dividing by S,

$$\frac{\delta S}{S} = \frac{\delta V_T}{V_T} - \frac{\delta Q_T}{Q_T} \, .$$

Since the uncertainty in Q_T and V_T are independent, this may be squared and the cross terms eliminated to yield:

$$\left(\frac{\delta S}{S}\right)^2 = \left(\frac{\delta V_T}{V_T}\right)^2 + \left(\frac{\delta Q_T}{Q_T}\right)^2 \, .$$

That is, the present uncertainty in the sensor sensitivity can be determined by quadrature summing the percent uncertainty in the transmitted heat flux during calibration with percent uncertainty in the measured sensor output voltage. The uncertainty δV_T in the sensor output voltage is estimated to be $\pm$ (4 microvolts + 1 percent of reading).

Since the output will be different for the different sensor types, the importance of the voltage uncertainty will also be different for the different sensor types. Table B-VI combines the voltage uncertainty with the uncertainty in Q_T obtained from Table B-V to obtain the total uncertainty in sensor sensitivity.

B-4.6 Comparison With Calibration Results

Qualitatively, the calibration results agree reasonably well with the results predicted from the error analysis. The laminated sensors showed more scatter than the other two sensor types, and the data scatter was generally greater at high sensor temperature. Quantitatively, however, the data showed more scatter than was predicted by the error analysis. A portion of this additional scatter may be due to the lead wire problems discussed in the body of the report. In addition, a review of the sensor calibration procedure is currently under way to identify any changes in equipment or procedures that would reduce data scatter.

TABLE B-VI

UNCERTAINTY IN OUTPUT VOLTAGE AND SENSOR SENSITIVITY

Parameter	T_R = 600K		T_R = 1200K	
	Q_i = 200 kw/m^2	Q_i = 800 kw/m^2	Q_i = 200 kw/m^2	Q_i = 800 kw/m^2
Q_T (kw/m^2)	169	702	59.2	589
δQ_T kw/m^2	11.0	17.6	13.0	21.3
δQ_T (percent of Q_T)	6.5	2.5	22.0	3.6
Nominal Output V_T (Microvolts)				
Embedded Thermocouples $S \approx 1.5$ $\mu v/(kw/m^2)$	254	1053	89	884
Laminated Sensor $S \approx 0.3$ $\mu v/(kw/m^2)$	51	211	18	177
Gardon Gauge $S \approx 1.0$ $\mu v/(kw/m^2)$	169	702	59	589
δV_T (Microvolts)				
Embedded Thermocouples	7	15	5	13
Laminated Sensor	5	6	4	6
Gardon Gauge	6	11	5	10
δV_T (percent of V_T)				
Embedded Thermocouples	2.8	1.4	5.6	1.5
Laminated Sensor	9.8	2.8	22.2	3.4
Gardon Gauge	3.6	1.6	8.5	1.7
δS (percent of S)				
Embedded Thermocouples	7.1	2.9	22.7	3.9
Laminated Sensor	11.8	3.8	31.3	5.0
Gardon Gauge	7.4	3.0	23.6	4.0

APPENDIX C

CALIBRATION DATA

Embedded Thermocouple Sensors

This Appendix presents the calibration data from embedded thermocouple sensors T-1 through T-7 and D-1 through D-4. The remaining embedded thermocouple sensors experienced failures during construction or installation before calibration data were obtained. All data for the sensors are presented although some of the high temperature, low heat flux points exhibit a large amount of scatter and are not representative of realistic operating conditions. The data for each sensor are presented in tabular form, as a plot of sensor microvolt output versus heat flux transmitted through the sensor, and as a plot of percent heat flux deviation versus sensor reference temperature. The heat flux transmitted values were calculated from incident heat flux measurements by accounting for absorption and losses from reradiation and convection. The percent heat flux deviation is the deviation of actual sensor output from the best straight line fit of the data through the origin expressed as a percent of the nominal maximum design heat flux of one megawatt per square meter.

Files T-2-A and D-3-A are sensor calibrations after the fifty hour thermal soak tests, and in both cases the sensor output was found to be low and erratic due to secondary junctions in the leadwires.

For each of the sensors, a sensor calibration constant was determined based on a least square line forced through the origin of the microvolt output versus heat flux transmitted plot. This value is presented below the tabular data. When the sensor is in operation, the heat flux is determined by the equation:

$$Q_{measured} = \frac{1}{sensitivity} \times microvolt\ output.$$

TABLE C-I

CALIBRATION RESULTS FOR EMBEDDED THERMOCOUPLE SENSOR T-1

Q TRANSMITTED KILOWATTS/M**2	T REFERENCE KELVIN	OUTPUT MICROVOLTS	SENSITIVITY OUTPUT/UNIT Q
587.76	1185.	928.	1.578
110.38	468.	186.	1.685
168.64	559.	271.	1.606
251.13	695.	409.	1.628
347.61	865.	589.	1.694
507.29	1104.	851.	1.677
585.99	1180.	947.	1.616
575.74	1208.	922.	1.601
471.39	1212.	742.	1.574
271.07	1207.	472.	1.741
149.53	1212.	271.	1.812
71.65	1170.	128.	1.786
277.11	1199.	415.	1.497
311.40	1093.	475.	1.525
354.94	887.	519.	1.462
371.81	745.	509.	1.368
375.19	707.	510.	1.359
272.57	1206.	399.	1.463
272.62	1207.	392.	1.437
577.03	1201.	829.	1.436
501.94	1110.	741.	1.476
347.90	901.	513.	1.474
249.34	728.	346.	1.387
169.79	587.	243.	1.431
107.45	482.	206.	1.917
268.85	1205.	379.	1.409
270.23	1208.	380.	1.406
269.04	1209.	379.	1.408
567.71	1208.	819.	1.442
492.33	1117.	721.	1.464
346.24	902.	506.	1.461
246.13	738.	344.	1.397
168.48	603.	239.	1.418
106.86	496.	197.	1.843
572.35	1201.	839.	1.465
491.80	1127.	740.	1.504
338.83	903.	510.	1.505
244.94	742.	347.	1.416
166.85	599.	246.	1.474
105.71	487.	199.	1.882

SENSOR CALIBRATION CONSTANT
BASED ON LEAST SQUARE LINE FORCED THROUGH ORIGIN OF OUTPUT VS. HEAT FLUX

S= 1.51   MICROVOLTS/KILOWATT/M**2

IN USE Q MEASURED = OUTPUT/S

Figure C-1   Voltage Output versus Heat Flux Transmitted through Embedded
Thermocouple Sensor T-1

Figure C-2   Heat Flux Deviation versus Sensor Reference Temperature for
Embedded Thermocouple Sensor T-1

TABLE C-II

CALIBRATION RESULTS FOR EMBEDDED THERMOCOUPLE SENSORS T-2 AND T-2A

Q TRANSMITTED KILOWATTS/M**2	T REFERENCE KELVIN	OUTPUT MICROVOLTS	SENSITIVITY OUTPUT/UNIT Q
570.28	1202.	709.	1.243
483.88	1106.	633.	1.308
342.99	882.	477.	1.390
241.37	700.	325.	1.346
167.37	572.	193.	1.153
454.59	1208.	504.	1.108
263.70	1206.	276.	1.046
142.21	1209.	101.	.710
72.53	1159.	45.	.620
566.65	1199.	558.	.984
111.22	533.	162.	1.456
237.38	779.	376.	1.583
164.71	635.	264.	1.602
592.48	1123.	626.	1.056
574.91	1173.	571.	.993
569.98	1182.	560.	.982
563.37	1190.	542.	.962
556.14	1204.	516.	.927
568.74	1167.	552.	.970
564.72	1183.	527.	.933
111.22	533.	162.	1.456
237.38	779.	376.	1.583
164.71	635.	264.	1.602

SENSOR CALIBRATION CONSTANT
BASED ON LEAST SQUARE LINE FORCED THROUGH ORIGIN OF OUTPUT VS. HEAT FLUX

S= 1.11   MICROVOLTS/KILOWATT/M**2

IN USE Q MEASURED = OUTPUT/S

NASA HEAT FLUX SENSOR CALIBRATION RESULTS

SENSOR SERIAL NUMBER T-2-A
AFTER   50 HOUR THERMAL SOAK

Q TRANSMITTED KILOWATTS/M**2	T REFERENCE KELVIN	OUTPUT MICROVOLTS	SENSITIVITY OUTPUT/UNIT Q
291.38	1140.	101.	.346
293.25	1148.	162.	.552
571.89	1174.	111.	.194
468.07	1047.	1655.	3.535
354.01	875.	204.	.576
218.79	645.	1155.	5.278
218.63	650.	1138.	5.205

SENSOR CALIBRATION CONSTANT
BASED ON LEAST SQUARE LINE FORCED THROUGH ORIGIN OF OUTPUT VS. HEAT FLUX

S= 1.87   MICROVOLTS/KILOWATT/M**2

The output of the sensor was found to be erratic in the Post Test Calibration after the 50 hour Thermal Ageing Test. This was found to be due to secondary junctions in the leadwire external to the sensor. The Post Test Calibration Data is not presented in Plot Form.

98

Figure C-3   Voltage Output versus Heat Flux Transmitted through Embedded Thermocouple Sensor T-2

Figure C-4   Heat Flux Deviation versus Sensor Reference Temperature for Embedded Thermocouple Sensor T-2

TABLE C-III

CALIBRATION RESULTS FOR EMBEDDED THERMOCOUPLE SENSOR T-3

Q TRANSMITTED KILOWATTS/M**2	T REFERENCE KELVIN	OUTPUT MICROVOLTS	SENSITIVITY OUTPUT/UNIT Q
100.85	489.	185.	1.834
139.36	1207.	201.	1.442
141.15	1203.	198.	1.402
142.40	1199.	204.	1.432
143.94	1198.	202.	1.403
146.40	1203.	214.	1.461
150.62	1207.	218.	1.447
563.30	1204.	744.	1.320
484.84	1088.	639.	1.317
340.82	871.	470.	1.378
242.70	702.	329.	1.355
167.36	577.	221.	1.320
110.82	484.	137.	1.236
567.91	1202.	765.	1.347
432.80	1203.	593.	1.370
257.76	1202.	344.	1.334
142.53	1202.	131.	.919
318.40	971.	534.	1.677
551.14	1201.	843.	1.529
466.03	1088.	725.	1.555
464.26	1089.	724.	1.559
338.46	888.	550.	1.624
234.79	717.	370.	1.575
161.14	584.	241.	1.495
101.38	477.	139.	1.370
396.55	1203.	595.	1.500

SENSOR CALIBRATION CONSTANT
BASED ON LEAST SQUARE LINE FORCED THROUGH ORIGIN OF OUTPUT VS. HEAT FLUX

$$S = 1.43 \quad MICROVOLTS/KILOWATT/M**2$$

$$IN \ USE \ Q \ MEASURED = OUTPUT/S$$

This Data represents two separate calibrations. The first 17 points were the initial calibration, and it was found that some of the Zynolite Coating had peeled off during the Calibration. The Sensor was recoated and a recalibration produced the additional 9 points. The sensor was then installed in the Vacuum Calibration Facility and experienced a thermocouple failure. The failure was found to be in the Leadwire External to the Sensor, and is believed to be due to vibration of the leadwires by the cooling air.
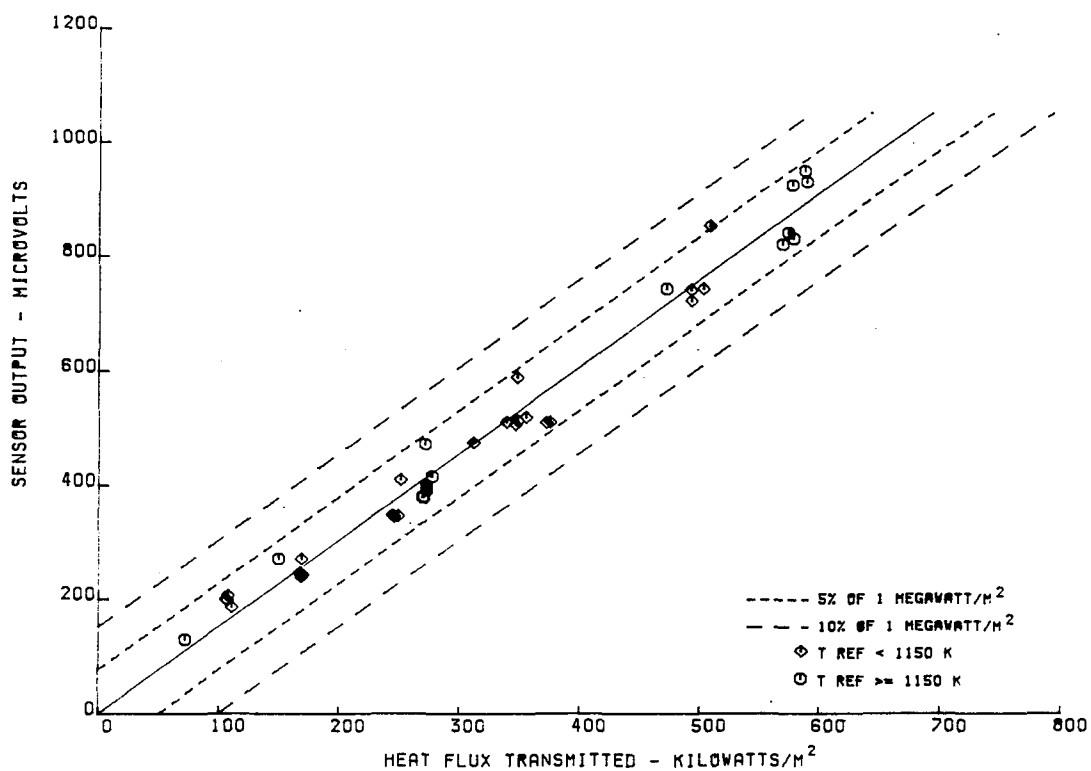
100

Figure C-5   Voltage Output versus Heat Flux Transmitted through Embedded
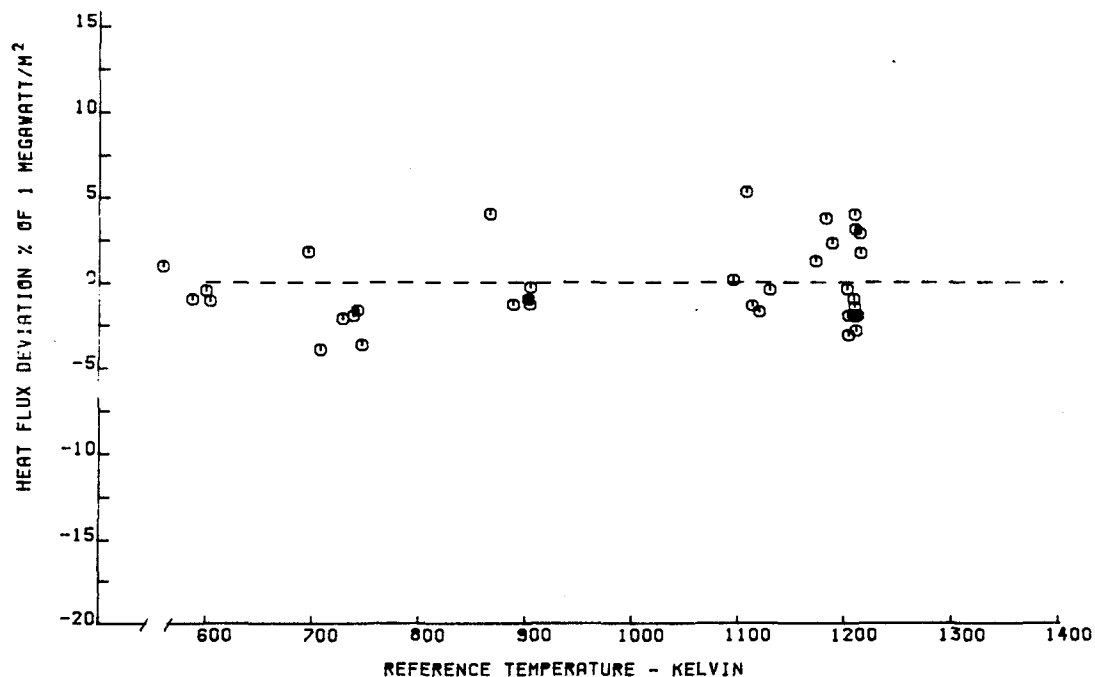Thermocouple Sensor T-3

Figure C-6   Heat Flux Deviation versus Sensor Reference Temperature for
Embedded Thermocouple Sensor T-3

TABLE C-IV

CALIBRATION RESULTS FOR EMBEDDED THERMOCOUPLE SENSOR T-4

Q TRANSMITTED KILOWATTS/M**2	T REFERENCE KELVIN	OUTPUT MICROVOLTS	SENSITIVITY OUTPUT/UNIT Q
652.15	1152.	1139.	1.746
643.25	1160.	1106.	1.719

SENSOR CALIBRATION CONSTANT
BASED ON LEAST SQUARE LINE FORCED THROUGH ORIGIN OF OUTPUT VS. HEAT FLUX

S= 1.73   MICROVOLTS/KILOWATT/M**2

IN USE Q MEASURED = OUTPUT/S

The hot side thermocouple failed after the 2nd point of the initial calibration. The failure was found to be in the leadwire external to the sensor, and is believed to be due to vibration of the leadwire by the cooling air.

Figure C-7   Voltage Output versus Heat Flux Transmitted through Embedded
             Thermocouple Sensor T-4

Figure C-8   Heat Flux Deviation versus Sensor Reference Temperature for
             Embedded Thermocouple Sensor T-4

103

TABLE C-V

CALIBRATION RESULTS FOR EMBEDDED THERMOCOUPLE SENSOR T-5

Q TRANSMITTED KILOWATTS/M**2	T REFERENCE KELVIN	OUTPUT MICROVOLTS	SENSITIVITY OUTPUT/UNIT Q
631.87	1202.	788.	1.247
523.27	1077.	653.	1.247
381.10	883.	481.	1.262
217.57	617.	267.	1.227
635.32	1199.	760.	1.196
488.89	1203.	595.	1.217
305.83	1199.	368.	1.203
118.43	1207.	125.	1.055
635.87	1204.	798.	1.254

SENSOR CALIBRATION CONSTANT
BASED ON LEAST SQUARE LINE FORCED THROUGH ORIGIN OF OUTPUT VS. HEAT FLUX

S= 1.22 MICROVOLTS/KILOWATT/M**2
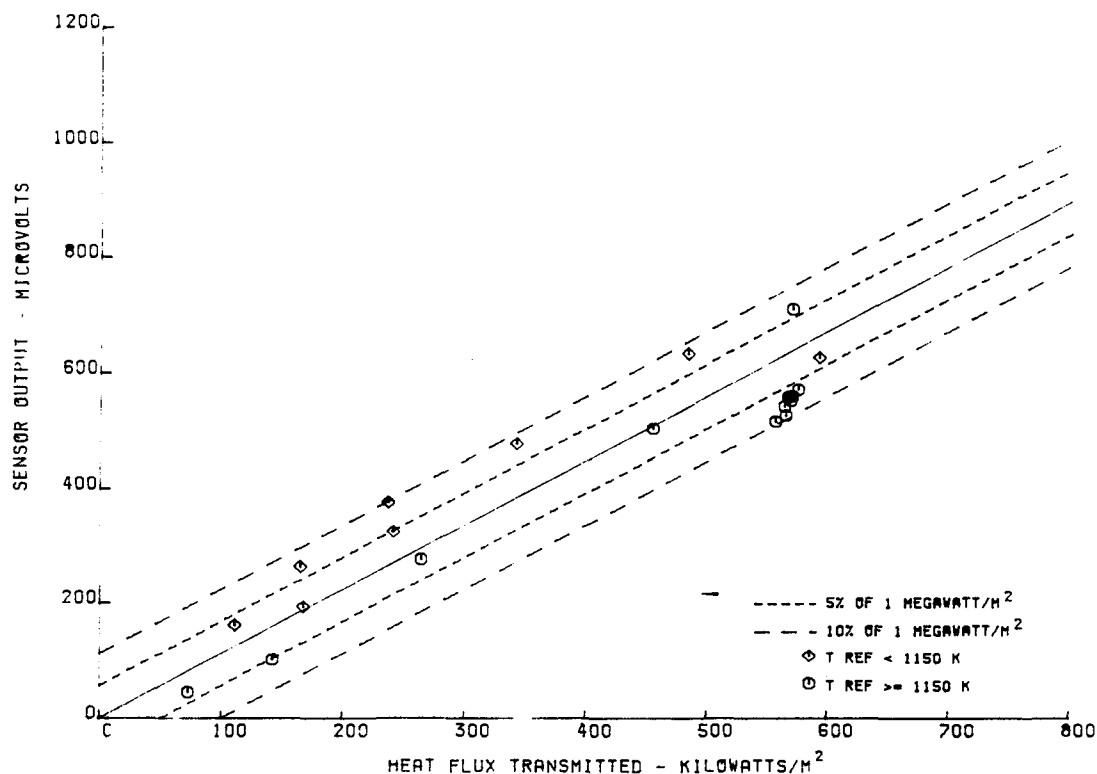
IN USE Q MEASURED = OUTPUT/S

Figure C-9   Voltage Output versus Heat Flux Transmitted through Embedded Thermocouple Sensor T-5

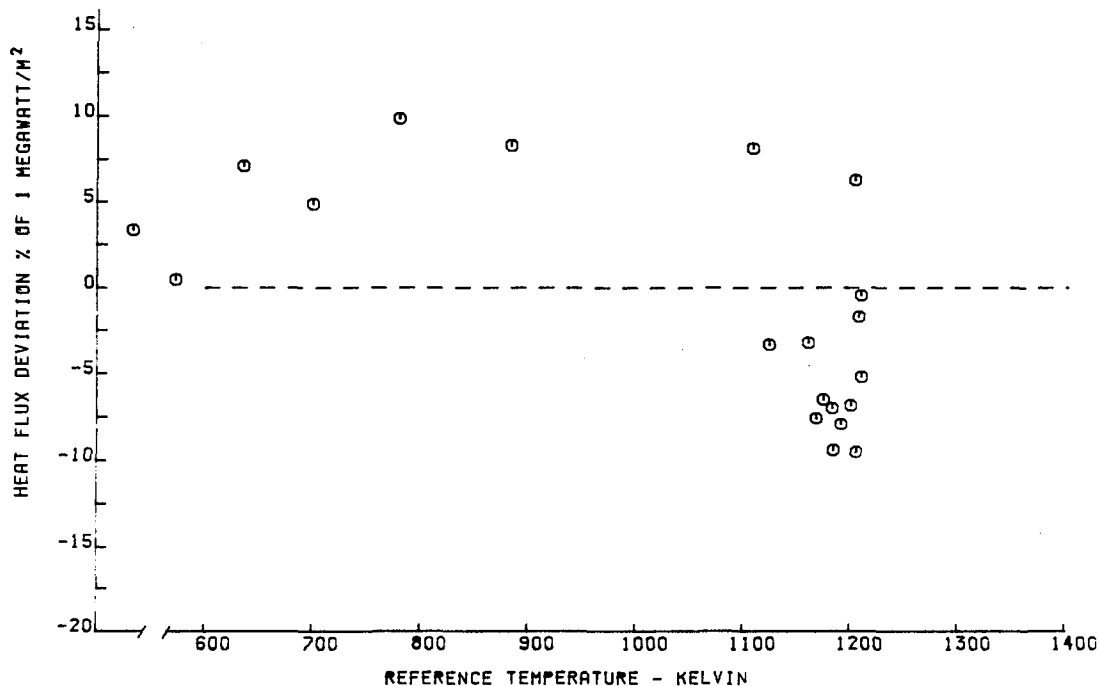**Figure C-10**   Heat Flux Deviation versus Sensor Reference Temperature for Embedded Thermocouple Sensor T-5

TABLE C-VI

CALIBRATION RESULTS FOR EMBEDDED THERMOCOUPLE SENSOR T-6

Q TRANSMITTED KILOWATTS/M**2	T REFERENCE KELVIN	OUTPUT MICROVOLTS	SENSITIVITY OUTPUT/UNIT Q
206.78	1179.	213.	1.030
199.46	1199.	243.	1.218
201.42	1198.	273.	1.355
201.25	1198.	316.	1.570
202.14	1196.	325.	1.607
200.64	1196.	315.	1.569
200.54	1196.	324.	1.615
202.48	1194.	312.	1.540

SENSOR CALIBRATION CONSTANT
BASED ON LEAST SQUARE LINE FORCED THROUGH ORIGIN OF OUTPUT VS. HEAT FLUX

S= 1.43   MICROVOLTS/KILOWATT/M**2

IN USE Q MEASURED = OUTPUT/S

The hot side thermocouple failed after the 9th point of the initial calibration. Post test analysis indicated that the failure was internal to the sensor.

Figure C-11   Voltage Output versus Heat Flux Transmitted through Embedded Thermocouple Sensor T-6

Figure C-12   Heat Flux Deviation versus Sensor Reference Temperature for Embedded Thermocouple Sensor T-6

TABLE C-VII

CALIBRATION RESULTS FOR EMBEDDED THERMOCOUPLE SENSOR T-7

Q TRANSMITTED KILOWATTS/M**2	T REFERENCE KELVIN	OUTPUT MICROVOLTS	SENSITIVITY OUTPUT/UNIT Q
236.07	560.	363.	1.537
143.17	1144.	155.	1.082
138.94	1163.	170.	1.223
141.51	1158.	173.	1.222
142.50	1155.	170.	1.192
630.42	1172.	836.	1.326
518.17	1048.	718.	1.385
375.16	858.	534.	1.423
222.75	614.	321.	1.441
631.98	1164.	837.	1.324
482.02	1175.	656.	1.360
126.32	1167.	159.	1.258

SENSOR CALIBRATION CONSTANT
BASED ON LEAST SQUARE LINE FORCED THROUGH ORIGIN OF OUTPUT VS. HEAT FLUX

S= 1.34 MICROVOLTS/KILOWATT/M**2

IN USE Q MEASURED = OUTPUT/S

During the initial calibration of this sensor the Chromel lead of the hot side thermocouple failed. The calibration was continued and the cold side reference temperature was used for data reduction. After test the failure was determined to be in the HARCO block and the leadwire was repaired.
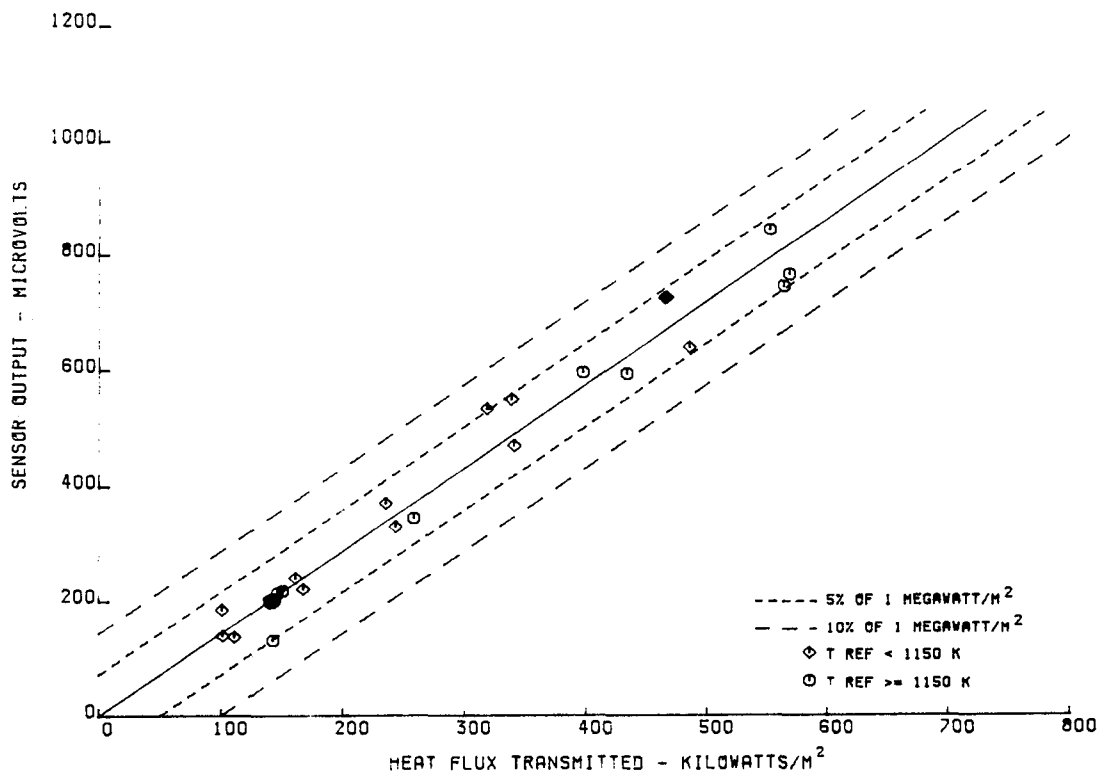
Figure C-13   Voltage Output versus Heat Flux Transmitted through Embedded Thermocouple Sensor T-7
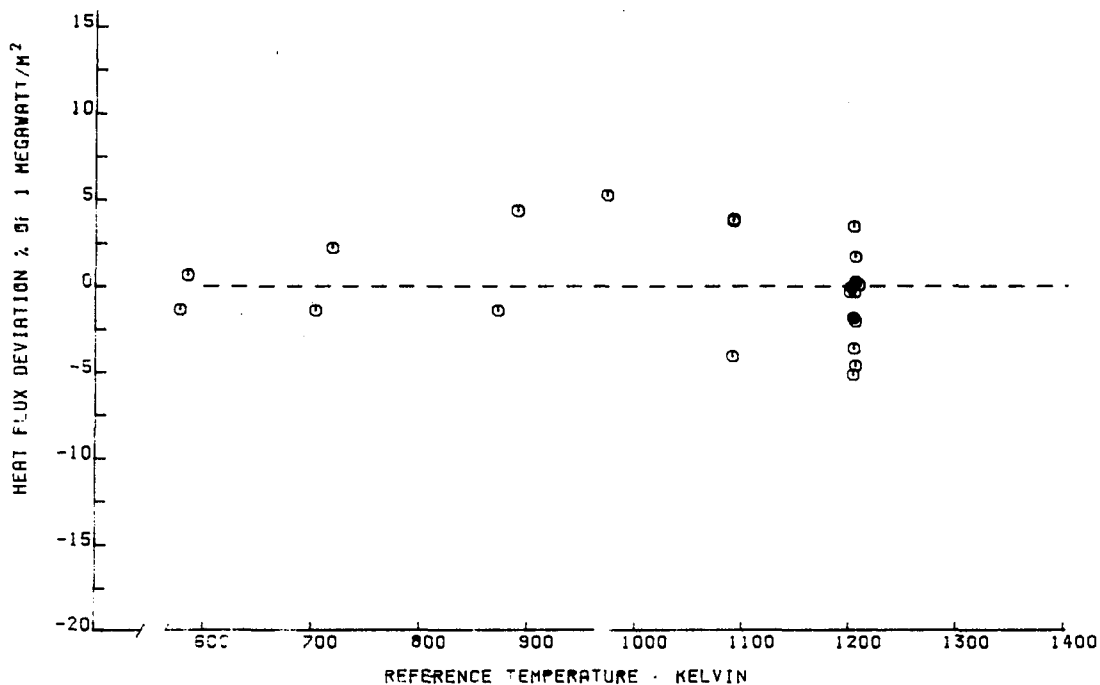

Figure C-14   Heat Flux Deviation versus Sensor Reference Temperature for Embedded Thermocouple Sensor T-7

TABLE C-VIII

CALIBRATION RESULTS FOR EMBEDDED THERMOCOUPLE SENSOR D-1

Q TRANSMITTED KILOWATTS/M**2	T REFERENCE KELVIN	OUTPUT MICROVOLTS	SENSITIVITY OUTPUT/UNIT Q
204.05	1175.	285.	1.396
203.96	1173.	276.	1.353
205.52	1172.	276.	1.342
205.62	1176.	288.	1.400
205.51	1177.	276.	1.342
630.54	1178.	817.	1.295
515.69	1028.	680.	1.318
377.45	850.	481.	1.274
222.99	607.	271.	1.215
622.59	1177.	811.	1.302
296.65	1177.	372.	1.253
480.27	1177.	638.	1.328
116.12	1179.	141.	1.214

SENSOR CALIBRATION CONSTANT
BASED ON LEAST SQUARE LINE FORCED THROUGH ORIGIN OF OUTPUT VS. HEAT FLUX

S= 1.3 MICROVOLTS/KILOWATT/M**2
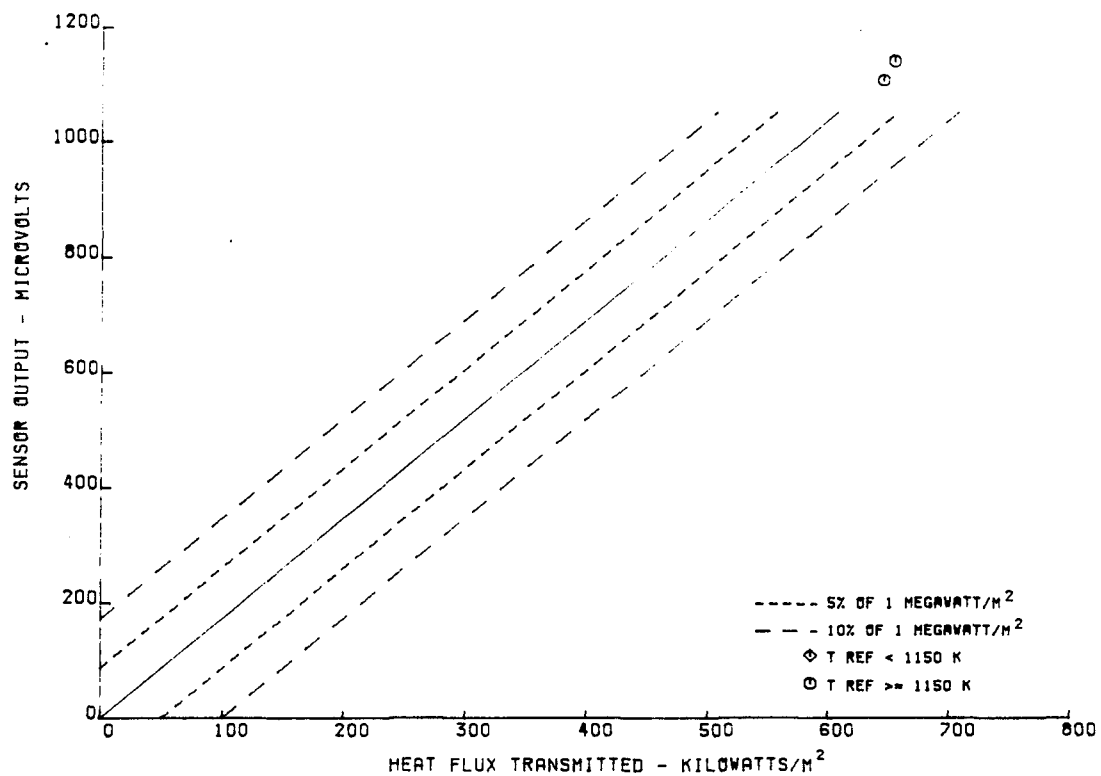
IN USE Q MEASURED = OUTPUT/S

Figure C-15   Voltage Output versus Heat Flux Transmitted through Embedded Thermocouple Sensor D-1
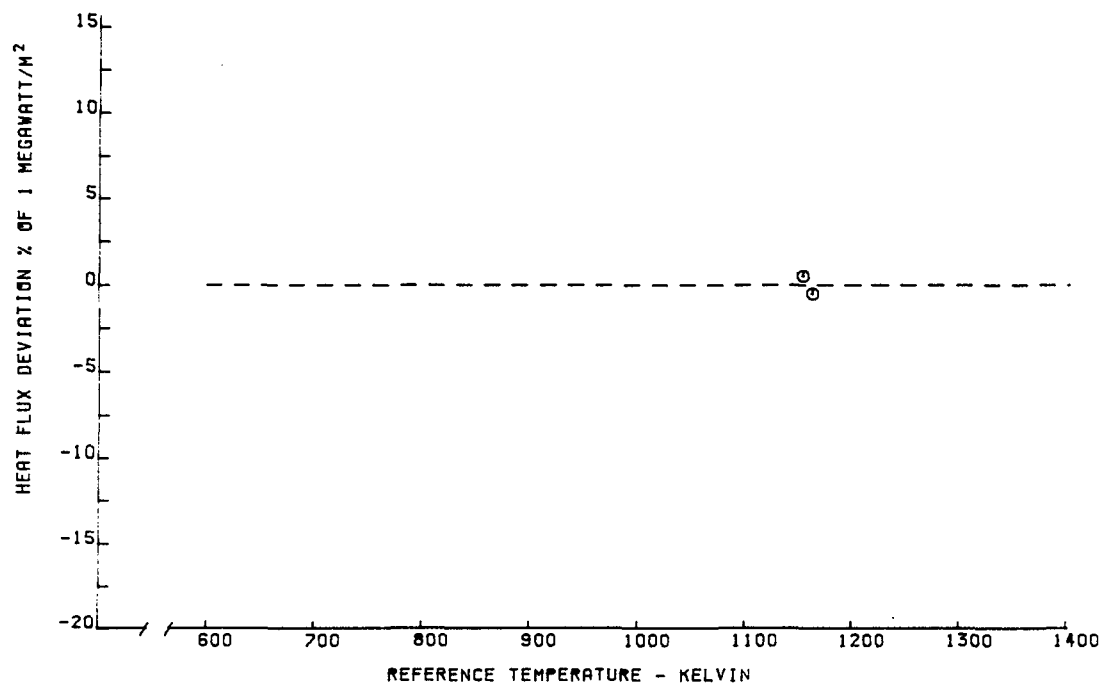

Figure C-16   Heat Flux Deviation versus Sensor Reference Temperature for Embedded Thermocouple Sensor D-1

TABLE C-IX

CALIBRATION RESULTS FOR EMBEDDED THERMOCOUPLE SENSOR D-2

Q TRANSMITTED KILOWATTS/M**2	T REFERENCE KELVIN	OUTPUT MICROVOLTS	SENSITIVITY OUTPUT/UNIT Q
291.22	729.	532.	1.826
202.53	1176.	322.	1.589
206.52	1169.	321.	1.554
205.93	1168.	317.	1.539
207.48	1165.	321.	1.547
620.42	1177.	1004.	1.618

SENSOR CALIBRATION CONSTANT
BASED ON LEAST SQUARE LINE FORCED THROUGH ORIGIN OF OUTPUT VS. HEAT FLUX

S= 1.62   MICROVOLTS/KILOWATT/M**2

IN USE Q MEASURED = OUTPUT/S

The hot side thermocouple failed after the 5th point of the initial calibration. The failure was found to be broken lead wire at the point where the leadwire exits the sensor, and is believed to be caused by vibration of the leadwire by the cooling air.
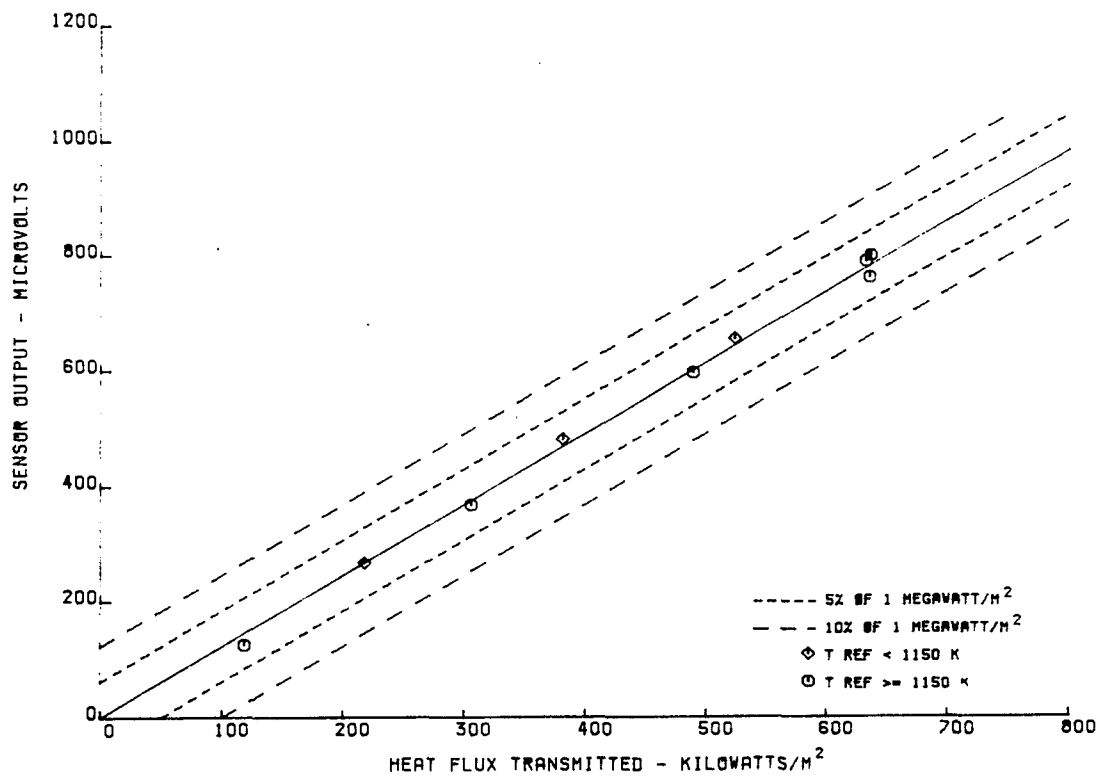
Figure C-17   Voltage Output versus Heat Flux Transmitted through Embedded
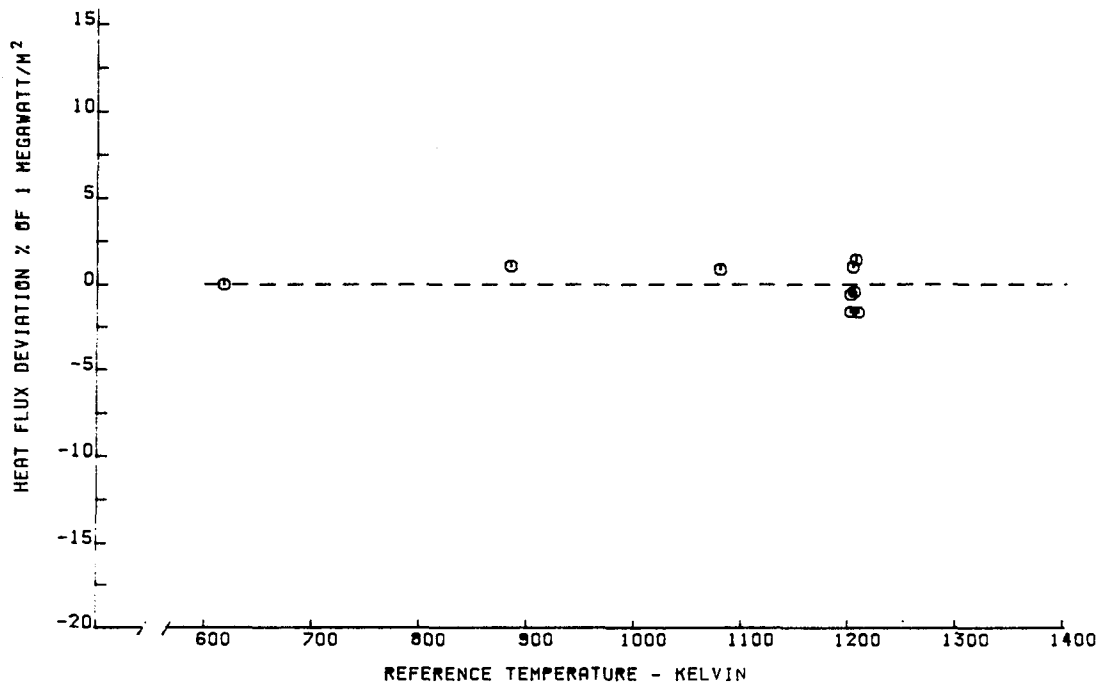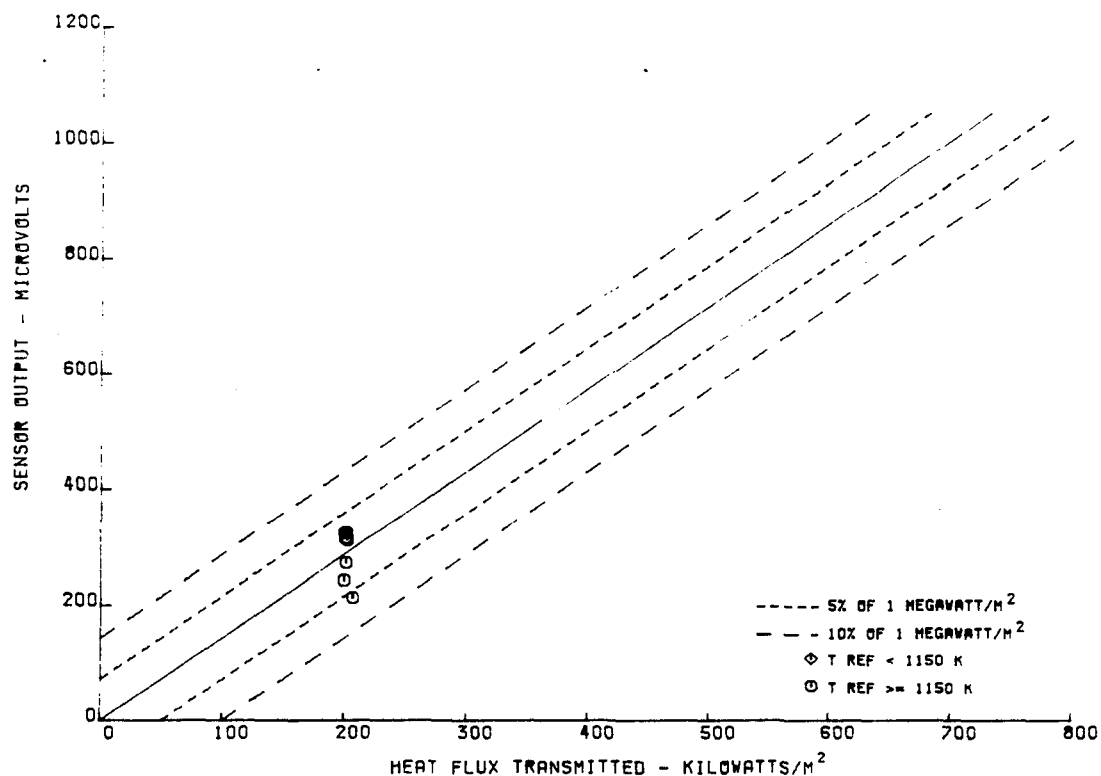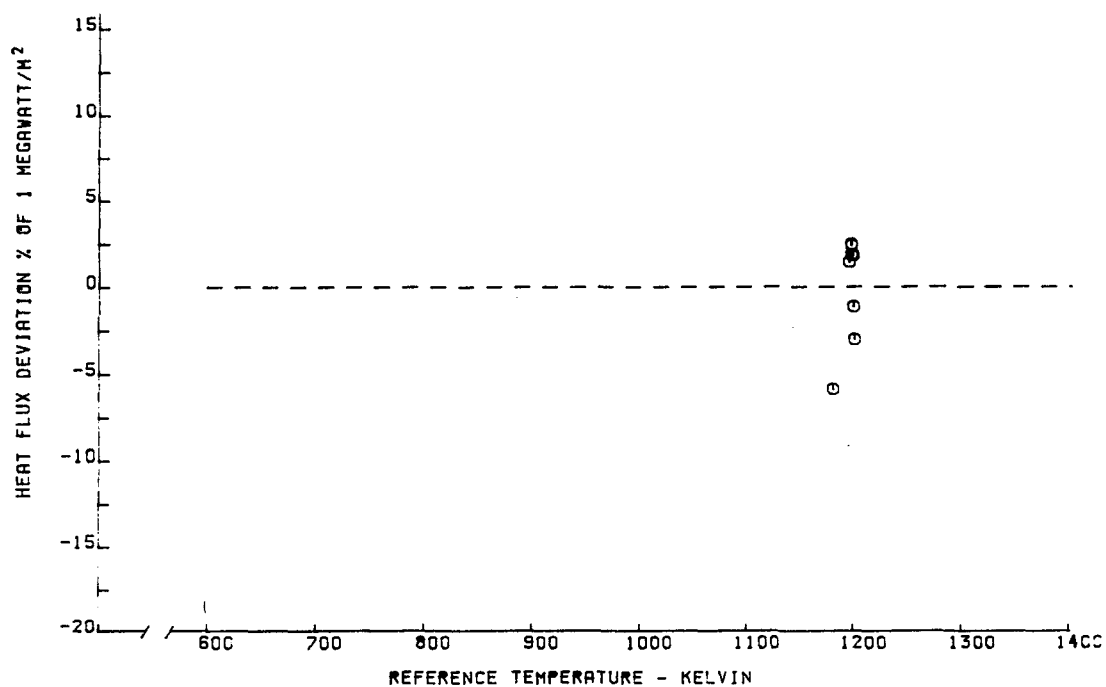Thermocouple Sensor D-2

Figure C-18   Heat Flux Deviation versus Sensor Reference Temperature for
Embedded Thermocouple Sensor D-2

113

TABLE C-X

CALIBRATION RESULTS FOR EMBEDDED THERMOCOUPLE SENSORS D-3 AND D-3A

Q TRANSMITTED KILOWATTS/M**2	T REFERENCE KELVIN	OUTPUT MICROVOLTS	SENSITIVITY OUTPUT/UNIT Q
197.53	856.	411.	2.080
127.63	1167.	251.	1.966
119.15	1168.	233.	1.955
129.19	1169.	207.	1.602
131.37	1164.	186.	1.415
130.96	1169.	178.	1.359
131.96	1164.	173.	1.310
131.32	1166.	176.	1.340
132.00	1164.	175.	1.325
625.18	1172.	1012.	1.618
518.98	1068.	919.	1.770
378.92	891.	740.	1.952
219.69	635.	337.	1.533
622.25	1178.	1003.	1.611
480.51	1172.	745.	1.550
309.11	1173.	436.	1.410
124.82	1174.	133.	1.065
318.41	1170.	427.	1.341
383.13	897.	757.	1.975

SENSOR CALIBRATION CONSTANT
BASED ON LEAST SQUARE LINE FORCED THROUGH ORIGIN OF OUTPUT VS. HEAT FLUX

S= 1.63   MICROVOLTS/KILOWATT/M**2

IN USE Q MEASURED = OUTPUT/S

NASA HEAT FLUX SENSOR CALIBRATION RESULTS

SENSOR SERIAL NUMBER D-3-A
AFTER 50 HOUR THERMAL SOAK

Q TRANSMITTED KILOWATTS/M**2	T REFERENCE KELVIN	OUTPUT MICROVOLTS	SENSITIVITY OUTPUT/UNIT Q
569.91	1171.	560.	.982
463.95	1053.	678.	1.461
351.48	875.	658.	1.872
214.99	670.	68.	.316
570.44	1172.	582.	1.020
433.30	1166.	311.	.717
285.48	1170.	21.	.073
133.53	1151.	179.	1.340

SENSOR CALIBRATION CONSTANT
BASED ON LEAST SQUARE LINE FORCED THROUGH ORIGIN OF OUTPUT VS. HEAT FLUX

S= 1.01   MICROVOLTS/KILOWATT/M**2

The output of the Sensor was found to be erratic in the Post Test Calibration after the 50 hour Thermal Ageing Test. This was found to be due to Secondary Junctions in the Leadwire External to the Sensor. The Post Test Calibration Data is not Presented in Plot Form.
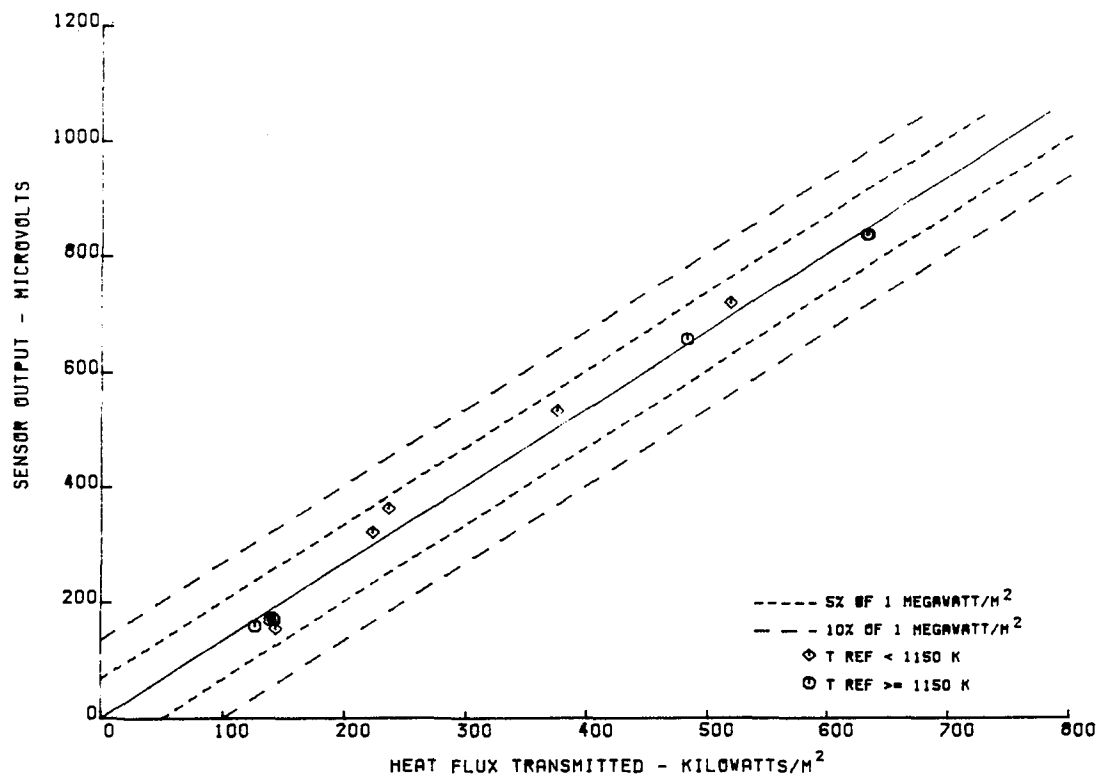
Figure C-19   Voltage Output versus Heat Flux Transmitted through Embedded
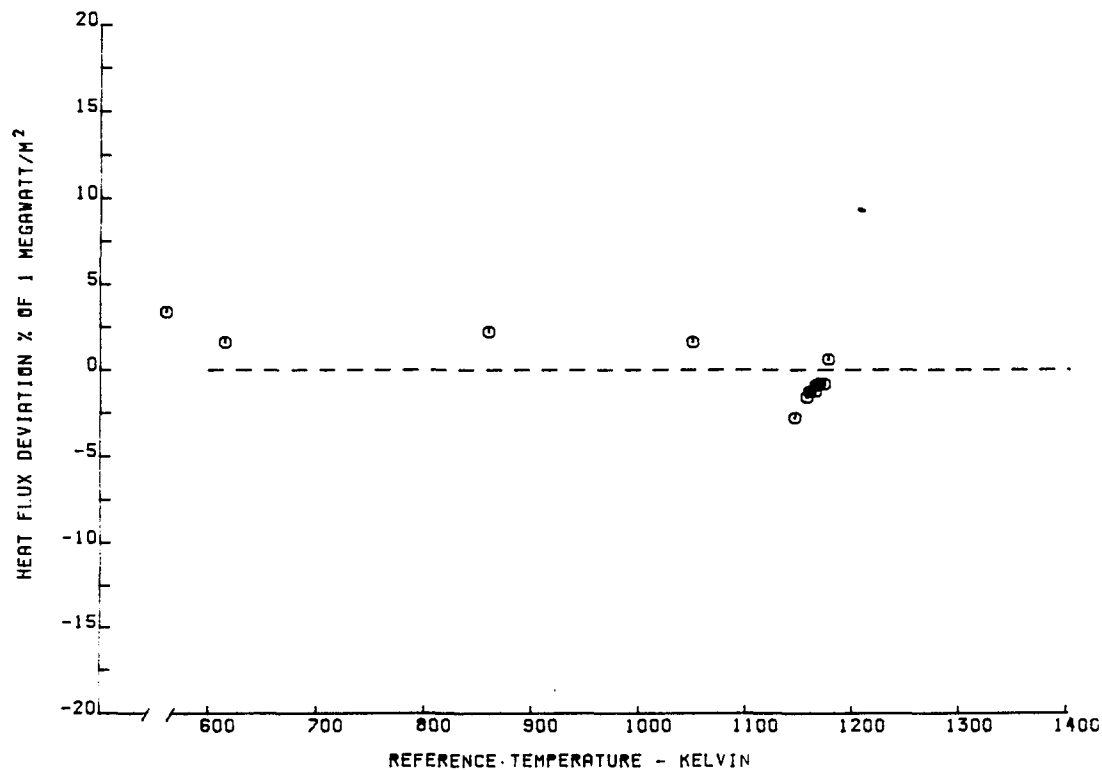   Thermocouple Sensor D-3

Figure C-20   Heat Flux Deviation versus Sensor Reference Temperature for
               Embedded Thermocouple Sensor D-3

115
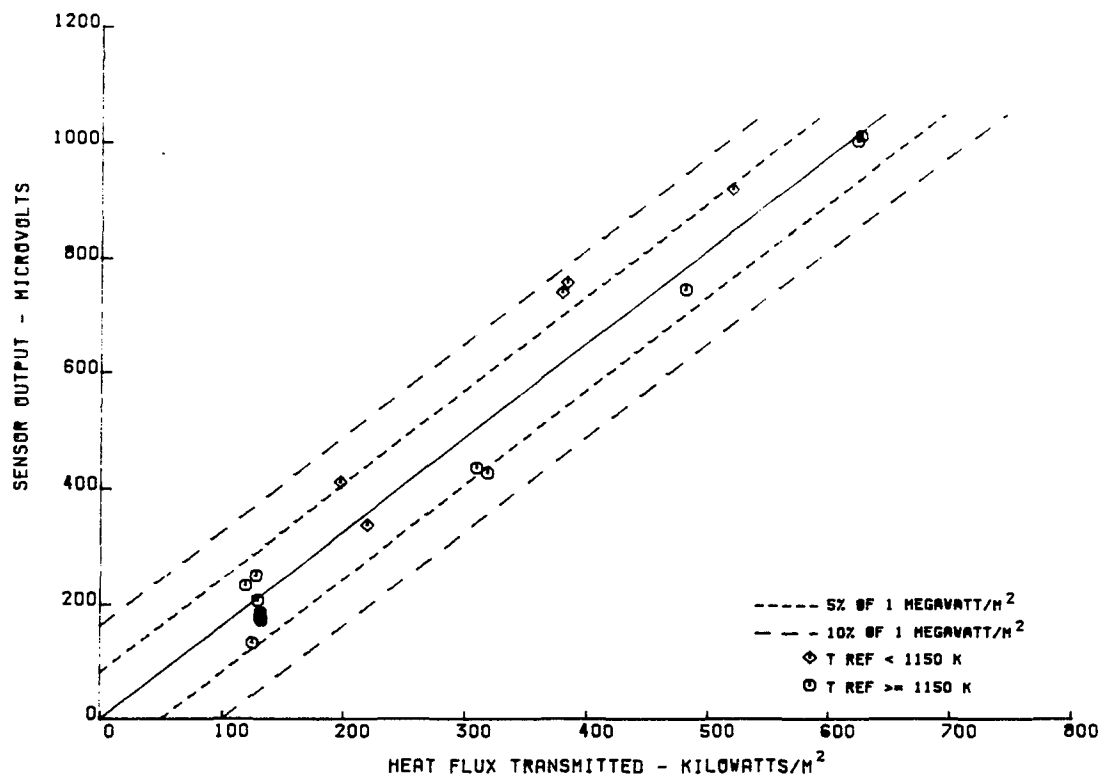
TABLE C-XI

CALIBRATION RESULTS FOR EMBEDDED THERMOCOUPLE SENSOR D-4

Q TRANSMITTED KILOWATTS/M**2	T REFERENCE KELVIN	OUTPUT MICROVOLTS	SENSITIVITY OUTPUT/UNIT Q
177.64	965.	278.	1.564
124.66	1173.	177.	1.419
128.23	1163.	189.	1.473
127.98	1163.	194.	1.515
128.01	1161.	190.	1.484
617.36	1173.	891.	1.443
515.16	1047.	763.	1.481
381.72	867.	566.	1.482
219.83	608.	285.	1.296
625.81	1155.	881.	1.407
479.19	1177.	670.	1.398
299.45	1180.	422.	1.409
123.18	1174.	158.	1.282

SENSOR CALIBRATION CONSTANT
BASED ON LEAST SQUARE LINE FORCED THROUGH ORIGIN OF OUTPUT VS. HEAT FLUX

S= 1.43   MICROVOLTS/KILOWATT/M**2
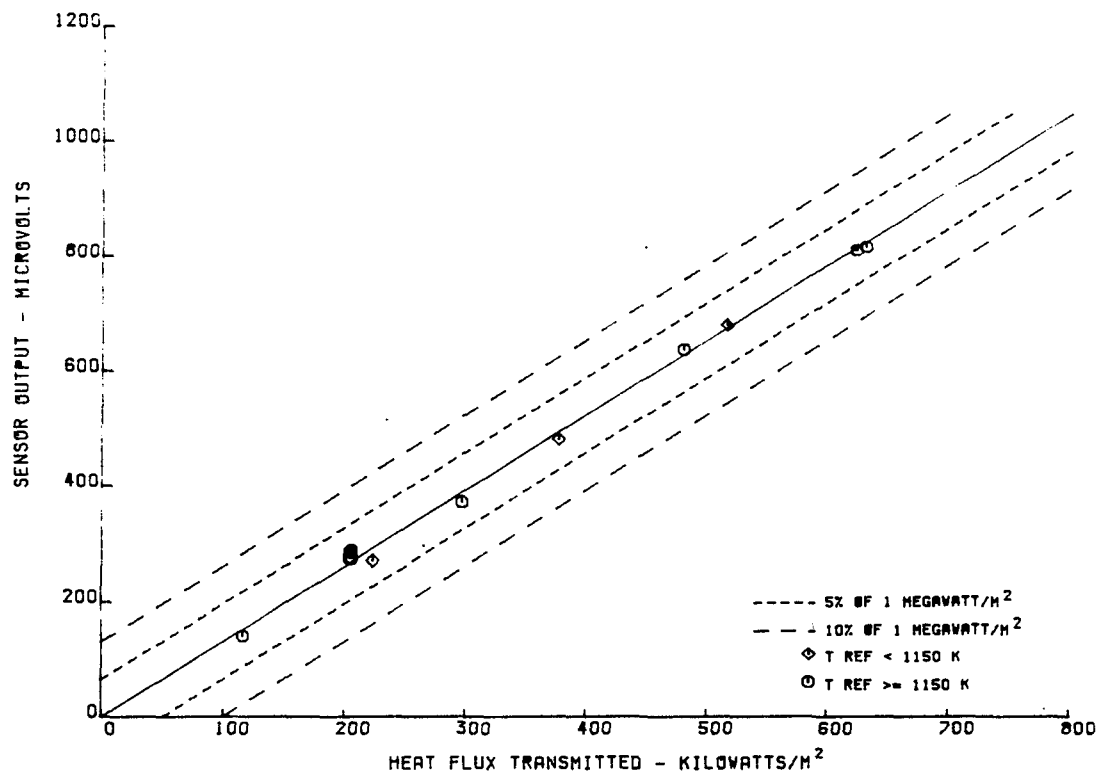
IN USE Q MEASURED = OUTPUT/S
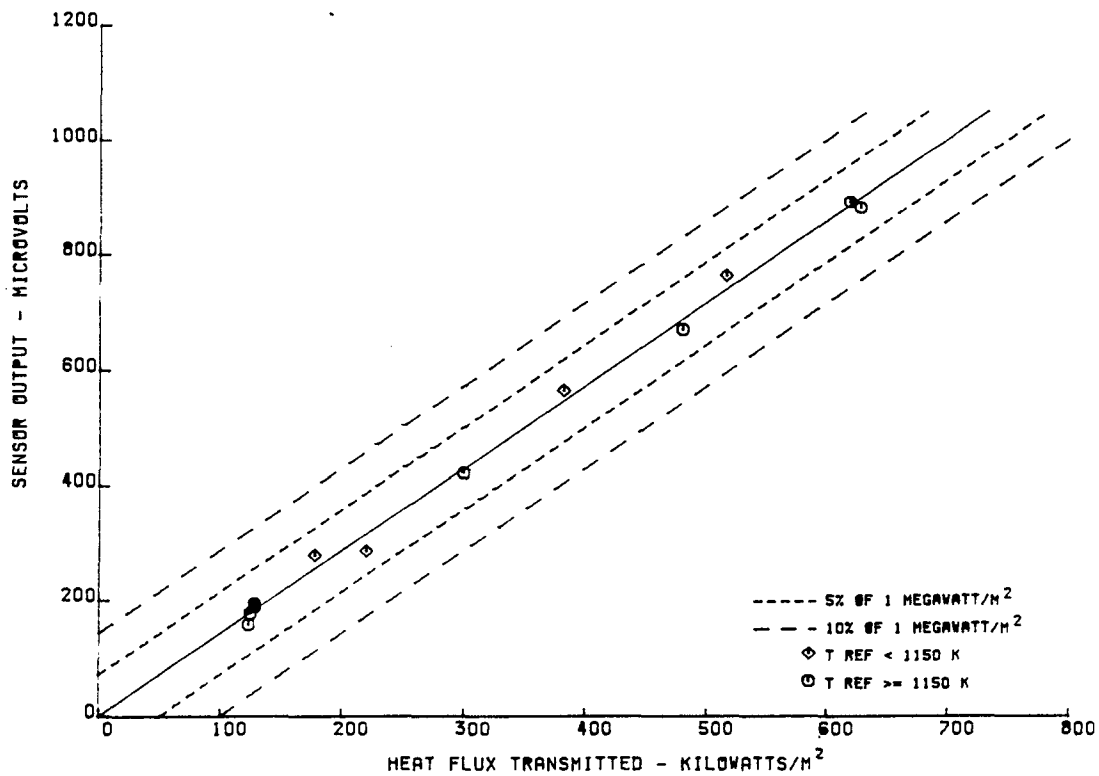
Figure C-21   Voltage Output versus Heat Flux Transmitted through Embedded
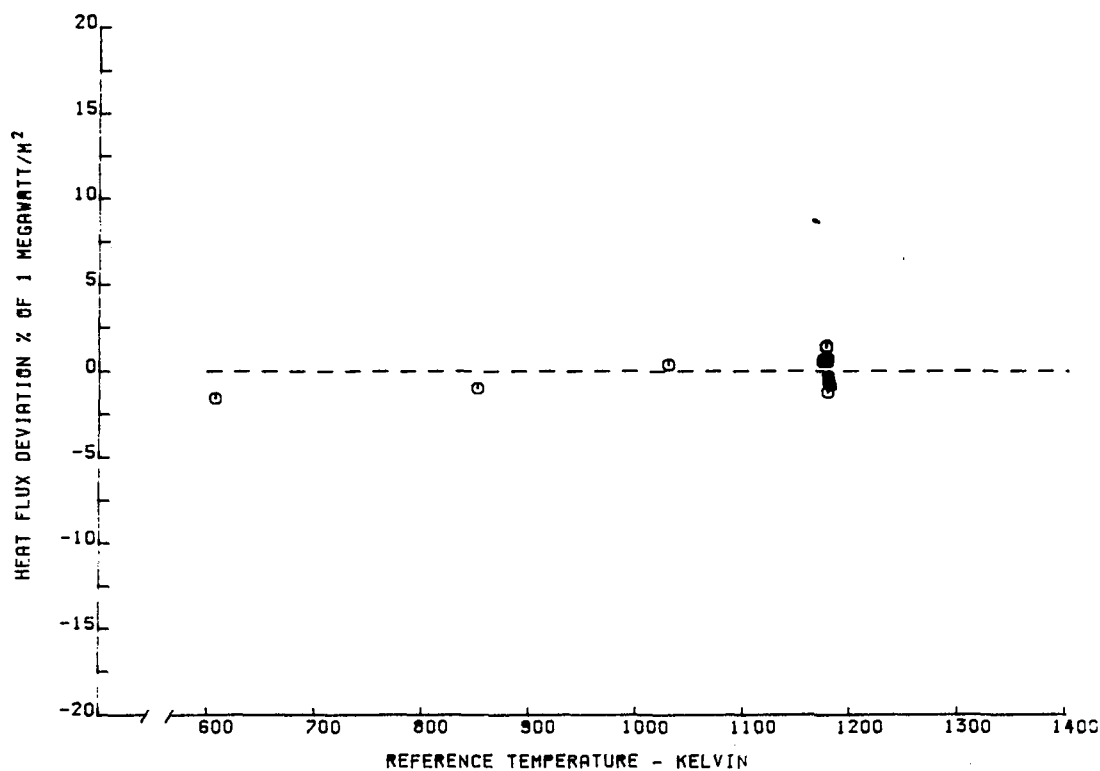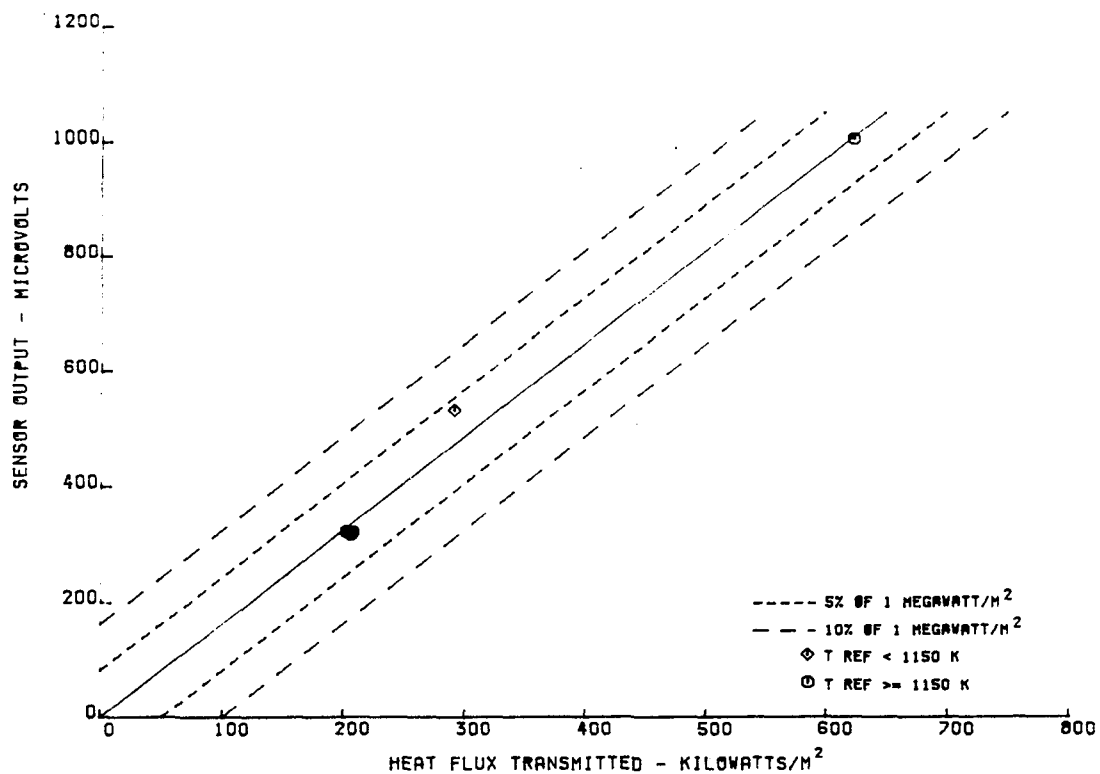   Thermocouple Sensor D-4
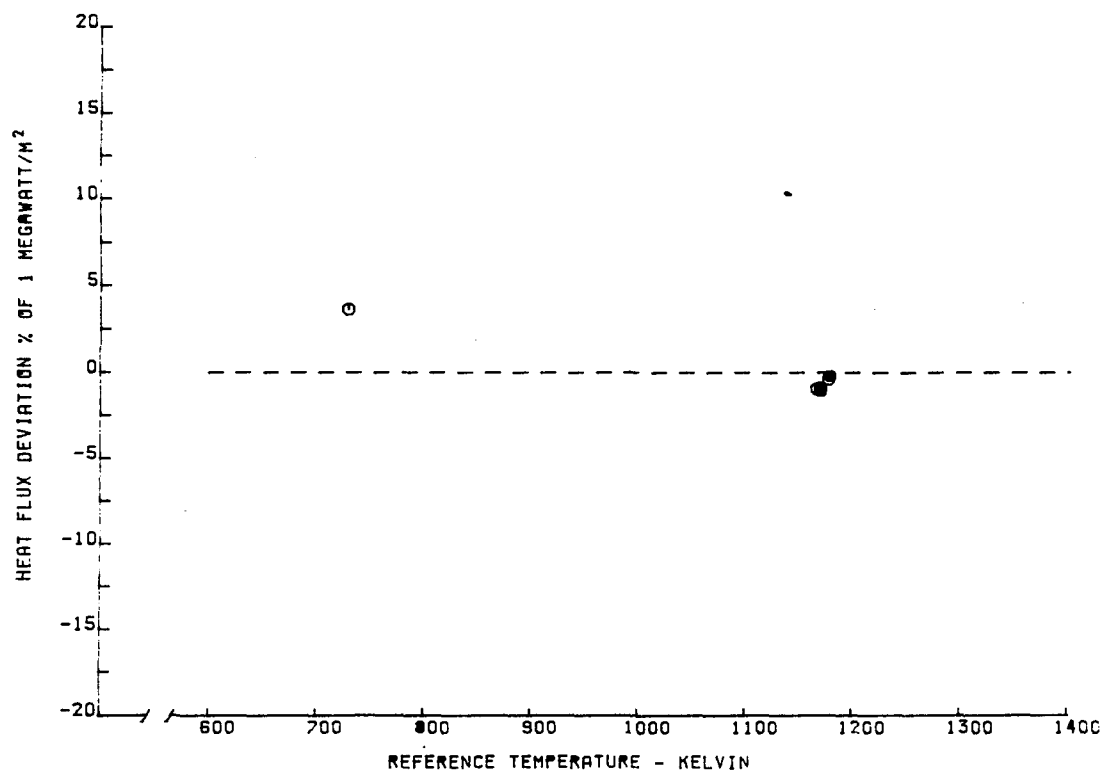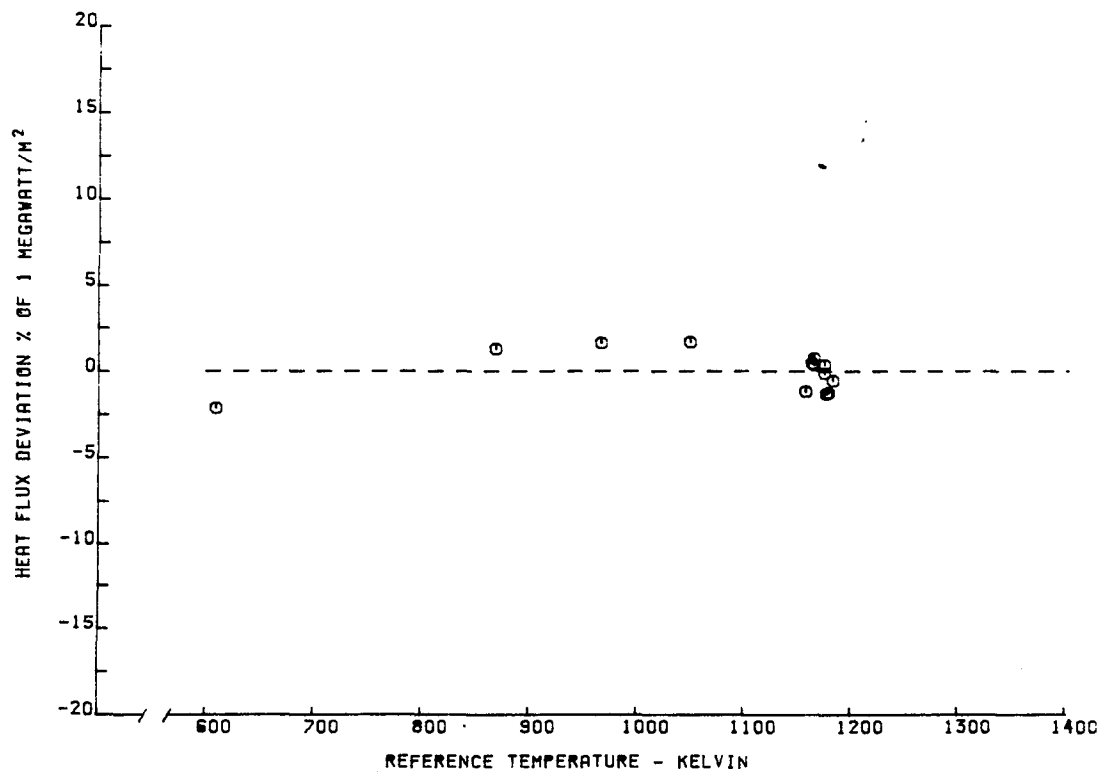

Figure C-22   Heat Flux Deviation versus Sensor Reference Temperature for
               Embedded Thermocouple Sensor D-4

CALIBRATION DATA

Laminated Sensors

This Appendix presents the calibration data from laminated sensors L-1 through L-11 in both corrected and uncorrected form, with the uncorrected data presented with a -UN suffix after the serial number. All data for the sensors are presented although some of the high temperature, low heat flux points exhibit a large amount of scatter and are not representative of realistic operating conditions. The data for each sensor are presented in tabular form, as a plot of sensor microvolt output versus heat flux transmitted through the sensor, and as a plot of percent heat flux deviation versus sensor reference temperature. The heat flux transmitted values were calculated from incident heat flux measurements by accounting for absorption and losses from reradiation and convection. The percent heat flux deviation is the deviation of actual sensor output from the best straight line fit of the data through the origin expressed as a percent of the nominal maximum design heat flux of one megawatt per square meter.

File L-1-A is a sensor recalibration after a fifty hour thermal soak, and the output was found to be low and erratic due to secondary junctions in the leadwire. File L-3-A is a recalibration of sensor L-3 after the thermal cycle test. The corrected data presented for the laminated sensors have been corrected to account for the variation in sensor sensitivity with sensor temperature as described in Appendix B and is thus normalized to a sensor temperature of 1150K. A sensor calibration constant has been determined for each sensor based on a least square line forced through the origin of the microvolt output versus heat flux transmitted plot. This value is presented below the tabulated data, and is valid only at a sensor temperature of 1150K. When the sensor is in use, the heat flux is determined by the relation:

$$Q_{measured} = \frac{1}{S - 2.5433 \times 10^{-4} (1150K - T_{reference})} \text{ X microvolt output.}$$

TABLE D-I

CALIBRATION RESULTS FOR LAMINATED SENSORS L-1 AND L-1A

Q TRANSMITTED KILOWATTS/M**2	T REFERENCE KELVIN	OUTPUT MICROVOLTS	SENSITIVITY OUTPUT/UNIT Q
219.05	569.	77.	.352
128.52	1153.	49.	.388
127.33	1152.	49.	.391
129.80	1150.	51.	.400
623.53	1199.	215.	.345
500.60	1063.	170.	.341
368.34	877.	126.	.343
217.40	634.	70.	.324
216.45	630.	69.	.321
606.41	1199.	195.	.322
602.34	1203.	190.	.316
460.93	1200.	164.	.355
290.68	1200.	109.	.375
110.03	1201.	74.	.677
110.37	1203.	79.	.720
201.41	1200.	104.	.518
106.38	1207.	69.	.652
140.06	1099.	78.	.562
169.46	979.	83.	.491
189.52	867.	72.	.383
201.88	755.	72.	.357
213.36	645.	76.	.357
218.31	577.	76.	.351
287.13	1200.	114.	.398
322.88	1089.	110.	.343
344.38	977.	117.	.340
363.06	867.	124.	.341
378.95	792.	135.	.357

SENSOR CALIBRATION CONSTANT
BASED ON LEAST SQUARE LINE FORCED THROUGH ORIGIN OF OUTPUT VS. HEAT FLUX

S= .37 MICROVOLTS/KILOWATT/M**2

THE ABOVE CALIBRATION CONSTANT AND MICROVOLT OUTPUTS ARE NORMALIZED TO 1150K
IN USE Q MEASURED = (RAW OUTPUT MICROVOLTS)/(S-2.5433*10**(-4)*(1150K-TREF))

SENSOR SERIAL NUMBER L-1-A
11-11-81 AFTER 50 HOUR THERMAL SOAK

Q TRANSMITTED KILOWATTS/M**2	T REFERENCE KELVIN	OUTPUT MICROVOLTS	SENSITIVITY OUTPUT/UNIT Q
535.11	1202.	38.	.072
451.20	1053.	35.	.077
346.44	891.	36.	.106
208.61	702.	29.	.142
630.55	793.	98.	.155

SENSOR CALIBRATION CONSTANT
BASED ON LEAST SQUARE LINE FORCED THROUGH ORIGIN OF OUTPUT VS. HEAT FLUX

S= .1 MICROVOLTS/KILOWATT/M**2

After the 50 hour thermal ageing test the sensor output was low and erratic, and
the Alumel lead failed during the post test calibration. The failure was traced to
the leadwire external to the sensor and secondary junctions were found in the
leadwire. The post test calibration data is not presented in plot form.

Figure D-1   Voltage Output versus Heat Flux Transmitted through Laminated Sensor L-1

Figure D-2   Heat Flux Deviation versus Sensor Reference Temperature for Laminated Sensor L-1

121

TABLE D-II

CALIBRATION RESULTS FOR LAMINATED SENSORS L-1-UN AND L-1A-UN

Q TRANSMITTED KILOWATTS/M**2	T REFERENCE KELVIN	OUTPUT MICROVOLTS	SENSITIVITY OUTPUT/UNIT Q
219.	570.	45.	.21
129.	1155.	50.	.39
127.	1155.	50.	.39
130.	1150.	52.	.40
624.	1200.	223.	.36
501.	1065.	160.	.32
368.	880.	101.	.27
217.	635.	42.	.19
216.	630.	41.	.19
606.	1200.	203.	.33
602.	1205.	199.	.33
461.	1200.	170.	.37
291.	1200.	113.	.39
110.	1200.	76.	.69
110.	1205.	81.	.73
201.	1200.	107.	.53
106.	1210.	71.	.67
140.	1100.	77.	.55
169.	980.	76.	.45
190.	870.	59.	.31
202.	755.	52.	.26
213.	645.	49.	.23
218.	575.	45.	.21
287.	1200.	118.	.41
323.	1090.	106.	.33
344.	980.	102.	.30
363.	870.	98.	.27
379.	795.	101.	.27

SENSOR CALIBRATION CONSTANT
BASED ON LEAST SQUARE LINE FORCED THROUGH ORIGIN OF OUTPUT VS. HEAT FLUX

S= .33 MICROVOLTS/KILOWATT/M**2

NASA HEAT FLUX SENSOR CALIBRATION RESULTS

SENSOR SERIAL NUMBER L-1-A-UN
11-11-81 AFTER 50 HOUR THERMAL SOAK

Q TRANSMITTED KILOWATTS/M**2	T REFERENCE KELVIN	OUTPUT MICROVOLTS	SENSITIVITY OUTPUT/UNIT Q
535.	1200.	46.	.09
451.	1055.	24.	.05
346.	890.	14.	.04
209.	700.	6.	.03
631.	795.	41.	.07

SENSOR CALIBRATION CONSTANT
BASED ON LEAST SQUARE LINE FORCED THROUGH ORIGIN OF OUTPUT VS. HEAT FLUX

S= .06 MICROVOLTS/KILOWATT/M**2

THE ABOVE CALIBRATION CONSTANT AND MICROVOLT OUTPUTS ARE NORMALIZED TO 1150K
IN USE Q MEASURED = (RAW OUTPUT MICROVOLTS)/(S-2.5433*10**(-4)*(1150K-TREF))

After the 50 hour thermal ageing test the sensor output was low and erratic, and
the Alumel lead failed during the post test calibration. The failure was traced to
the leadwire external to the sensor and secondary junctions were found in the
leadwire. The post test calibration data is not presented in plot form.
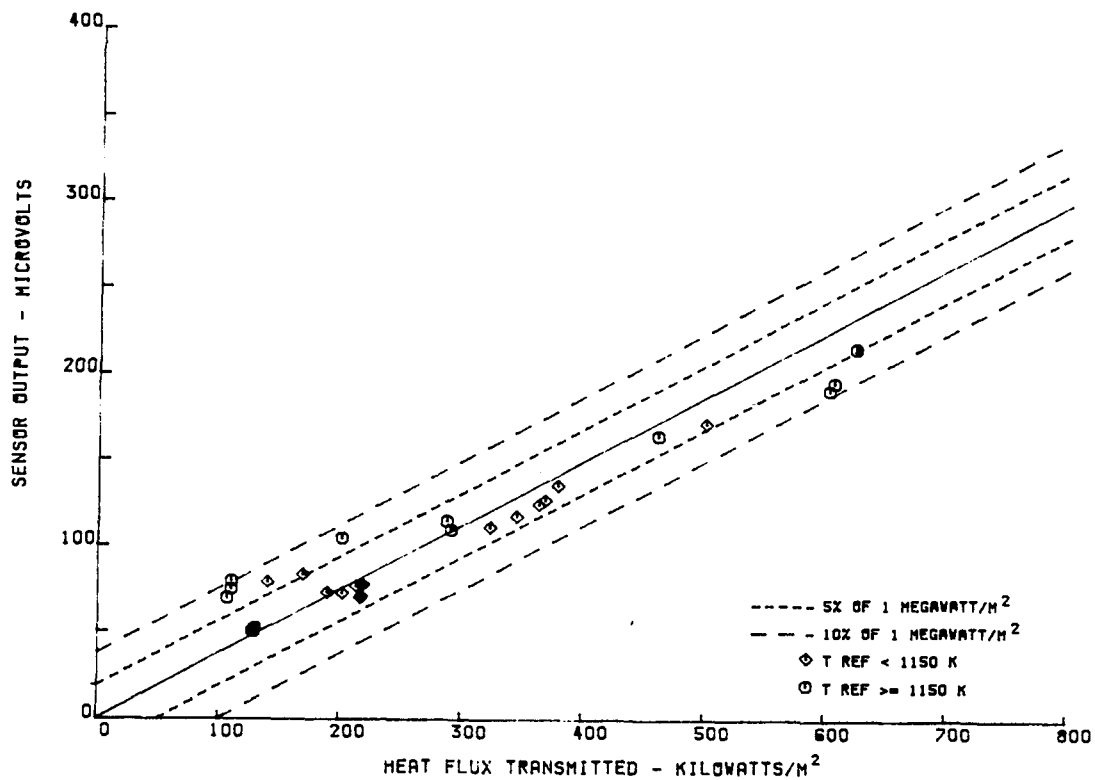
Figure D-3   Voltage Output versus Heat Flux Transmitted through Laminated
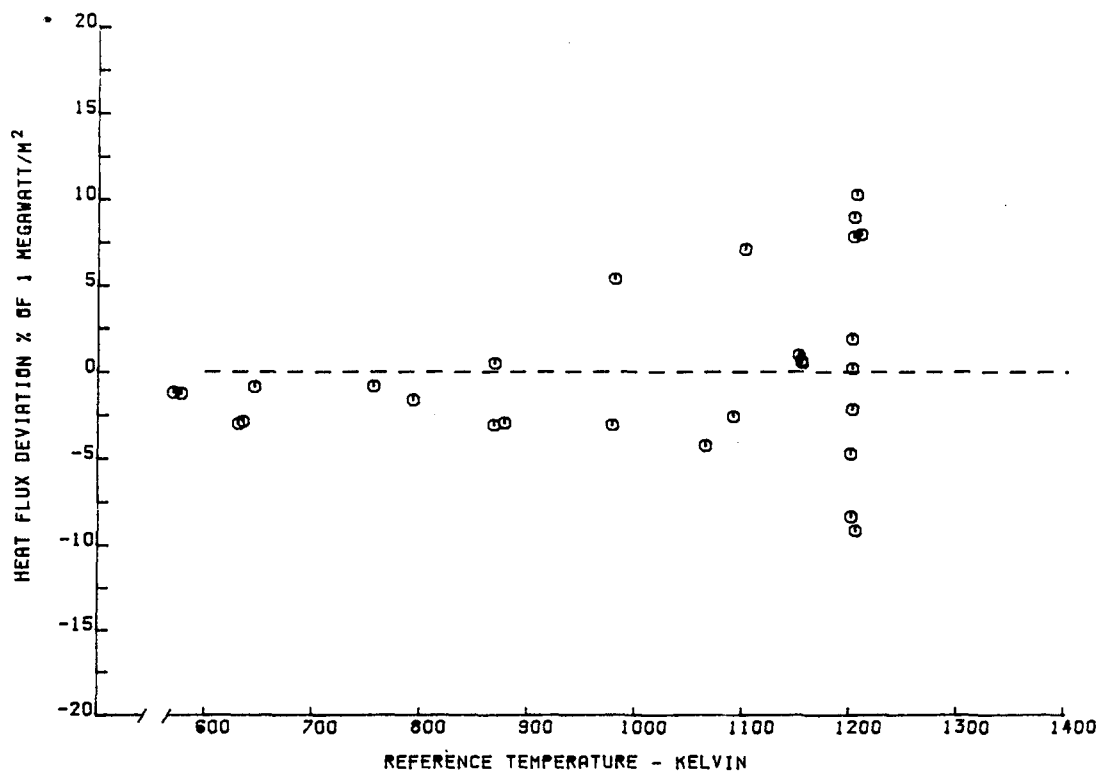   Sensor L-1-UN

Figure D-4   Heat Flux Deviation versus Sensor Reference Temperature for
              Laminated Sensor L-1-UN

123

TABLE D-III

CALIBRATION RESULTS FOR LAMINATED SENSOR L-2

Q TRANSMITTED KILOWATTS/M**2	T REFERENCE KELVIN	OUTPUT MICROVOLTS	SENSITIVITY OUTPUT/UNIT Q
114.59	1188.	58.	.513
610.84	1201.	208.	.340
487.16	1058.	167.	.343
361.91	887.	122.	.337
213.94	639.	63.	.298
608.32	1192.	206.	.339
443.20	1203.	159.	.358
282.18	1199.	115.	.409
85.40	1117.	44.	.523
61.76	1061.	25.	.411
136.09	1122.	63.	.469
112.24	1197.	27.	.246
113.07	1190.	57.	.511
113.28	1197.	34.	.305
603.42	1207.	215.	.356
500.81	1095.	178.	.357
367.98	913.	132.	.359
215.95	659.	83.	.388
607.21	1202.	211.	.348
467.19	1202.	173.	.371
290.58	1199.	94.	.324
118.50	1190.	46.	.394

SENSOR CALIBRATION CONSTANT
BASED ON LEAST SQUARE LINE FORCED THROUGH ORIGIN OF OUTPUT VS. HEAT FLUX

S= .36   MICROVOLTS/KILOWATT/M**2

THE ABOVE CALIBRATION CONSTANT AND MICROVOLT OUTPUTS ARE NORMALIZED TO 1150K
IN USE Q MEASURED = (RAW OUTPUT MICROVOLTS)/(S-2.5433*10**(-4)*(1150K-TREF))

This sensor was calibrated in the quartz lamp bank facility, and removed from the facility. The sensor was reinstalled in the facility for a thermal cycling test, and the Alumel lead failed after one thermal cycle. The failure was external to the sensor and is believed due to vibration of the leadwire by the cooling air.
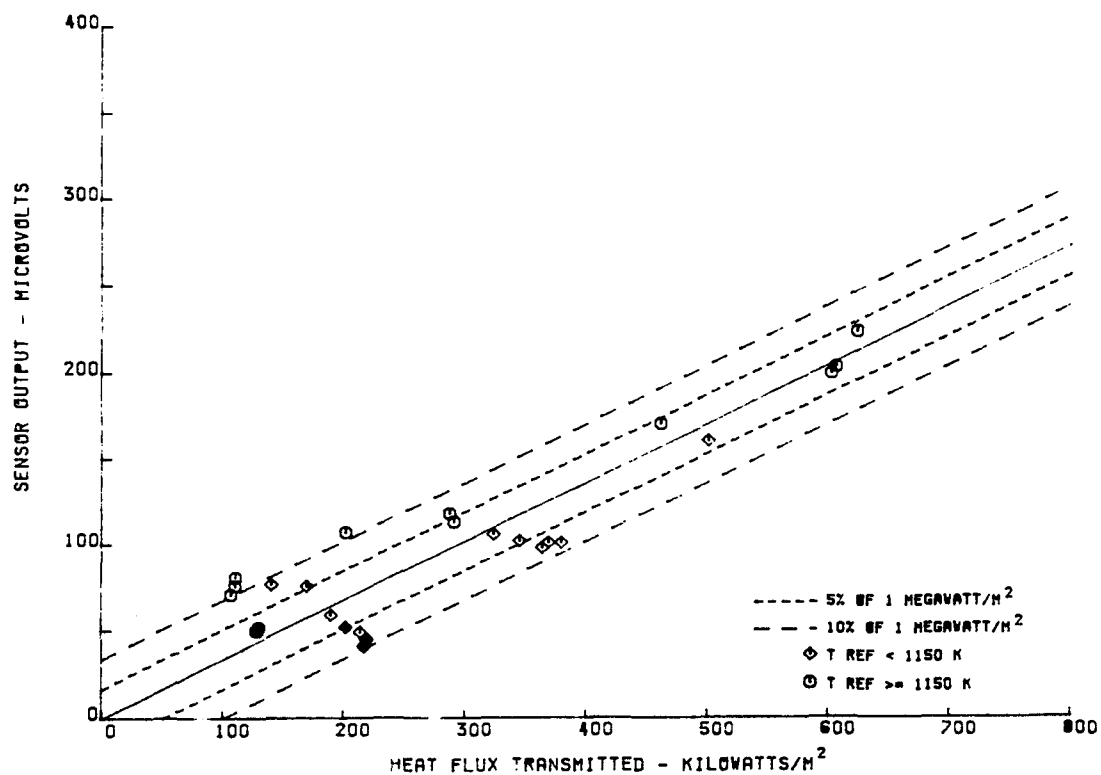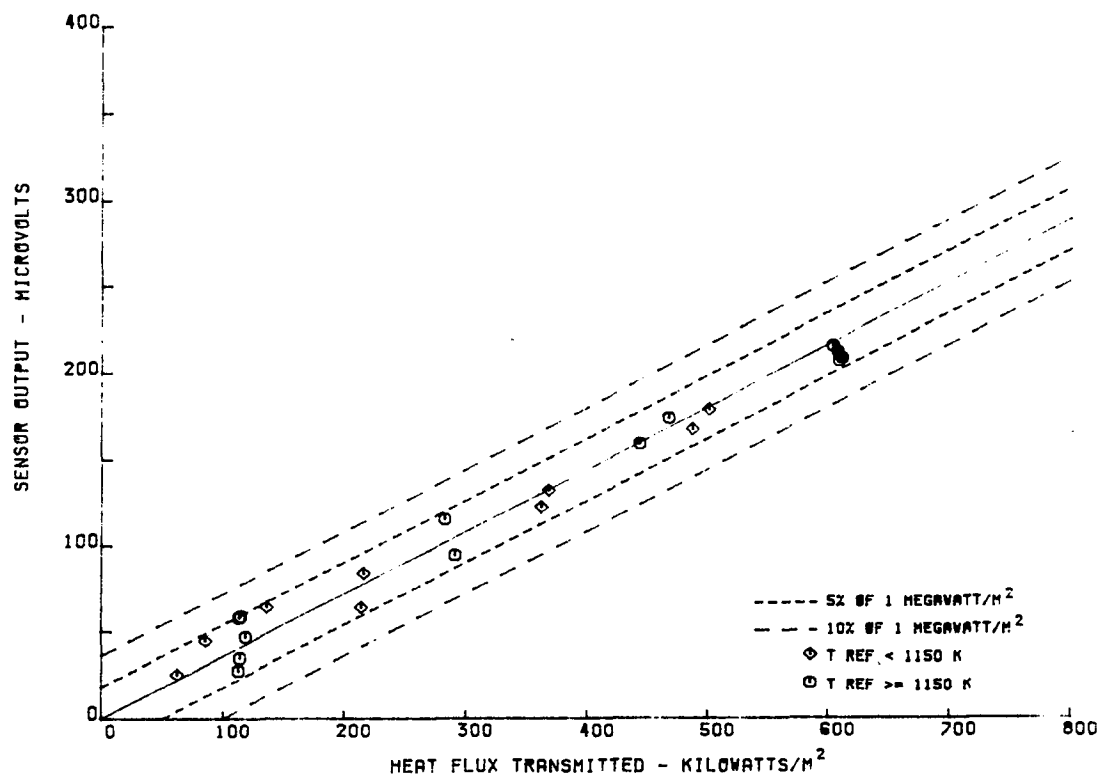
Figure D-5 Voltage Output versus Heat Flux Transmitted through Laminated Sensor L-2
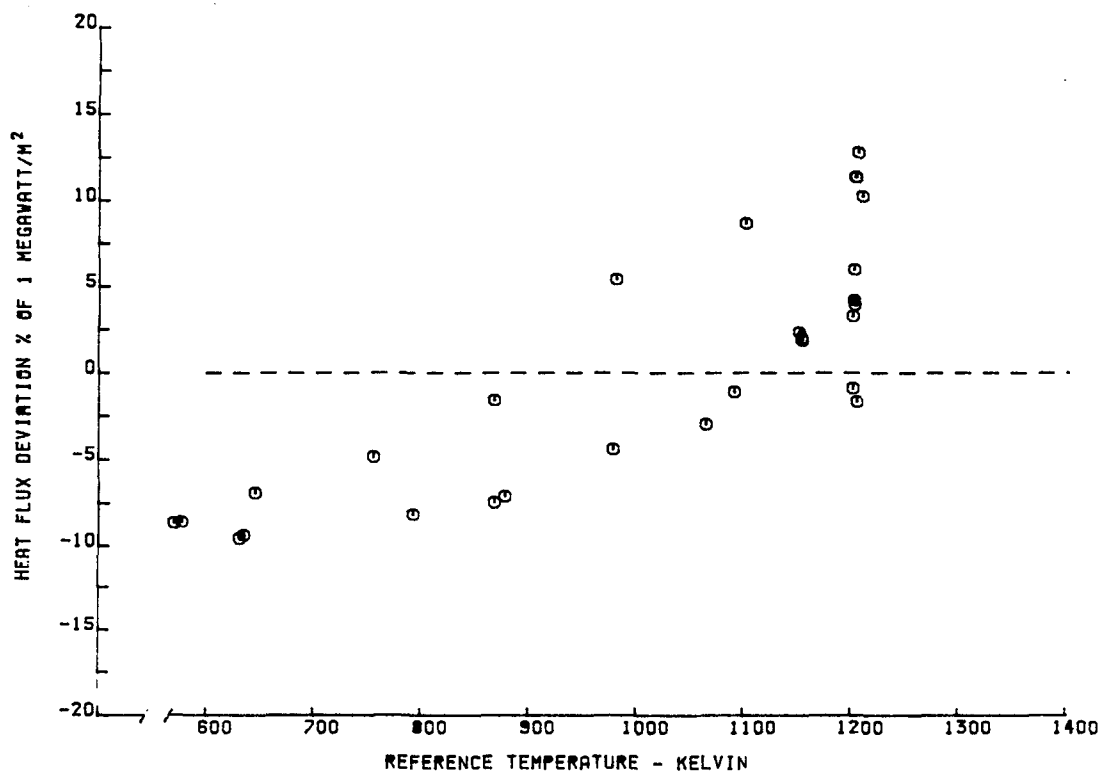

Figure D-6 Heat Flux Deviation versus Sensor Reference Temperature for Laminated Sensor L-2

TABLE D-IV

CALIBRATION RESULTS FOR LAMINATED SENSOR L-2-UN

Q TRANSMITTED KILOWATTS/M**2	T REFERENCE KELVIN	OUTPUT MICROVOLTS	SENSITIVITY OUTPUT/UNIT Q
115.	1190.	60.	.52
611.	1200.	216.	.35
487.	1060.	156.	.32
362.	890.	98.	.27
214.	640.	36.	.17
608.	1195.	213.	.35
443.	1205.	165.	.37
282.	1200.	119.	.42
85.	1120.	44.	.52
62.	1060.	24.	.39
136.	1125.	63.	.46
112.	1200.	29.	.26
113.	1190.	59.	.52
113.	1195.	36.	.32
603.	1210.	224.	.37
501.	1095.	172.	.34
368.	915.	110.	.30
216.	660.	57.	.26
607.	1205.	220.	.36
467.	1205.	180.	.39
291.	1200.	98.	.34
119.	1190.	48.	.41

SENSOR CALIBRATION CONSTANT
BASED ON LEAST SQUARE LINE FORCED THROUGH ORIGIN OF OUTPUT VS. HEAT FLUX

S= .35   MICROVOLTS/KILOWATT/M**2

THE ABOVE CALIBRATION CONSTANT AND MICROVOLT OUTPUTS ARE NORMALIZED TO 1150K
IN USE Q MEASURED = (RAW OUTPUT MICROVOLTS)/(S-2.5433*10**(-4)*(1150K-TREF))

This sensor was calibrated in the quartz lamp bank facility, and removed from the
facility. The sensor was reinstalled in the facility for a thermal cycling test, and
the Alumel lead failed after one thermal cycle. The failure was external to the sensor
and is believed due to vibration of the leadwire by the cooling air.

Figure D-7   Voltage Output versus Heat Flux Transmitted through Laminated
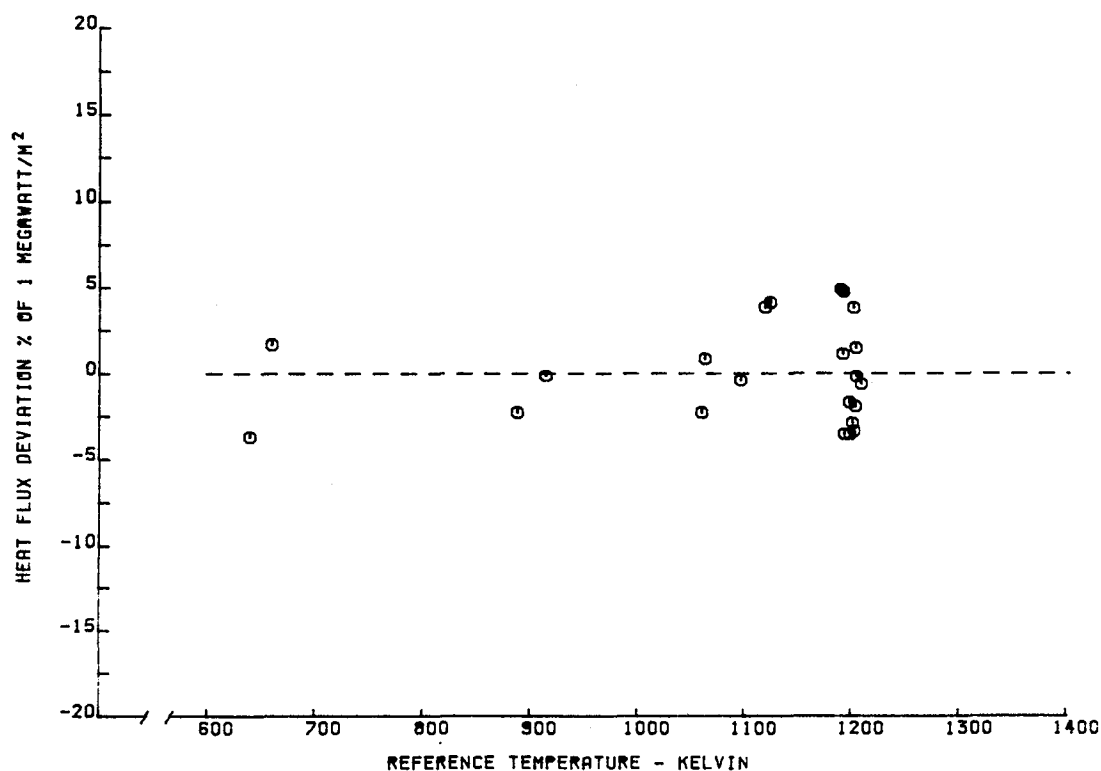Sensor L-2-UN

Figure D-8   Heat Flux Deviation versus Sensor Reference Temperature for
Laminated Sensor L-2-UN

127

TABLE D-V

CALIBRATION RESULTS FOR LAMINATED SENSOR L-3

Q TRANSMITTED KILOWATTS/M**2	T REFERENCE KELVIN	OUTPUT MICROVOLTS	SENSITIVITY OUTPUT/UNIT Q
192.05	933.	63.	.330
137.72	1160.	84.	.614
135.03	1164.	96.	.714
673.24	1200.	219.	.325
527.86	1040.	168.	.319
394.03	868.	131.	.332
230.54	630.	70.	.305
230.06	620.	69.	.304
660.05	1200.	209.	.317
496.79	1197.	165.	.334
307.95	1202.	101.	.330
128.08	1188.	34.	.271
124.80	1199.	70.	.564
124.79	1202.	72.	.579
125.54	1197.	25.	.202
498.03	1082.	170.	.342
604.42	1199.	206.	.341
497.70	1073.	173.	.349
365.77	898.	142.	.389
215.27	639.	82.	.385
607.68	1195.	212.	.350
458.90	1199.	159.	.347
291.25	1199.	95.	.327
114.57	1193.	36.	.320

SENSOR CALIBRATION CONSTANT
BASED ON LEAST SQUARE LINE FORCED THROUGH ORIGIN OF OUTPUT VS. HEAT FLUX

S= .35   MICROVOLTS/KILOWATT/M**2

THE ABOVE CALIBRATION CONSTANT AND MICROVOLT OUTPUTS ARE NORMALIZED TO 1150K
IN USE Q MEASURED = (RAW OUTPUT MICROVOLTS)/(S-2.5433*10**(-4)*(1150K-TREF))

128

Figure D-9   Voltage Output versus Heat Flux Transmitted through Laminated Sensor L-3

Figure D-10   Heat Flux Deviation versus Sensor Reference Temperature for Laminated Sensor L-3

TABLE D-VI

CALIBRATION RESULTS FOR LAMINATED SENSOR L-3A

Q TRANSMITTED KILOWATTS/M**2	T REFERENCE KELVIN	OUTPUT MICROVOLTS	SENSITIVITY OUTPUT/UNIT Q
582.21	1203.	191.	.328
479.58	1082.	166.	.346
360.74	907.	129.	.358
220.25	672.	74.	.339

SENSOR CALIBRATION CONSTANT
BASED ON LEAST SQUARE LINE FORCED THROUGH ORIGIN OF OUTPUT VS. HEAT FLUX

S= .34   MICROVOLTS/KILOWATT/M**2

THE ABOVE CALIBRATION CONSTANT AND MICROVOLT OUTPUTS ARE NORMALIZED TO 1150K
IN USE Q MEASURED = (RAW OUTPUT MICROVOLTS)/(S-2.5433*10**(-4)*(1150K-TREF))

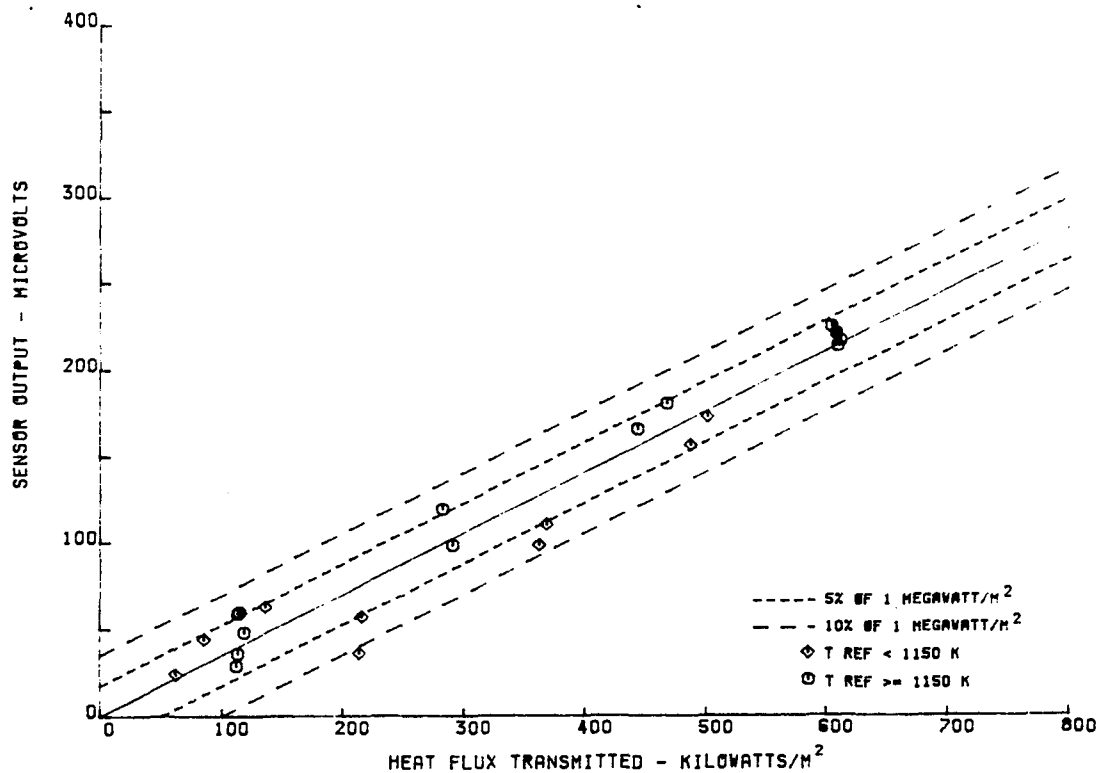This data is from the post test recalibration of sensor L-3 after a 50 cycle thermal test.

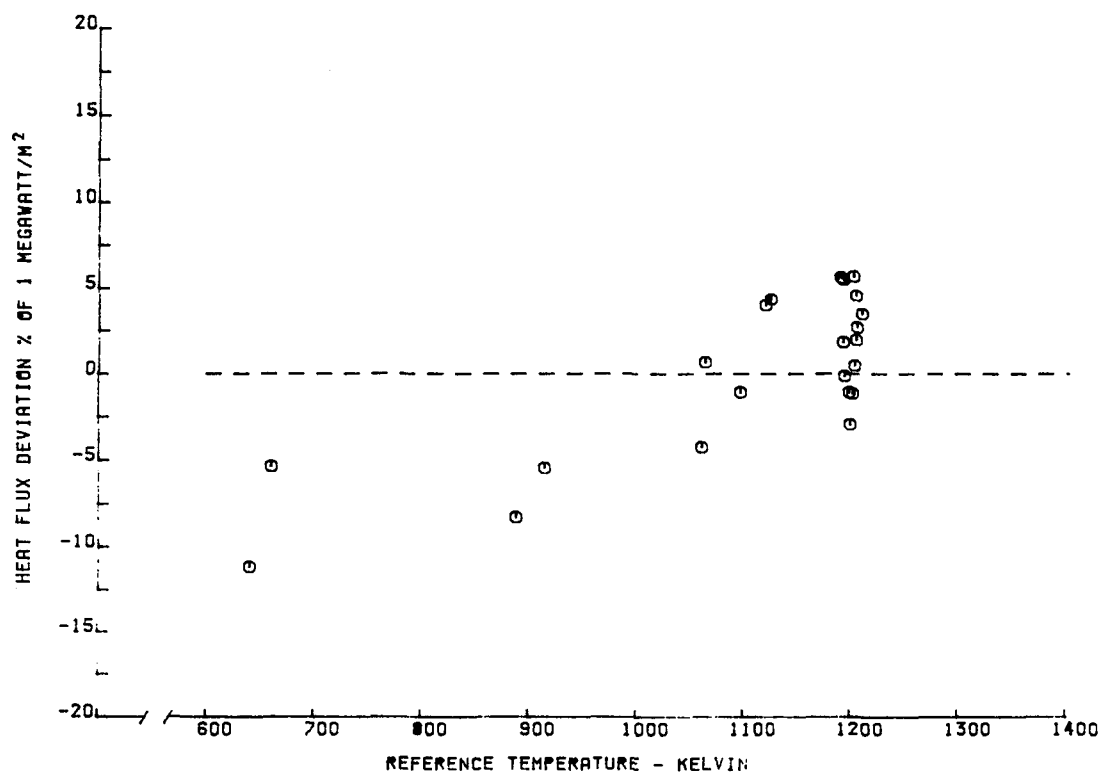Figure D-11   Voltage Output versus Heat Flux Transmitted through Laminated Sensor L-3A

Figure D-12   Heat Flux Deviation versus Sensor Reference Temperature for Laminated Sensor L-3A

TABLE D-VII

CALIBRATION RESULTS FOR LAMINATED SENSOR L-3-UN

Q TRANSMITTED KILOWATTS/M**2	T REFERENCE KELVIN	OUTPUT MICROVOLTS	SENSITIVITY OUTPUT/UNIT Q
192.	935.	53.	.28
138.	1160.	85.	.62
135.	1165.	97.	.72
673.	1200.	228.	.34
528.	1040.	154.	.29
394.	870.	103.	.26
231.	630.	40.	.17
230.	620.	39.	.17
660.	1200.	218.	.33
497.	1200.	172.	.35
308.	1205.	106.	.34
128.	1190.	36.	.28
125.	1200.	72.	.58
125.	1200.	74.	.59
126.	1200.	27.	.22
498.	1085.	162.	.33
604.	1200.	214.	.35
498.	1075.	164.	.33
365.	900.	119.	.33
215.	640.	55.	.26
608.	1195.	220.	.36
459.	1200.	165.	.36
291.	1200.	99.	.34
115.	1195.	38.	.33

SENSOR CALIBRATION CONSTANT
BASED ON LEAST SQUARE LINE FORCED THROUGH ORIGIN OF OUTPUT VS. HEAT FLUX

S= .33   MICROVOLTS/KILOWATT/M**2

THE ABOVE CALIBRATION CONSTANT AND MICROVOLT OUTPUTS ARE NORMALIZED TO 1150K
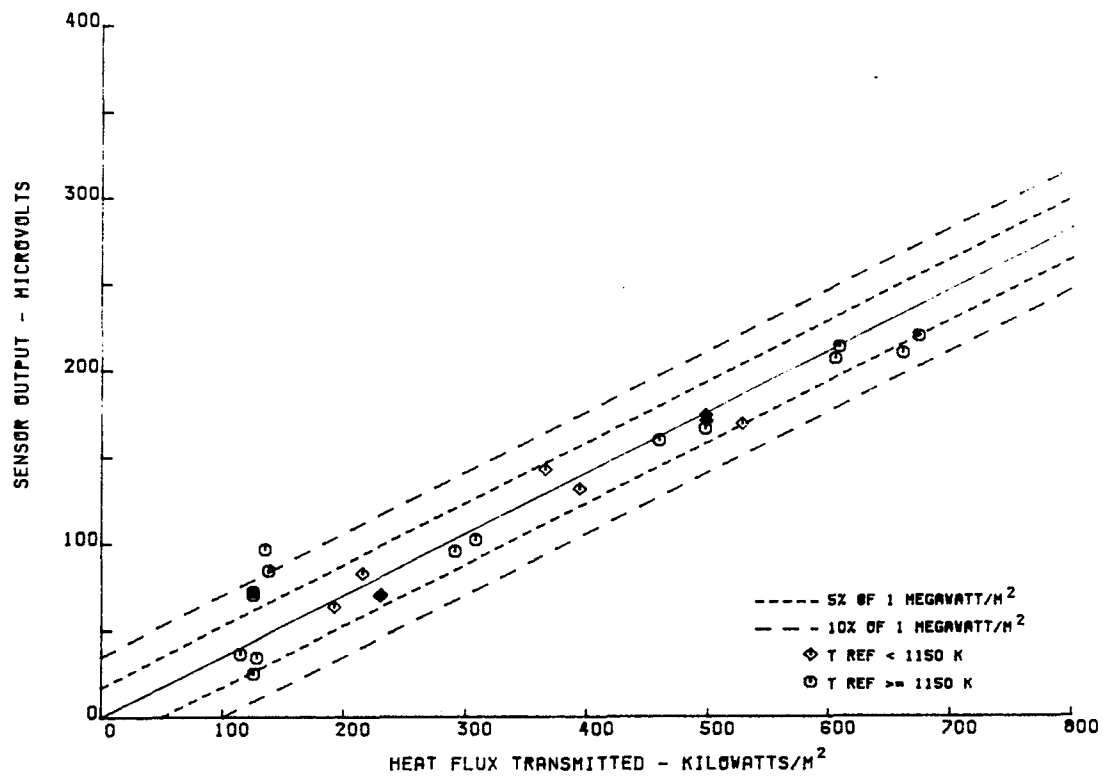IN USE Q MEASURED = (RAW OUTPUT MICROVOLTS)/(S-2.5433*10**(-4)*(1150K-TREF))
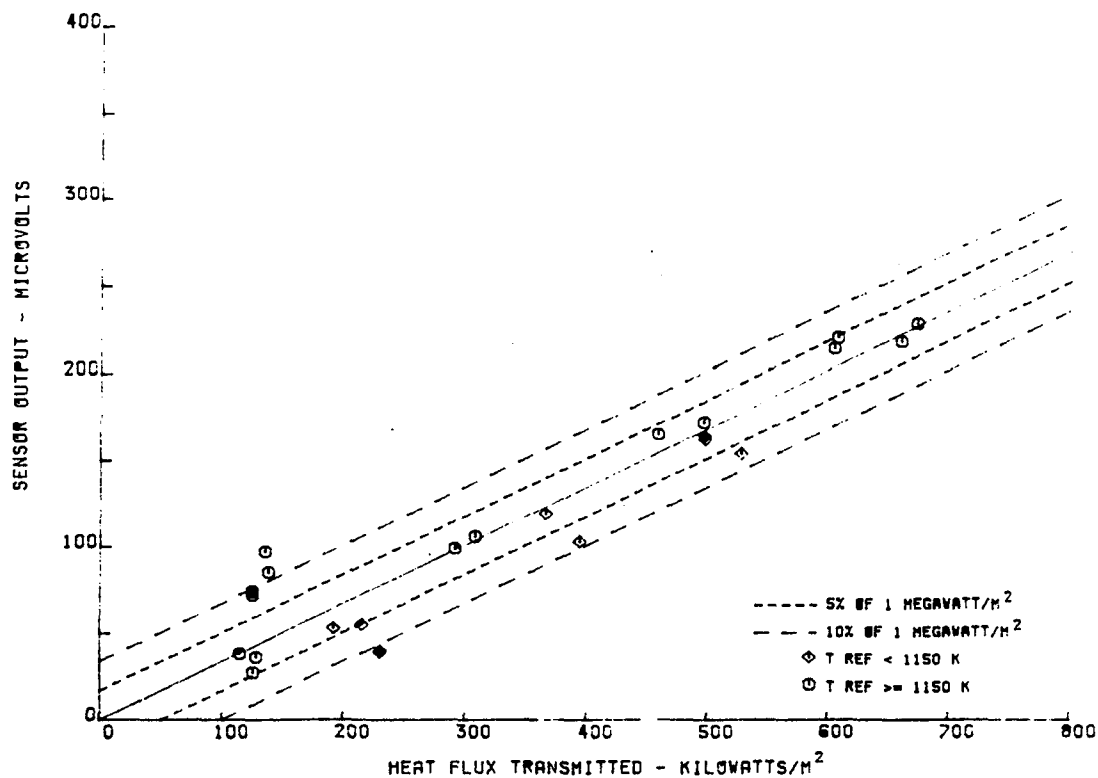
Figure D-13   Voltage Output versus Heat Flux Transmitted through Laminated
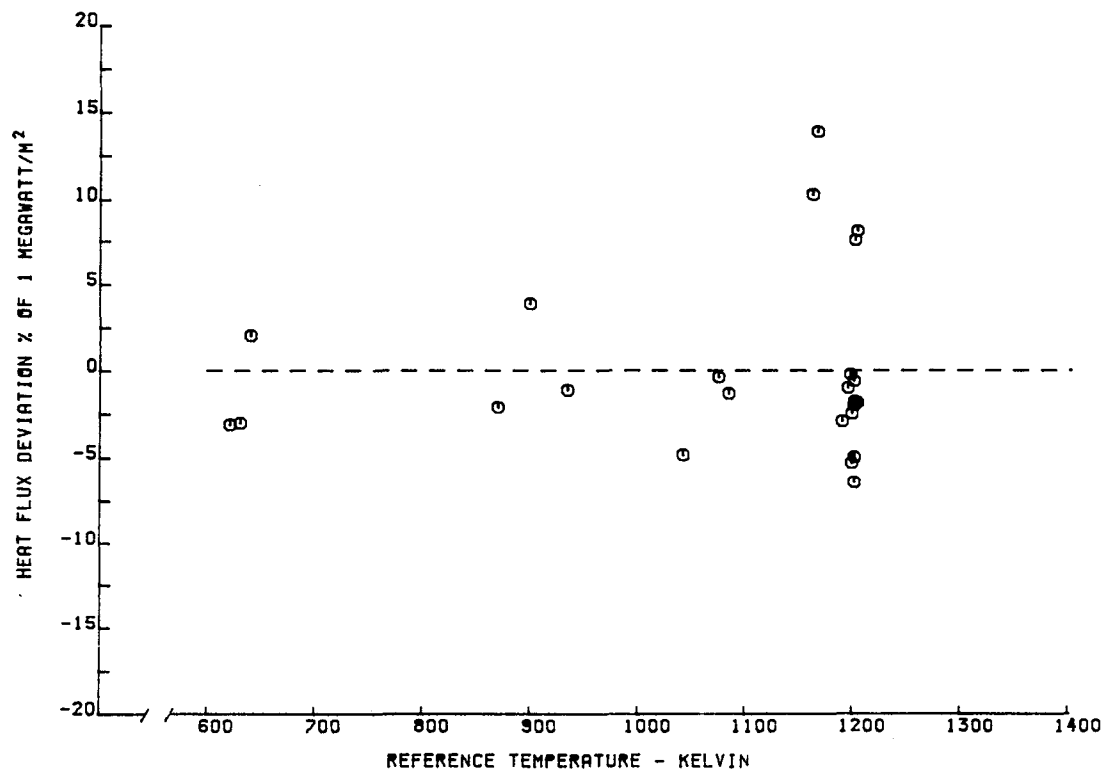Sensor L-3-UN
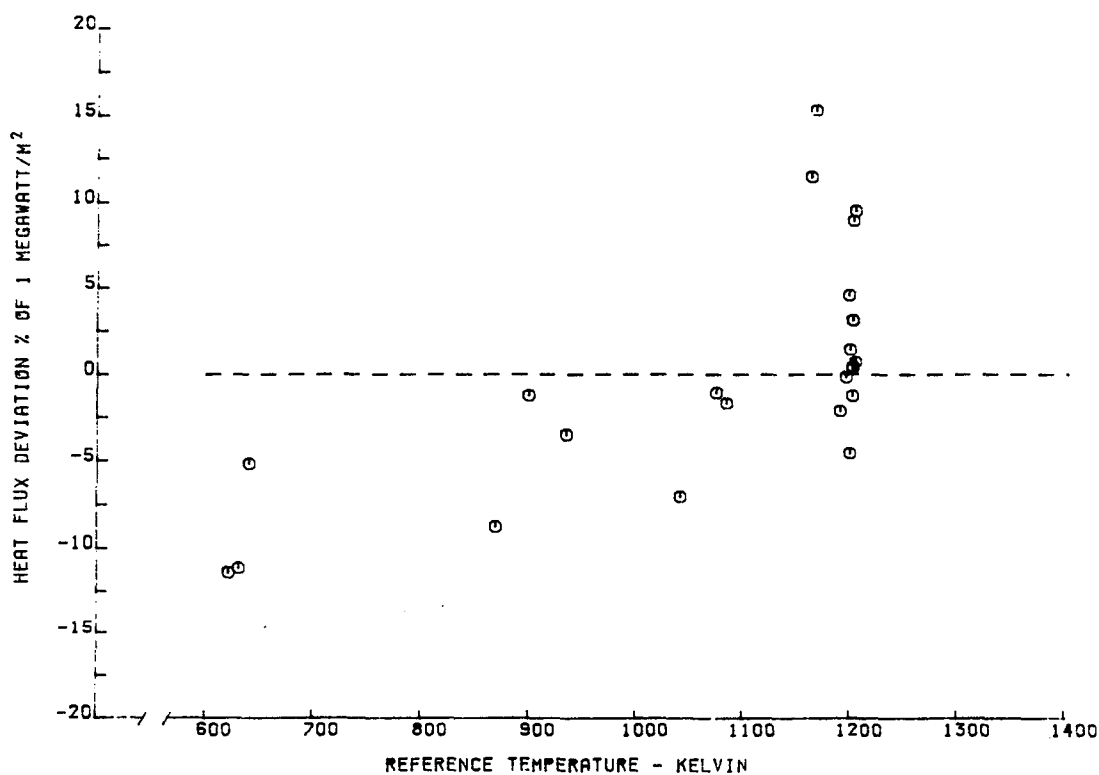
Figure D-14   Heat Flux Deviation versus Sensor Reference Temperature for
Laminated Sensor L-3-UN

TABLE D-VIII

CALIBRATION RESULTS FOR LAMINATED SENSOR L-3A-UN

Q TRANSMITTED KILOWATTS/M**2	T REFERENCE KELVIN	OUTPUT MICROVOLTS	SENSITIVITY OUTPUT/UNIT Q
582.	1205.	199.	.34
480.	1080.	158.	.33
361.	905.	107.	.30
220.	670.	48.	.22

SENSOR CALIBRATION CONSTANT
BASED ON LEAST SQUARE LINE FORCED THROUGH ORIGIN OF OUTPUT VS. HEAT FLUX

S= .31   MICROVOLTS/KILOWATT/M**2

THE ABOVE CALIBRATION CONSTANT AND MICROVOLT OUTPUTS ARE NORMALIZED TO 1150K
IN USE Q MEASURED = (RAW OUTPUT MICROVOLTS)/(S-2.5433*10**(-4)*(1150K-TREF))
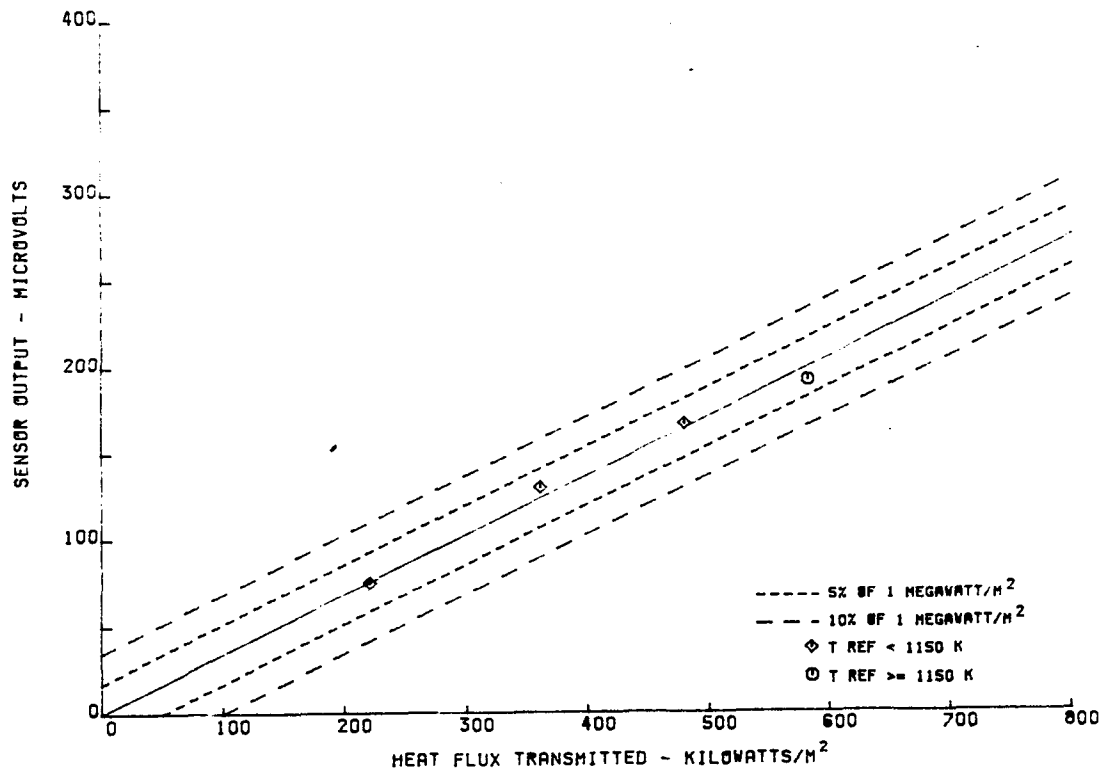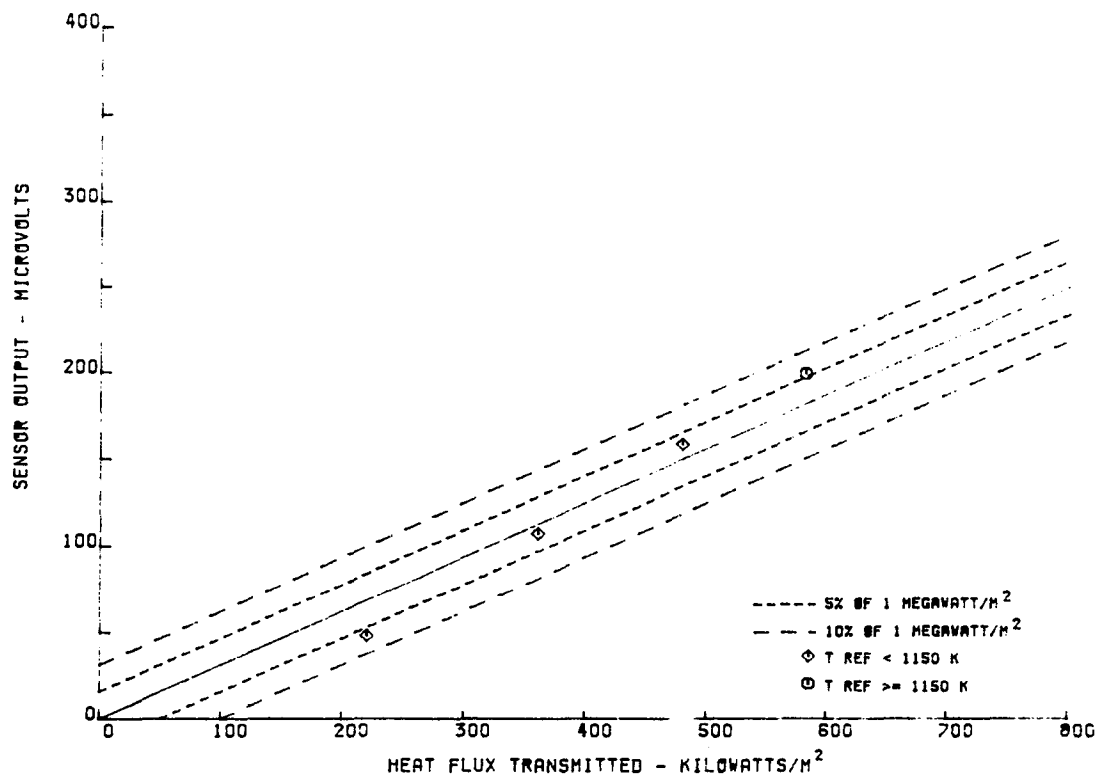
Figure D-15   Voltage Output versus Heat Flux Transmitted through Laminated
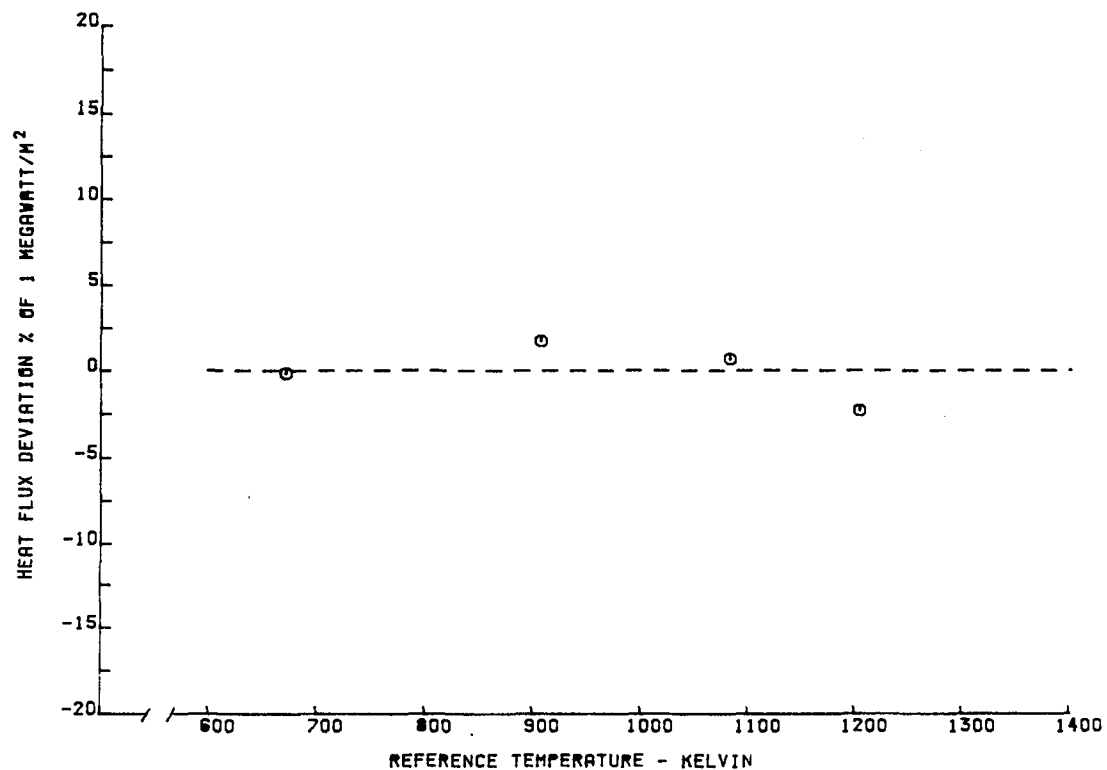Sensor L-3A-UN
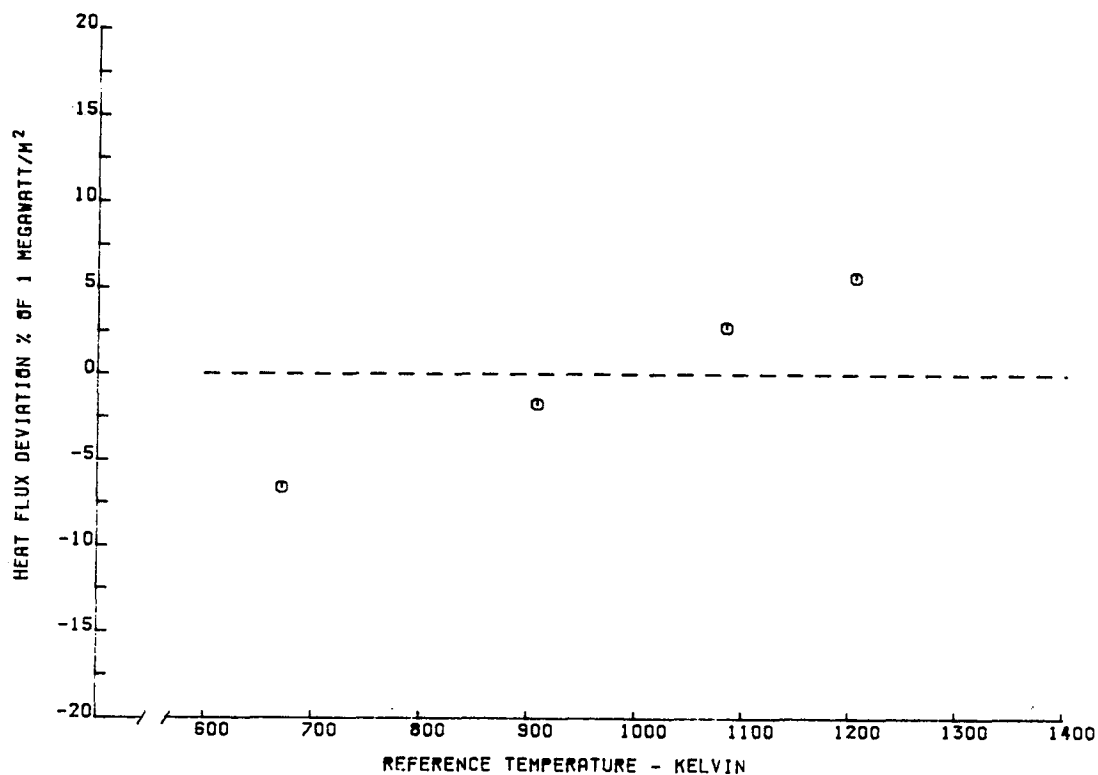
Figure D-16   Heat Flux Deviation versus Sensor Reference Temperature for
Laminated Sensor L-3A-UN

135

TABLE D-IX

CALIBRATION RESULTS FOR LAMINATED SENSOR L-4

Q TRANSMITTED KILOWATTS/M**2	T REFERENCE KELVIN	OUTPUT MICROVOLTS	SENSITIVITY OUTPUT/UNIT Q
129.75	1188.	47.	.367
128.21	1190.	54.	.426
130.62	1187.	64.	.495
129.20	1189.	62.	.485
161.73	1087.	72.	.448
127.04	1198.	68.	.538
124.84	1197.	81.	.652
125.57	1203.	37.	.297
124.41	1204.	31.	.251
122.94	1204.	32.	.262
128.75	1195.	41.	.322
124.03	1204.	23.	.187
125.97	1198.	22.	.178
127.25	1189.	87.	.689
653.01	1203.	261.	.399
541.59	1079.	230.	.425
391.49	877.	158.	.403
230.59	637.	75.	.325
662.76	1190.	257.	.387
499.01	1201.	204.	.409
315.09	1203.	146.	.465
124.04	1200.	23.	.188
125.32	1200.	19.	.154
207.13	1200.	96.	.465
204.50	1202.	110.	.539
125.51	1200.	28.	.226
127.37	1194.	61.	.483
127.19	1194.	60.	.476
124.15	1202.	61.	.494
125.36	1200.	63.	.505
124.81	1202.	71.	.571
124.86	1194.	73.	.589
121.68	1204.	31.	.257
122.10	1203.	39.	.322
123.87	1198.	40.	.326
125.77	1195.	43.	.346
126.76	1189.	88.	.699
124.92	1200.	28.	.227
125.78	1199.	33.	.265
127.20	1192.	83.	.657
125.55	1198.	39.	.314
124.99	1200.	41.	.331

SENSOR CALIBRATION CONSTANT
BASED ON LEAST SQUARE LINE FORCED THROUGH ORIGIN OF OUTPUT VS. HEAT FLUX

S= .4 MICROVOLTS/KILOWATT/M**2

THE ABOVE CALIBRATION CONSTANT AND MICROVOLT OUTPUTS ARE NORMALIZED TO 1150K
IN USE Q MEASURED = (RAW OUTPUT MICROVOLTS)/(S-2.5433*10**(-4)*(1150K-TREF))
This data represents three separate calibration tests on the sensor. During these tests various
cooling air configurations were investigated to provide additional cooling for the leadwires.
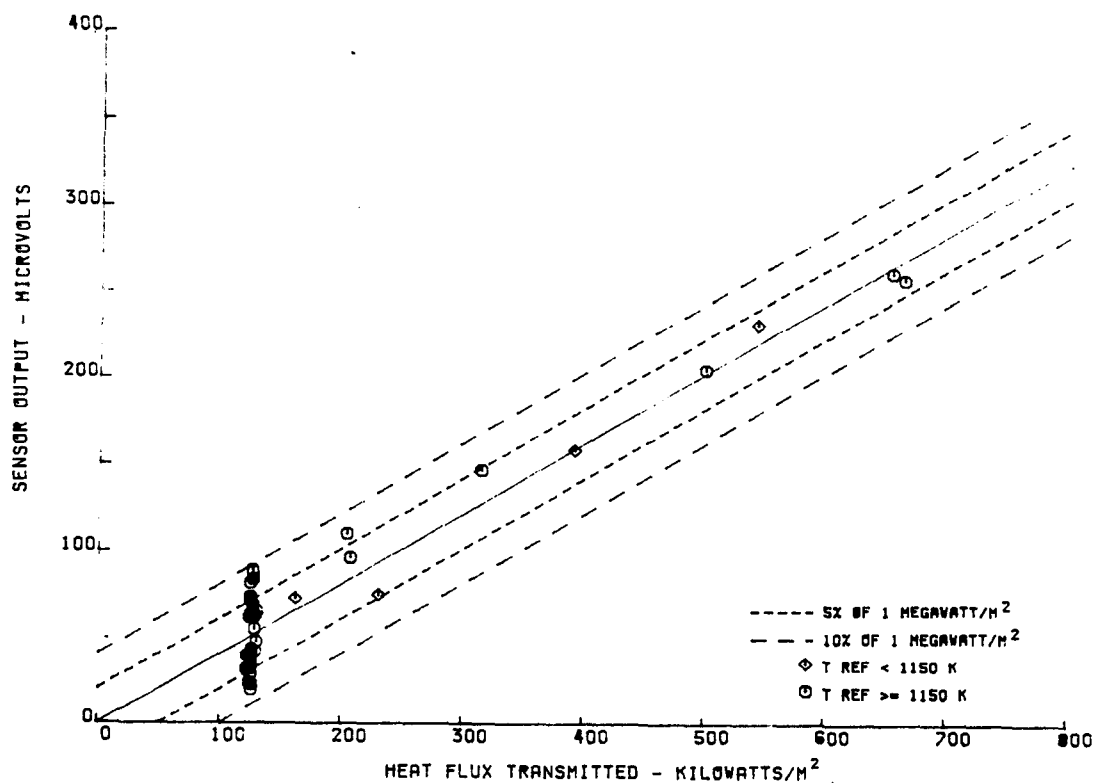
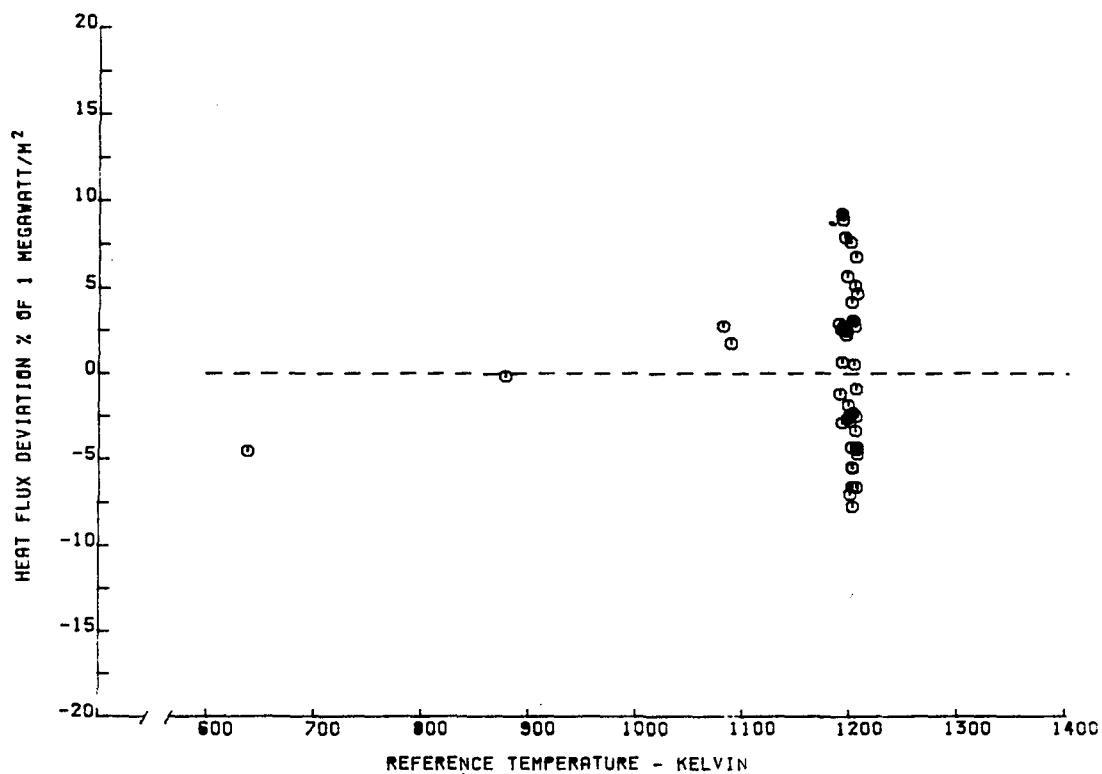Figure D-17   Voltage Output versus Heat Flux Transmitted through Laminated
Sensor L-4

Figure D-18   Heat Flux Deviation versus Sensor Reference Temperature for
Laminated Sensor L-4

137

TABLE D-X

CALIBRATION RESULTS FOR LAMINATED SENSOR L-4-UN

Q TRANSMITTED KILOWATTS/M**2	T REFERENCE KELVIN	OUTPUT MICROVOLTS	SENSITIVITY OUTPUT/UNIT Q
130.	1190.	49.	.38
128.	1190.	56.	.44
131.	1190.	66.	.51
129.	1190.	64.	.50
162.	1085.	70.	.43
127.	1200.	70.	.55
125.	1200.	83.	.66
126.	1205.	39.	.31
124.	1205.	33.	.27
123.	1205.	34.	.28
129.	1195.	43.	.33
124.	1205.	25.	.20
126.	1200.	24.	.19
127.	1190.	89.	.70
653.	1205.	270.	.41
542.	1080.	221.	.41
391.	880.	131.	.33
231.	640.	45.	.20
663.	1190.	264.	.40
499.	1200.	211.	.42
315.	1205.	151.	.48
124.	1200.	25.	.20
125.	1200.	21.	.17
207.	1200.	99.	.48
205.	1205.	113.	.55
126.	1200.	30.	.24
127.	1195.	63.	.49
127.	1195.	62.	.49
124.	1205.	63.	.51
125.	1200.	65.	.52
125.	1200.	73.	.58
125.	1195.	75.	.60
122.	1205.	33.	.27
122.	1205.	41.	.34
124.	1200.	42.	.34
126.	1195.	45.	.36
127.	1190.	90.	.71
125.	1200.	30.	.24
126.	1200.	35.	.28
127.	1195.	85.	.67
126.	1200.	41.	.33
125.	1200.	43.	.34

SENSOR CALIBRATION CONSTANT
BASED ON LEAST SQUARE LINE FORCED THROUGH ORIGIN OF OUTPUT VS. HEAT FLUX

S= .4 MICROVOLTS/KILOWATT/M**2

THE ABOVE CALIBRATION CONSTANT AND MICROVOLT OUTPUTS ARE NORMALIZED TO 1150K
IN USE Q MEASURED = (RAW OUTPUT MICROVOLTS)/(S-2.5433*10**(-4)*(1150K-TREF))

This data represents three separate calibration tests on the sensor. During these tests various cooling air configurations were investigated to provide additional cooling for the leadwires.
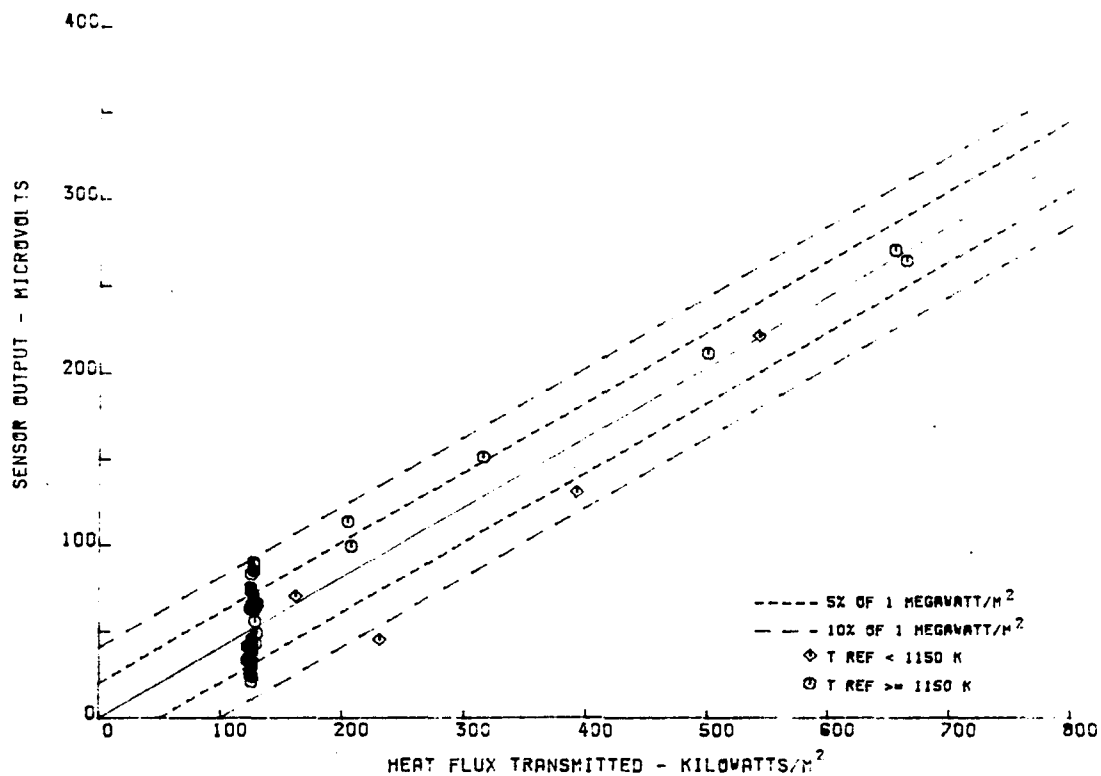
138

Figure D-19   Voltage Output versus Heat Flux Transmitted through Laminated Sensor L-4-UN

Figure D-20   Heat Flux Deviation versus Sensor Reference Temperature for Laminated Sensor L-4-UN

TABLE D-XI

CALIBRATION RESULTS FOR LAMINATED SENSOR L-5

Q TRANSMITTED KILOWATTS/M**2	T REFERENCE KELVIN	OUTPUT MICROVOLTS	SENSITIVITY OUTPUT/UNIT Q
178.78	907.	53.	.296
107.52	1193.	5.	.053
529.83	1202.	138.	.262
451.20	1089.	108.	.241
339.67	917.	77.	.226
212.55	686.	43.	.202
549.36	1203.	130.	.237
418.06	1200.	102.	.245
272.84	1201.	49.	.181
112.98	1199.	12.	.111

SENSOR CALIBRATION CONSTANT
BASED ON LEAST SQUARE LINE FORCED THROUGH ORIGIN OF OUTPUT VS. HEAT FLUX

S= .22   MICROVOLTS/KILOWATT/M**2

THE ABOVE CALIBRATION CONSTANT AND MICROVOLT OUTPUTS ARE NORMALIZED TO 1150K
IN USE Q MEASURED = (RAW OUTPUT MICROVOLTS)/(S-2.5433*10**(-4)*(1150K-TREF))

140

Figure D-21   Voltage Output versus Heat Flux Transmitted through Laminated
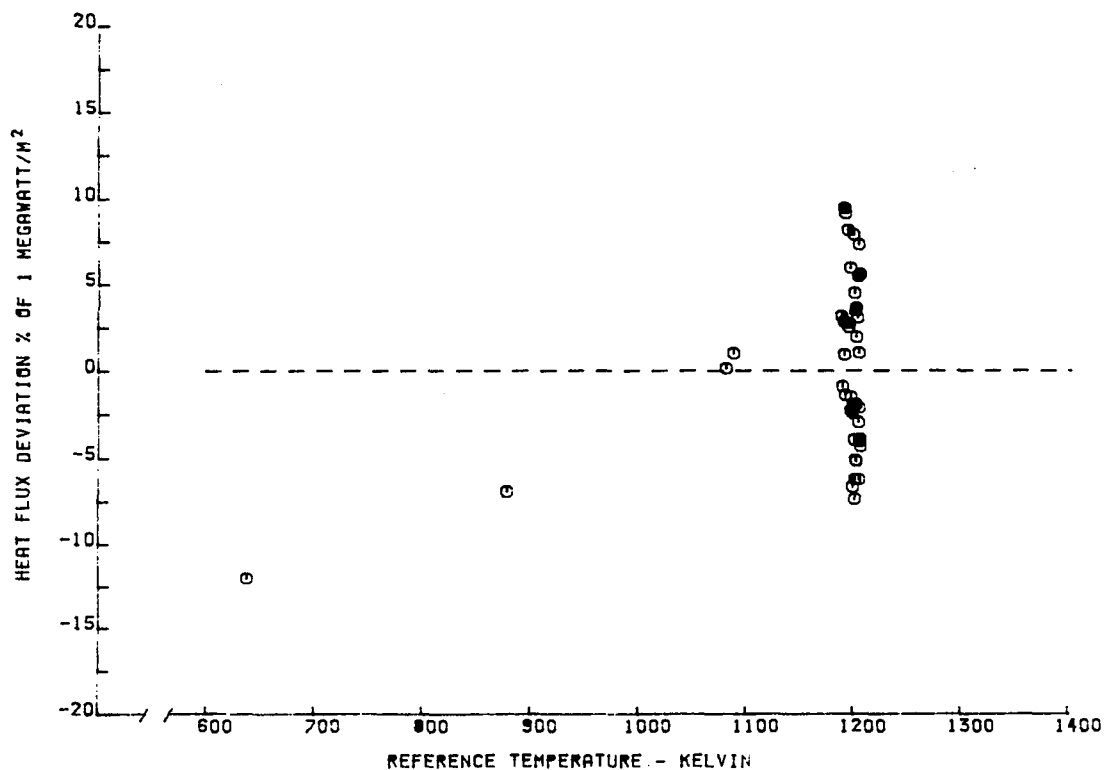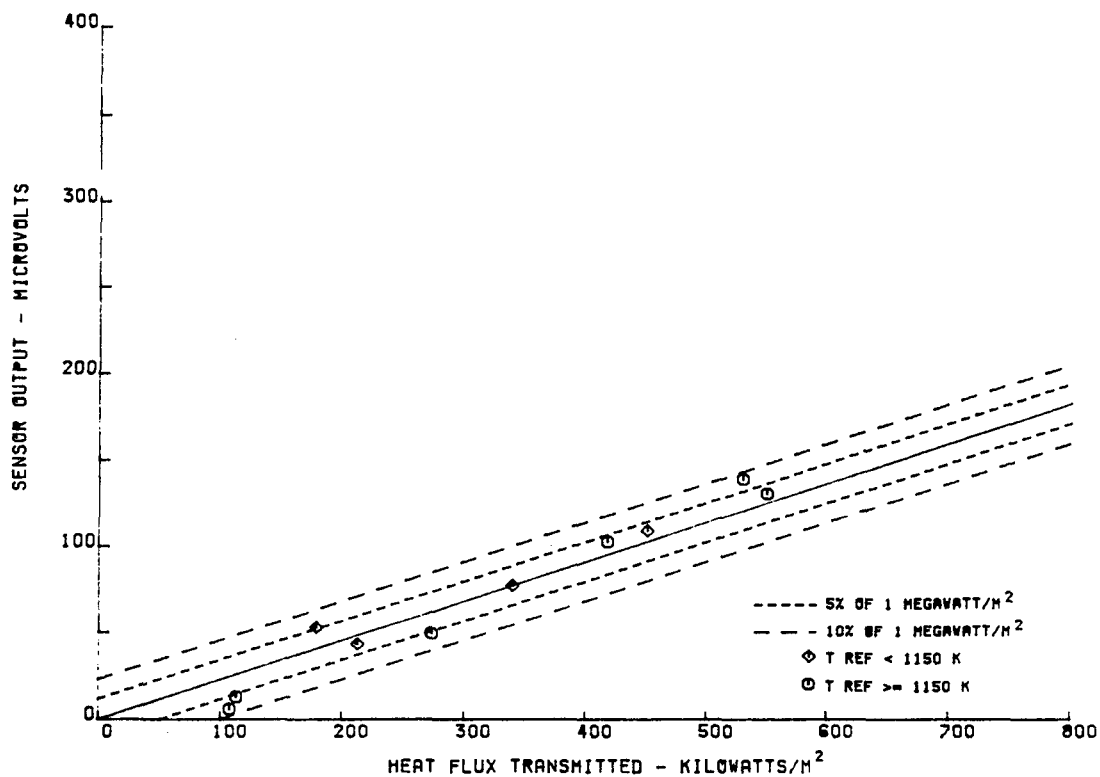Sensor L-5

Figure D-22   Heat Flux Deviation versus Sensor Reference Temperature for
Laminated Sensor L-5

TABLE D-XII

CALIBRATION RESULTS FOR LAMINATED SENSOR L-5-UN

Q TRANSMITTED KILOWATTS/M**2	T REFERENCE KELVIN	OUTPUT MICROVOLTS	SENSITIVITY OUTPUT/UNIT Q
179.	905.	42.	.23
108.	1195.	7.	.07
530.	1200.	146.	.28
451.	1090.	102.	.23
340.	920.	57.	.17
213.	685.	18.	.08
549.	1205.	138.	.25
418.	1200.	108.	.26
273.	1200.	53.	.19
113.	1200.	14.	.12

SENSOR CALIBRATION CONSTANT
BASED ON LEAST SQUARE LINE FORCED THROUGH ORIGIN OF OUTPUT VS. HEAT FLUX

S= .21   MICROVOLTS/KILOWATT/M**2

THE ABOVE CALIBRATION CONSTANT AND MICROVOLT OUTPUTS ARE NORMALIZED TO 1150K
IN USE Q MEASURED = (RAW OUTPUT MICROVOLTS)/(S-2.5433*10**(-4)*(1150K-TREF))

Figure D-23   Voltage Output versus Heat Flux Transmitted through Laminated Sensor L-5-UN
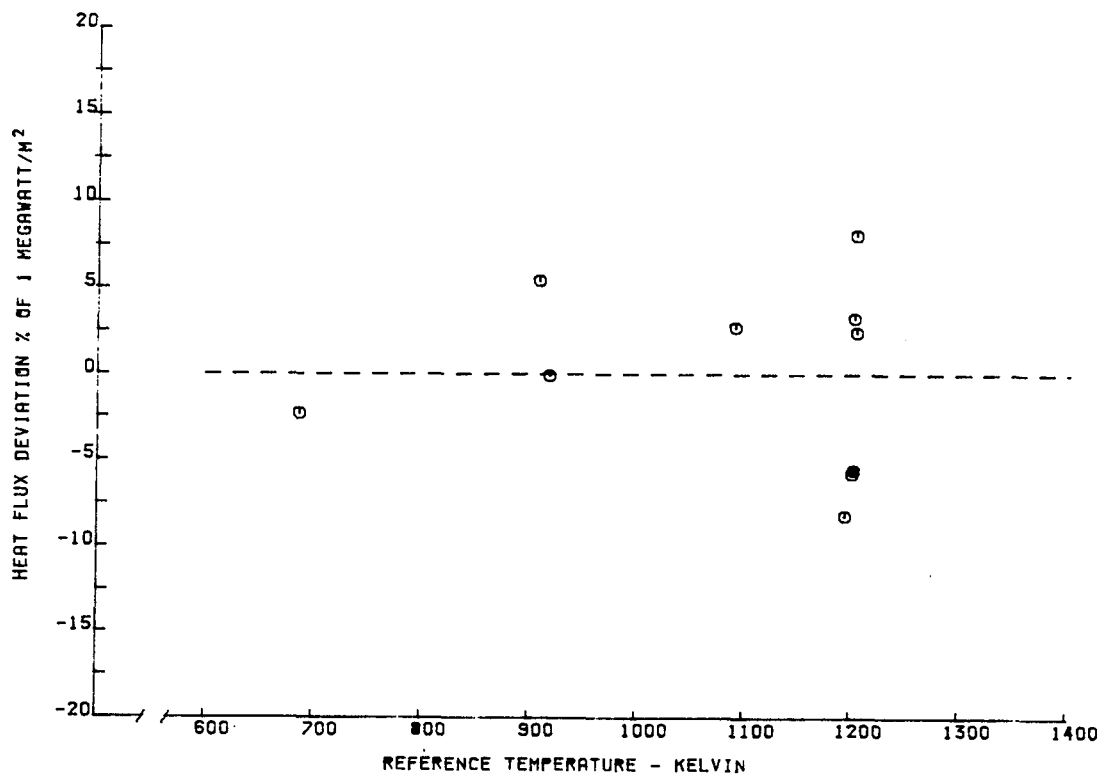

Figure D-24   Heat Flux Deviation versus Sensor Reference Temperature for Laminated Sensor L-5-UN

TABLE D-XIII

CALIBRATION RESULTS FOR LAMINATED SENSOR L-6

Q TRANSMITTED KILOWATTS/M**2	T REFERENCE KELVIN	OUTPUT MICROVOLTS	SENSITIVITY OUTPUT/UNIT Q
178.24	947.	80.	.449
120.59	1175.	52.	.432
550.99	1200.	147.	.268
458.36	1073.	117.	.257
348.79	902.	82.	.237
215.45	659.	36.	.171
552.18	1200.	146.	.265
421.93	1202.	119.	.282
270.63	1203.	73.	.270
113.38	1198.	30.	.269

SENSOR CALIBRATION CONSTANT
BASED ON LEAST SQUARE LINE FORCED THROUGH ORIGIN OF OUTPUT VS. HEAT FLUX

S= .27   MICROVOLTS/KILOWATT/M**2

THE ABOVE CALIBRATION CONSTANT AND MICROVOLT OUTPUTS ARE NORMALIZED TO 1150K
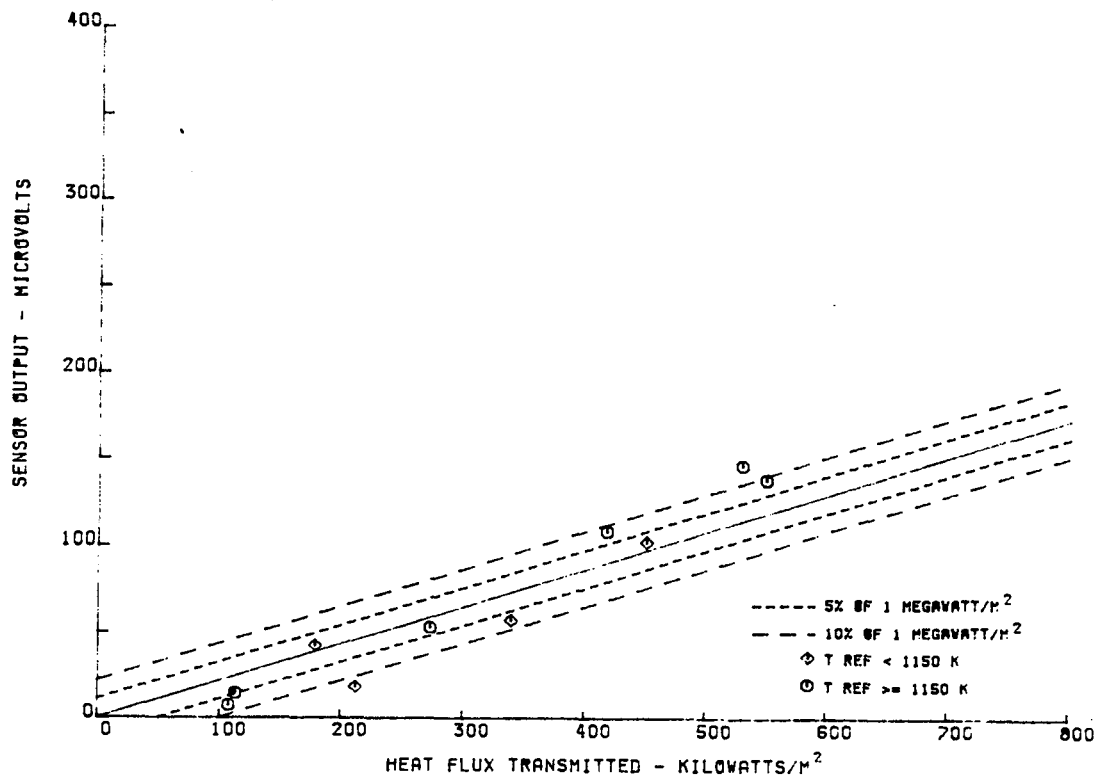 IN USE Q MEASURED = (RAW OUTPUT MICROVOLTS)/(S-2.5433*10**(-4)*(1150K-TREF))

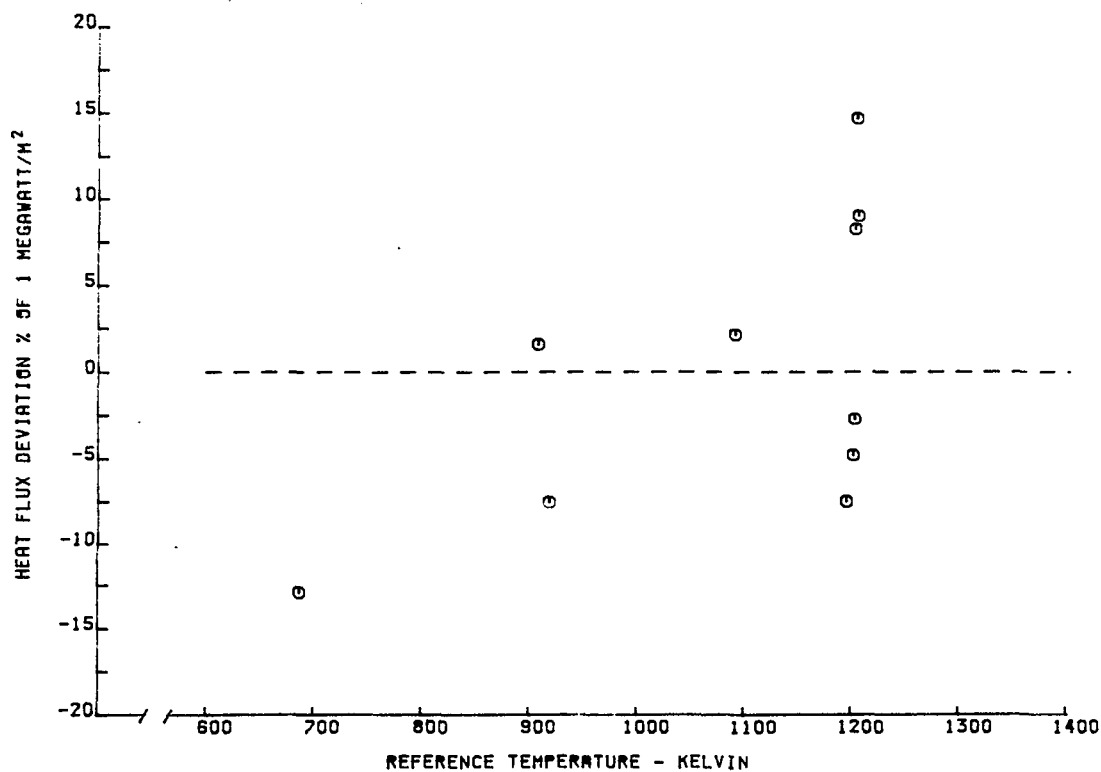Figure D-25   Voltage Output versus Heat Flux Transmitted through Laminated Sensor L-6

Figure D-26   Heat Flux Deviation versus Sensor Reference Temperature for Laminated Sensor L-6

TABLE D-XIV

CALIBRATION RESULTS FOR LAMINATED SENSOR L-6-UN

NASA HEAT FLUX SENSOR CALIBRATION RESULTS

SENSOR SERIAL NUMBER L-6-UN
11-19-81 LAMP CAL

Q TRANSMITTED KILOWATTS/M**2	T REFERENCE KELVIN	OUTPUT MICROVOLTS	SENSITIVITY OUTPUT/UNIT Q
178.	945.	71.	.40
121.	1175.	53.	.44
551.	1200.	155.	.28
458.	1075.	109.	.24
349.	900.	61.	.17
215.	660.	10.	.05
552.	1200.	154.	.28
422.	1205.	125.	.30
271.	1205.	77.	.28
113.	1200.	32.	.28

SENSOR CALIBRATION CONSTANT
BASED ON LEAST SQUARE LINE FORCED THROUGH ORIGIN OF OUTPUT VS. HEAT FLUX

S= .26 MICROVOLTS/KILOWATT/M**2

THE ABOVE CALIBRATION CONSTANT AND MICROVOLT OUTPUTS ARE NORMALIZED TO 1150K
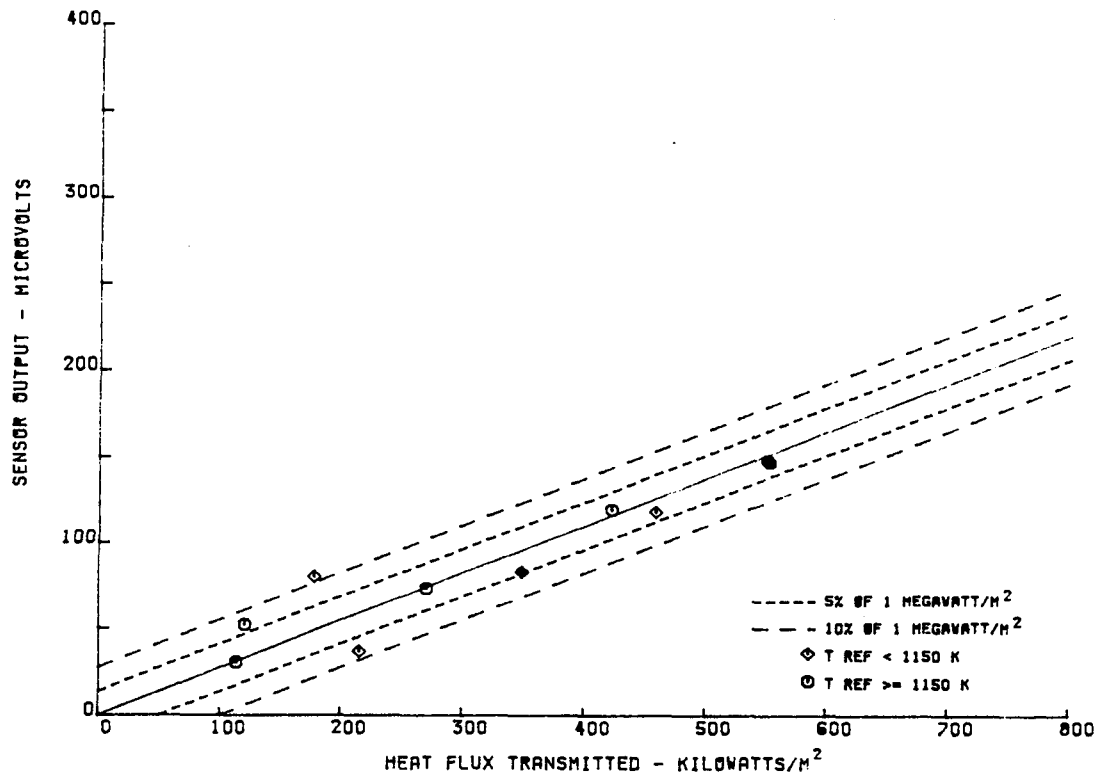IN USE Q MEASURED = (RAW OUTPUT MICROVOLTS)/(S-2.5433*10**(-4)*(1150K-TREF))

Figure D-27   Voltage Output versus Heat Flux Transmitted through Laminated
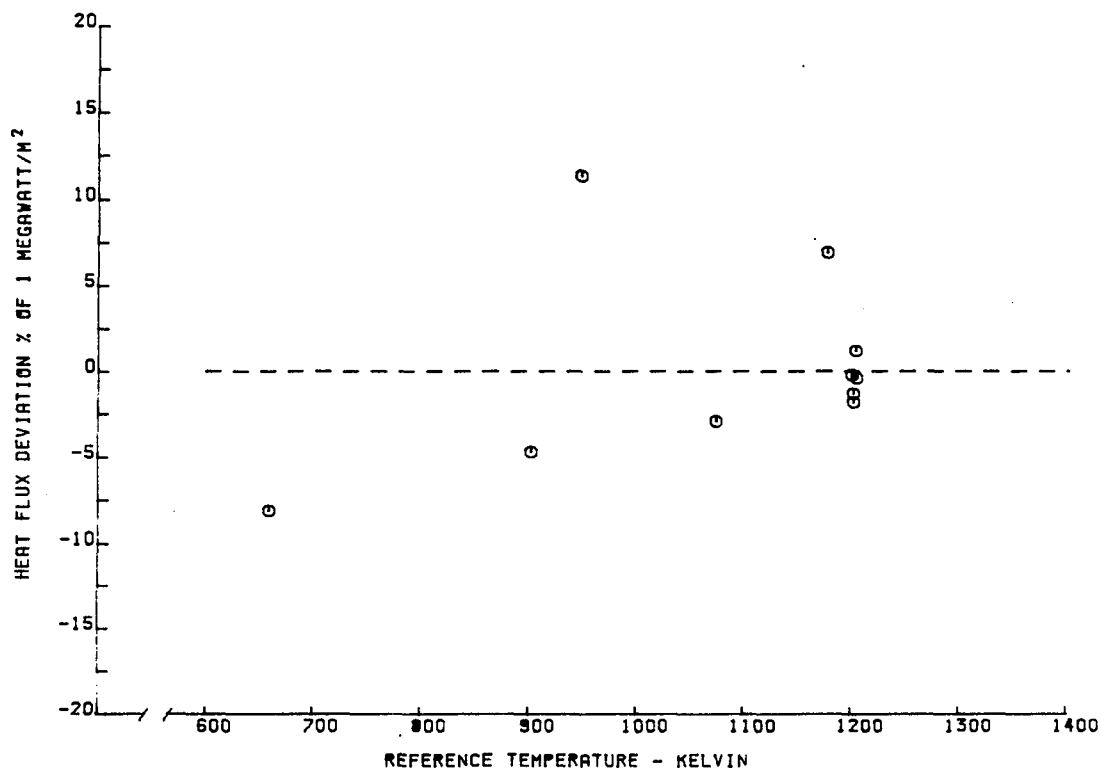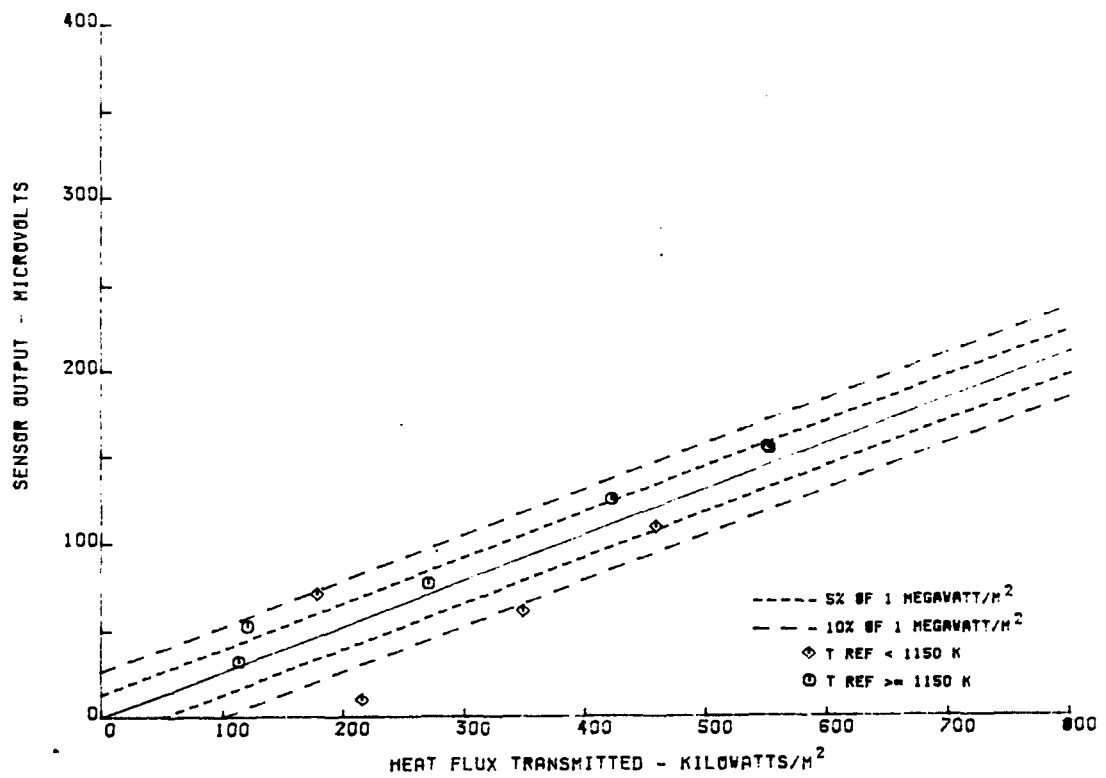Sensor L-6-UN

Figure D-28   Heat Flux Deviation versus Sensor Reference Temperature for
Laminated Sensor L-6-UN

TABLE D-XV

CALIBRATION RESULTS FOR LAMINATED SENSOR L-7

Q TRANSMITTED KILOWATTS/M**2	T REFERENCE KELVIN	OUTPUT MICROVOLTS	SENSITIVITY OUTPUT/UNIT Q
169.32	1003.	42.	.249
125.72	1170.	62.	.495
567.97	1202.	157.	.277
464.39	1056.	124.	.267
346.34	882.	79.	.229
218.75	649.	45.	.209
571.01	1198.	157.	.276
443.67	1202.	129.	.290
262.46	1199.	76.	.292
124.44	1198.	69.	.558

SENSOR CALIBRATION CONSTANT
BASED ON LEAST SQUARE LINE FORCED THROUGH ORIGIN OF OUTPUT VS. HEAT FLUX

S= .28   MICROVOLTS/KILOWATT/M**2

THE ABOVE CALIBRATION CONSTANT AND MICROVOLT OUTPUTS ARE NORMALIZED TO 1150K
IN USE Q MEASURED = (RAW OUTPUT MICROVOLTS)/(S-2.5433*10**(-4)*(1150K-TREF))

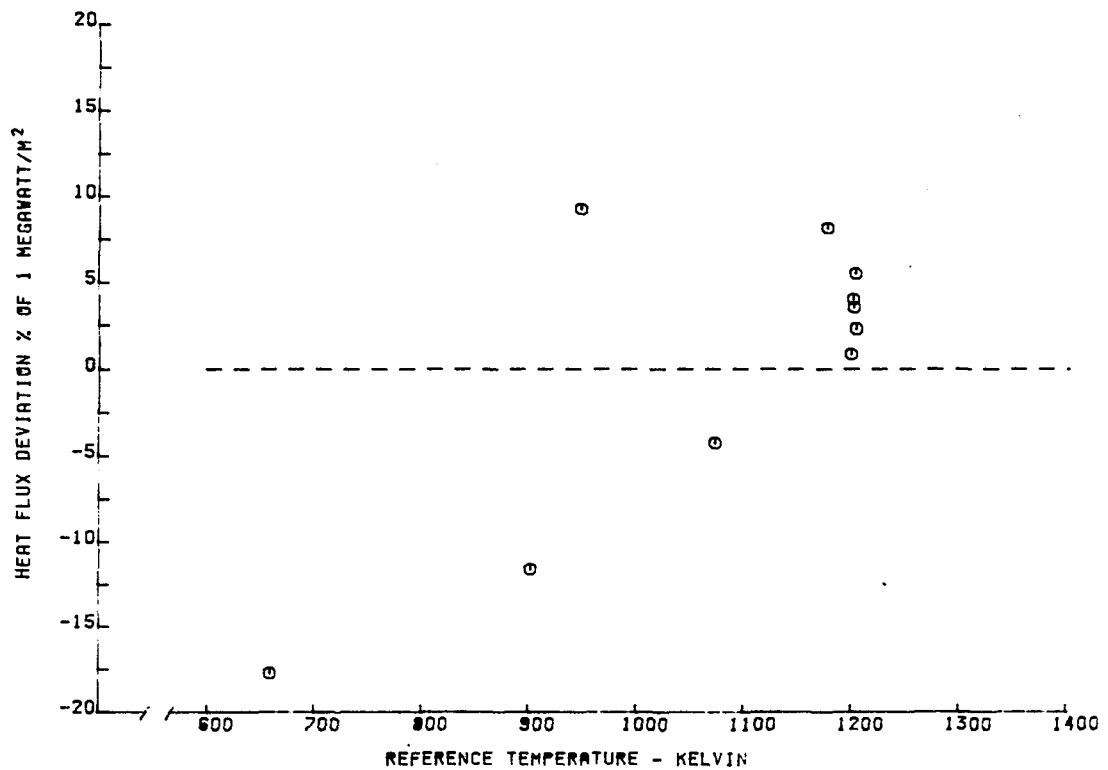Figure D-29   Voltage Output versus Heat Flux Transmitted through Laminated
Sensor L-7

Figure D-30   Heat Flux Deviation versus Sensor Reference Temperature for
Laminated Sensor L-7

TABLE D-XVI

CALIBRATION RESULTS FOR LAMINATED SENSOR L-7-UN

Q TRANSMITTED KILOWATTS/M**2	T REFERENCE KELVIN	OUTPUT MICROVOLTS	SENSITIVITY OUTPUT/UNIT Q
169.	1005.	36.	.21
126.	1170.	63.	.50
568.	1205.	165.	.29
464.	1055.	113.	.24
346.	885.	56.	.16
219.	650.	18.	.08
571.	1200.	165.	.29
444.	1205.	135.	.30
262.	1200.	80.	.30
124.	1200.	71.	.57

SENSOR CALIBRATION CONSTANT
BASED ON LEAST SQUARE LINE FORCED THROUGH ORIGIN OF OUTPUT VS. HEAT FLUX

S= .27   MICROVOLTS/KILOWATT/M**2

THE ABOVE CALIBRATION CONSTANT AND MICROVOLT OUTPUTS ARE NORMALIZED TO 1150K
IN USE Q MEASURED = (RAW OUTPUT MICROVOLTS)/(S-2.5433*10**(-4)*(1150K-TREF))
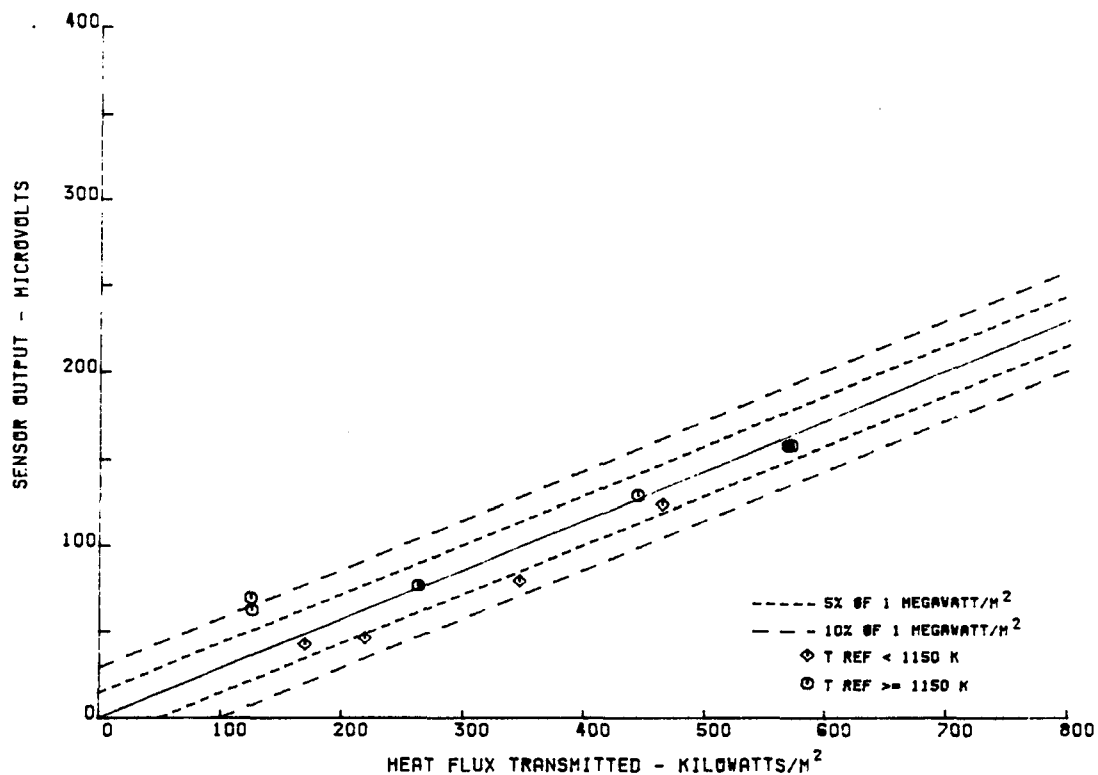
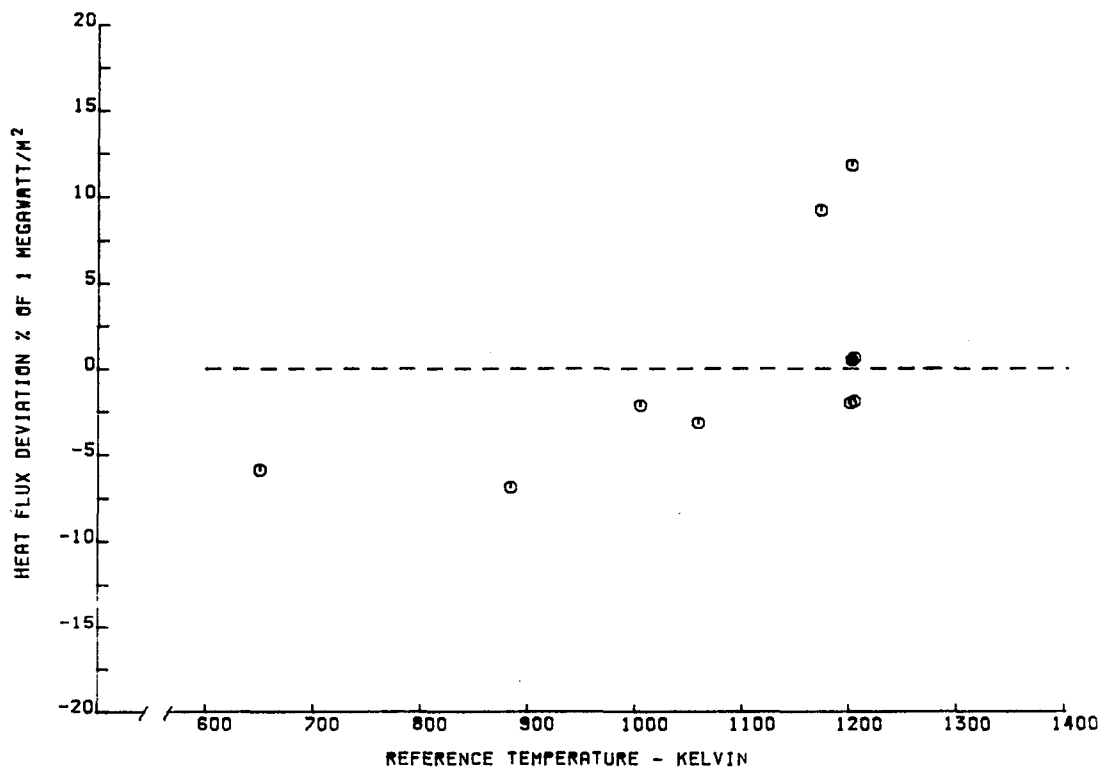Figure D-31   Voltage Output versus Heat Flux Transmitted through Laminated
Sensor L-7-UN

Figure D-32   Heat Flux Deviation versus Sensor Reference Temperature for
Laminated Sensor L-7-UN

TABLE D-XVII

CALIBRATION RESULTS FOR LAMINATED SENSOR L-8

Q TRANSMITTED KILOWATTS/M**2	T REFERENCE KELVIN	OUTPUT MICROVOLTS	SENSITIVITY OUTPUT/UNIT Q
546.12	1202.	124.	.228
466.92	1070.	101.	.217
355.29	884.	73.	.208
217.80	645.	41.	.192
559.16	1200.	126.	.226
425.71	1200.	93.	.219
275.47	1205.	54.	.196
115.81	1201.	5.	.047
122.60	1190.	16.	.136
189.37	931.	64.	.340
551.65	1202.	126.	.229
347.62	940.	68.	.197

SENSOR CALIBRATION CONSTANT
BASED ON LEAST SQUARE LINE FORCED THROUGH ORIGIN OF OUTPUT VS. HEAT FLUX

S= .21   MICROVOLTS/KILOWATT/M**2

THE ABOVE CALIBRATION CONSTANT AND MICROVOLT OUTPUTS ARE NORMALIZED TO 1150K
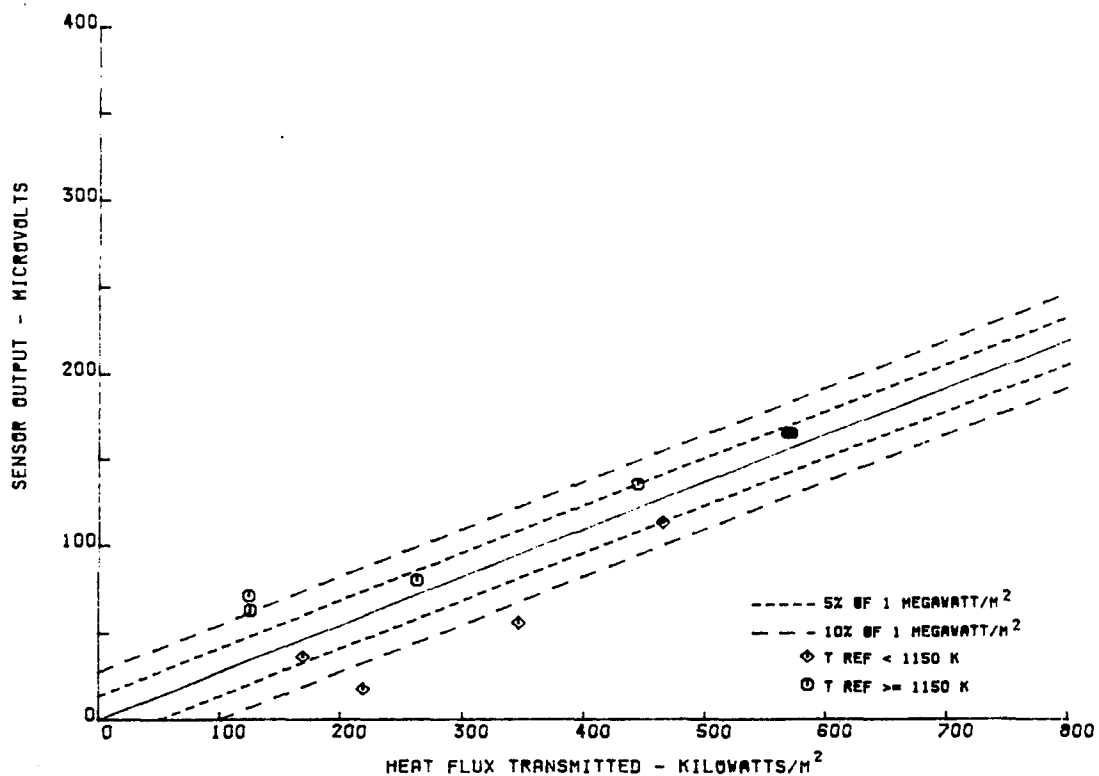IN USE Q MEASURED = (RAW OUTPUT MICROVOLTS)/(S-2.5433*10**(-4)*(1150K-TREF))

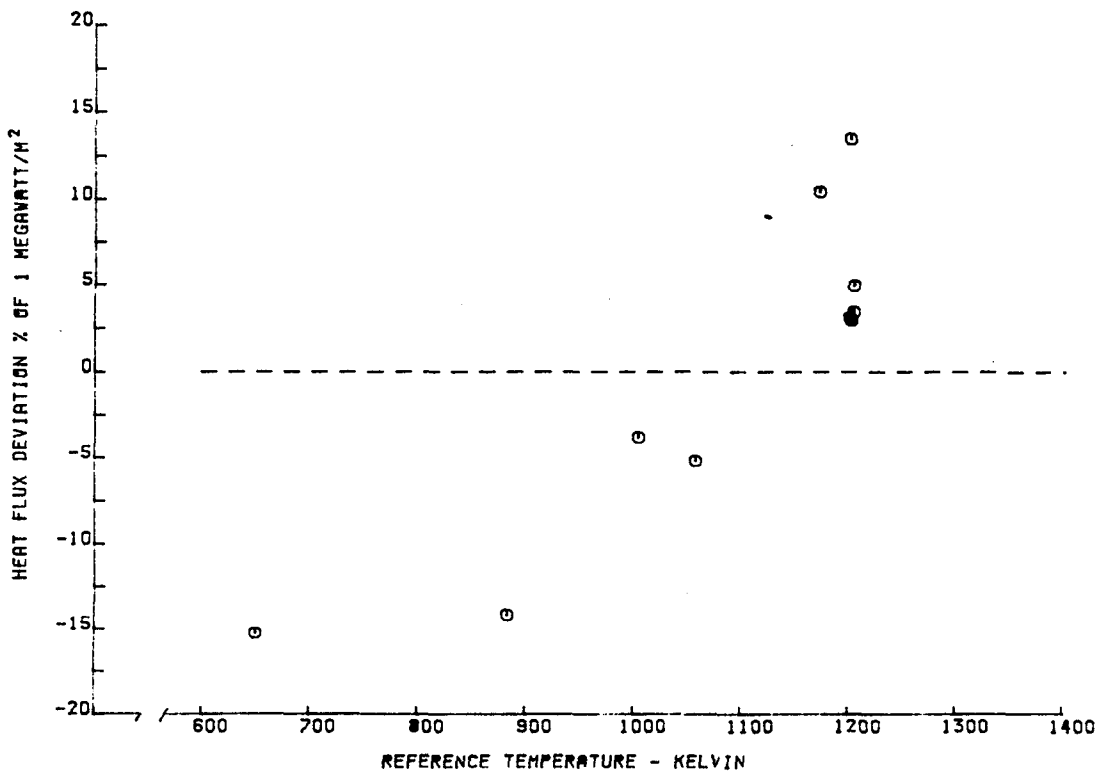Figure D-33   Voltage Output versus Heat Flux Transmitted through Laminated
Sensor L-8

Figure D-34   Heat Flux Deviation versus Sensor Reference Temperature for
Laminated Sensor L-8

153

TABLE D-XVIII

CALIBRATION RESULTS FOR LAMINATED SENSOR L-8-UN

Q TRANSMITTED KILOWATTS/M**2	T REFERENCE KELVIN	OUTPUT MICROVOLTS	SENSITIVITY OUTPUT/UNIT Q
546.	1205.	132.	.24
467.	1070.	92.	.20
355.	885.	50.	.14
218.	645.	14.	.06
559.	1200.	134.	.24
426.	1200.	99.	.23
275.	1205.	58.	.21
116.	1200.	7.	.06
123.	1190.	18.	.15
189.	930.	54.	.29
552.	1200.	134.	.24
348.	940.	50.	.14

SENSOR CALIBRATION CONSTANT
BASED ON LEAST SQUARE LINE FORCED THROUGH ORIGIN OF OUTPUT VS. HEAT FLUX

S= .2   MICROVOLTS/KILOWATT/M**2

THE ABOVE CALIBRATION CONSTANT AND MICROVOLT OUTPUTS ARE NORMALIZED TO 1150K
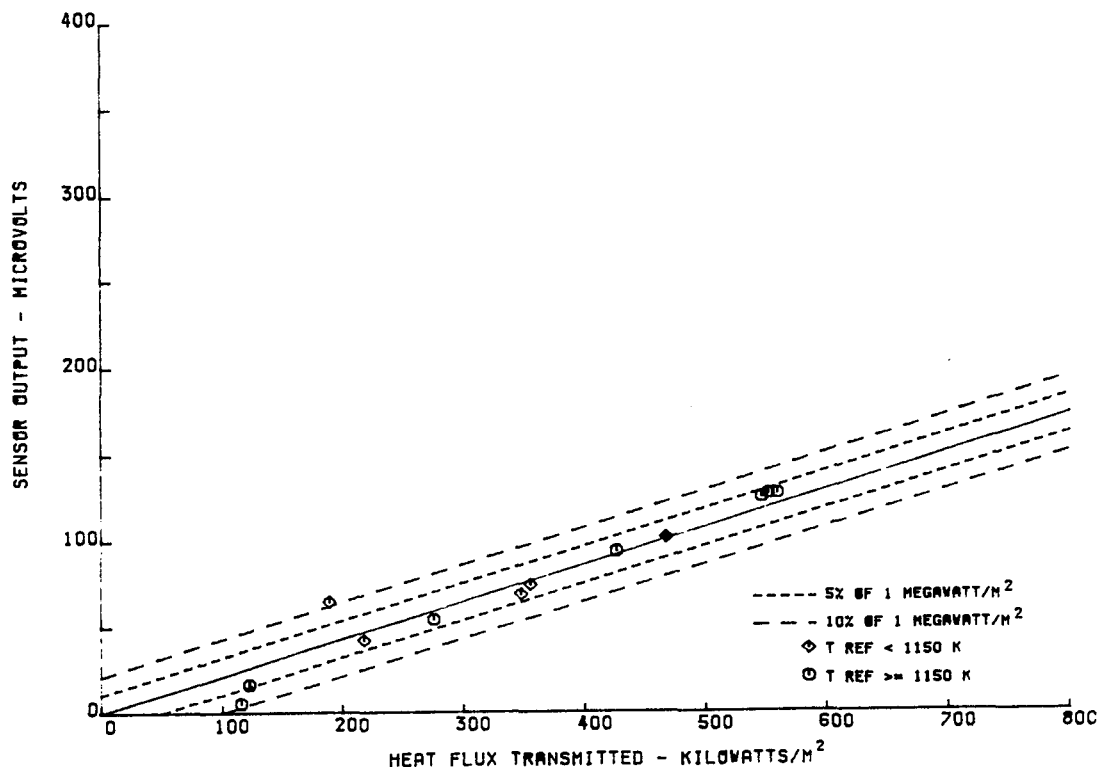IN USE Q MEASURED = (RAW OUTPUT MICROVOLTS)/(S-2.5433*10**(-4)*(1150K-TREF))

Figure D-35   Voltage Output versus Heat Flux Transmitted through Laminated
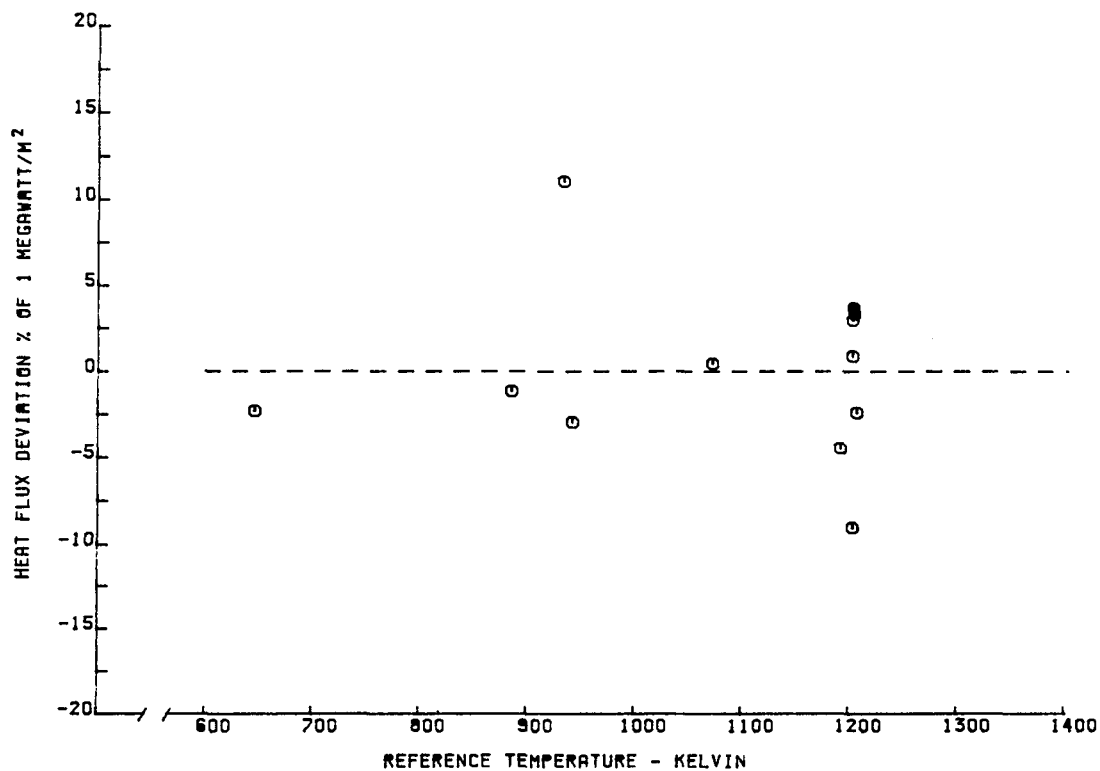Sensor L-8-UN

Figure D-36   Heat Flux Deviation versus Sensor Reference Temperature for
Laminated Sensor L-8-UN

155

TABLE D-XIX

CALIBRATION RESULTS FOR LAMINATED SENSOR L-9

Q TRANSMITTED KILOWATTS/M**2	T REFERENCE KELVIN	OUTPUT MICROVOLTS	SENSITIVITY OUTPUT/UNIT Q
177.70	983.	44.	.250
555.05	1203.	182.	.328
467.03	1059.	143.	.307
357.61	892.	108.	.303
226.65	668.	70.	.312
562.64	1199.	175.	.312
426.93	1203.	133.	.312
272.86	1204.	71.	.261
121.59	1191.	56.	.466

SENSOR CALIBRATION CONSTANT
BASED ON LEAST SQUARE LINE FORCED THROUGH ORIGIN OF OUTPUT VS. HEAT FLUX

S= .31   MICROVOLTS/KILOWATT/M**2

THE ABOVE CALIBRATION CONSTANT AND MICROVOLT OUTPUTS ARE NORMALIZED TO 1150K
IN USE Q MEASURED = (RAW OUTPUT MICROVOLTS)/(S-2.5433*10**(-4)*(1150K-TREF))
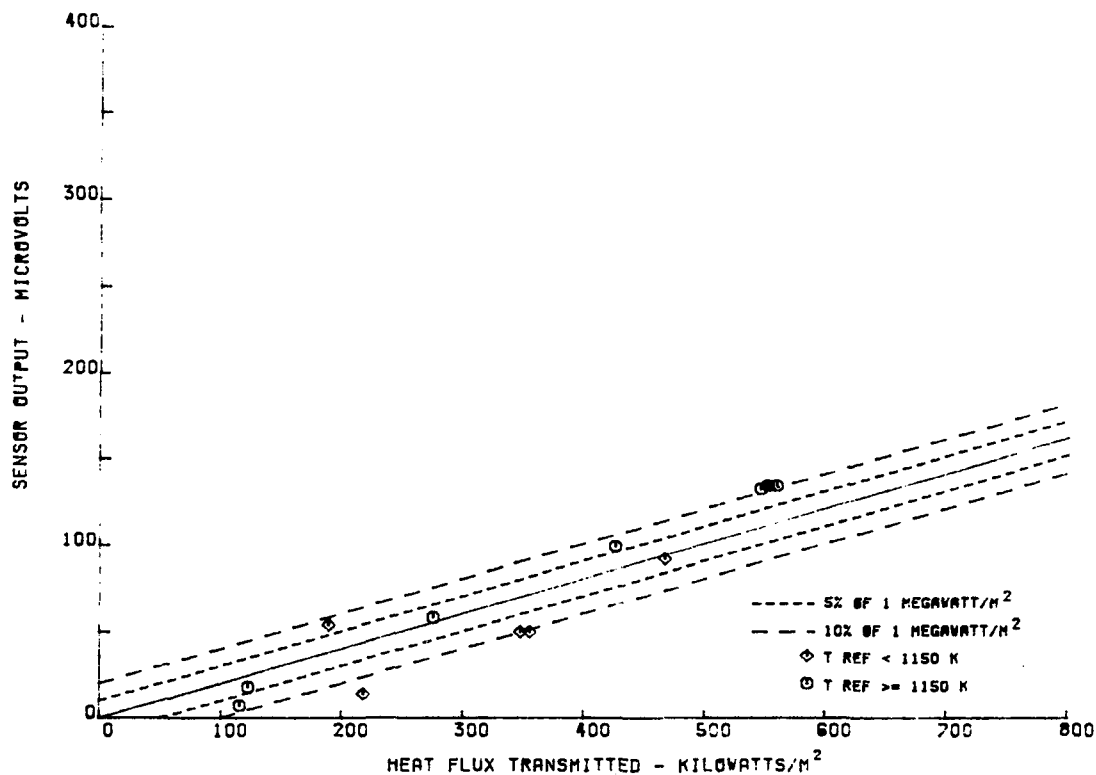
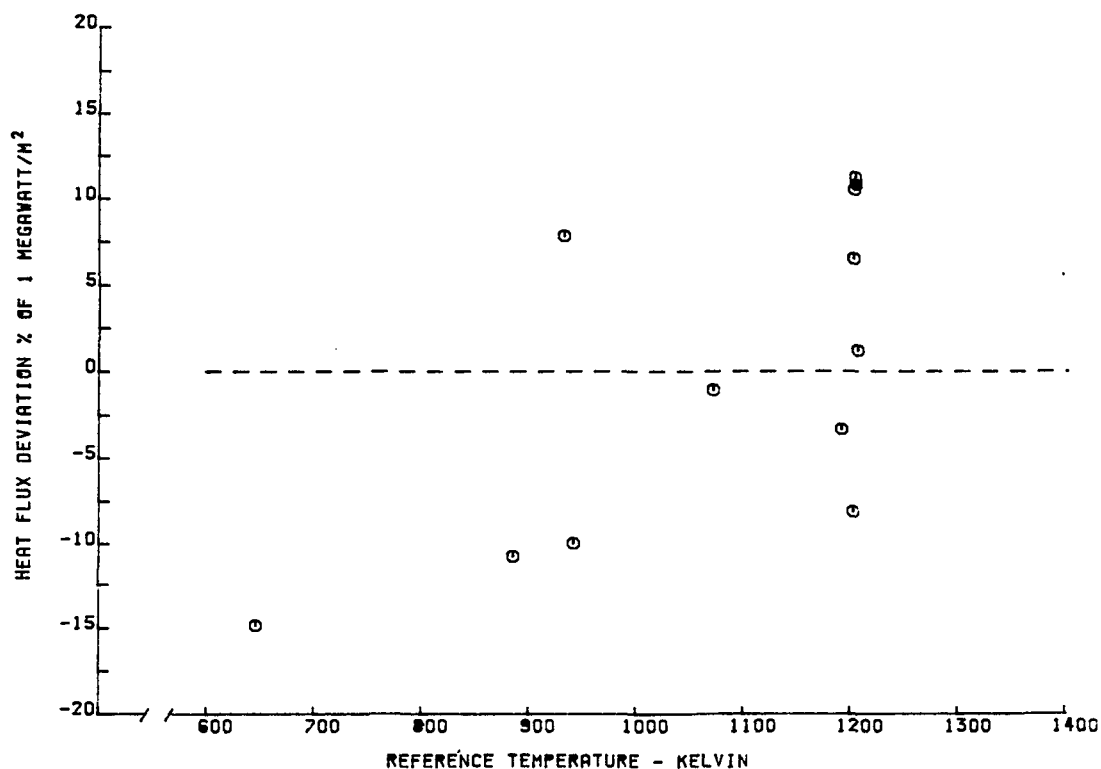Figure D-37   Voltage Output versus Heat Flux Transmitted through Laminated
Sensor L-9

Figure D-38   Heat Flux Deviation versus Sensor Reference Temperature for
Laminated Sensor L-9

157

TABLE D-XX

CALIBRATION RESULTS FOR LAMINATED SENSOR L-9-UN

Q TRANSMITTED KILOWATTS/M**2	T REFERENCE KELVIN	OUTPUT MICROVOLTS	SENSITIVITY OUTPUT/UNIT Q
178.	985.	37.	.21
555.	1205.	190.	.34
467.	1060.	133.	.28
358.	890.	85.	.24
227.	670.	43.	.19
563.	1200.	183.	.33
427.	1205.	139.	.33
273.	1205.	75.	.27
122.	1190.	58.	.48

SENSOR CALIBRATION CONSTANT
BASED ON LEAST SQUARE LINE FORCED THROUGH ORIGIN OF OUTPUT VS. HEAT FLUX

S= .29 MICROVOLTS/KILOWATT/M**2

THE ABOVE CALIBRATION CONSTANT AND MICROVOLT OUTPUTS ARE NORMALIZED TO 1150K
IN USE Q MEASURED = (RAW OUTPUT MICROVOLTS)/(S-2.5433*10**(-4)*(1150K-TREF))
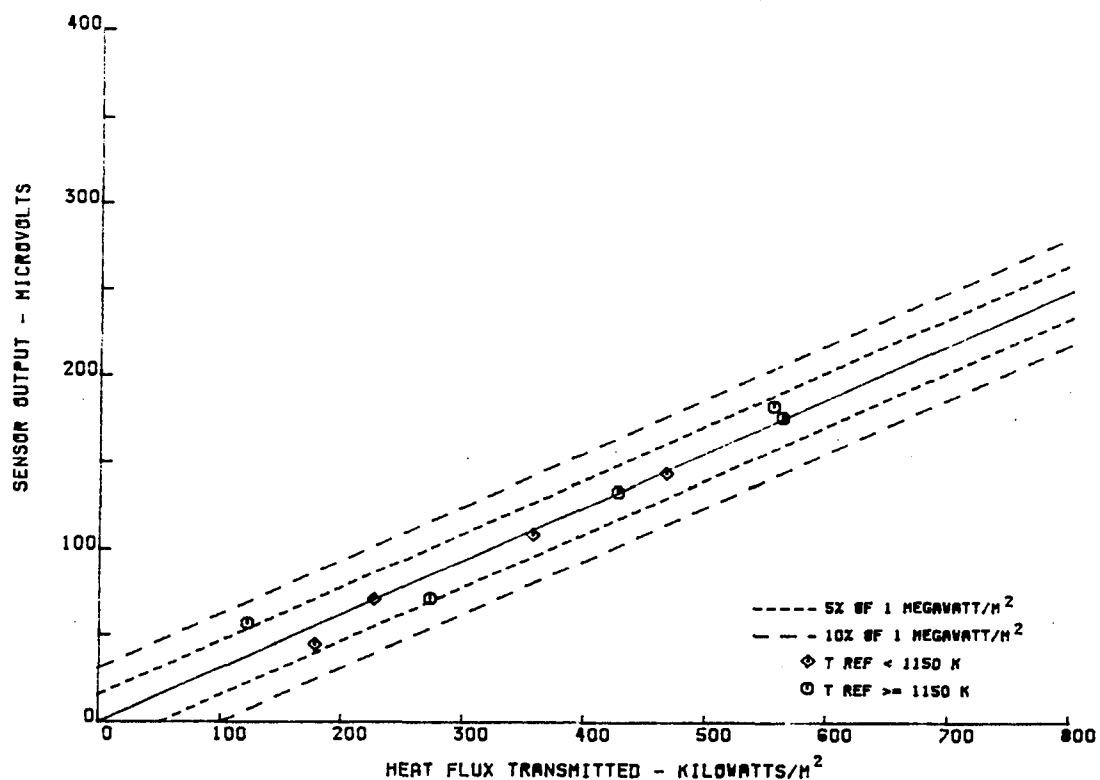
Figure D-39   Voltage Output versus Heat Flux Transmitted through Laminated
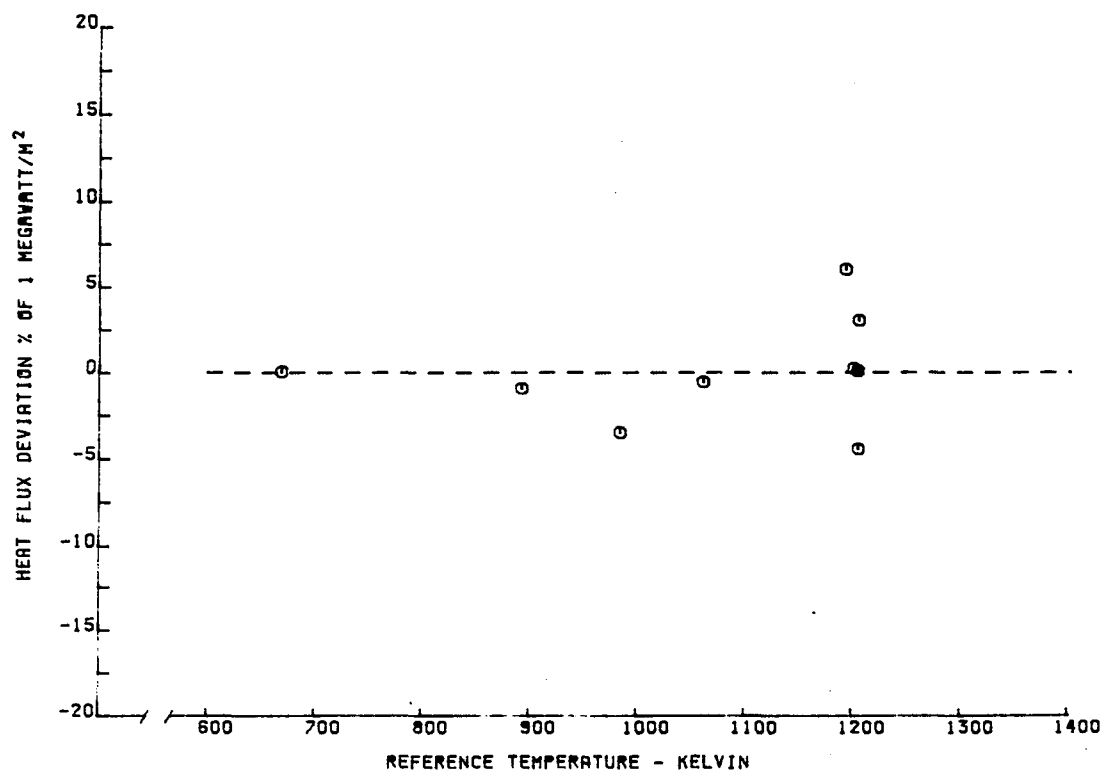Sensor L-9-UN

Figure D-40   Heat Flux Deviation versus Sensor Reference Temperature for
Laminated Sensor L-9-UN

159

TABLE D-XXI

CALIBRATION RESULTS FOR LAMINATED SENSOR L-10

Q TRANSMITTED KILOWATTS/M**2	T REFERENCE KELVIN	OUTPUT MICROVOLTS	SENSITIVITY OUTPUT/UNIT Q
178.79	979.	52.	.295
557.06	1205.	166.	.298
464.70	1079.	126.	.271
350.48	903.	93.	.265
220.89	670.	53.	.244
559.84	1199.	155.	.278
421.16	1200.	128.	.305
277.27	1204.	78.	.281
119.52	1197.	66.	.556

SENSOR CALIBRATION CONSTANT
BASED ON LEAST SQUARE LINE FORCED THROUGH ORIGIN OF OUTPUT VS. HEAT FLUX

S= .29   MICROVOLTS/KILOWATT/M**2

THE ABOVE CALIBRATION CONSTANT AND MICROVOLT OUTPUTS ARE NORMALIZED TO 1150K
IN USE Q MEASURED = (RAW OUTPUT MICROVOLTS)/(S-2.5433*10**(-4)*(1150K-TREF))
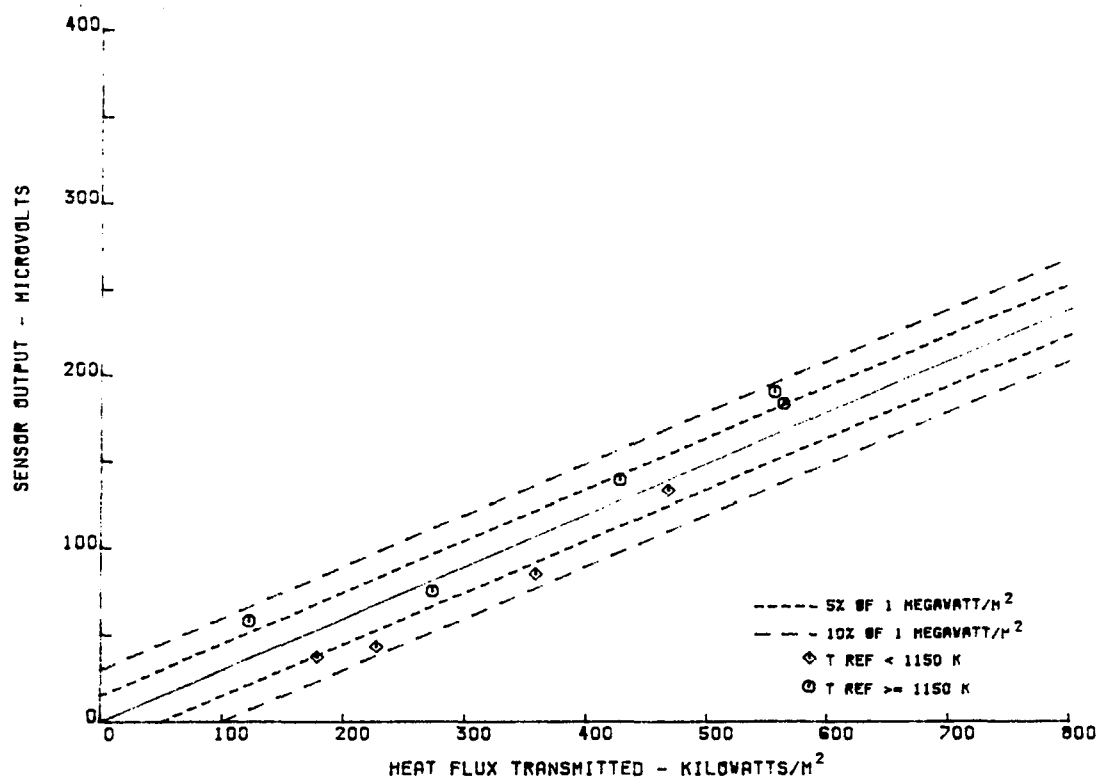
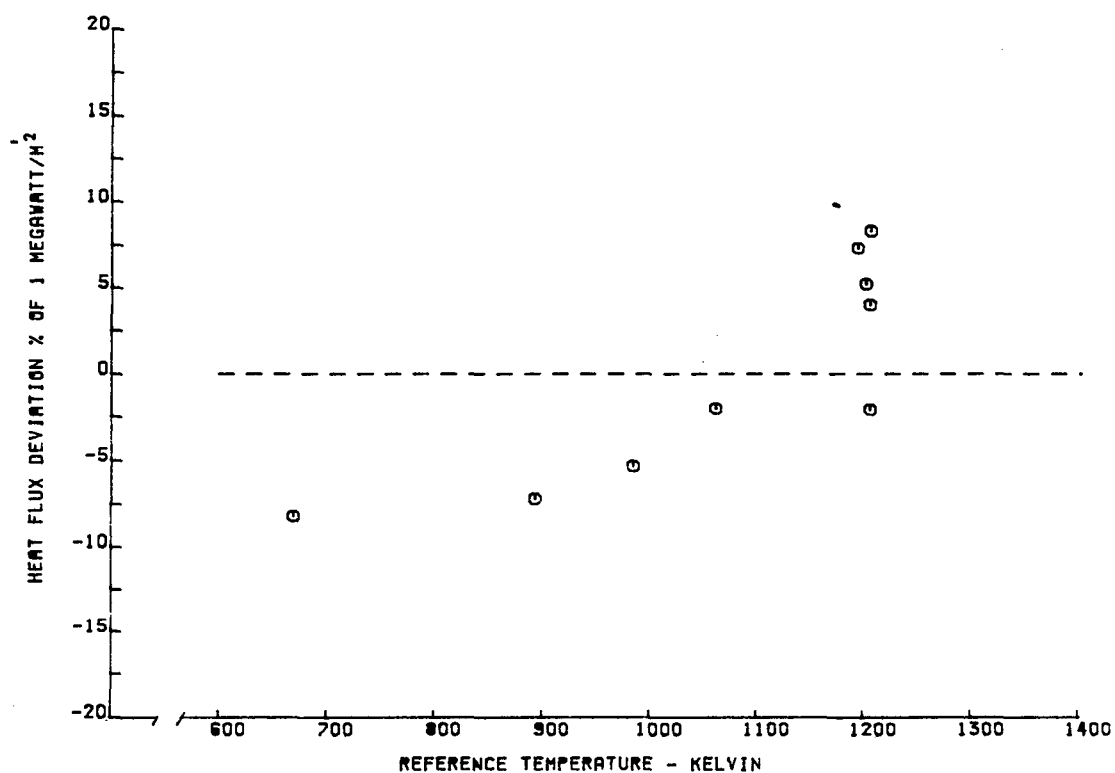Figure D-41   Voltage Output versus Heat Flux Transmitted through Laminated Sensor L-10

Figure D-42   Heat Flux Deviation versus Sensor Reference Temperature for Laminated Sensor L-10

TABLE D-XXII

CALIBRATION RESULTS FOR LAMINATED SENSOR L-10-UN

Q TRANSMITTED KILOWATTS/M**2	T REFERENCE KELVIN	OUTPUT MICROVOLTS	SENSITIVITY OUTPUT/UNIT Q
179.	980.	45.	.25
557.	1205.	174.	.31
465.	1080.	118.	.25
350.	905.	71.	.20
221.	670.	27.	.12
560.	1200.	163.	.29
421.	1200.	134.	.32
277.	1205.	82.	.30
120.	1200.	68.	.57

SENSOR CALIBRATION CONSTANT
BASED ON LEAST SQUARE LINE FORCED THROUGH ORIGIN OF OUTPUT VS. HEAT FLUX

S= .28   MICROVOLTS/KILOWATT/M**2

THE ABOVE CALIBRATION CONSTANT AND MICROVOLT OUTPUTS ARE NORMALIZED TO 1150K
IN USE Q MEASURED = (RAW OUTPUT MICROVOLTS)/(S-2.5433*10**(-4)*(1150K-TREF))
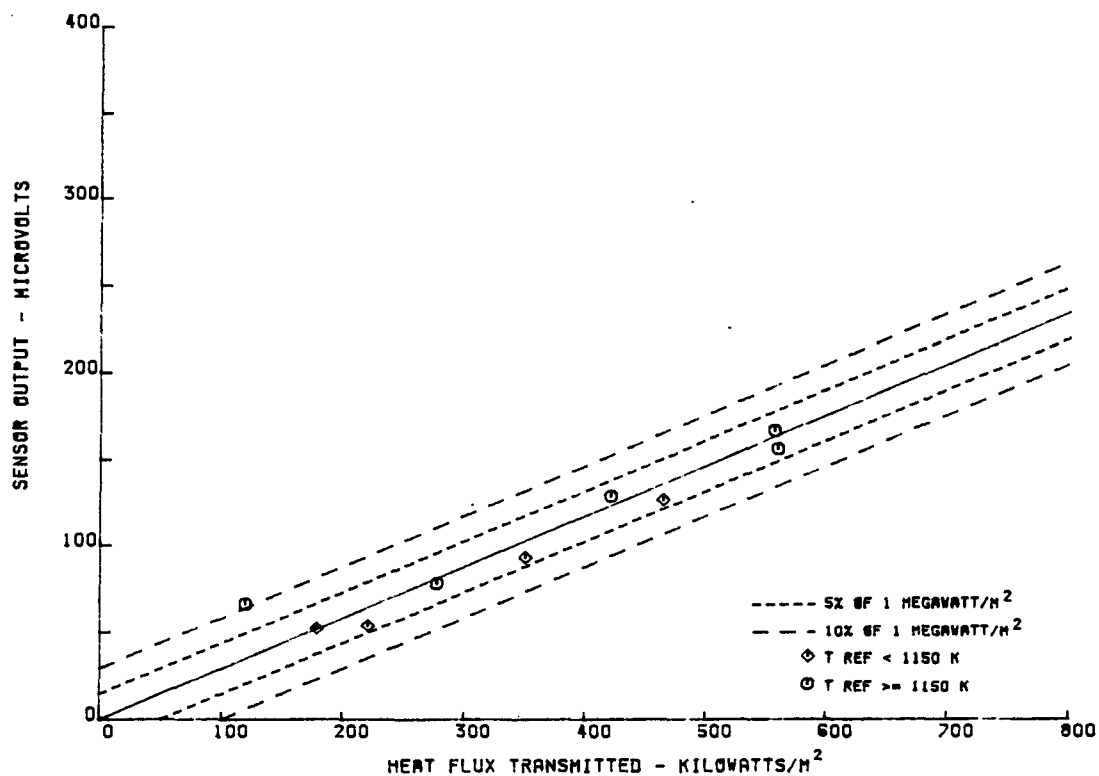
Figure D-43   Voltage Output versus Heat Flux Transmitted through Laminated
Sensor L-10-UN

Figure D-44   Heat Flux Deviation versus Sensor Reference Temperature for
Laminated Sensor L-10-UN

TABLE D-XXIII

CALIBRATION RESULTS FOR LAMINATED SENSOR L-11

Q TRANSMITTED KILOWATTS/M**2	T REFERENCE KELVIN	OUTPUT MICROVOLTS	SENSITIVITY OUTPUT/UNIT Q
193.60	910.	75.	.391
553.68	1200.	187.	.339
459.80	1074.	146.	.319
348.32	894.	112.	.323
220.42	673.	64.	.293
568.62	1204.	183.	.322
432.83	1201.	149.	.345
273.41	1200.	80.	.294
122.42	1190.	54.	.447

SENSOR CALIBRATION CONSTANT
BASED ON LEAST SQUARE LINE FORCED THROUGH ORIGIN OF OUTPUT VS. HEAT FLUX

S= .33   MICROVOLTS/KILOWATT/M**2

THE ABOVE CALIBRATION CONSTANT AND MICROVOLT OUTPUTS ARE NORMALIZED TO 1150K
IN USE Q MEASURED = (RAW OUTPUT MICROVOLTS)/(S-2.5433*10**(-4)*(1150K-TREF))

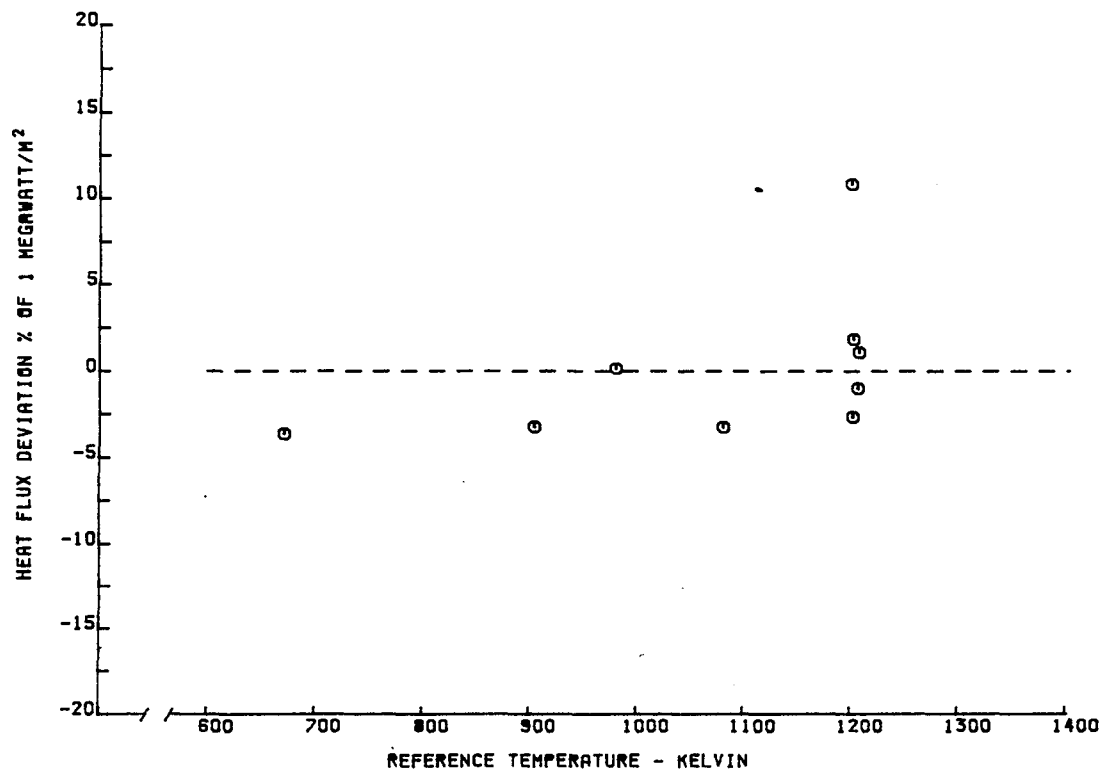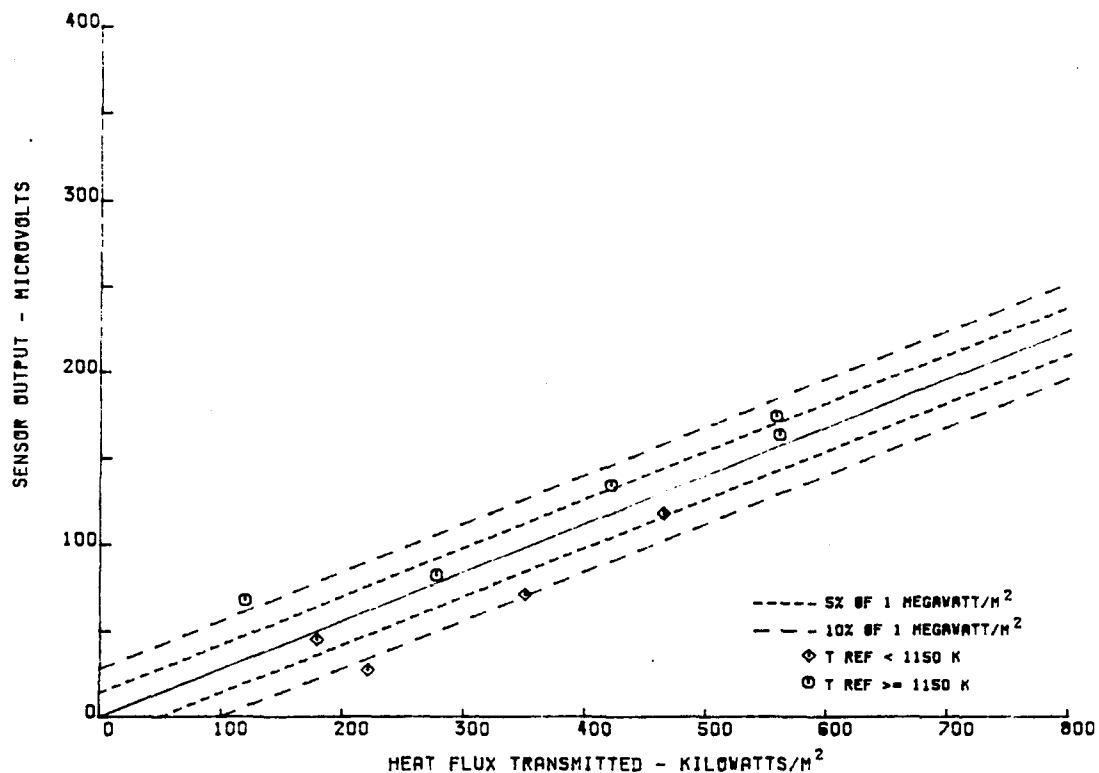Figure D-45   Voltage Output versus Heat Flux Transmitted through Laminated
Sensor L-11

Figure D-46   Heat Flux Deviation versus Sensor Reference Temperature for
Laminated Sensor L-11

165

TABLE D-XXIV

CALIBRATION RESULTS FOR LAMINATED SENSOR L-11-UN

Q TRANSMITTED KILOWATTS/M**2	T REFERENCE KELVIN	OUTPUT MICROVOLTS	SENSITIVITY OUTPUT/UNIT Q
194.	910.	64.	.33
554.	1200.	195.	.35
460.	1075.	138.	.30
348.	895.	90.	.26
220.	675.	38.	.17
569.	1205.	191.	.34
433.	1200.	155.	.36
273.	1200.	84.	.31
122.	1190.	56.	.46

SENSOR CALIBRATION CONSTANT
BASED ON LEAST SQUARE LINE FORCED THROUGH ORIGIN OF OUTPUT VS. HEAT FLUX

S= .31   MICROVOLTS/KILOWATT/M**2

THE ABOVE CALIBRATION CONSTANT AND MICROVOLT OUTPUTS ARE NORMALIZED TO 1150K
IN USE Q MEASURED = (RAW OUTPUT MICROVOLTS)/(S-2.5433*10**(-4)*(1150K-TREF))

Figure D-47   Voltage Output versus Heat Flux Transmitted through Laminated
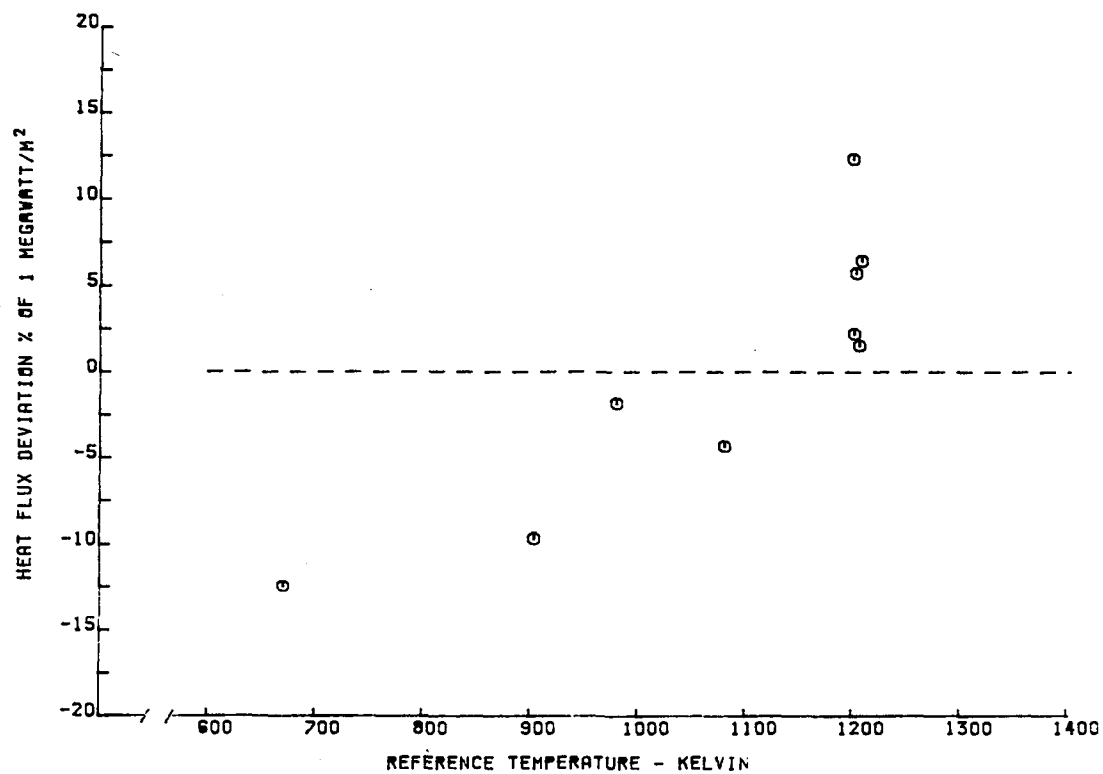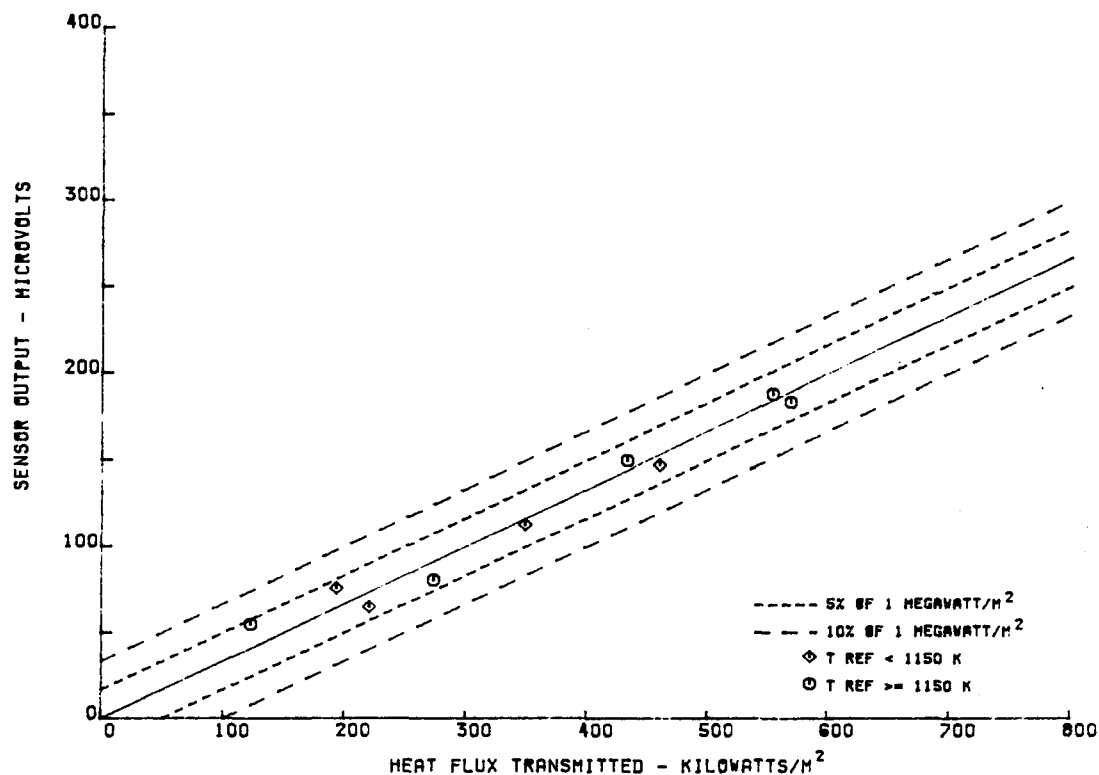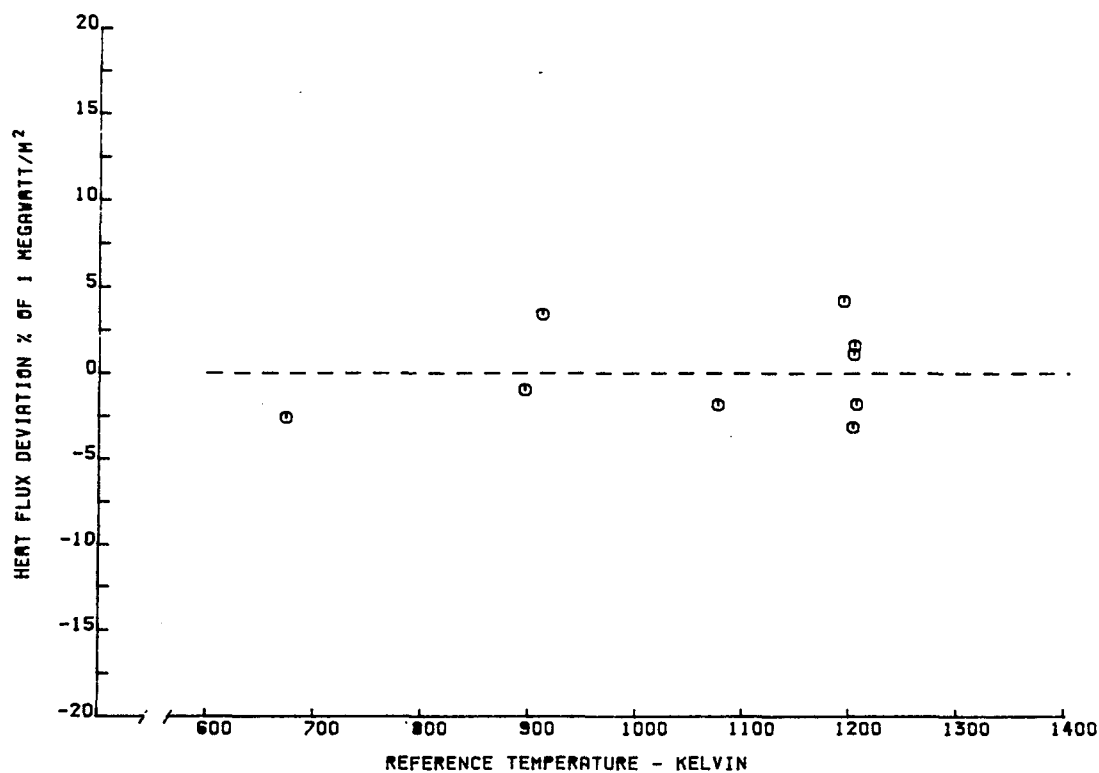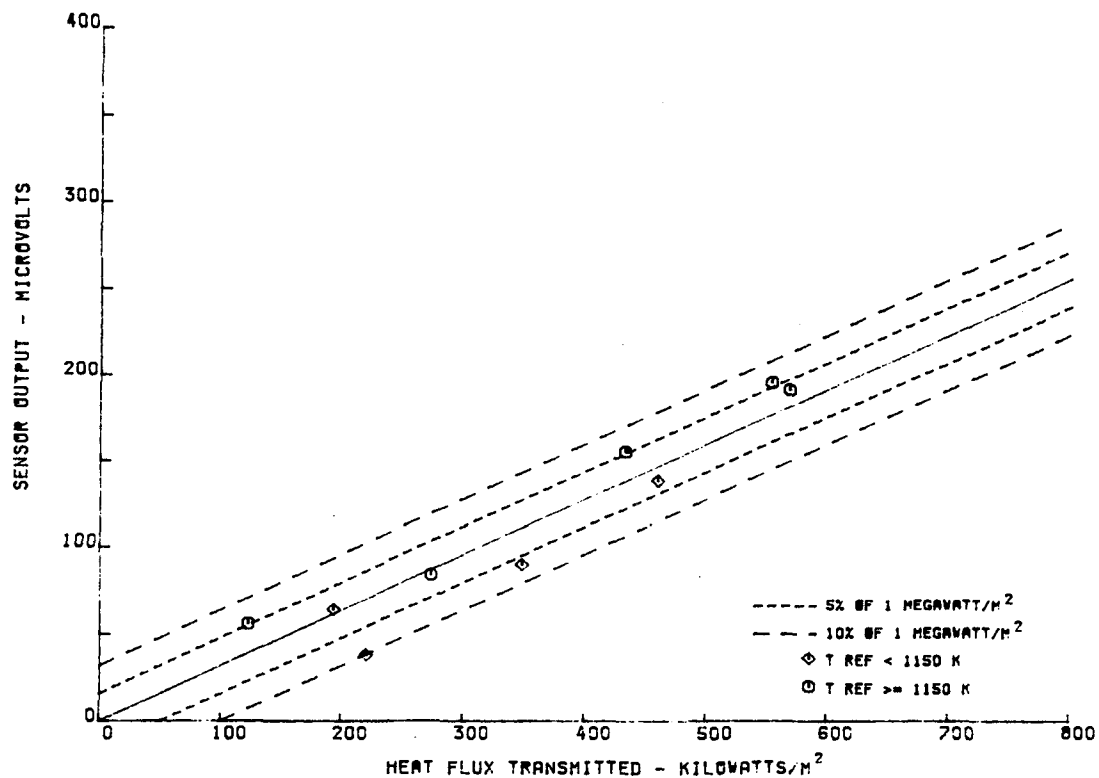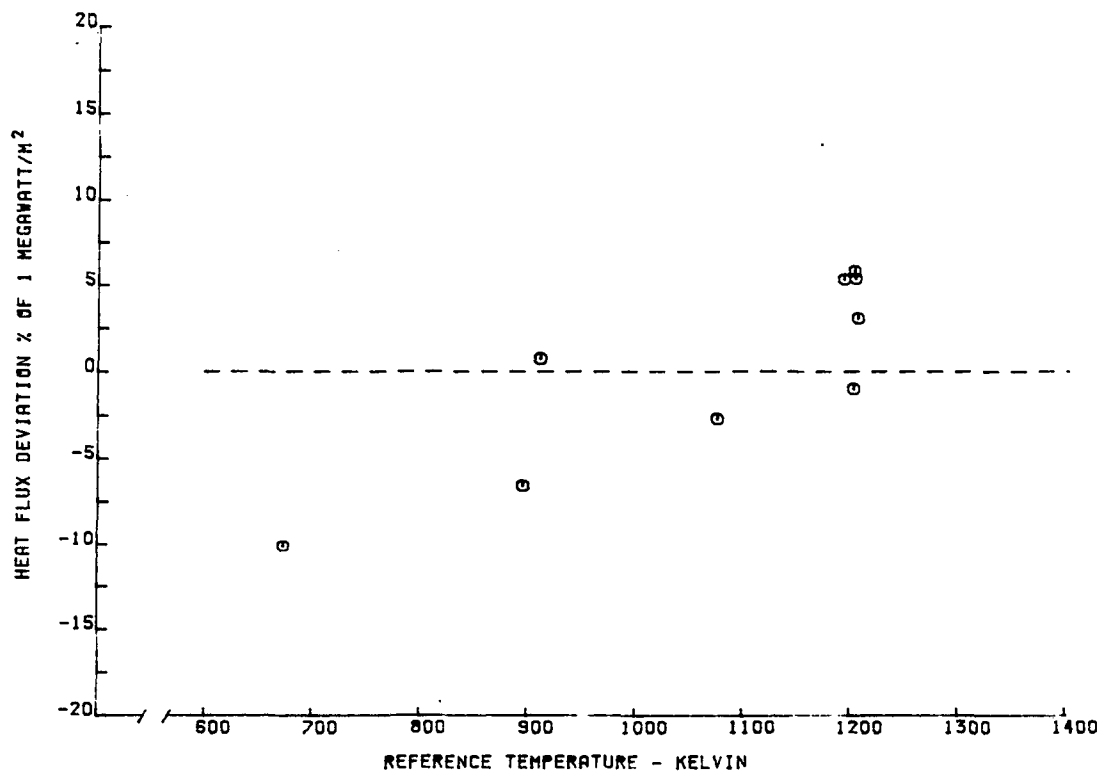Sensor L-11-UN

Figure D-48   Heat Flux Deviation versus Sensor Reference Temperature for
Laminated Sensor L-11-UN

APPENDIX E

CALIBRATION DATA

Gardon Gauge Sensors

This Appendix presents the calibration data from Gardon gauge sensors G-1 through G-9. All data from the calibration are presented although some of the high temperature, low heat flux points exhibit a large amount of scatter and are not representative of realistic operating conditions. The data for each sensor are presented in tabular form, as a plot of sensor microvolt output versus heat flux transmitted through the sensor, and as a plot of percent heat flux deviation versus sensor reference temperature. The heat flux transmitted values were calculated from incident heat flux measurements by accounting for absorption and losses from reradiation and convection. The percent heat flux deviation is the deviation of actual sensor output from the best straight line fit of the data through the origin expressed as a percent of the nominal maximum design heat flux of one megawatt per square meter.

File G-1-A is the calibration of sensor serial number G-1 with an air filled cavity, and the G-1 file is the calibration of the same sensor rebuilt with a ceramic filled cavity. Files G-3-A and G-9-A are recalibrations of these sensors after the thermal cycle tests.

A sensor calibration constant has been determined for each sensor based on a least square line forced through the origin of the microvolt output versus heat flux transmitted plot. This value is presented below the tabulated data. In use, the heat flux would be determined according to the relation:

$$Q_{measured} = \frac{1}{S} \times \text{microvolt output.}$$

TABLE E-I

CALIBRATION RESULTS FOR GARDON GAUGE SENSOR G-1

Q TRANSMITTED KILOWATTS/M**2	T REFERENCE KELVIN	OUTPUT MICROVOLTS	SENSITIVITY OUTPUT/UNIT Q
122.62	1171.	141.	1.149
622.76	1174.	555.	.891
512.56	1058.	463.	.903
371.19	878.	368.	.991
220.17	634.	245.	1.112
620.69	1178.	552.	.889
477.33	1173.	425.	.890
300.02	1173.	276.	.919
122.26	1172.	143.	1.169
124.17	1167.	139.	1.119

SENSOR CALIBRATION CONSTANT
BASED ON LEAST SQUARE LINE FORCED THROUGH ORIGIN OF OUTPUT VS. HEAT FLUX

S= .94   MICROVOLTS/KILOWATT/M**2

IN USE Q MEASURED = OUTPUT/S

This calibration data was taken with the cavity filled with GA-100 ceramic cement. The sensor was also calibrated in the three filament vacuum facility. The sensor experienced a leadwire failure external to the sensor caused by mechanical damage during handling.
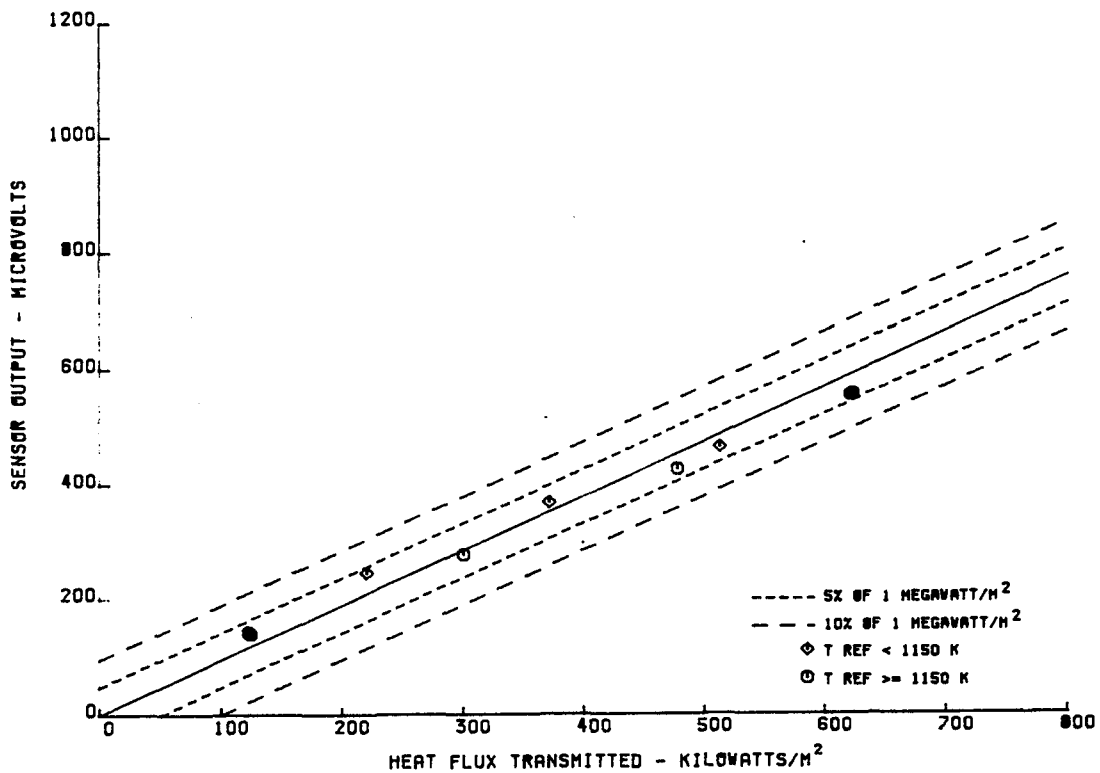
Figure E-1   Voltage Output versus Heat Flux Transmitted through Gardon
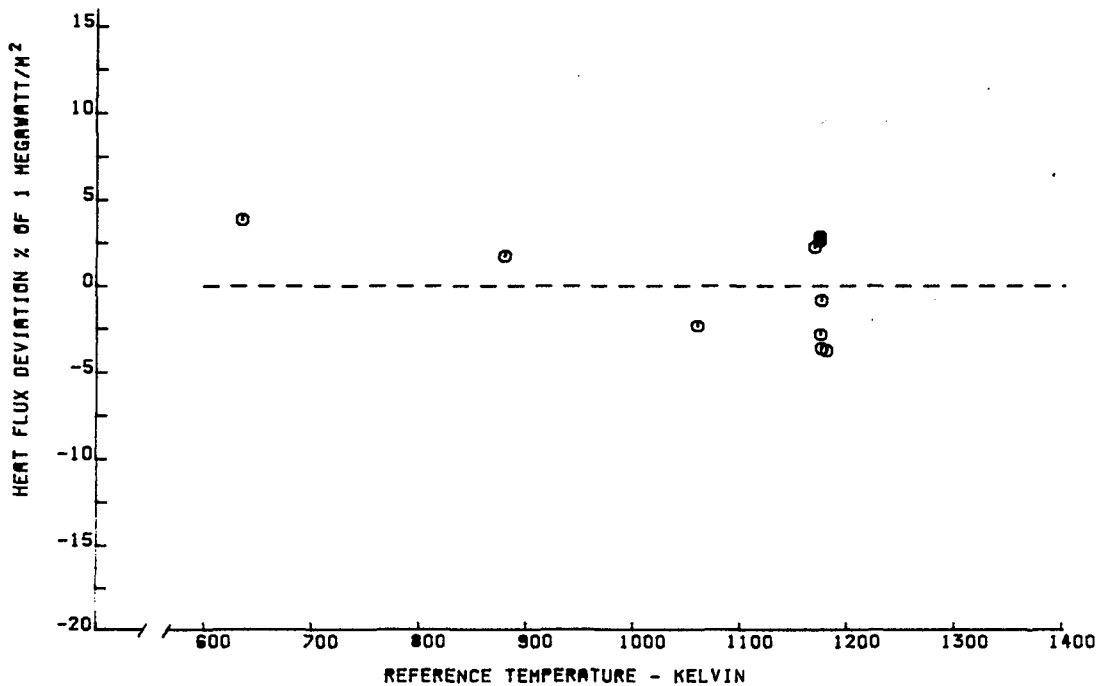   Gauge Sensor G-1

Figure E-2   Heat Flux Deviation versus Sensor Reference Temperature for
              Gardon Gauge Sensor G-1

TABLE E-II

CALIBRATION RESULTS FOR GARDON GAUGE SENSOR G-1A

Q TRANSMITTED KILOWATTS/M**2	T REFERENCE KELVIN	OUTPUT MICROVOLTS	SENSITIVITY OUTPUT/UNIT Q
191.56	870.	250.	1.305
147.37	1173.	194.	1.316
150.23	1162.	191.	1.271
620.33	1173.	725.	1.168
514.41	1053.	624.	1.213
218.91	614.	294.	1.343
626.88	1159.	730.	1.164
482.09	1172.	567.	1.176
307.27	1175.	370.	1.204
126.94	1168.	137.	1.079
126.95	1169.	144.	1.134

SENSOR CALIBRATION CONSTANT
BASED ON LEAST SQUARE LINE FORCED THROUGH ORIGIN OF OUTPUT VS. HEAT FLUX

S= 1.2   MICROVOLTS/KILOWATT/M**2

IN USE Q MEASURED = OUTPUT/S

This calibration data was taken with an air filled cavity and a thin sheet of Hastelloy-X covering the Cold Side Surface to provide aerodynamic integrity. After the calibration testing, the Hastelloy-X foil was removed and the cavity was filled with GA-100 ceramic cement for further testing.
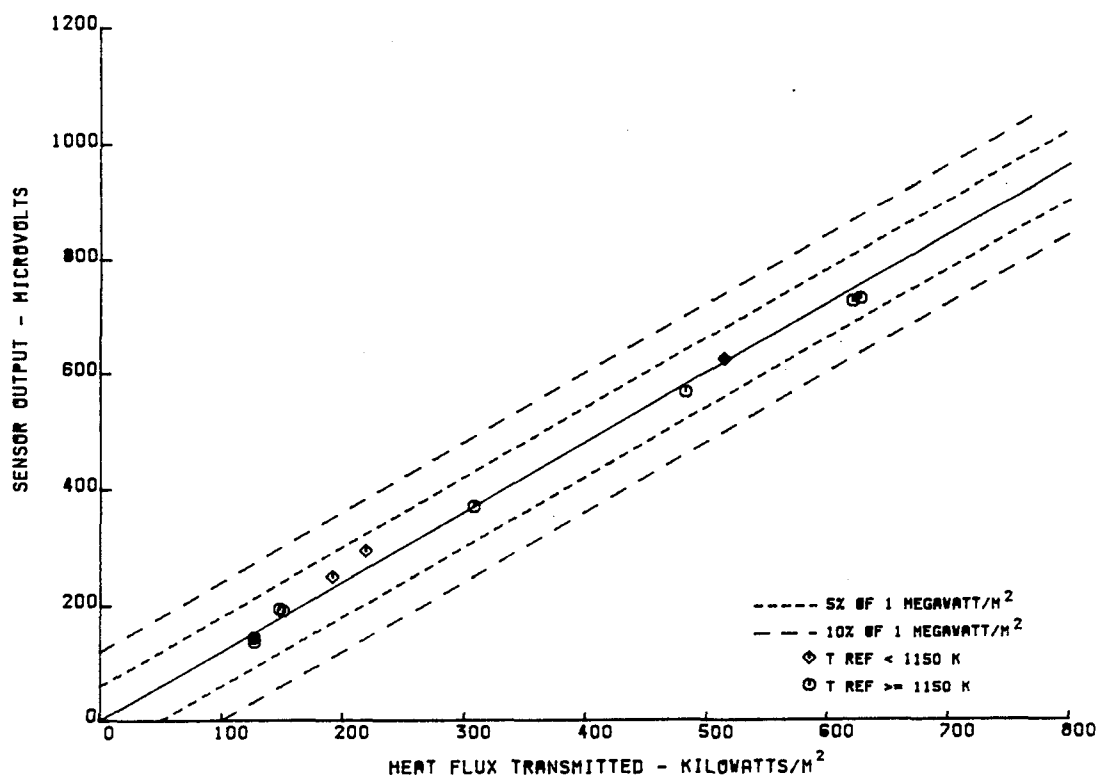
Figure E-3   Voltage Output versus Heat Flux Transmitted through Gardon
Gauge Sensor G-1A

Figure E-4   Heat Flux Deviation versus Sensor Reference Temperature for
Gardon Gauge Sensor G-1A

TABLE E-III

CALIBRATION RESULTS FOR GARDON GAUGE SENSOR G-2

Q TRANSMITTED KILOWATTS/M**2	T REFERENCE KELVIN	OUTPUT MICROVOLTS	SENSITIVITY OUTPUT/UNIT Q
219.39	706.	287.	1.308
209.02	807.	275.	1.315
121.40	1194.	246.	2.026
123.29	1194.	236.	1.914
127.42	1185.	149.	1.169
123.14	1198.	135.	1.096
647.70	1172.	769.	1.187
531.46	1065.	667.	1.255
395.32	848.	544.	1.376
229.67	602.	270.	1.175
646.40	1158.	777.	1.202
495.10	1173.	590.	1.191
322.83	1172.	400.	1.239

SENSOR CALIBRATION CONSTANT
BASED ON LEAST SQUARE LINE FORCED THROUGH ORIGIN OF OUTPUT VS. HEAT FLUX

S= 1.27   MICROVOLTS/KILOWATT/M**2

IN USE Q MEASURED = OUTPUT/S

The Chromel thermocouple lead failed after the 12th point of the initial calibration.
The failure was determined to be in the leadwire external to the sensor.

Figure E-5   Voltage Output versus Heat Flux Transmitted through Gardon Gauge Sensor G-2

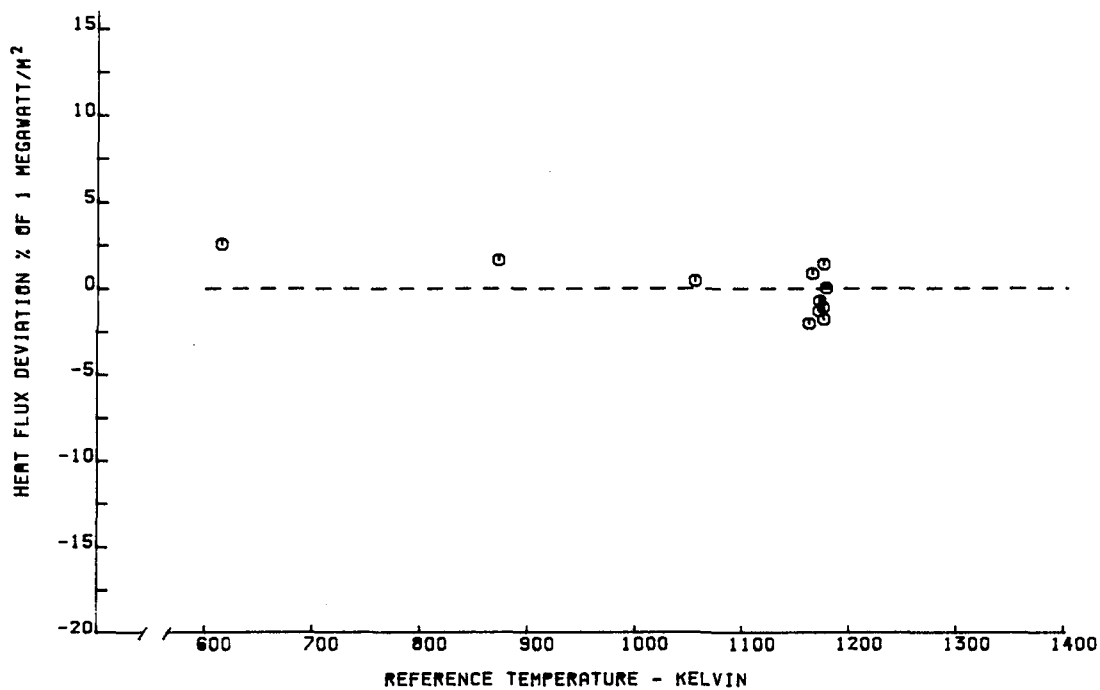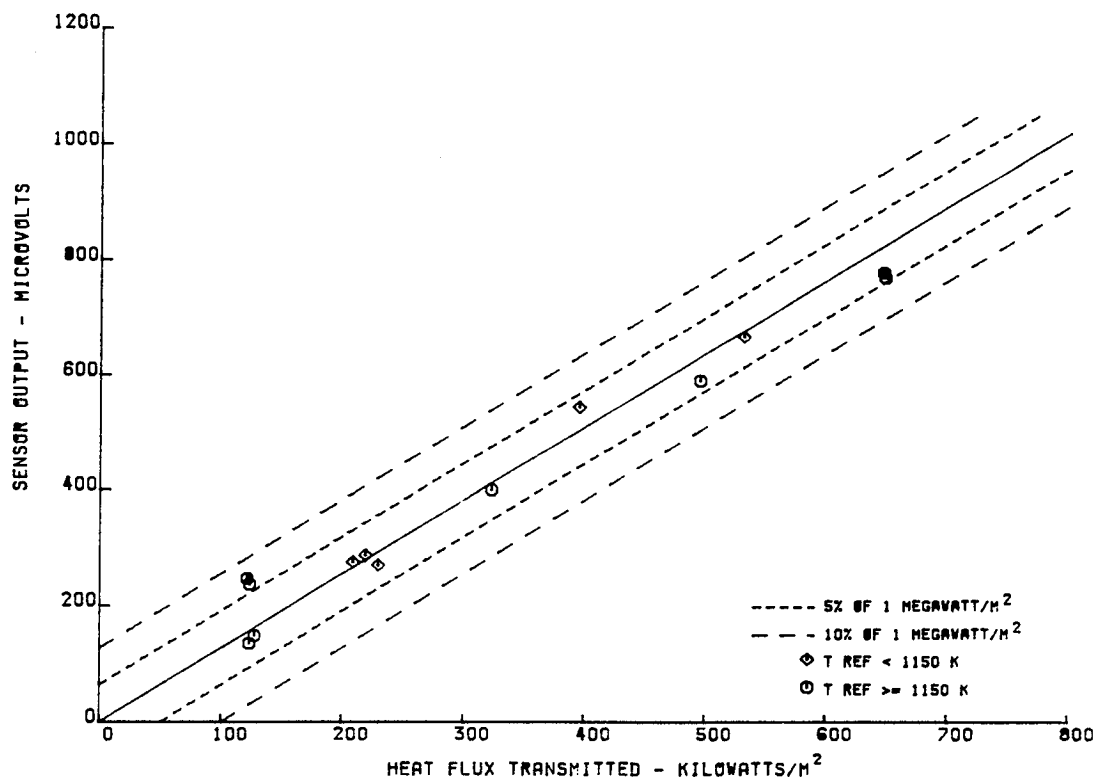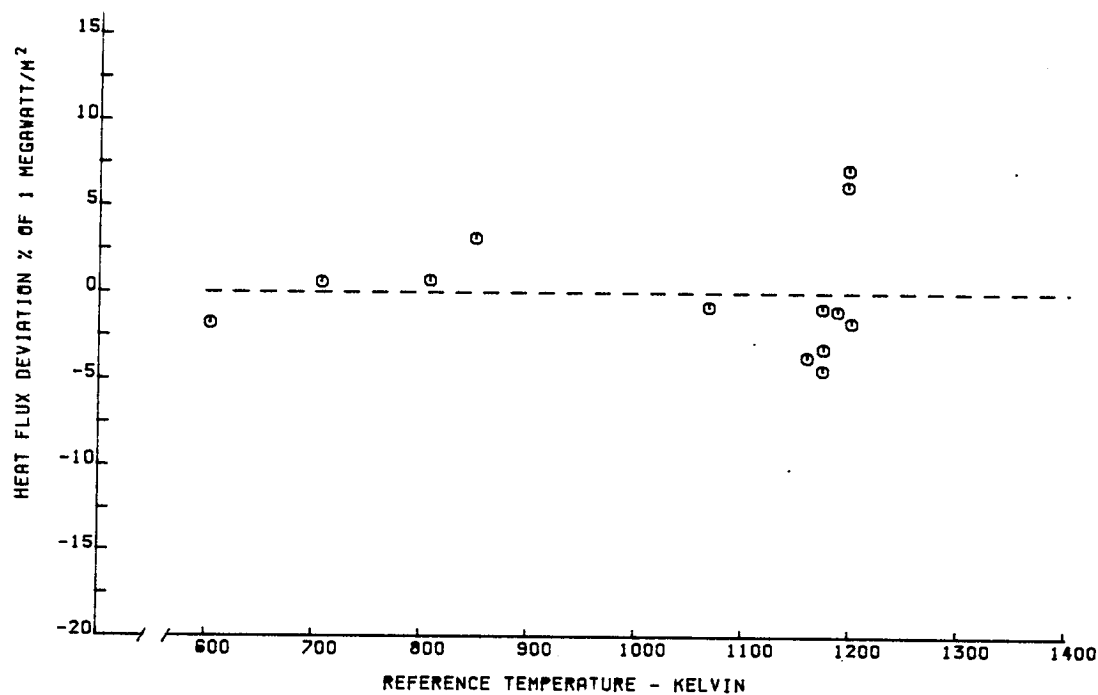**Figure E-6**   Heat Flux Deviation versus Sensor Reference Temperature for Gardon Gauge Sensor G-2

175

TABLE E-IV

CALIBRATION RESULTS FOR GARDON GAUGE SENSORS G-3 AND G-3A

Q TRANSMITTED KILOWATTS/M**2	T REFERENCE KELVIN	OUTPUT MICROVOLTS	SENSITIVITY OUTPUT/UNIT Q
212.81	787.	247.	1.160
130.48	1175.	139.	1.065
131.67	1174.	136.	1.032
130.51	1169.	237.	1.815
130.71	1171.	228.	1.744
646.40	1173.	608.	.940
536.40	1052.	538.	1.002
389.20	854.	401.	1.030
228.83	614.	209.	.913
649.66	1154.	615.	.946
496.25	1175.	455.	.916
316.65	1172.	304.	.960
130.79	1173.	114.	.871
382.16	1177.	355.	.928
386.85	1164.	361.	.933
380.96	1169.	399.	1.047
380.32	1171.	413.	1.085
384.60	1174.	432.	1.123

SENSOR CALIBRATION CONSTANT
BASED ON LEAST SQUARE LINE FORCED THROUGH ORIGIN OF OUTPUT VS. HEAT FLUX

S= 1.02 MICROVOLTS/KILOWATT/M**2

IN USE Q MEASURED = OUTPUT/S

SENSOR SERIAL NUMBER G-3-A
AFTER 50 HOUR SOAK

Q TRANSMITTED KILOWATTS/M**2	T REFERENCE KELVIN	OUTPUT MICROVOLTS	SENSITIVITY OUTPUT/UNIT Q
126.95	1176.	519.	4.088
585.31	1173.	2794.	4.773
479.82	1064.	1997.	4.161
359.60	907.	1438.	3.998
220.88	679.	2391.	10.824
586.48	1173.	2771.	4.724
451.80	1170.	2412.	5.338
295.83	1170.	1506.	5.090
126.86	1174.	359.	2.829
577.84	1174.	1991.	3.445
575.86	1172.	1998.	3.469

SENSOR CALIBRATION CONSTANT
BASED ON LEAST SQUARE LINE FORCED THROUGH ORIGIN OF OUTPUT VS. HEAT FLUX

S= 4.59 MICROVOLTS/KILOWATT/M**2

This sensor visually exhibited a non-uniform temperature profile on the cold side, and a poor lamination from the diffusion bonding is suspected. After the 50 hour thermal ageing test, the output was erratic, and this was traced to secondary junctions in the leadwires external to the sensor. The data from after the thermal ageing is not presented in plot form.
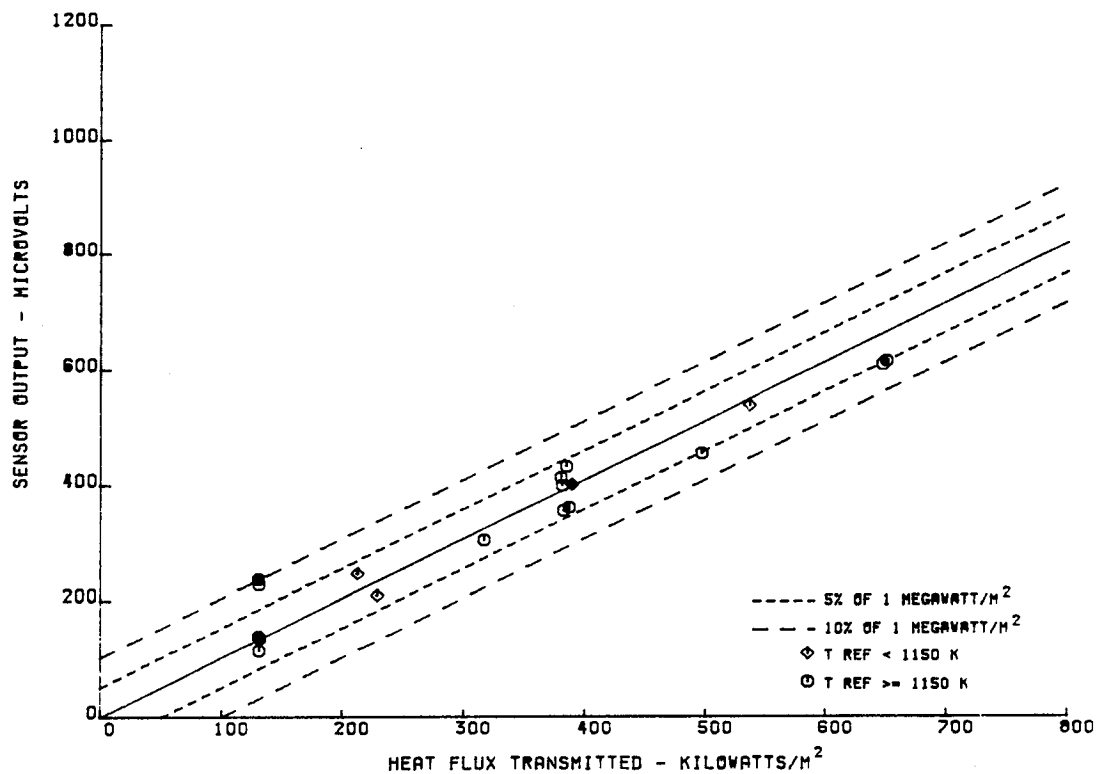
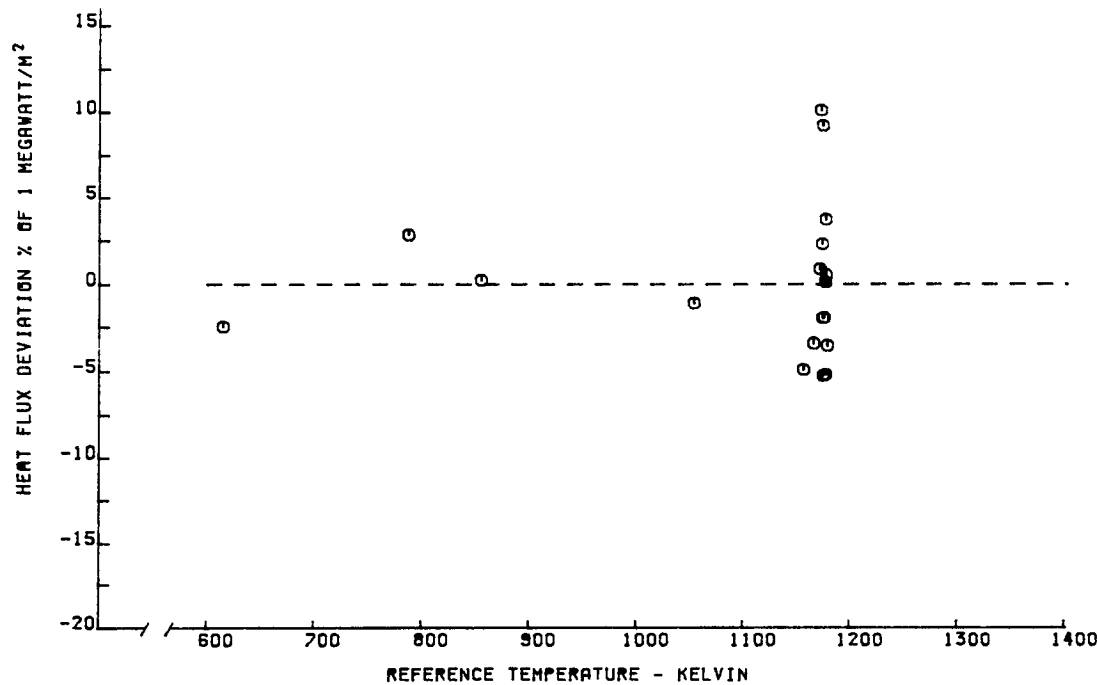Figure E-7   Voltage Output versus Heat Flux Transmitted through Gardon
Gauge Sensor G-3

Figure E-8   Heat Flux Deviation versus Sensor Reference Temperature for
Gardon Gauge Sensor G-3

TABLE E-V

CALIBRATION RESULTS FOR GARDON GAUGE SENSOR G-4

Q TRANSMITTED KILOWATTS/M**2	T REFERENCE KELVIN	OUTPUT MICROVOLTS	SENSITIVITY OUTPUT/UNIT Q
198.60	882.	359.	1.807
130.75	1172.	218.	1.667
651.15	1174.	1067.	1.638
538.55	1041.	916.	1.700
389.61	857.	689.	1.768
229.05	609.	387.	1.689
648.78	1174.	1066.	1.643
499.18	1173.	832.	1.666
314.13	1175.	531.	1.690
132.16	1174.	192.	1.452
386.24	1174.	655.	1.695
385.33	1173.	706.	1.832
373.67	1173.	711.	1.902
386.26	1172.	734.	1.900
383.55	1175.	697.	1.817

SENSOR CALIBRATION CONSTANT
BASED ON LEAST SQUARE LINE FORCED THROUGH ORIGIN OF OUTPUT VS. HEAT FLUX

S= 1.72 MICROVOLTS/KILOWATT/M**2

IN USE Q MEASURED = OUTPUT/S
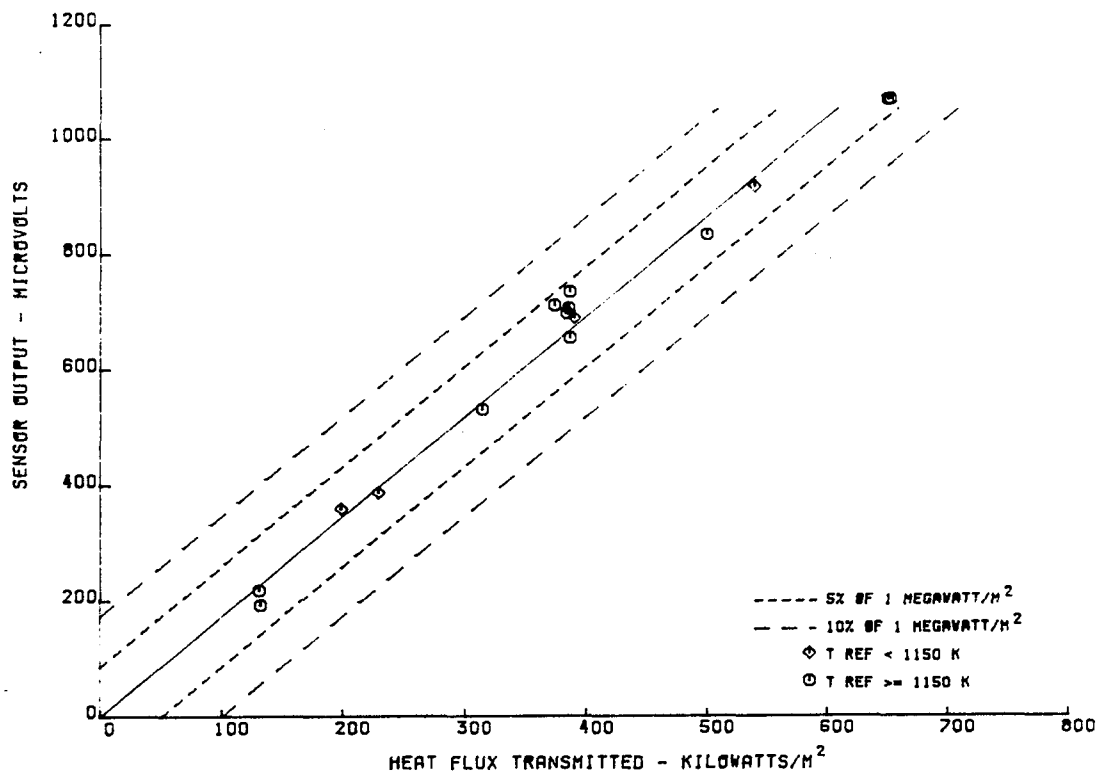
Figure E-9   Voltage Output versus Heat Flux Transmitted through Gardon
              Gauge Sensor G-4

Figure E-10   Heat Flux Deviation versus Sensor Reference Temperature for
              Gardon Gauge Sensor G-4

TABLE E-VI

CALIBRATION RESULTS FOR GARDON GAUGE SENSOR G-5

Q TRANSMITTED KILOWATTS/M**2	T REFERENCE KELVIN	OUTPUT MICROVOLTS	SENSITIVITY OUTPUT/UNIT Q
140.56	1134.	158.	1.124
128.61	1172.	119.	.925
632.74	1174.	577.	.911
529.93	1052.	496.	.935
367.06	977.	392.	1.067
204.83	825.	238.	1.161

SENSOR CALIBRATION CONSTANT
BASED ON LEAST SQUARE LINE FORCED THROUGH ORIGIN OF OUTPUT VS. HEAT FLUX

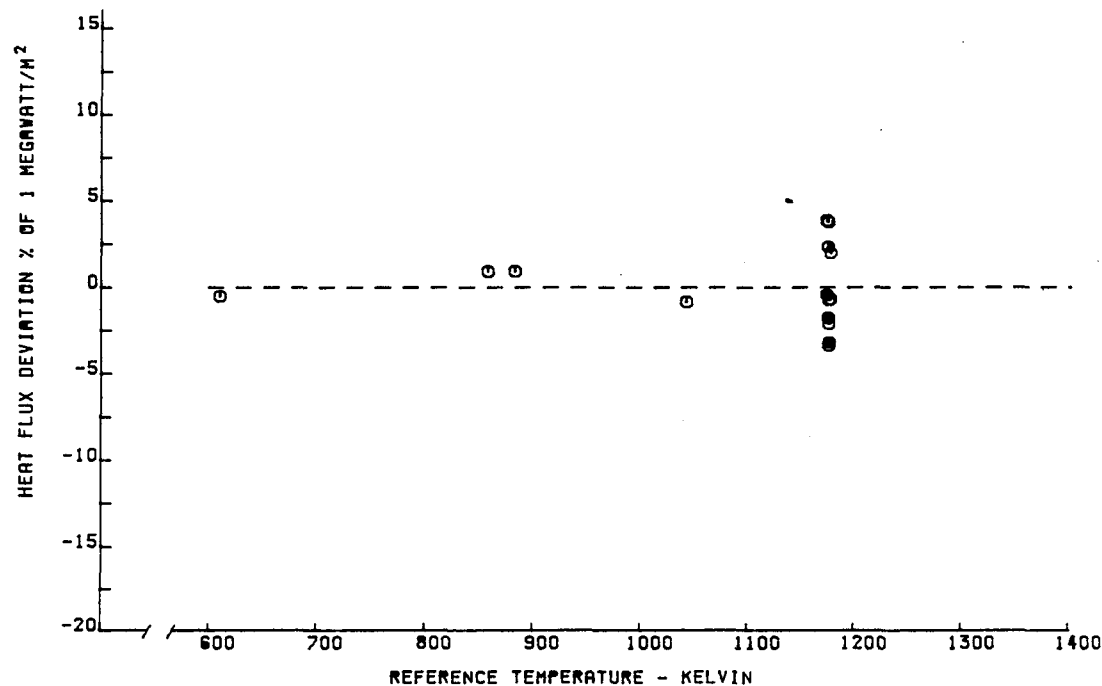S= .98   MICROVOLTS/KILOWATT/M**2

IN USE Q MEASURED = OUTPUT/S

This sensor expereienced a leadwire failure after the 6th point of the initial calibration, and the failure was found to be at the point where the leadwire exits the sensor. The cause of failure is believed to be vibration caused by the cooling air.
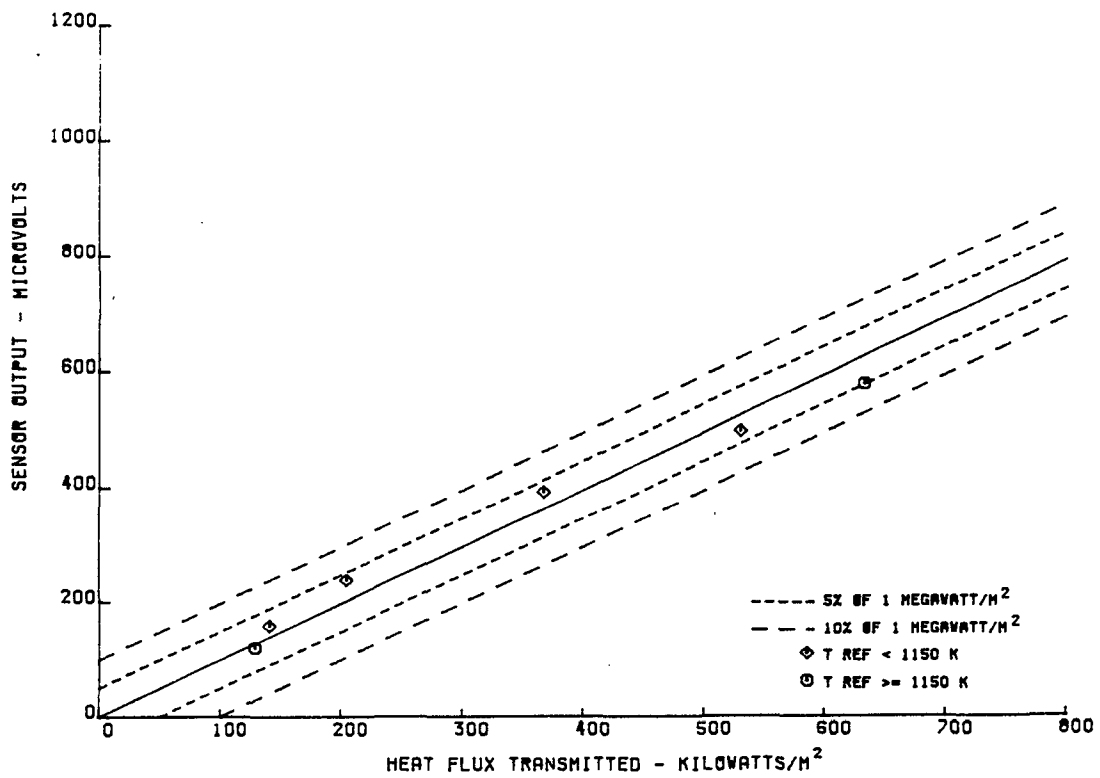
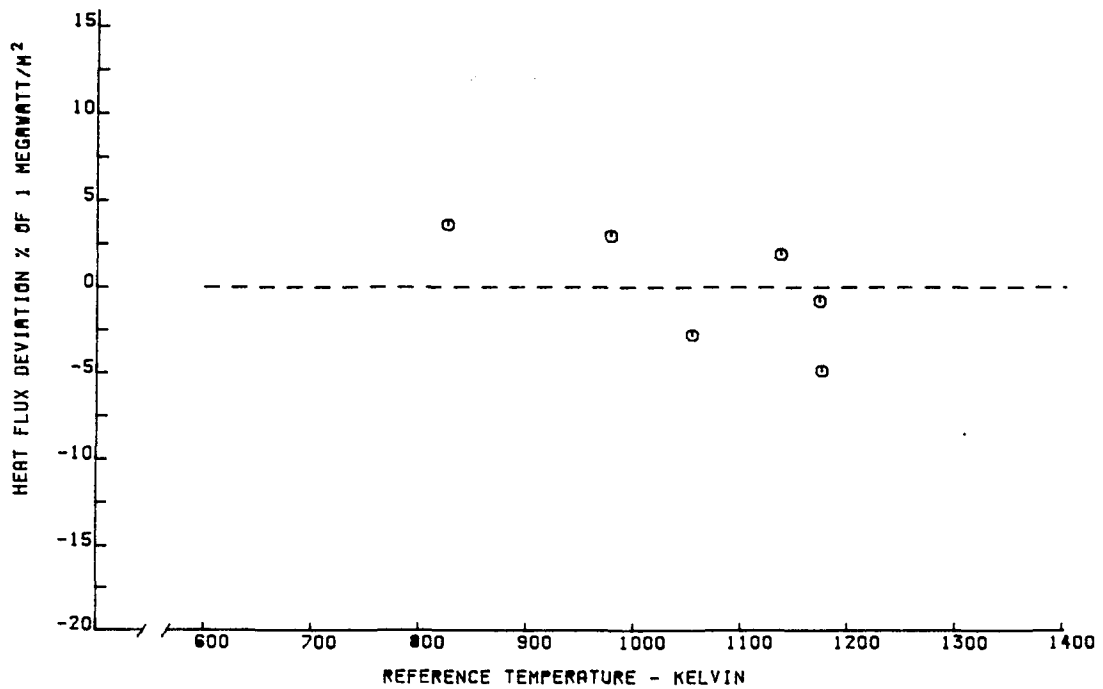Figure E-11   Voltage Output versus Heat Flux Transmitted through Gardon
Gauge Sensor G-5

Figure E-12   Heat Flux Deviation versus Sensor Reference Temperature for
Gardon Gauge Sensor G-5

TABLE E-VII

CALIBRATION RESULTS FOR GARDON GAUGE SENSOR G-6

Q TRANSMITTED KILOWATTS/M**2	T REFERENCE KELVIN	OUTPUT MICROVOLTS	SENSITIVITY OUTPUT/UNIT Q
142.06	1132.	166.	1.168
651.52	1173.	669.	1.026
529.53	1006.	589.	1.112
386.72	823.	413.	1.067
227.09	594.	252.	1.109
644.82	1150.	660.	1.023
495.61	1175.	511.	1.031
312.82	1174.	321.	1.026
129.57	1170.	137.	1.057

SENSOR CALIBRATION CONSTANT
BASED ON LEAST SQUARE LINE FORCED THROUGH ORIGIN OF OUTPUT VS. HEAT FLUX

S= 1.05   MICROVOLTS/KILOWATT/M**2

IN USE Q MEASURED = OUTPUT/S

The Alumel lead to the cold side of this sensor failed during the 20th cycle of a 50 cycle thermal test. The open was determined to be in the leadwire external to the sensor.
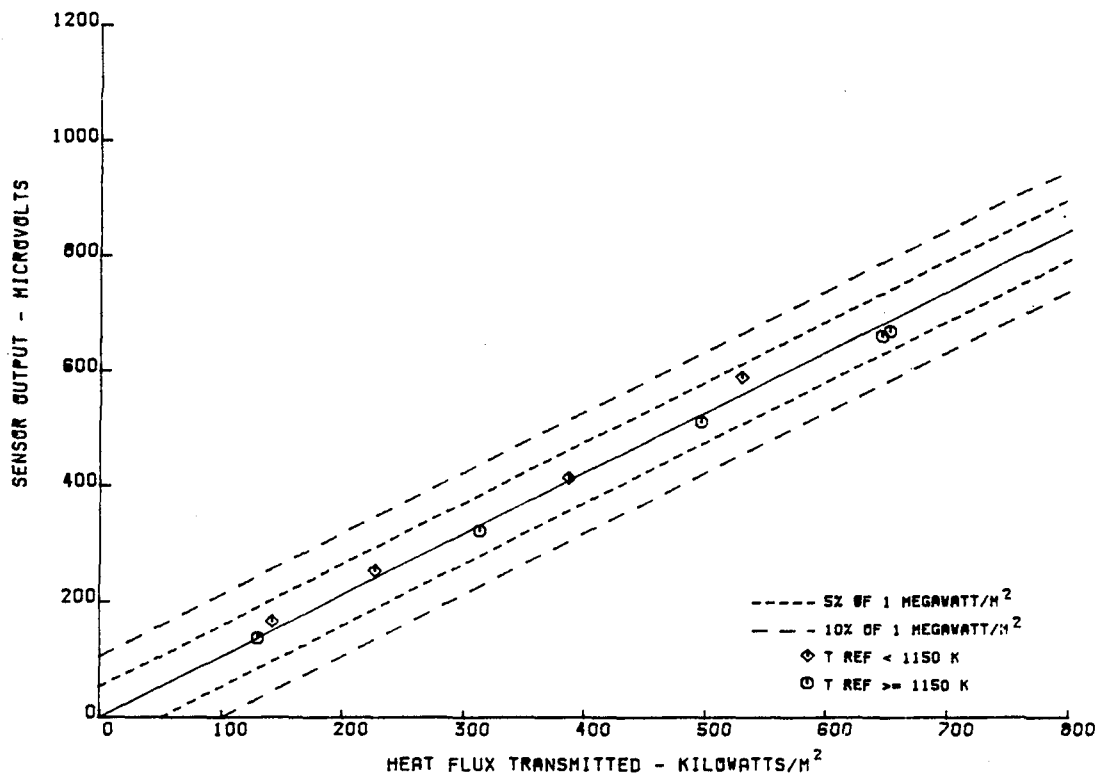
Figure E-13   Voltage Output versus Heat Flux Transmitted through Gardon
Gauge Sensor G-6

Figure E-14   Heat Flux Deviation versus Sensor Reference Temperature for
Gardon Gauge Sensor G-6

183

TABLE E-VIII

CALIBRATION RESULTS FOR GARDON GAUGE SENSOR G-7

Q TRANSMITTED KILOWATTS/M**2	T REFERENCE KELVIN	OUTPUT MICROVOLTS	SENSITIVITY OUTPUT/UNIT Q
178.51	986.	172.	.963
129.06	1175.	117.	.906
576.94	1172.	545.	.944
478.79	1045.	475.	.992
364.06	881.	374.	1.027

SENSOR CALIBRATION CONSTANT
BASED ON LEAST SQUARE LINE FORCED THROUGH ORIGIN OF OUTPUT VS. HEAT FLUX

S= .97   MICROVOLTS/KILOWATT/M**2

IN USE Q MEASURED = OUTPUT/S

The Center Alumel lead failed after the 5th point of the initial calibration of this sensor. The open was determined to be in the leadwire external to the sensor.

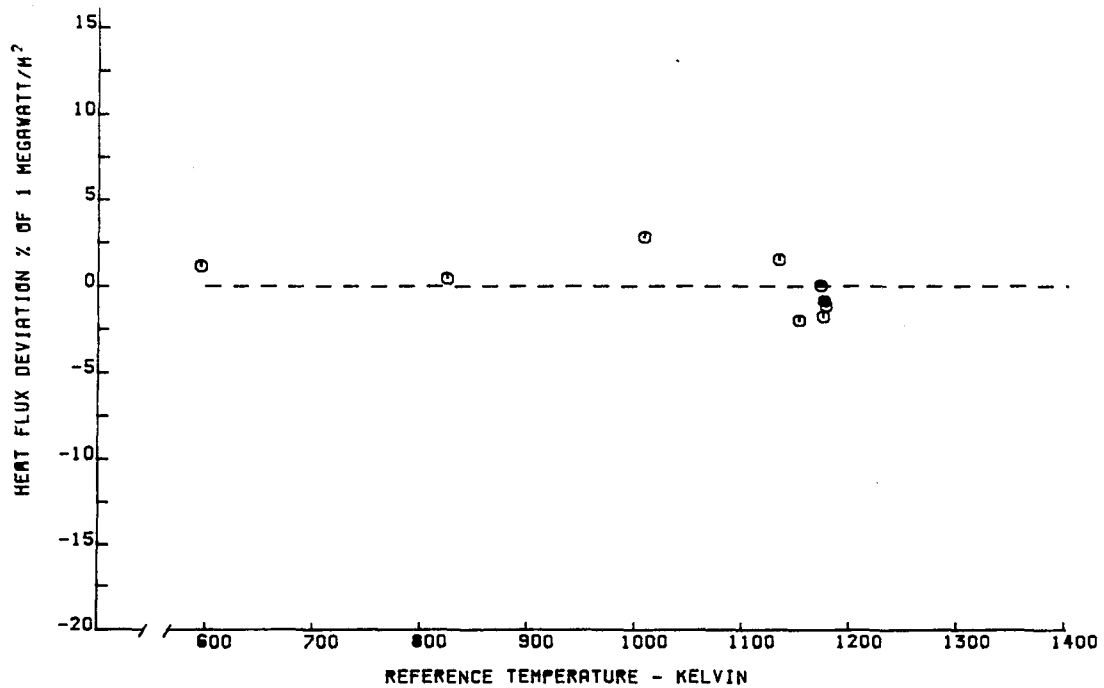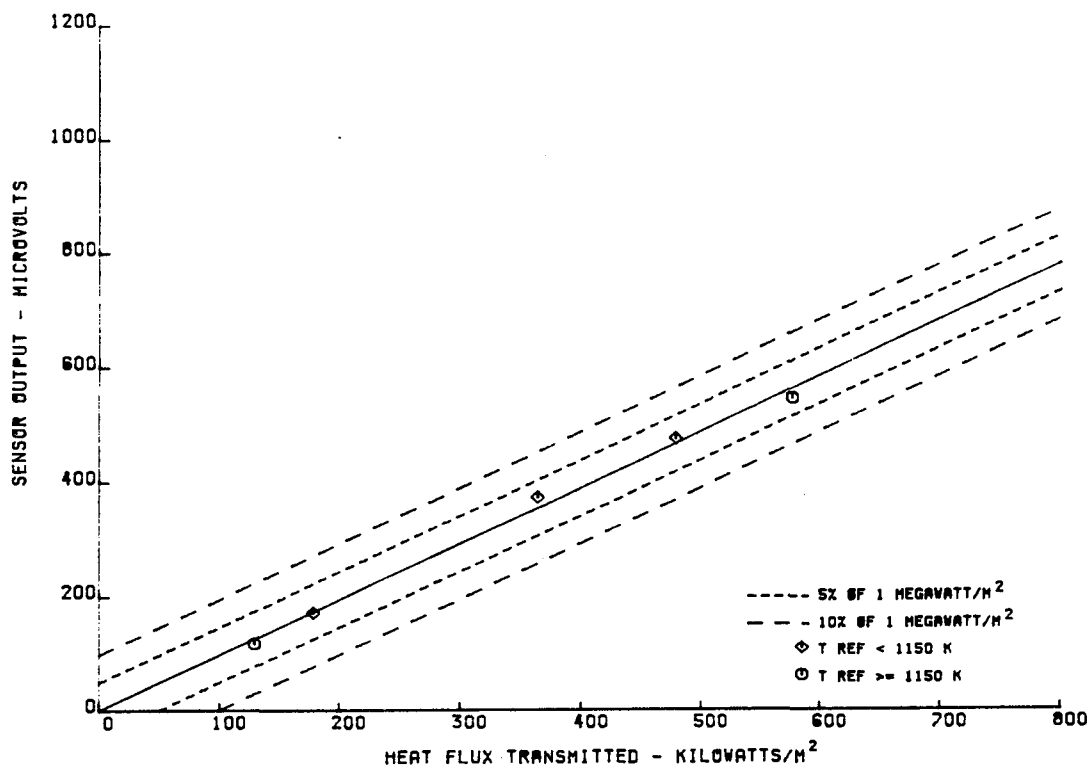Figure E-15   Voltage Output versus Heat Flux Transmitted through Gardon
Gauge Sensor G-7

Figure E-16   Heat Flux Deviation versus Sensor Reference Temperature for
Gardon Gauge Sensor G-7

185

TABLE E-IX

CALIBRATION RESULTS FOR GARDON GAUGE SENSOR G-8

Q TRANSMITTED KILOWATTS/M**2	T REFERENCE KELVIN	OUTPUT MICROVOLTS	SENSITIVITY OUTPUT/UNIT Q
220.00	691.	245.	1.113
131.20	1169.	129.	.983
592.53	1172.	597.	1.007
491.20	1032.	525.	1.068
365.30	861.	389.	1.064
224.38	632.	241.	1.074
590.24	1169.	614.	1.040
446.85	1174.	475.	1.062
290.13	1173.	324.	1.116
130.65	1172.	134.	1.025

SENSOR CALIBRATION CONSTANT
BASED ON LEAST SQUARE LINE FORCED THROUGH ORIGIN OF OUTPUT VS. HEAT FLUX

S= 1.05   MICROVOLTS/KILOWATT/M**2

IN USE Q MEASURED = OUTPUT/S

Figure E-17   Voltage Output versus Heat Flux Transmitted through Gardon
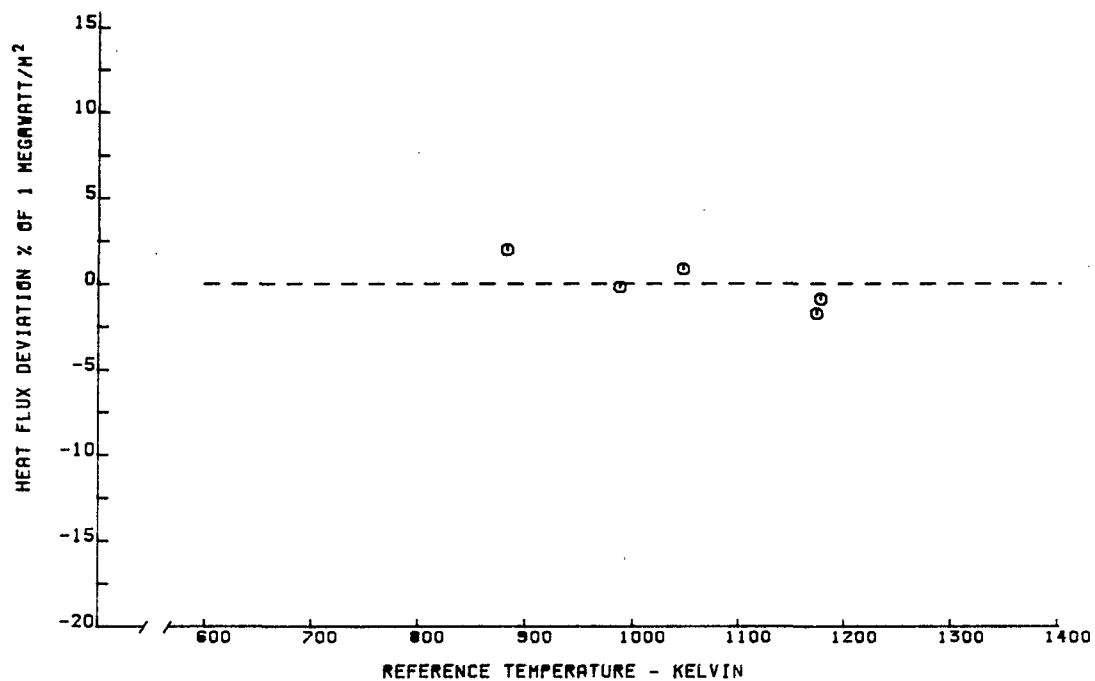   Gauge Sensor G-8

Figure E-18   Heat Flux Deviation versus Sensor Reference Temperature for
               Gardon Gauge Sensor G-8

TABLE E-X

CALIBRATION RESULTS FOR GARDON GAUGE SENSOR G-9

Q TRANSMITTED KILOWATTS/M**2	T REFERENCE KELVIN	OUTPUT MICROVOLTS	SENSITIVITY OUTPUT/UNIT Q
170.40	1024.	136.	.798
128.36	1174.	91.	.708
575.27	1172.	488.	.848
479.30	1050.	401.	.836
360.39	866.	315.	.874
223.61	635.	195.	.872
584.76	1160.	470.	.803
442.38	1171.	379.	.856
293.22	1173.	257.	.876
128.27	1173.	96.	.748

SENSOR CALIBRATION CONSTANT
BASED ON LEAST SQUARE LINE FORCED THROUGH ORIGIN OF OUTPUT VS. HEAT FLUX

S= .83 MICROVOLTS/KILOWATT/M**2

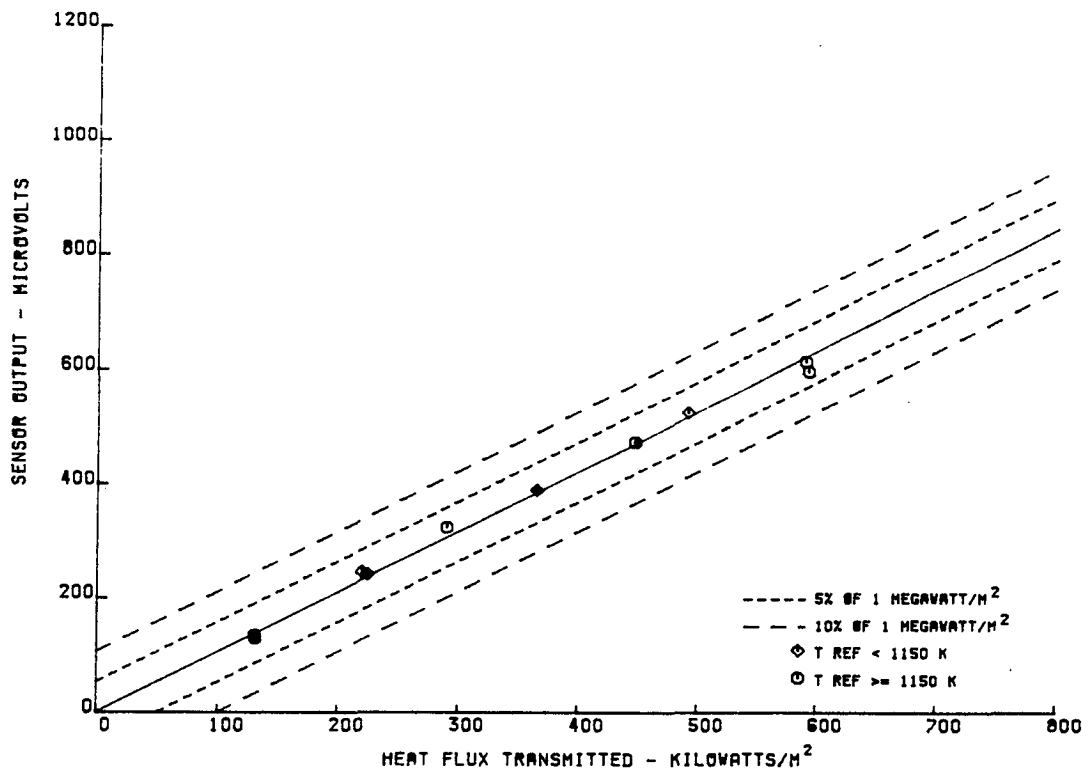IN USE Q MEASURED = OUTPUT/S

Figure E-19   Voltage Output versus Heat Flux Transmitted through Gardon
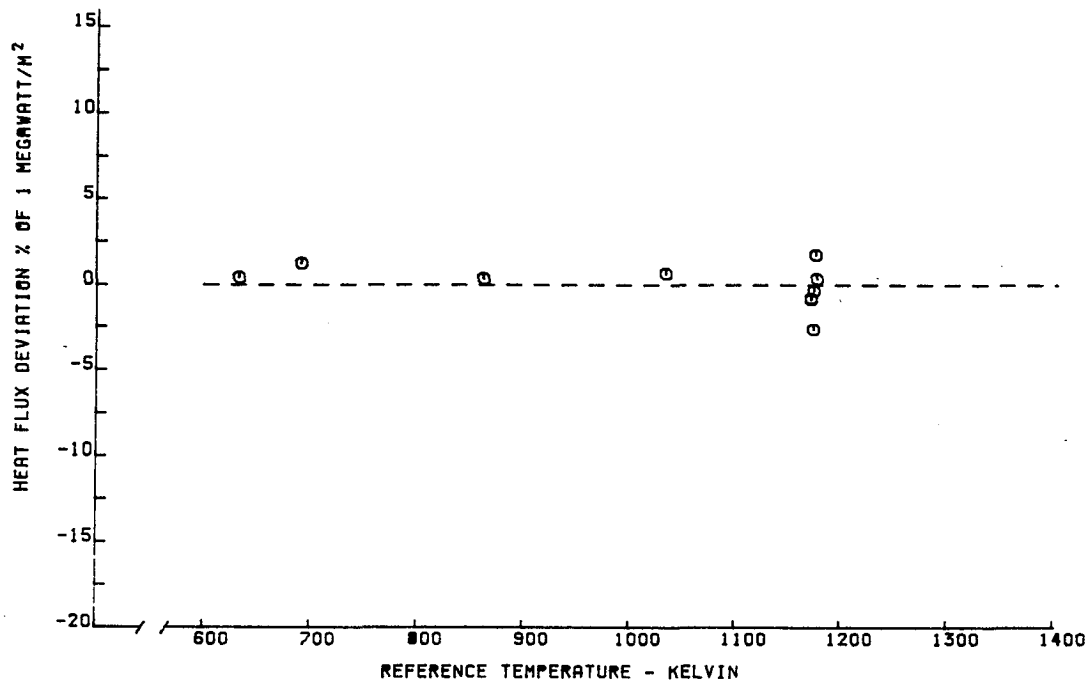Gauge Sensor G-9
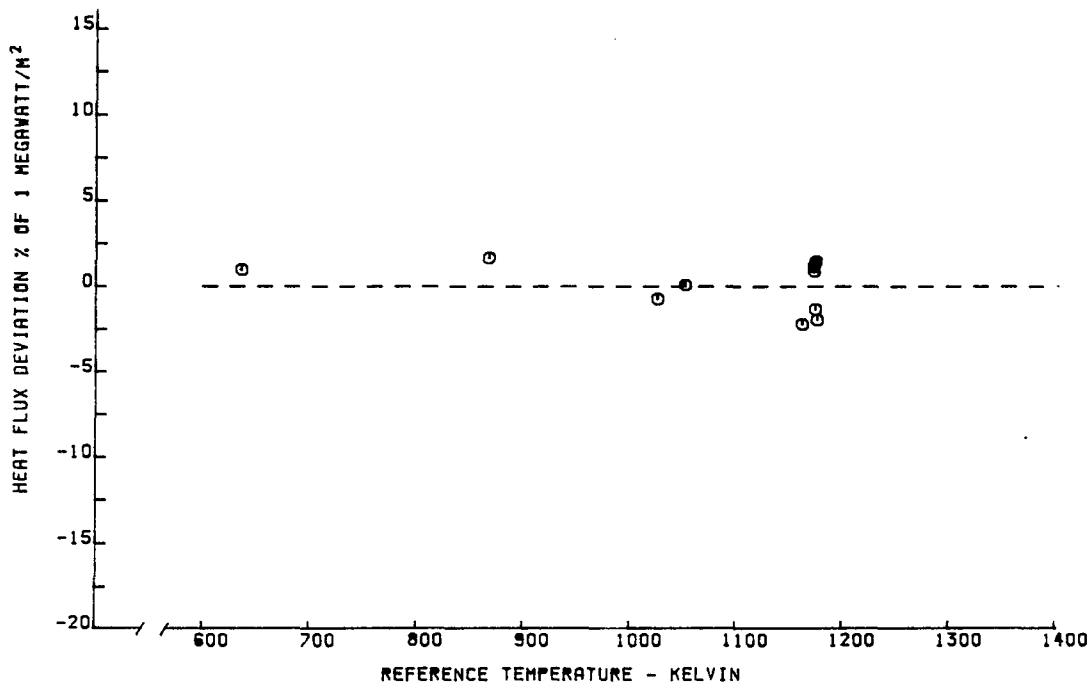
Figure E-20   Heat Flux Deviation versus Sensor Reference Temperature for
Gardon Gauge Sensor G-9

189

TABLE E-XI

CALIBRATION RESULTS FOR GARDON GAUGE SENSOR G-9A

Q TRANSMITTED KILOWATTS/M**2	T REFERENCE KELVIN	OUTPUT MICROVOLTS	SENSITIVITY OUTPUT/UNIT Q
47.15	927.	44.	.933
126.59	1173.	106.	.837
593.62	1177.	541.	.911
484.67	1048.	413.	.852
364.29	859.	301.	.826
223.94	629.	217.	.968
592.48	1167.	545.	.919
448.98	1172.	410.	.913
293.03	1173.	283.	.965
130.48	1167.	92.	.705

SENSOR CALIBRATION CONSTANT
BASED ON LEAST SQUARE LINE FORCED THROUGH ORIGIN OF OUTPUT VS. HEAT FLUX

S= .89   MICROVOLTS/KILOWATT/M**2

IN USE Q MEASURED = OUTPUT/S

This is data from the post test recalibration of sensor G-9 after the 50 cycle thermal test.
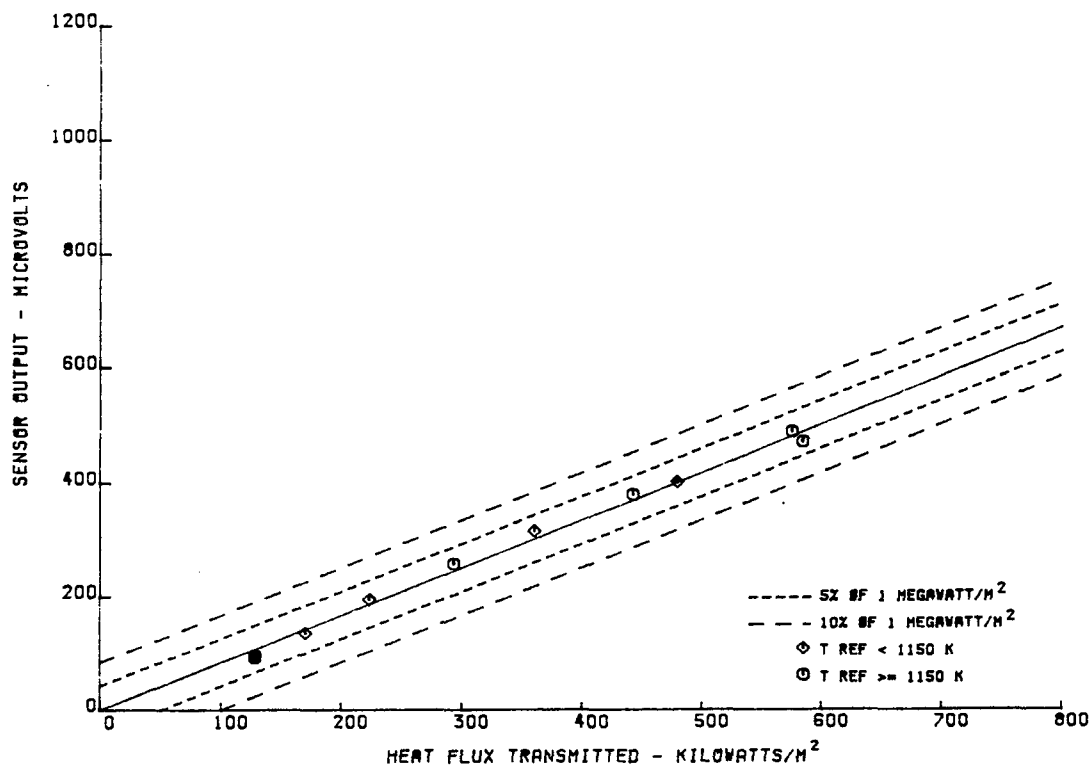
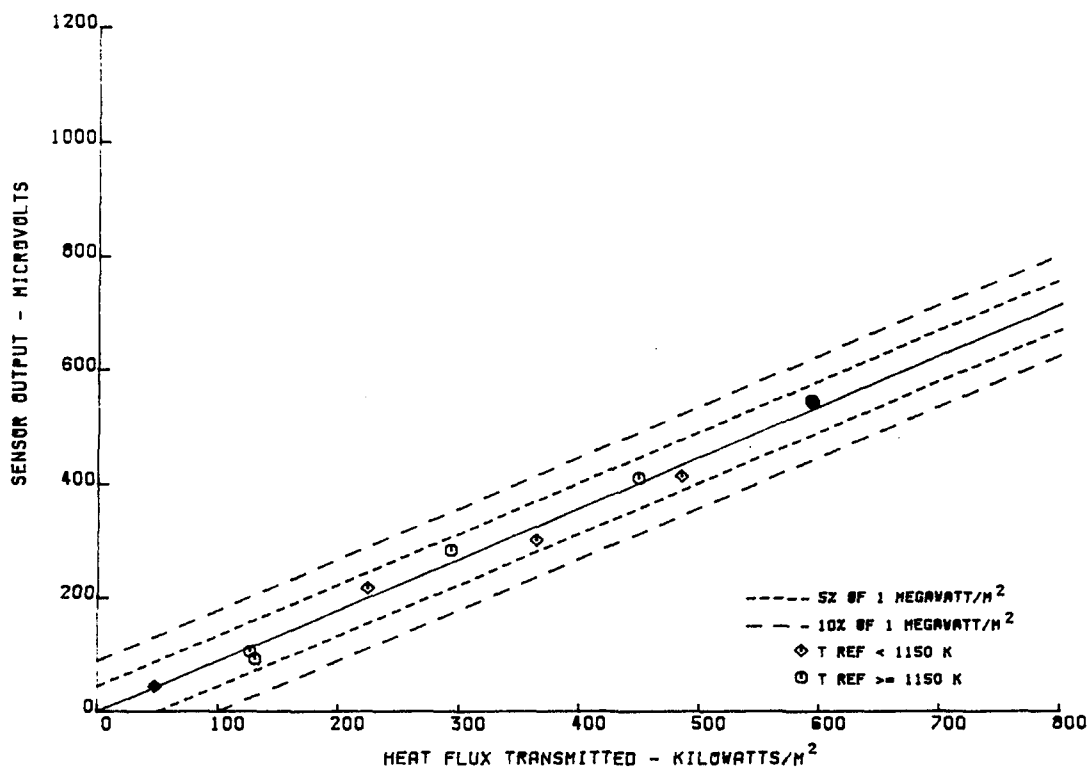Figure E-21   Voltage Output versus Heat Flux Transmitted through Gardon
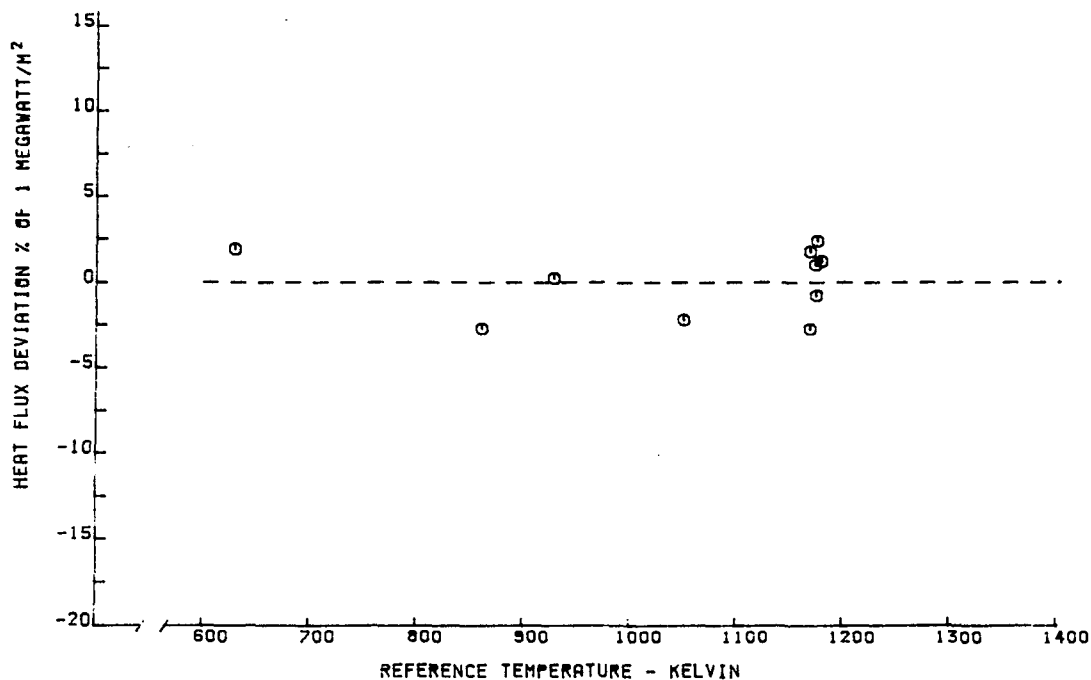Gauge Sensor G-9A

Figure E-22   Heat Flux Deviation versus Sensor Reference Temperature for
Gardon Gauge Sensor G-9A

CONTRACT REPORT DISTRIBUTION LIST

Instrumentation R&D Branch

Each addressee will receive one copy unless indicated otherwise.

NASA Lewis Research Center
21000 Brookpark Road
Cleveland, OH 44135
Attn: M.S. 77-1
(50 copies)

NASA Lewis Research Center
21000 Brookpark Road
Cleveland, OH 44135
Attn: Leonard W. Schopen, M.S. 501-11

NASA Scientific and Technical
  Information Facility
P. O. Box 33
College Park, MD 20740
Attn: Acquisitions Branch
(22 copies)

NASA Lewis Research Center
21000 Brookpark Road
Cleveland, OH 44135
Attn: Library, M.S. 60-3
(2 copies)

NASA Lewis Research Center
21000 Brookpark Road
Cleveland, OH 44135
Attn: Report Control Office, M.S. 5-5

General Electric Company
Aircraft Engine Group
Evendale, OH 45215
Attn: Wayne Shaffernocker, MSH-78
       Ronald Wise, MSH-78

Stanford University
Stanford, CA 94305
Attn: Dr. R. J. Moffat
       Asst. Prof., Mech. Engr.
       Dir. Thermoscience
         Measurement Center

Air Force Wright Aeronautical
  Laboratory
Wright Patterson AFB, OH 45433
Attn: R. Cox/POTC

Air Force Wright Aeronautical
  Laboratory
Wright Patterson AFB, OH 45433
Attn: Everett E. Bailey/AFWAL/NASA-PO

Air Force Wright Aeronautical
  Laboratory
Wright Patterson AFB, OH 45433
Attn: Deborah Finnerty/POTC

Air Force Wright Aeronautical
  Laboratory
Wright Patterson AFB, OH 45433
Attn: M. Roquemore/POSF

Roto Data, Inc.
10200 Anderson Way
Cincinnati, OH 45242
Attn: David Davidson

UTRC/OATL
Palm Beach Gardens Facility
West Palm Beach, FL 33402
Attn: John T. Carroll
       Bldg. 30 (MS R-23)

Lewis Engineering Company
238 Wate Street
Naugatuck, CT 06770
Attn: C. B. Stegner

Arnold Engineering
  Development Center
Arnold Air Force Station, TN 37389
Attn: Marshall Kingery

Hitec Corporation
Nardone Industrial Park
Westford, MA 01886
Attn: Steve Wnuk

General Electric Company
Aircraft Engine Group
1000 Western Avenue
Lynn, MA 01910
Attn: George Leperch, A129dD

General Electric Company
Aircraft Equipment Division
50 Fordham Road
Wilmington, MA 01887
Attn: Ronald J. Casagrande

Detroit Diesel Allison
Box 894
Indianapolis, IN 46206
Attn: John Custer, W-16

Detroit Diesel Allison
Box 894
Indianapolis, IN 46206
Attn: Ken Cross

Detroit Diesel Allison
Box 894
Indianapolis, IN 46206
Attn: David Willis

Detroit Diesel Allison
Box 894
Indianapolis, IN 46206
Attn: Ralph Fox

Battelle Columbus Laboratories
505 King Avenue
Columbus, OH 43201
Attn: Ross G. Luce, Energy &
      Thermal Tech. Section

Teledyne CAE
1350 Laskey Road
Toledo, OH 43612
Attn: R. Hugh Gaylord

Garret-AiResearch
P. O. Box 5217
Phoenix, AZ 85010
Attn: N. Fred Pratt

FluiDyne Engr. Corporation
5900 Olson Memorial Highway
Minneapolis, MN 55422
Attn: T. Matsuura

AVCO Corporation
Lycoming Division
550 South Main Street
Stratford, CT 06497
Attn: E. Twarog, Mgr.
      Electronics and Instr.

Thermonetics Corporation
1028 Garnet Avenue
San Diego, CA 92109
Attn: H. F. Poppendiek

Battelle Columbus Laboratories
505 King Avenue
Columbus, OH 43201
Attn: M. M. Lemcoe

Peter K. Stein
5602 East Monterosa
Phoenix, AZ 85018

Pratt & Whitney Aircraft
Main Plant
P. O. Box 2691
West Palm Beach, FL 33402
Attn: John Prosser (MS C-04)

National Bureau of Standards
Washington, DC 20234
Attn: Ray Dils

National Bureau of Standards
Washington, DC 20234
Attn: George Burns
      Inst. for Basic Research

General Electric Company
P. O. Box 8
Schenectady, NY 12301
Attn: Dr. David Skelley
      Bldg. K-1, Rm. 3B24

Mechanical Technology, Inc.
968 Albany-Shaker Road
Latham, NY 12110
Attn: R. Hohenberg

Boeing Aerospace Company
Engineering Laboratories
Seattle, WA 98124
Attn: Darrell R. Harting

Engelhard
Engelhard Industries Div.
228 East 10th Street
Newport, KY 41075
Attn: Ronald G. Braun

Williams Research
2280 West Maple Road
Walled Lake, MI 48088
Attn: Henry Moore, Head
      Instr. Dept.

Virginia Polytechnic Institute
  and State University
Mechanical Engineering Dept.
Blacksburg, VA 24061
Attn: W. F. O'Brien, Jr.

Naval Post Graduate School
Department of Aeronautics (Code 67)
Monterey, CA 93940
Attn: Prof. R. P. Shreeve

Pennsylvania State University
233 Hammond Building
University Park, PA 16802
Attn: Prof. B. Lakshminarayana

Kulite Semiconductor Products, Inc.
1039 Hoyt Avenue
Ridgefield, NJ 07657
Attn: John R. Hayer

Bolt Beranek and Newman, Inc.
50 Moulton Street
Cambridge, MA 02138
Attn: Richard E. Hayden

Caterpillar Tractor Company
Technical Center, Building F
100 Northeast Adams Street
Peoria, IL 61629
Attn: Mr. Donald Wilson

Air Force Wright Aeronautical
  Laboratory
Wright Patterson AFB, OH 45433
Attn: Mr. Charles Bentz/POTC
      Hot Section Technology

AVCO Corporation
Lycoming Division
550 South Main Street
Stratford, CT 06497
Attn: Mr. K. Collinge
      IRAD Mechanical Projects
        Manager

Eaton Corporation
Box 766
Southfield, MI 48037
Attn: Mr. Lamont Eltinge
      Director of Research

Public Service Electric & Gas Company
80 Park Plaza
Newark, NJ 07101
Attn: Dr. Melvin L. Zwillenberg
      Research & Development Dept.

Raychem Corporation
300 Constitution Drive
Menlo Park, CA 94025
Attn: Dr. David C. Chappelear
      Director of Corporate
        Research & Development

Fabrication Development Laboratory
Owens/Corning Fiberglas
Technical Center
Granville, OH 43023
Attn: Mr. Hugh W. Bradley, Jr.

Xerox Electro-Optical Systems
1616 North Fort Myer Drive, 16th Floor
Arlington, VA 22209
Attn: Mr. Clifford I. Cummings
      Manager, Intelligence &
        Reconnaissance

Construction Materials Support Group
Owens/Corning Fiberglas
CMG Process Technology Laboratory
Granville, OH 43023
Attn: Mr. J. W. Scott

Thermogage Inc.
330 Allegany Street
Frostburg, Maryland 21532

Attn: Charles E. Brookley

Hycal Engineering
12105 Los Nietos Rd.
Sante Fe Springs, CA 90670

Attn: William Clayton

Medtherm Corporation
P.O. Box 412
Huntsville, AL 35804

Attn: Larry Jones

Rocketdyne
6633 Canoga Ave
Canoga Park, CA 91304

Attn: Dr. John C. Lee

Combustion Engineering
Dept 9005-03D1
Windsor, CT 06095

Attn: John Fishburn

RdF Corporation
23 Elm Ave.
Hudson N.H. 03051

Attn: Frank Hines

Babcock & Wilcox R&D Division
P.O. Box 835
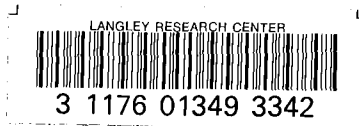Alliance, OH 44601

Attn: Harold Wahle

JEC Lasers Inc.
253 Crooks Ave
Patterson, NJ

Attn: Mr. John Wasko

NASA Langley Research Center
Hamilton, VA 23665   MS-234

Attn: R.E. Wright Jr.

DO NOT REMOVE SLIP FROM MATERIAL

Delete your name from this slip when returning material to the library.

NAME	MS
S. Borg	234

NASA Langley (Rev. May 1988)   RIAD N-75